THESE / UNIVERSITE DE BREST
sous le sceau de l'Université européenne de Bretagne

pour obtenir le titre de
DOCTEUR DE l'UNIVERSITE DE BREST
Mention Sciences de la Terre
Ecole Doctorale des Sciences de la Mer

présentée par
Estelle Leroux

Préparée à 'Unité Mixte de recherche (n°6538)
Institut Universitaire Européen de la Mer
Domaines Océaniques

« Quantification des flux sédimentaires et de la subsidence du bassin Provençal – **Annexes : Volume II** »

Thèse soutenue le 14 mai 2012 devant le jury composé de :

Cécile Robin
Maître de conférence, Université de Rennes 1 / *Rapporteur*
Jean-Loup Rubino
Expert rang Professeur, Pau / *Rapporteur*
Philippe Joseph
Professeur ENSPM, Rueil Malmaison / *Examinateur*
Michel Séranne
Chercheur CNRS, Université de Montpellier / *Examinateur*
Jacques Deverchère
Professeur, Université de Brest / *Examinateur*
Christian Gorini
Professeur UPMC, Istep / examinateur et Co-directeur de thèse
Laurence Droz
Chercheur CNRS, UMR6538, Brest Co-Directrice de thèse (Invitée)
Daniel Aslanian
Chercheur IFREMER, Brest / Tuteur
Marina Rabineau
Chercheur CNRS, UMR6538, Brest / Tutrice

Liste des publications et communications

PUBLICATIONS ACCEPTEES, SOUMISES OU EN PREPARATION

(I) F. Bache, S.-M. Popescu, M. Rabineau, C. Gorini, J.-P. Suc, G. Clauzon, J.-L. Olivet, J.-L. Rubino, M.-C. Melinte-Dobrinescu, F. Estradan, L. Londeix, R. Armijo, B. Meyer, L. Jolivet, G. Jouannic, **E. Leroux**, D. Aslanian, A.T. Dos Reis, L. Macochain, N. Dumurdzanov, I. Zagorchev, V. Lesić, D. Tomić, M. Namik, Çagatay, J.-P. Brun, D. Sokoutis, I. Csato, G. Ucarkus and Z. Çakir, **2012**. A two step process for the reflooding of the Mediterranean after the Messinian Salinity Crisis. *Basin Research* 23, 1-29.

(II) M. Rabineau, **E. Leroux**, F. Bache, D. Aslanian, C. Gorini, L. Droz, M. Moulin, D. Granjeon, J.-L. Olivet, **(submitted)**. Quantification of Pliocene-Quaternary Subsidence and isostatic readjustment related to the Messinian Crisis (using paleobathymetric markers in the *Gulf of Lions*), *Earth & Planetary Sciences*, xxx, xx-xx..

(III) F. Bache, J. Gargani, J.-P. Suc, C. Gorini, M. Rabineau, J.-L. Olivet, S.-M. Popescu, **E. Leroux**, G. Jouannic, D. Do Couto, J.-L. Rubino, G. Clauzon & A. T. Dos Reis, **(submitted)**. Detailed process of the peak of the Messinian Salinity Crisis : Evidences from the Gulf of Lions (NW Mediterranean), *Earth & Planetary Sciences*, xxx, xx-xx.

(IV) **E. Leroux**, M. Rabineau, D. Aslanian, D. Granjeon, C. Gorini, L. Droz **(in preparation)**. Stratigraphic simulations on the Gulf of Lion platform : results on plioquaternary subsidence and climatic implications.

(V) D. Aslanian, M. Rabineau, F. Klingelhoefer, M. Moulin, P. Schnurle, A. Gailler, F. Bache, **E. Leroux**, C. Gorini, A. Droxler, N. Eguchi, J. Kuroda, K. Alain, F. Roure & B. Haq. Structure and evolution of the Gulf of Lions : the Sardinia seismic experiment and the GOLD (Gulf of Lions Drilling) project, *Leading Edge*, xxx, xx-xx.

AUTRES PUBLICATIONS

C. Satra, J. Boyer, S. Berné, M. Tesson, P. Guennoc, A.-S. Alix, M.A. Bassetti, G. Jouet, **E. Leroux**, J.P. Mazé, A. Normand, D. Pierre, C. Labaune, B. Gensous and K. Guérin, **2004**. Projet Beachmed. Rapport final de phase C : Présentation des données. In : D.G. 2004-21 (Editor). Ifremer, Brest.

COMMUNICATIONS SCIENTIFIQUES

• **E. Leroux**, M. Rabineau, D. Aslanian, D. Granjeon, C. Gorini, L. Droz Simulations Stratigraphiques des dépôts plio-quaternaires de la plate-forme du Golfe du Lion : Etude de la subsidence. **ASF 2009**, Rennes (Poster).
• Réunion GDR Marges 2010, SGF, Paris, France (Communication orale).
• Réunion de travail 2010, IFP, France (Communication orale).
• **E. Leroux**, M. Rabineau, D. Aslanian, D. Granjeon, C. Gorini, L. Droz Simulations Stratigraphiques des dépôts plio-quaternaires de la plate-forme du Golfe du Lion : Etude de la subsidence.**RST 2010**, Bordeaux (Poster).

COMMUNICATIONS DE VULGARISATION SCIENTIFIQUE

• Stage résidentiel CIES 2011, Rennes (France).

• TCM (Très Court Métrage de vulgarisation scientifique) réalisé puis présenté lors du festival du Très Court-Métrage de vulgarisation scientifique, Edition 2010 (http ://www.nicomaque.org/projets/tcm).

Publications

I. Une remontée biphasée du niveau marin après la crise de salinité messinienne (Bache *et al.*, 2012).

II. Quantification de la subsidence plio-quaternaire et des réajustements isostatiques liés à la crise messinienne au travers de marqueurs paléobathymétriques dans le Golfe du Lion (Rabineau *et al.*, 2012 *(soumis)*)

III. Scénario au paroxysme de la crise de salinité messinienne : mise en évidence à partir de marqueurs géologiques dans le Golfe du Lion (Méditerranée Occidentale) (Bache *et al.*, 2012 *(soumis)*).

IV. Structure et évolution de la marge du Golfe du Lion : la campagne Sardinia et le projet de forage profond GOLD (Aslanian *et al.*, 2012 *(soumis)*).

Basin Research

Basin Research (2011) 23, 1–29, doi: 10.1111/j.1365-2117.2011.00521.x

A two step process for the reflooding of the Mediterranean after the Messinian Salinity Crisis

François Bache,*,†,‡ Speranta-Maria Popescu,§ Marina Rabineau,¶ Christian Gorini,*,† Jean-Pierre Suc,*,† Georges Clauzon,** Jean-Louis Olivet,†† Jean-Loup Rubino,‡‡ Mihaela Carmen Melinte-Dobrinescu,§§ Ferran Estrada,¶¶ Laurent Londeix,*** Rolando Armijo,§ Bertrand Meyer,*,† Laurent Jolivet,††† Gwénaël Jouannic,‡‡‡ Estelle Leroux,¶,†† Daniel Aslanian,†† Antonio Tadeu Dos Reis,§§§ Ludovic Mocochain,¶¶¶ Nikola Dumurdžanov,**** Ivan Zagorchev,†††† Vesna Lesić,‡‡‡‡ Dragana Tomić,‡‡‡‡ M. Namık Çağatay,§§§§ Jean-Pierre Brun,¶¶¶¶ Dimitrios Sokoutis,***** Istvan Csato,††††† Gülsen Ucarkus§§§§ and Ziyadin Çakır§§§§

*UPMC Univ, Paris 06, UMR 7193, ISTEP, F-75005, Paris, France
†CNRS, UMR 7193, ISTEP, F-75005, Paris, France
‡GNS Science, P.O. BOX 30368, Lower Hutt 5040, New Zealand
§Laboratoire de Tectonique, Institut de Physique du Globe de Paris (UMR 7154 CNRS), Paris Cedex, France
¶IUEM, Domaines océaniques (UMR 6538), 1 place Nicolas Copernic, 29280, Plouzané, France
**C.E.R.E.G.E. (UMR 6635), Université Paul Cézanne, Europôle de l'Arbois, BP 80, 13545, Aix-en-Provence Cedex 04, France
††IFREMER, Géosciences marines, LGG, BP 70, 29280, Plouzané Cedex, France
‡‡TOTAL, TG/ISS, CSTJF, Avenue Laribeau, 64018, Pau Cedex, France
§§National Institute of Marine Geology and Geoecology, 23-25 Dimitrie Onciul street, P.O. Box 34-51, 70318, Bucharest, Romania
¶¶Instituto de Ciencias del Mar de Barcelona, C.S.I.C., Paseo Juan de Borbon s/n, 08039, Barcelona, Spain
***Université Bordeaux 1, UMR 5805 CNRS 'EPOC', avenue des Facultés, 33405, Talence cedex, France
†††ISTO (UMR 6113), Université d'Orléans, 45071, Orléans Cedex 2, France
‡‡‡Université Paris-Sud, Laboratoire IDES, UMR 8148, Orsay, F-91405, France
§§§Departamento de Oceanografia Geologica/UERJ-Brazil, Rua São Francisco Xavier, 524, 48 Andar, Maracaña, Rio de Janeiro RJ CEP, 20.550-900, Brazil
¶¶¶Laboratoire de Géologie (UMR 8538), Ecole Normale Supérieure, 24 rue Lhomond, 75231, Paris, Cedex 05, France
****Sts. Cyril and Methodius University, Faculty of Mining and Geology, Goce Delčev 89, 2000, Štip, Republic of Macedonia
††††Geological Institute, Bulgarian Academy of Sciences, 1113, Sofia, Bulgaria
‡‡‡‡Geolomagnetic Institute, Kraljice Natalije 45, 11000, Belgrad, Republic of Serbia
§§§§Istanbul Technical University, School of Mines and Eurasia Institute of Earth Sciences, Maslak, 34469, Istanbul, Turkey
¶¶¶¶Géosciences Rennes (UMR 6118), Université Rennes 1, 35042, Rennes Cedex, France
*****ISES, Vrije Universiteit Amsterdam, 1081, HV Amsterdam, The Netherlands
†††††Department of Geology, Collin College, 2800 Spring Creek Pkwy, Plano, TX, 75075, USA

ABSTRACT

The Messinian Salinity Crisis is well known to have resulted from a significant drop of the Mediterranean sea level. Considering both onshore and offshore observations, the subsequent reflooding is generally thought to have been very sudden. We present here offshore seismic evidence from the Gulf of Lions and re-visited onshore data from Italy and Turkey that lead to a new concept of a two-step reflooding of the Mediterranean Basin after the Messinian Salinity Crisis. The refilling was first moderate and relatively slow accompanied by transgressive ravinement, and later on very rapid, preserving the subaerial Messinian Erosional Surface. The amplitude of these two successive rises of sea level has been estimated at ≤ 500 m for the first rise and 600–900 m for the second rise. Evaporites from the central Mediterranean basins appear to have been deposited principally at the beginning of the first step of reflooding. After the second step, which preceeded the Zanclean Global Stratotype Section and Point, successive connections with the Paratethyan Dacic Basin, then the Adriatic

Correspondence: F. Bache, GNS Science, P.O. BOX 30368, Lower Hutt 5040, New Zealand. E-mail: f.bache@gns.cri.nz

foredeep, and finally the Euxinian Basin occurred, as a consequence of the continued global rise in sea level. A complex morphology with sills and sub-basins led to diachronous events such as the so-called 'Lago Mare'. This study helps to distinguish events that were synchronous over the entire Mediterranean realm, such as the two-step reflooding, from those that were more local and diachronous. In addition, the shoreline that marks the transition between these two steps of reflooding in the Provence Basin provides a remarkable palaeogeographical marker for subsidence studies.

INTRODUCTION

The almost complete desiccation of the Mediterranean Sea in the Messinian resulted in the deposition of thick evaporites in the central basins (Hsü *et al.*, 1973; Rouchy & Caruso, 2006) and the cutting of deep fluvial canyons (Chumakov, 1973; Clauzon, 1973, 1978, 1980a, 1982, 1990; Savoye & Piper, 1991) (Fig. 1). The termination of the Messinian Salinity Crisis (MSC), i.e. the reflooding of the Mediterranean Basin, is classically considered to have been very sudden (Hsü *et al.*, 1973; Clauzon & Cravatte, 1985; Pierre *et al.*, 1998; Blanc, 2002; Lofi *et al.*, 2003). The generally accepted age for this event is that of the Zanclean Global Stratotype Section and Point (GSSP) at 5.332 Ma (Table 1; Hilgen & Langereis, 1993; van Couvering *et al.*, 2000; Lourens *et al.*, 2004). Offshore, this very rapid event is reflected by the sharp contact between the Messinian evaporites and Zanclean mudrocks (Cita *et al.*, 1978) or the Zanclean prograding sediments downlapping directly on the Messinian Erosional Surface (MES) (Lofi *et al.*, 2003). Onshore, this contact is often reflected by the prograding sedimentary filling of Gilbert-type fan deltas within the Zanclean rias without any onlapping transgressive parasequence (Fig. 2; Clauzon, 1990). In the earliest Pliocene, the Mediterranean Basin was starved of terrigenous sediments (Cita *et al.*, 1978, 1999a), which concentrated within the rias. In several rias from southern France and northeastern Spain, the clayey bottomset beds of the Gilbert-type fan deltas have been dated by foraminifers from the *Sphaeroidinellopsis* Acme Zone (Civis, 1977; Clauzon & Cravatte, 1985; Zheng & Cravatte, 1986) in agreement with the nannofossil record (Matias I Sendra, 1990). The Gilbert-type fan deltas have been identified as infilling Messinian fluvial canyons all around the Mediterranean Basin and in adjacent territories as illustrated in Fig. 1.

The question of the suddenness of the Mediterranean reflooding has been reopened since a progressive reflooding of the Mediterranean was advocated by Krijgsman *et al.* (1999a), possibly preceding the earliest Zanclean

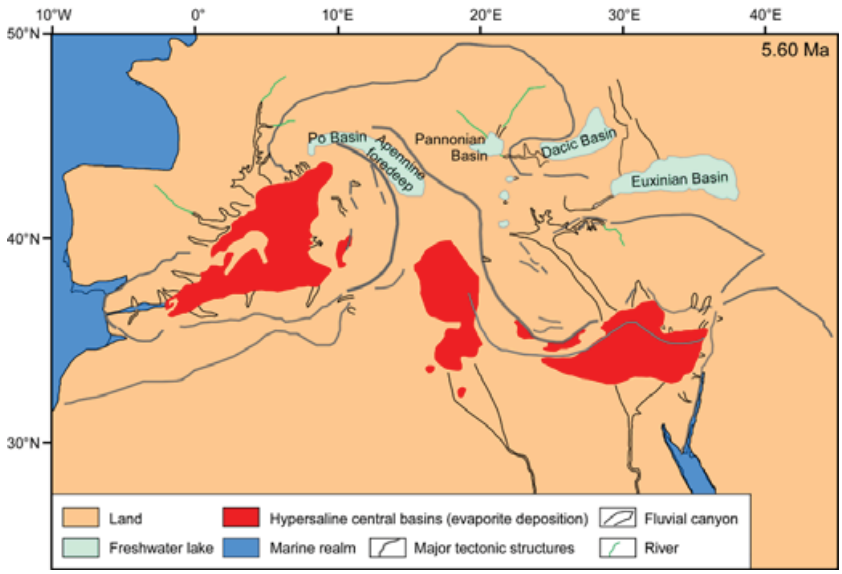

Fig. 1. Map of the Messinian central basin evaporites and fluvial canyons identified around the Mediterranean Basin and adjacent territories during the peak of the Messinian Salinity Crisis (5.60–5.56? Ma). At that time, the water level in the Mediterranean Basin was some 1600 m lower than the global sea level. Major tectonic structures and corresponding topographic highs are drawn according to Jolivet *et al.* (2006) also valid for Figs 16, 19, 20 and 22. Map of central basin evaporites is from Rouchy & Caruso (2006). Map of fluvial canyons is from field observations of some of us (G. C., J.-P. S., J.-L. R., L. M.) and from the related literature (Nile area: Chumakov, 1967, 1973; Bentz & Hughes, 1981; Said, 1982; Goudie, 2005; Lybia: Griffin, 2002; Drake *et al.*, 2008; Nicolai, 2008; Paillou *et al.*, 2009; North Tunisia: El Euch – El Koundi *et al.*, 2009; Antalya Basin, South Turkey: Poisson *et al.*, 2011; Southeastern Spain: Soria *et al.*, 2008; Northwestern Italy: Breda *et al.*, 2007). Map of the Po Basin and Apennine foredeep is from Boccaletti *et al.* (1990) and Clauzon *et al.* (1997), that of the Dacic Basin from Clauzon *et al.* (2005), that of the Pannonian Basin from Csato *et al.* (2007), and that of the Euxinian Basin to Gillet *et al.* (2007).

Table 1. Key ages used in this paper, arranged from the oldest to the youngest, with information on their origin (events, proxies, localities, relevant references)

Age (Ma)	Events	Proxies	Localities	References	Concerned parts of this paper
5.31	•Entrance of Mediterranean marine waters into the Black Sea, Euxinian Basin	*Ceratolithus acutus* and *Triquetrorhabdulus rugosus* (nannofossils) recorded at 840.07 m depth with Mediterranean diatoms and dinoflagellate cysts, age calibration by nannofossil biostratigraphy and pollen cyclostratigraphy correlated with oxygen isotope stratigraphy	DSDP Site 380 (Black Sea)	Popescu *et al.* (2010) Popescu (2006) Schrader (1978)	Section "Tentative age model of the reflooding process and suggested resulting palaeogeographical changes" Figs 20 and 22
5.332	•Base of Trubi, Zanclean GSSP	Bio- and magnetostratigraphy, astrochronology	Eraclea Minoa (Sicily)	Lourens *et al.* (2004) van Couvering *et al.* (2000) Hilgen & Langereis (1993)	Introduction Section "Eraclea Minoa (Sicily)" Figs 9, 11 and 22
5.345	•Lower occurrence	*Ceratolithus acutus* (nannofossil)	Atlantic Ocean	Raffi *et al.* (2006)	Introduction Sections "Maccarone (Apiro, Marche)", "The Dardanelles Strait area" Figs 4, 11 and 12
5.36	•Entrance of Mediterranean marine waters into the Apennines foredeep (AFC)	First record of Mediterranean nannofossils, foraminifers, dinoflagellate cysts, age calibration by relationship between pollen record and eccentricity	Maccarone (Apennines foredeep)	**This paper** Popescu *et al.* (2007)	Sections "Maccarone (Apiro, Marche)", "Tentative age model of the reflooding process and suggested resulting palaeogeographical changes" Figs 11, 19 and 22
5.45	•High sea-level water exchanges between the Mediterranean and Dacic Basin (DBC), Eastern Paratethys	Evidence of Eastern Paratethyan dinoflagellate cysts (*Galeacysta etrusca*, etc.) half a dark-light cycle above the base of Arenazzolo	Eraclea Minoa (Sicily)	**This paper**	Sections "Eraclea Minoa (Sicily)", "Tentative age model of the reflooding process and suggested resulting palaeogeographical changes" Figs 10, 17 and 22
5.46	•End of Step I of reflooding followed by instantaneous Step II	Base of Arenazzolo (6.5 dark–light alternations below the Zanclean GSSP, regarded as precession forced)	Eraclea Minoa (Sicily)	**This paper**	Section "Tentative age model of the reflooding process and suggested resulting palaeogeographical changes" Figs 10, 15 and 22
5.555 ± 0.06	•Ash layer	Radiometric age ($^{39}Ar/^{40}Ar$)	Maccarone (Apennines foredeep)	Cosentino *et al.* (2009)	Section "Maccarone (Apiro, Marche)" Fig. 11

Table 1 (continued)

Age (Ma)	Events	Proxies	Localities	References	Concerned parts of this paper
5.60	•Halite in central basins •Second sea-level fall (>1000 m) •Closure of the Rifian corridor	16–17 precession cycles of Primary Lower Gypsum Continuous dinoflagellate cyst and pollen records (chronologically calibrated by bio-, magnetostratigraphy and oxygen isotope stratigraphy) indicating increased coastal conditions at the Atlantic outlet of the Rifian corridor	Apennines foredeep, Sorbas Salé (Atlantic Morocco)	CIESM *et al.* (2008) Krijgsman *et al.* (1999b) Warny *et al.* (2003)	Section "Maccarone (Apiro, Marche)" Fig. 1 and 22
5.96	•Evaporites in marginal basins •Beginning of the MSC •First sea-level fall (*ca.* 150 m)	Bio- and magnetostratigraphy, astrochronology of the first evaporites	Sorbas (SE Spain), Sicily	Krijgsman *et al.* (1999b) Gautier *et al.* (1994)	Section "Eraclea Minoa (Sicily)" Fig. 22

Ages in bold characters are suggested in this paper. For ages corresponding to several events (5.96 and 5.6 Ma), the latter are indicated from the oldest (at the bottom) to the youngest (at the top). The relevant parts of this paper are indicated.

(Cavazza & Decelles, 1998; Cornée *et al.*, 2006). The problem also arises when considering the Sicilian Caltanissetta Basin (Fig. 3), a piggy-back basin located at that time some 150–200 km northward of its present-day position (Boccaletti *et al.*, 1990; Casero, 2004; Jolivet *et al.*, 2006). The interpretation of the environmental setting of the basin is controversial, representing either a deep Mediterranean central basin that was subsequently uplifted (Hsü *et al.*, 1973; Krijgsman *et al.*, 1999a; Rouchy & Caruso, 2006; Roveri & Manzi, 2006; Krijgsman & Meijer, 2008; Roveri *et al.*, 2008a,b), assuming synchronism of these evaporites with those of the Mediterranean central basins; or a marginal (even though relatively deep) domain (Brolsma, 1975; Butler *et al.*, 1995; Clauzon *et al.*, 1996; Popescu *et al.*, 2009) assuming that the evaporites in this basin are older than those of the central basins. This question has been discussed for a long time (Hsü *et al.*, 1973) and is still intensely debated (e.g. Rouchy & Caruso, 2006; CIESM, 2008). Recent data acquired offshore Tunisia (Sicily Strait) support the hypothesis that the Caltanissetta Basin was rather a marginal basin even if it deepens significantly from North to South (El Euch – El Koundi *et al.*, 2009).

A very rapid process for the Mediterranean reflooding after the MSC was until now considered satisfactory as finer resolution data based on biostratigraphy or seismic data were not available. This paper reviews recent offshore seismic evidence from the Gulf of Lions and its relationship with boreholes (Bache *et al.*, 2009) showing two types of erosional surfaces in regressive and transgressive conditions, respectively. We re-visited and completed recently published onshore data documenting the post-MSC marine transgression in different palaeoenvironmental contexts, particularly from Italy (Sicily: Londeix *et al.*, 2007; Popescu *et al.*, 2009; Marche: Popescu *et al.*, 2007) and Turkey (Melinte-Dobrinescu *et al.*, 2009) (Fig. 3). Several published and new age determinations will be repeatedly used in this article. To help the reader, they have been summarized in Table 1, pointing out which event they date and how and where they have been obtained within the relative literature. Nannofossils have been intensively used for defining the chronostratigraphic position of the exposed sections considered here (see Popescu *et al.*, 2007; Melinte-Dobrinescu *et al.*, 2009) following the chart shown in Fig. 4 (Berggren *et al.*, 1995; Raffi *et al.*, 2006), in which the two steps in deposition of the Messinian evaporites proposed by Clauzon *et al.* (1996) are indicated, a distinction which is now widely accepted (CIESM, 2008; Ryan, 2011). After displaying data from the Gulf of Lions that illustrate a post-MSC reflooding of the Mediterranean in two steps, we discuss the extension of this model to the eastern basin and its potential chronology. We then consider the geodynamic causes and attempt to quantify the associated sea-level changes, leading to a revision of the late Messinian–early Zanlcean eustatic events in the Mediterranean region (see the map of Fig. 3 for most of the localities cited in the article).

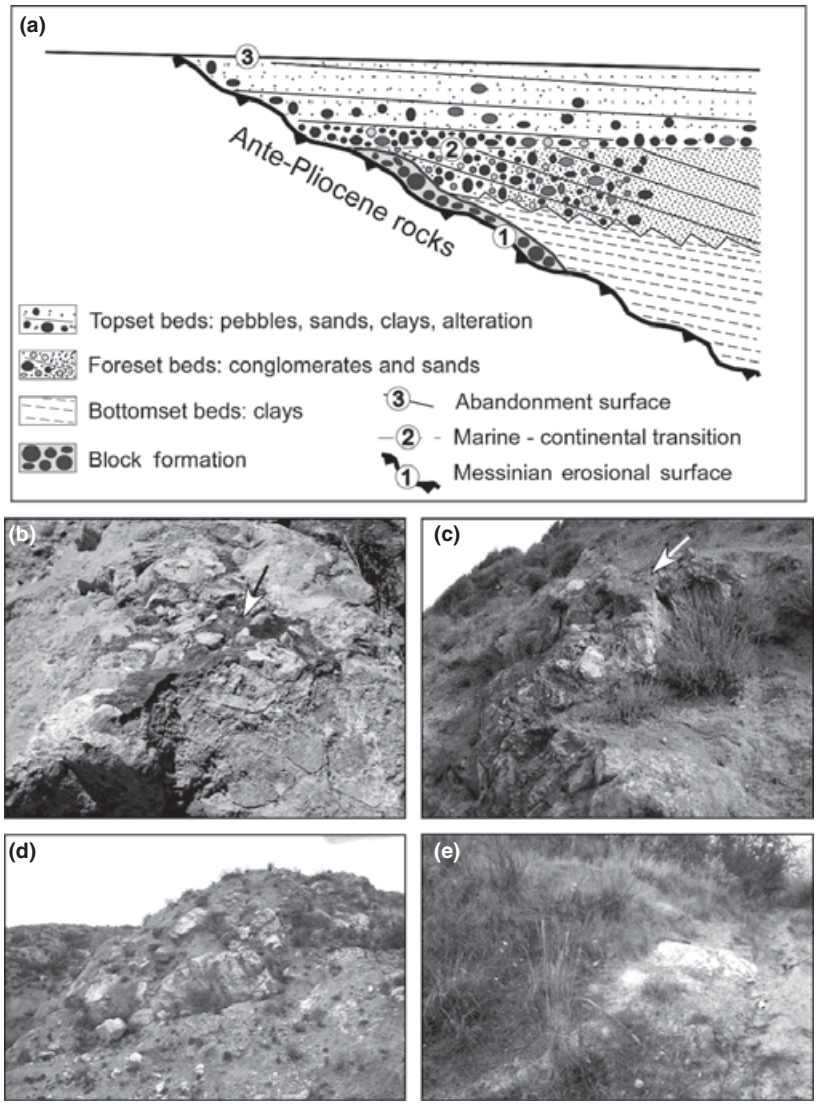

Fig. 2. Gilbert-type fan deltas (Gilbert, 1885, 1890) need a significant accommodation space. This was provided by erosion and very fast flooding in the case of the Mediterranean in early Zanclean time. (a) Characteristic organization of Zanclean Gilbert-type fan deltas (Clauzon, 1990). They are composed of a prograding subaqueous part (clayey bottomset beds and conglomeratic to sandy foreset beds, the sedimentary dip of which may reach 30–35°) and an aggrading subaerial part (conglomeratic to sandy almost horizontal topset beds often affected by significant alteration). Two key chronological surfaces bound them: the Messinian Erosional Surface at the base (1), and the abandonment surface at the top (3). The diachronous subaqueous-continental (i.e. marine-continental in this case study) transition is sandwiched between the foreset beds and the topset beds (2), corresponding to a condensed layer (often a lignite). (b) Carros Breccia (Nice, SE France) overlain by an iron crust (indicated by the arrow). (c) Breccias of Salzidere (Bandirma, Turkey, southern coastline of the Marmara Sea) overlain by an iron-rich crust (indicated by the arrow). (d) Coarse fluvial deposit with reworked blocks of Messinian gypsum within the Messinian fluvial canyon at Garrucha (Vera Basin, southeastern Spain). (e) Coarse fluvial deposit with reworked blocks of Messinian gypsum within the Messinian fluvial canyon at San Ippolito (Volterra area, Central Italy).

OFFSHORE DATA

The Western Mediterranean potentially records any connection with the Atlantic Ocean due to its location near the Strait of Gibraltar. Within the Western Mediterranean, the Gulf of Lions is exceptional in that its Neogene sedimentary strata have not been significantly deformed except for salt-related tectonics in the deep basin (Gaullier, 1993; Dos Reis *et al.*, 2008) and no significant post-sedimentation uplift has occurred in the deep basin. This area can thus be considered as a good reference for sea-level variations in the whole Mediterranean Basin. In addition, the Gulf of Lions has been characterized by a relatively high total subsidence rate, which has continuously created accomodation space (Steckler & Watts, 1980; Bessis, 1986; Burrus, 1989; Rabineau *et al.*, 2005; Bache *et al.*, 2010). This configuration, together with the availability of numerous offshore data (seismic profiles, boreholes), has permitted accurate descriptions of the transition between the Messinian halite identified in the central Mediterranean basins and the Zanclean prograding sediments (Gorini, 1993; Lofi, 2002; Lofi *et al.*, 2005; Bache, 2008; Lofi & Berné, 2008; Bache *et al.*, 2009). Here, we will review these observations.

Fig. 3. Location map of the studied areas with most of the main localities cited in the text and in Table 1. The map was created using GeoMapApp System developed by Haxby *et al.* (2010). 1, Gulf of Lions (seismic profiles and boreholes), details are given in Fig. 5; 2, Eraclea Minoa in the Caltanissetta Basin (onshore sections); 3, Maccarone (onshore section near Apiro); 4, Dardanelles Strait area (onshore sections).

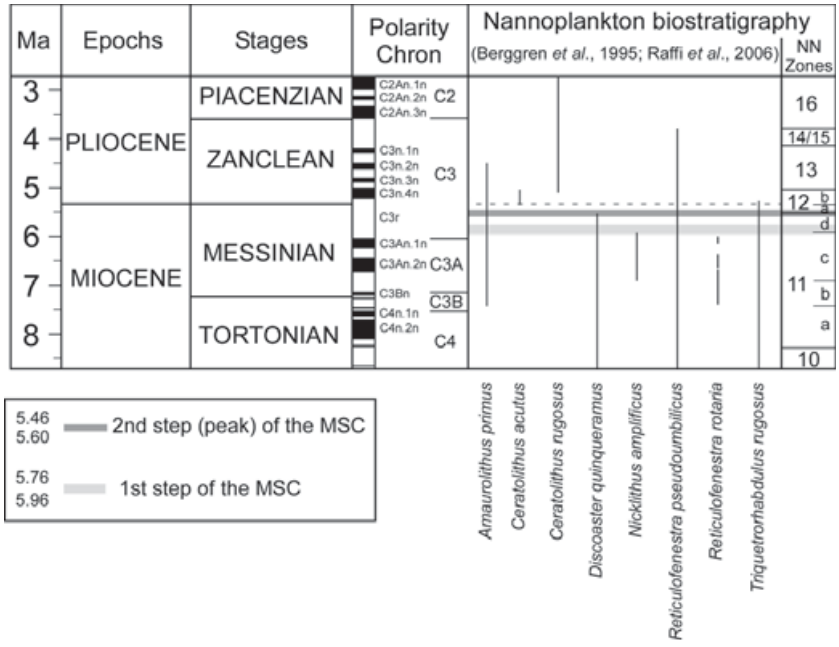

Fig. 4. Chronostratigraphy and nannoplankton biostratigraphy of the Late Miocene and Early–Middle Pliocene. Ages of stages, polarity chrons refer to Lourens *et al.* (2004), NN zonation to Berggren *et al.* (1995) and Raffi *et al.* (2006), age of nannoplankton events to Raffi *et al.* (2006). The grey strips correspond to the generally accepted (CIESM, 2008) two steps of the MSC (Clauzon *et al.*, 1996). See also Melinte-Dobrinescu *et al.* (2009) for more details concerning this nannoplankton chart.

Seismic profiles

Three key surfaces intercalated between the precrisis Miocene and the Pliocene deposits can be identified in the Gulf of Lions (Fig. 5).

The first key-surface ('f' on Fig. 5) is the 'MES' also named 'Margin Erosional Surface' by Lofi & Berné (2008). This surface corresponds to the discordant contact between the Miocene deposits ('a' on Fig. 5) and the overlying prograding Pliocene and Pleistocene sequence ('g' on Fig. 5). This pervasive erosional surface has long been identified in the Rhône Valley (Denizot, 1952; Clauzon, 1973, 1982) and on the Gulf of Lions shelf (Ryan & Cita, 1978; Gennesseaux & Lefèbvre, 1980; Lefèbvre, 1980; Gorini, 1993; Guennoc *et al.*, 2000; Dos Reis, 2001; Lofi, 2002; Dos Reis *et al.*, 2005, 2008; Lofi *et al.*, 2005). Mapping of this surface shown in Fig. 6 revealed a pattern of up to fifth order dendritic drainage and represents a subaerial landscape (Gennesseaux & Lefèbvre, 1980; Gorini *et al.*, 1993; Guennoc *et al.*, 2000; Lofi *et al.*, 2005). Beneath the shelf, the sudden reflooding at the end of the MSC is supported by the Zanclean prograding sediments downlapping directly on the MES (Lofi *et al.*, 2003). The MES therefore represents the preserved subaerial landscape just before reflooding, which is generally dated at 5.332 Ma (Table 1; see also the 'Introduction'). The landscape corresponding to the onset of the drawdown has not been preserved on the shelf because of uninterrupted subaerial exposure during the Messinian drawdown.

The second key-surface is the 'Basal Erosional Surface' (BES) ('b' on Fig. 5), which corresponds to the discordant contact between precrisis Miocene deposits and the syn-crisis detrital deposits (Maillard *et al.*, 2006). At the present time, a controversy exists concerning its

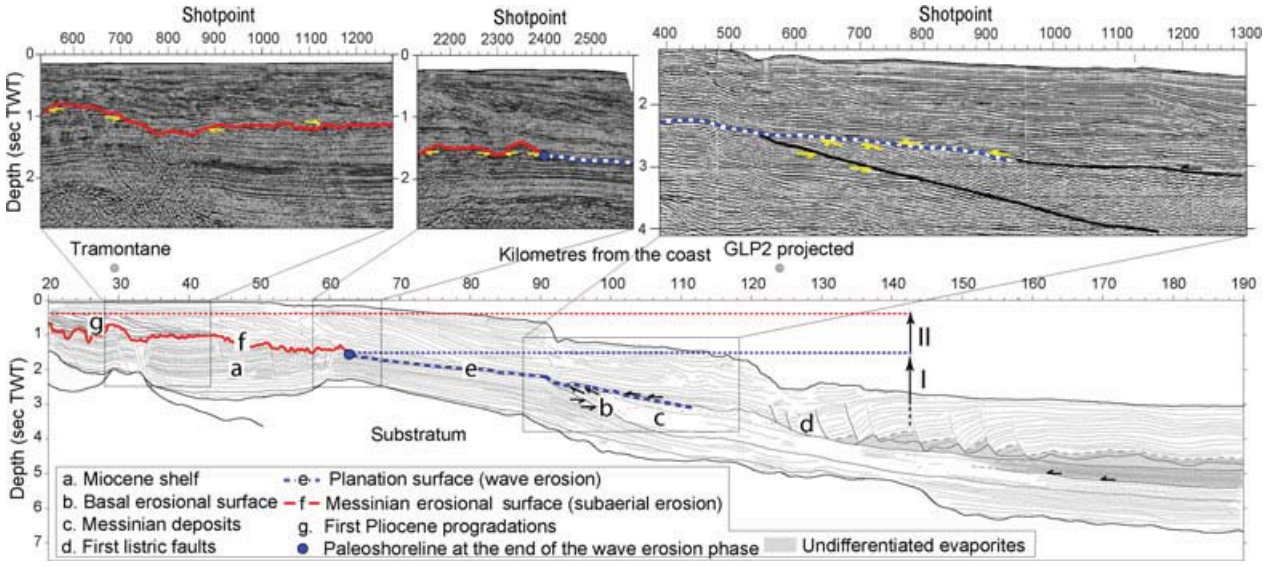

Fig. 5. Line drawing and details of seismic lines perpendicular and parallel to the margin of the Gulf of Lions showing the major key surfaces related to the Messinian Salinity Crisis. Location of seismic profiles on Fig. 6. See uninterpreted seismic profile on Fig. S1.

significance. On the basis of detailed mapping of this surface, Bache (2008) and Bache *et al.* (2009) considered the 'BES' as the marker of the Messinian drawdown in the basin ('b' on Fig. 5). In contrast, Lofi & Berné (2008) interpreted this surface as a pre-MSC discordance related to sub-marine slope canyon erosional systems and placed the 'BES' higher in the Miocene series. A full discussion concerning the consequences of these interpretations is beyond the scope of this article, but can be found in Bache *et al.* (2009).

Finally, the third surface (planation surface 'e' on Fig. 5) is a straight and smooth surface that is locally conformable with the underlying precrisis series (between 64 and 90 km from the coast on Fig. 5), but that is also locally erosional (90–100 km; Fig. 5) as it truncates the underlying syn-crisis series (Bache, 2008; Bache *et al.*, 2009). Above this surface, sedimentary units are characterized by onlap termination of seismic reflectors in the deepest part and downlap termination in the shallower part (Figs 5 and 7). The limit between the MES and the planation surface 'e' is clear and occurs at a constant two-way travel time of 1.6 s over most of the shelf (Figs 5–7). Towards the basin, the limit of salt deposition represents the maximum extent of erosion. The planation surface 'e' thus extends over 50 km, from the shelf to the basin (Fig. 6).

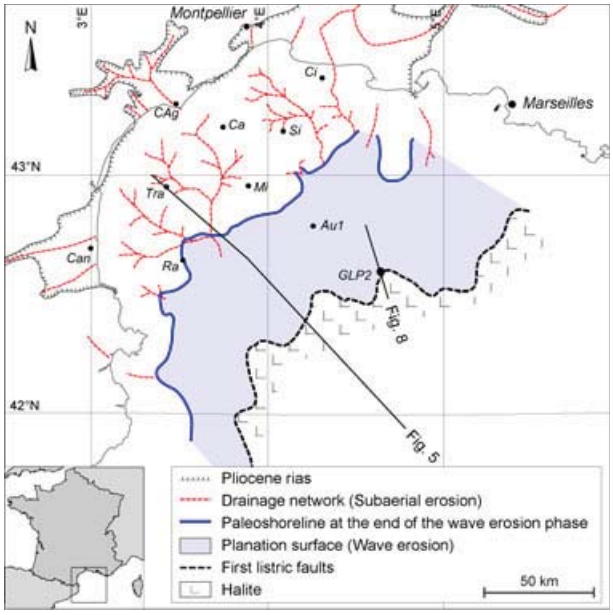

Fig. 6. Subsurface mapping of the basal Pliocene of the Gulf of Lions showing the limits between the various topographic zones (from the basin to the margin: halite, planation surface 'e', Messinian Erosional Surface) and location of line drawings shown in Figs 5 and 8. Boreholes: *Ca*, Calmar; *Ci*, Cicindelle; *Si*, Sirocco1; *Mi*, Mistral1; *Tra*, Tramontane1; *Ra*, Rascasse1; *Au1*, Autan1; *CAg*, Cap d'Agde1; *Can*, Canet1.

Boreholes

Boreholes located on the shelf (Fig. 6) show that the MES truncates Miocene sediments and underlies the earliest Pliocene sediments (Cravatte *et al.*, 1974; Gorini *et al.*, 1993; Guennoc *et al.*, 2000; Lofi *et al.*, 2003). The youngest Miocene sediments were found in the Tramontane1 well and were dated as Tortonian (Cravatte *et al.*, 1974), i.e. between 11.61 and 7.25 Ma (Lourens *et al.*, 2004). The record of the Upper Miocene sediments is missing, having been removed by subaerial erosion during the MSC. The amplitude of erosion during the MSC reaches at least 1 km in the central part of the Languedoc shelf (Lofi *et al.*, 2005; Bache, 2008; Bache *et al.*, 2009).

Boreholes Autan1 and GLP2 drilled on the slope (Fig. 6) cross-surface 'e' respectively in its landward and seaward areas (Fig. 5). In the Autan1 borehole, a very

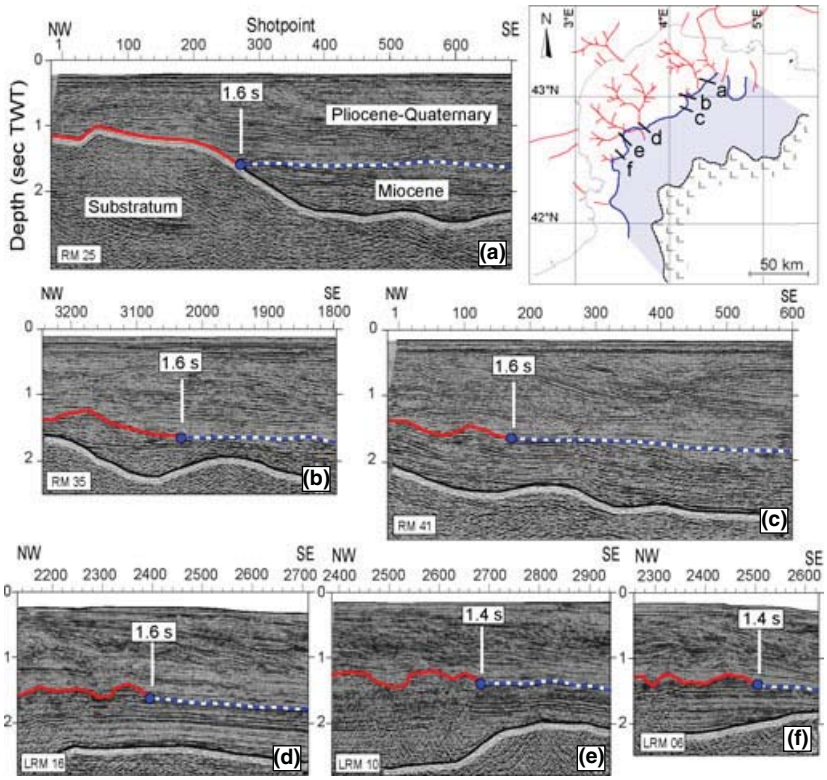

Fig. 7. Detail of the transition from the Messinian Erosional Surface (subaerial erosion 'f') to the planation surface 'e'. The boundary between these two surfaces is located at a constant two-way travel time of 1.6 s over the entire margin (a–d). Near the Pyrenees, the boundary is located at a two-way travel time of around 1.4 s (e, f). This boundary represents the shoreline just before 5.46 Ma. Modified from Bache *et al.* (2009). See uninterpreted seismic profiles on Fig. S2.

sharp contact occurring at 2424 m depth is described between a littoral to mid-shelf Upper Miocene environment and an outer shelf – upper slope earliest Pliocene environment (Cravatte *et al.*, 1974). In the GLP2 borehole (Guennoc *et al.*, 2000), salt and anhydrite deposits alternating with calcareous clays related to the MSC have been described in the well (between 3703 and 3437 m) and underlie the planation surface 'e' (Fig. 8). Fifty metres of azoic sandy clays intercalated with micaceous sandstone have been drilled between the salt deposits and the lowermost Pliocene clays.

ONSHORE DATA

Three main areas will be considered here (Sicily, Marche and Dardanelles; Fig. 3), which show common characteristics of the terminal MSC in various palaeoenvironments. We will then discuss the presence of coarse block deposits between the MES and Gilbert-type fan delta sediments (i.e. the Block Formation of Fig. 2) which have now been observed throughout the Mediterranean region.

Eraclea Minoa (Sicily)

The cyclic pattern of the Sicilian Upper Evaporites (six gypsum – clay cyclothems) has been described by many authors (Fig. 9a; Decima & Wezel, 1971; Nesteroff & Glaçon, 1977; Homewood *et al.*, 1992; Bonaduce & Sgarrella, 1999; Rouchy & Caruso, 2006; Krijgsman & Meijer, 2008; Manzi *et al.*, 2009), especially in the Eraclea Minoa key-section (Figs 3 and 9c). The calibration of the Upper Evaporites with the Astronomical Tuned Neogene Time Scale (ATNTS2004: Lourens *et al.*, 2004) from 5.52 to 5.332 Ma has been proposed considering a continuous sedimentation in the Sicilian Basin during the peak of the MSC (Krijgsman & Meijer, 2008; Roveri *et al.*, 2008a,b). Each sequence ranges from brackish (gypsum and lowermost clay) to marine (clay overlain by diatomite and turbidites, i.e. the highest relative sea level) (Homewood *et al.*, 1992). This interpretation is supported by geochemistry (Pierre & Fontes, 1979), foraminifers (Nesteroff & Glaçon, 1977), dinoflagellate cysts (Londeix *et al.*, 2007) and pollen grains (Suc & Bessais, 1990; Fauquette *et al.*, 2006).

Here, we focus on the uppermost cycle, constituted by the last gypsum bed overlain by clays (Lago Mare Unit) and silts (Arenazzolo Unit), immediately below the Trubi carbonates (Fig. 9). Following Cita & Colombo (1979), we emphasize the distinction between the Lago Mare and Arenazzolo deposits, often improperly grouped within the Arenazzolo Unit (Decima & Wezel, 1971; Bonaduce & Sgarrella, 1999) or a 'Lago Mare – Arenazzolo' Unit (Rouchy & Caruso, 2006). From bottom to top, the Lago Mare, Arenazzolo and Trubi formations represent quite different environmental conditions: (i) brackish shallow-water conditions as shown by the faunal content (ostracods; dreissenids, i.e. freshwater bivalves coming from the Dacic and Euxinian basins: Fig. 1), (ii) a higher energy littoral environment and (iii) open marine conditions, as shown by foraminiferal fauna (Cita & Colombo, 1979) and dinoflagellate cyst flora (Londeix *et al.*, 1999, 2007). An intense debate arose from the discrepancies and large

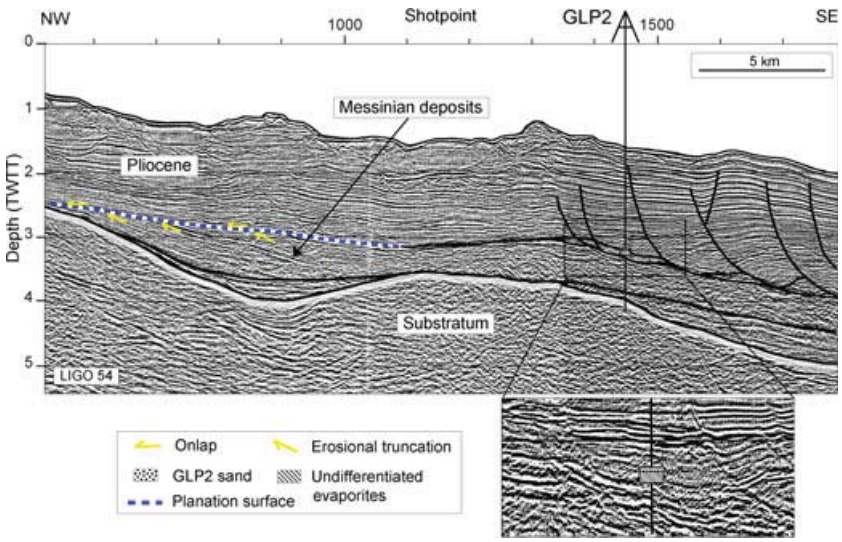

Fig. 8. Ligo 54 profile crossing the GLP2 borehole. The erosional nature of the planation surface 'e' and the transgressive nature of sediments deposited above it are outlined by arrows. The 50 m of azoic sand described in the GLP2 borehole could correspond to the transgressive sands eroded from upstream by the wave erosion (planation surface 'e'). Location of seismic profiles on Fig. 6. See uninterpreted seismic profile on Fig. S3.

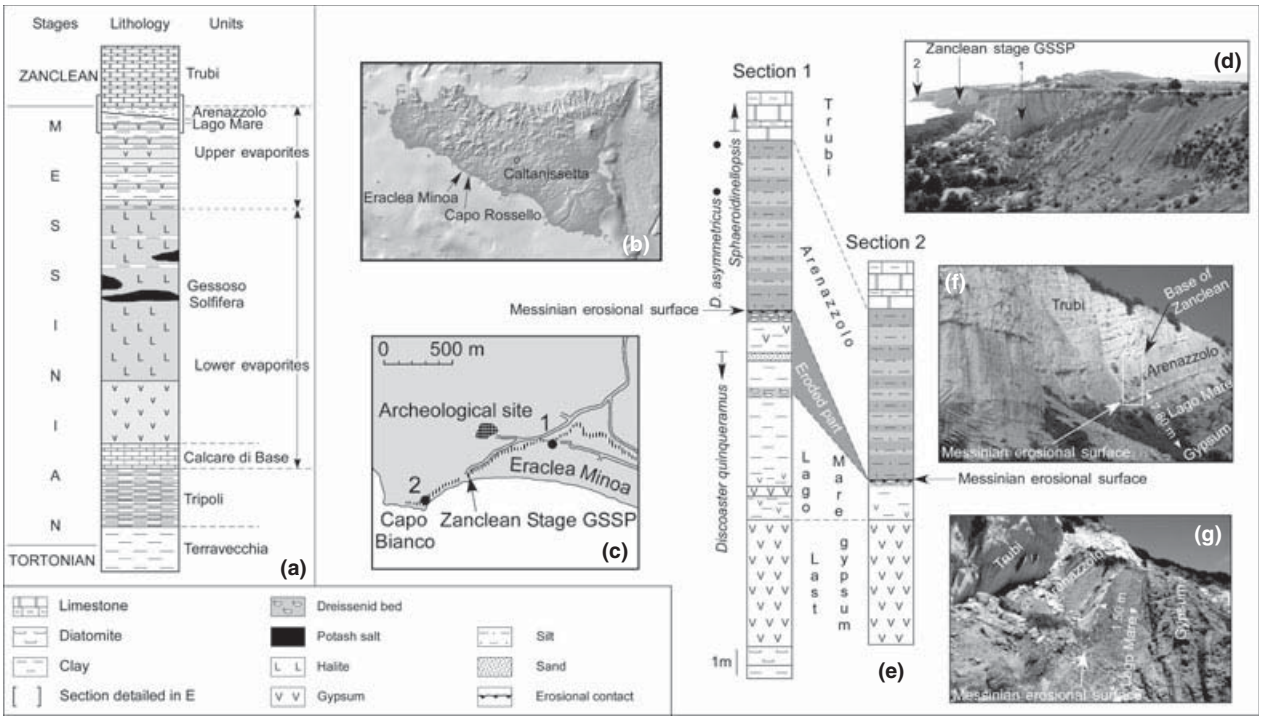

Fig. 9. Eraclea Minoa (southern Sicily). (a) Simplified classical stratigraphic succession of the Tortonian to Zanclean Sicilian series (Decima & Wezel, 1971). (b) Location of Eraclea Minoa and Capo Rossello in Sicily. (c) Location map of the two studied sections at Eraclea Minoa. (d) View of the eastern part of the Eraclea Minoa succession with location of Sections 1 and 2, and of the Zanclean Stage GSSP. (e) Eraclea Minoa Sections 1 and 2 compared: the grey surface shows the missing part (eroded) of Lago Mare in Section 2. Nannoplankton data according to A. Di Stefano (pers. comm.) and our own results. (f) View of Section 1. The white box corresponds to the girdled stratigraphic interval in (a). (g) View of Section 2.

uncertainties about the palaeo-water depth estimates for the Trubi deposition. Using quantitative studies on benthic foraminifers, Brolsma (1978) proposed 100–1000 m, whereas Cita & Colombo (1979) proposed 1400–2400 m, using benthic foraminifers and the sharp sedimentary contrast between the uppermost Messinian and lowermost Zanclean deposits, in both exposed sections and DSDP (Deep Sea Drilling Project) wells. Disagreement also concerns the location of the most significant environmental change. Cita & Gartner (1973) and Cita *et al.* (1999b) proposed the location of the environmental break at the base of the Trubi, emphasizing the presence of a sharp and even unconformable contact. Brolsma (1975) interpreted the Arenazzolo Unit as a transitional interval leading to the Trubi conditions and proposed locating the environmental break between the Lago Mare and Are-

nazzolo units. The Zanclean GSSP was eventually established at the base of the Trubi (van Couvering *et al.*, 2000).

At Eraclea Minoa, two sections located on both sides of the Zanclean GSSP were studied (Londeix *et al.*, 2007; Popescu *et al.*, 2009) (Fig. 9c and d).

Section 1 (Fig. 9e and f) starts with clays and diatomitic turbidites underlying the highest gypsum bed of the Sicilian Upper Evaporites. This bed is overlain by the Lago Mare Unit (7.80 m thick), constituted by clay deposits, which includes in its upper part three characteristic layers (two dreissenid coquina layers, 25 and 40 cm thick respectively, and a 32 cm thick white sand layer between the two previous layers). The Lago Mare Unit is followed by the silty Arenazzolo Unit (5.60 m thick) comprising 6.5 dark–light alternations (Figs 9e and 10a). The upper part of this section corresponds to the Trubi Unit and is constituted by cyclic carbonates and marls. The position of the Zanclean GSSP, placed at the base of the Trubi Unit, is indicated on Fig. 9f.

We performed new analyses of nannofossils from the Eraclea Minoa Section 1 to better characterize the major environmental changes affecting the Lago Mare, Arenazzolo and Trubi units. The calcareous nannoplankton identified in the Lago Mare Unit of Section 1 includes, among other taxa, *Nicklithus amplificus*, *Amaurolithus primus*, *Coccolithus pelagicus*, *Discoaster quinqueramus*, *Helicosphaera carteri s.l.*, *Helicosphaera intermedia*, *Pontosphaera multipora*, small-sized reticulofenestrids, *Reticulofenestra pseudoumbilicus*, *Sphenolithus* group *abies/moriformis*, *Triquetrorhabulus striatus* and *Triquetrorhabulus rugosus* (Fig. 9e). Considering that the Sicilian Upper Evaporites that end the Sicilian Messinian evaporitic series are significantly younger than 5.96 Ma (the robust age of the beginning of the MSC; Table 1), *N. amplificus* (highest occurrence at 5.939 Ma: Raffi *et al.*, 2006; Fig. 4) could be reworked. This nannoflora, which includes *D. quinqueramus* (highest occurrence at 5.54 Ma: Raffi *et al.*, 2006; Fig. 4), precedes Zone NN12 and hence might be related to the Subzone NN11d (Fig. 4). Londeix *et al.* (2007) studied dinoflagellate cysts from the successive uppermost part of the Eraclea Minoa section (Lago Mare and Arenazzolo units) and lowermost part of the classic Capo Rossello section (Fig. 9b) (lowermost Trubi). The dinoflagellate cyst assemblage of the Lago Mare Unit is dominated (>60%) by *Lingulodinium machaerophorum* and *Homotryblium* spp. (Fig. 10e) that indicate coastal to lagoonal environments (Londeix *et al.*, 2007). The presence of Cretaceous reworked dinoflagellate cysts on top of the Lago Mare Unit results from an increased terrestrial input, and was considered to announce the major erosional episode of the Mediterranean desiccation phase (Londeix *et al.*, 2007). The Arenazzolo Unit is characterized by an increase in more marine dinoflagellate cysts assemblages (occurrences of *Impagidinium* spp.) showing fluctuations between dominant outer shelf conditions and inner shelf to coastal conditions (everywhere <50% coastal, apart from two incursions; Londeix *et al.*, 2007), documenting a significant rise of sea level at the base followed by secondary fluctuations of sea level. The Trubi dinoflagellate cyst assemblage with *Impagidinium patulum* mostly documents open marine conditions (Fig. 10e). To summarize, the dinoflagellate cyst study from Eraclea Minoa (Section 1; Fig. 9e) and the nearby equivalent Capo Rossello section *p.p.* by Londeix *et al.* (2007) suggests that Lago Mare deposits represent a coastal to brackish-lagoonal environment, Arenazzolo deposits correspond to inner and outer shelf marine conditions, and Trubi deposits to open marine conditions. The difference in bathymetry between Arenazzolo and Trubi might have been only 100–150 m. We obtain similar results using pollen analysis (Fig. 10d) and especially the '*Pinus*/Halophytes' ratio (P/H). In the P/H ratio, the increasing relative frequency of *Pinus* (an easily water-transported pollen grain) correlates with the increasing offshore distance, in opposition to that of halophytes

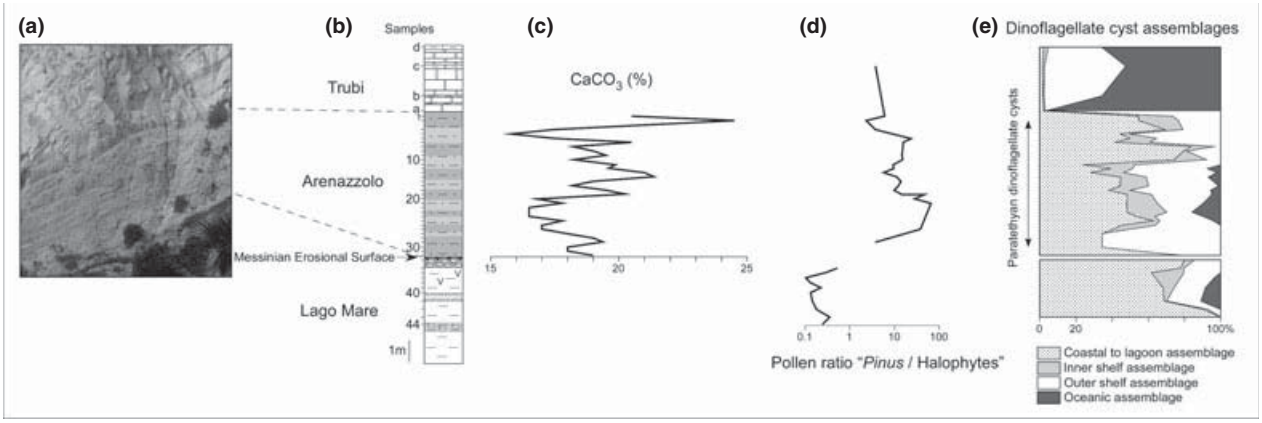

Fig. 10. Environmental significance of Lago Mare, Arenazzolo and Trubi deposits in Sicily; age of Arenazzolo. (a) View of the dark–light bands at Eraclea Minoa (Section 1) as reported on Fig. 9b. (b) Upper part of Section 1 of Eraclea Minoa. Studied samples: 1–44 from Eraclea Minoa (Section 1), a–d from Capo Rossello. Same legend as in Fig. 8. (c) Total $CaCO_3$ content from the Arenazzolo Unit at Section 1 of Eraclea Minoa. (d) Pollen ratio '*Pinus*/Halophytes' (logarithmic abscissa scale). (e) Dinoflagellate cyst assemblages with respect to their environmental (coastal to oceanic) significance. Distribution of Paratethyan dinoflagellate cysts is indicated.

(plants restricted to coastal environments) (Suc *et al.*, 1995). We interpret the abrupt and intense changes in the pollen ratio P/H (Fig. 10d) as indicating that the rise in sea level preceding Arenazzolo corresponds to a significant increase in the distality at the locality. On the other hand, the continuing process of sea-level rise at the base of Trubi apparently did not coincide with an increased distality. Accordingly, palynological data (dinoflagellate cysts and pollen grains) support the interpretation that the most significant break in marine influence occurred between the Lago Mare and Arenazzolo units. We must indicate that Eastern Paratethyan dinoflagellate cysts (*Galeacysta etrusca* mostly) are regularly recorded from 60 cm above the base of Arenazzolo practically up to its top (Fig. 10e; Londeix *et al.*, 2007; Popescu *et al.*, 2009).

Section 2 (Fig. 9e and g) is markedly different from Section 1: the Lago Mare Unit is significantly thinner (1.50 m thick only) and truncated at its top, ending with a single residual 2 cm thick coquina layer rich in dreissenids; the Arenazzolo Unit (same thickness as at Section 1) clearly onlaps the Lago Mare clays (Fig. 9g) and, according to our new nannofossil analyses, contains typical 'Pliocene' specimens, *Helicosphaera selli* and *Discoaster asymmetricus*, while *Ceratolithus acutus* was not recorded (Fig. 9e). We therefore conclude that the upper part of the Lago Mare of Section 1 has been eroded in Section 2, and that the erosional contact between Arenazzolo and Lago Mare should correspond to the MES (Fig. 9e) and, hence, the peak of the MSC with the major sea-level drawdown.

Here, we consider that desiccation of the Mediterranean is not expressed by intensely marked erosion, probably because the locality occupied an interfluvial position in a semi-arid area with limited erosion and condensed sedimentation (Suc & Bessais, 1990; Fauquette *et al.*, 2006) as known in other peri-Mediterranean localities (Vera Basin, Cuevas de Almanzora section: Clauzon, 1980b; Dardanelles Strait area, Intepe section: Melinte-Dobrinescu *et al.*, 2009). However, significant and coeval erosion is suggested by several offshore wells in the area such as Zagara 1 and Venere 1 (Fig. 3) and by seismic profiles where Lower Pliocene deposits immediately overlie the Upper Miocene, so-called Terravecchia (VI.D.E.P.I. Database: fttp://www.videpi.com/mappa.php). This interpretation is also supported by the offshore data from Tunisia, which indicate that the dramatic sea-level drop that caused evaporite deposition in the Mediterranean central basins and the cutting of fluvial canyons on their margins occurred after the deposition of a thick marginal evaporitic succession similar to the Sicilian series (Fig. 9a; El Euch – El Koundi *et al.*, 2009).

The 6.5 dark–light alternations observed at Section 1 within the Arenazzolo Unit (Figs 9e and 10a and b; see also: Decima & Wezel, 1971; : fig. 9), already indicated by Brolsma (1975) at Capo Rossello, resemble the precession-related carbonate cycles of the overlying Trubi (Hilgen & Langereis, 1989). To clarify the cause of the dark–light alternations of the Arenazzolo Unit, we estimated its $CaCO_3$ content by measurement of the escaped CO_2 as reaction to HCl using a Bernard calcimeter. The values are shown in Fig. 10c: on the whole, dark bands correspond to higher carbonate contents, with a more reliable relationship in the upper Arenazzolo. Although variations in Arenazzolo $CaCO_3$ only fluctuate between 15% and 25%, at a lower level than in the Trubi (60–80%: Hilgen & Langereis, 1989), in the same way, we speculate that the dark–light alternations can be similarly used as a chronometer to estimate by precession-tuning the age of the base of Arenazzolo on the basis of the continuity in sedimentation between Arenazzolo and Trubi (Londeix *et al.*, 2007).

Maccarone (Apiro, Marche)

The Maccarone section (Figs 3 and 11a) belongs to the reference area for the Apennine foredeep, where reworked marginal gypsum is observable beneath a thick clayey-turbiditic series (the Di Tetto Formation) devoid of foraminifers in its lower part (Carloni *et al.*, 1974; Popescu *et al.*, 2007), i.e. the p-ev$_1$b sequence of Roveri *et al.* (2001) (Fig. 11a). This formation is overlain by the Colombacci clay-limestone alternations and topped by the Lower Zanclean open-marine Argille Azzurre (>700 m in thickness within the foredeep, 210 m at Maccarone located on the edge of the foredeep) (Roveri & Manzi, 2006). The Maccarone section benefits from three precise ages near its base and top (Fig. 11a): (i) an ash layer first dated at 5.51 ± 0.05 Ma using $^{39}Ar/^{40}Ar$ (Odin *et al.*, 1997), but recently, re-dated at 5.555 ± 0.06 Ma (Table 1; Cosentino *et al.*, 2009) as considered in Fig. 11, and (ii) the evidence of the C3n.4n (i.e. Thvera) normal palaeomagnetic Chron (Gennari *et al.*, 2008), the base and top of which are respectively dated at 5.235 and 4.997 Ma (Lourens *et al.*, 2004). As a consequence, the base of the Argille Azzurre Formation, just preceding the *Sphaeroidinellopsis* Acme (Zone MPl1), is reasonably dated at 5.332 Ma by Gennari *et al.* (2008). This chronological calibration of the section has been recently strenghtened by Popescu *et al.* (2007) who recorded the first evidence of *C. acutus* at 133 m in the section (Fig. 11a), the marker of the nannoplankton Subzone NN12b (Fig. 4) whose Lowest Occurrence is dated at 5.345 Ma (Table 1; Raffi *et al.*, 2006). Popescu *et al.* (2007) demonstrated that the increased distance from palaeoshoreline indicated by a sudden doubling of disaccate pollen grains at *ca.* 110 m in the section (Fig. 11a; Bertini, 1992, 2006) was caused by the entrance of marine waters into the Apennine foredeep, almost coeval with the earliest influx of Paratethyan surface waters. The above-mentioned age model of the section (Fig. 11a) allows us to propose a new cyclostratigraphy, based on the pollen record studied by Bertini (1992, 2006), which differs from that of Roveri & Manzi (2006) and Gennari *et al.* (2008). We use the pollen ratio (SE/AE) 'Subtropical Elements/

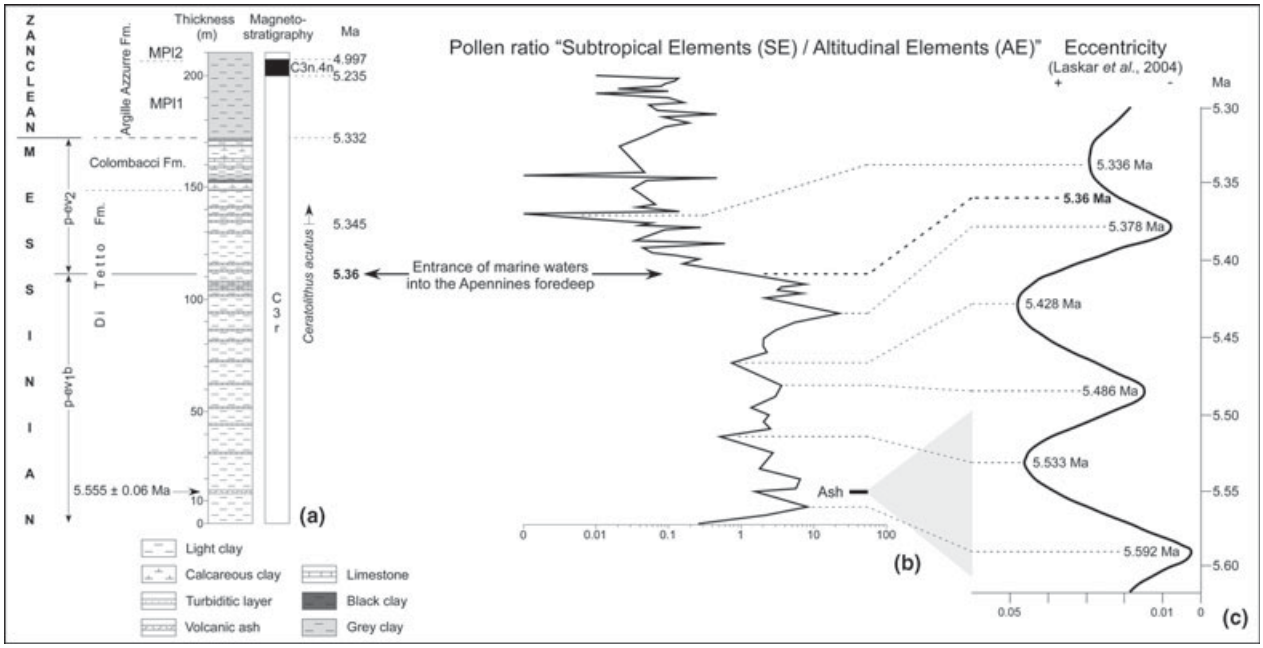

Fig. 11. Maccarone (Apiro, Marche). (a) Litho-, bio- and chronostratigraphy. Ages of palaeomagnetic Chron C3n.4n and of the base of Zanclean are from Lourens *et al.* (2004), age of the Lowest Occurrence of *Ceratolithus acutus* is from Raffi *et al.* (2006). Age (5.36 Ma) in bold characters is the estimated age of the entrance of marine waters into the Apennine foredeep. Lithology from Popescu *et al.* (2007). Magnetostratigraphy: Messinian sediments (G. Napoleone, pers. comm.), Zanclean sediments (Gennari *et al.*, 2008). (b) Pollen ratio 'Subtropical Elements (SE)/Altitudinal Elements (AE)' (logarithmic abscissa scale) from Bertini (1992, 2006), plotted on the log of the Maccarone section. (c) Eccentricity curve between 5.62 and 5.30 Ma (Laskar *et al.*, 2004), plotted on the orbital time-scale. Uncertainty on the age of the ash is indicated by the grey range.

Altitudinal Elements', i.e. mostly Taxodiaxeae plus other subtropical plants (*Engelhardia*, *Nyssa*, Arecaceae, Cyrillaceae-Clethraceae, etc.) vs. the *Cedrus–Tsuga–Abies–Picea* altitudinal forest complex (Fig. 11b). The curve expresses the amount of pollen grains of low-altitude thermophilous forests (i.e. SE) relative to those of coniferous forests growing in significantly cooler conditions at higher altitude (i.e. AE). Maxima of SE in the pollen records represent spreading of thermophilous forests during warmer phases, while maxima of AE correspond to descents of the altitudinal forest belts as a response to cooler phases, making this index very useful for climate reconstructions at the foot of high mountains (Popescu, 2001). It is established that, in contrast to Late Pleistocene, Pliocene and Early Pleistocene cooling phases occurred during times of high eccentricity and the warmer phases correspond to low eccentricity (Li *et al.*, 1998). This relationship was applied to a well-dated long section by Popescu (2001) and Popescu *et al.* (2006a), who correlated the highest values of the SE/AE ratio with minima of eccentricity and its lowest values with maxima of eccentricity. Considering the time-window 5.60–5.30 Ma that corresponds to deposition of the Maccarone section, it is worth noting that three eccentricity minima (warmer phases) appear at 5.592, 5.486 and 5.378 Ma respectively (Fig. 11c; Laskar *et al.*, 2004). In-between, the highest value of the SE/AE ratio is directly correlated with the lowermost minimum of eccentricity at 5.378 Ma, consistent with the first occurrence of *C. acutus* at 5.345 Ma (Fig. 11a). Then, the underlying maxima of SE/AE are correlated with the successive minima of eccentricity (at 5.486 and 5.592 Ma) and the inserted minima of SE/AE are correlated with the maxima of eccentricity (at 5.428 and 5.533 Ma) (Fig. 11b and c).

The Dardanelles Strait area

In this area, two kinds of sedimentary records have been observed (Fig. 12; Melinte-Dobrinescu *et al.*, 2009). At Intepe (Fig. 12a), an apparently continuous section (Fig. 12b), with bay to lagoon environments and a constant nannoflora allows, by using the first appearance of *C. acutus* (at 5.345 Ma; Table 1) (Fig. 12b and c), the precise location of the MSC below this point. A thin bed of lignite was observed below a thin rubefied (i.e. fired) clayey bed transformed into porcellanite. This contact (Fig. 12b and c) has been interpreted as evidence of local emersion and correlated with the peak of the MSC (Melinte-Dobrinescu *et al.*, 2009). These authors correlated the lignite with the marginal evaporites (the first step of the MSC; Clauzon *et al.*, 1996). However, a few hundred metres northwards, Melinte-Dobrinescu *et al.* (2009) pointed out thick sandy foreset beds (dipping at 25° to the West) of a Gilbert-type fan delta, with clayey bottomset beds exposed along the northern shoreline of the Dardanelles Strait at Seddülbahir where the first appearance of *C. acutus* (i.e. at 5.345 Ma; Table 1) has been recorded (Fig. 12b and

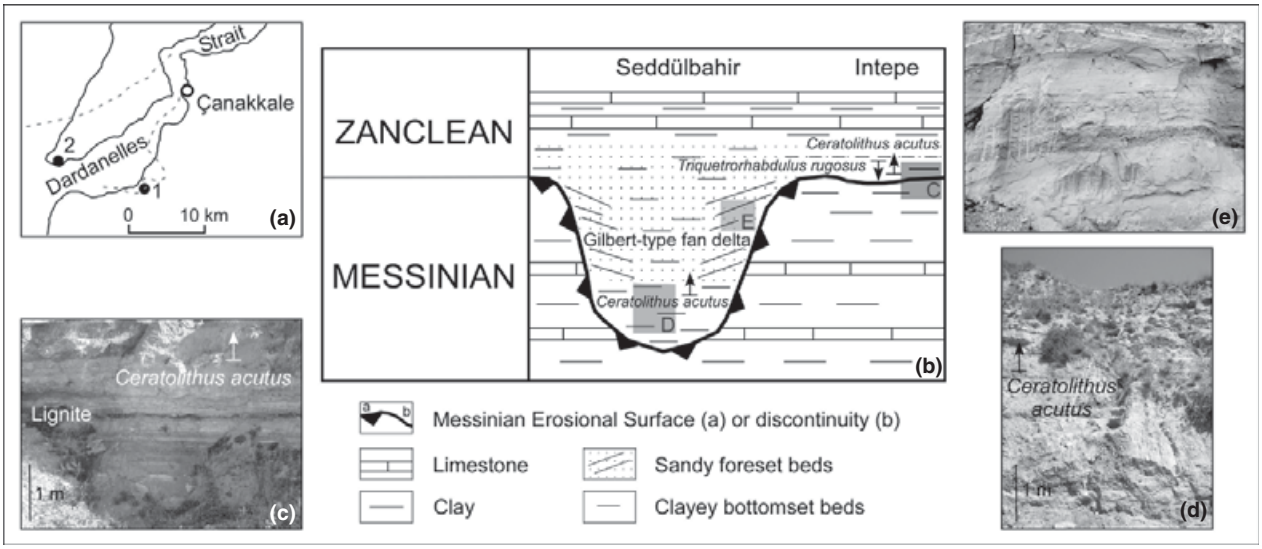

Fig. 12. Two types of Messinian – Zanclean deposit organization in the area of the Dardanelles Strait. (a) Location map. 1, Intepe; 2, Seddülbahir. The dotted grey line displays the local coastline at the end of reflooding of the Mediterranean after the MSC. (b) Intepe, a bay-lagoon locality, and Seddülbahir where a Gilbert-type fan delta infils a ria resulting from a Messinian fluvial canyon, with location of photographs c–e. (c) Middle part of the Intepe section showing the lignite overlain by rubefied (fired) clays. (d) Seddülbahir: clayey bottomset beds of the Gilbert-type fan delta. (e) Sandy foreset beds of the Gilbert-type fan delta northward Intepe.

d). The Zanclean Gilbert-type fan delta infills a Messinian fluvial canyon (Fig. 12a and b), where the MES was identified at several points. In both localities (Seddülbahir and Intepe), the lowermost clays just above the MES (Seddülbahir) or the Messinian subaerial exposure (Intepe) show a record of *T. rugosus*, which is an accurate biostratigraphic nannofossil marker (Fig. 4). *Ceratolithus acutus* appears above (Fig. 12b–d) (Melinte-Dobrinescu *et al.*, 2009). *Triquetrorhabdulus rugosus* disappears in the upper part of the Intepe section (Fig. 12) at 5.279 Ma (Fig. 4: Raffi *et al.*, 2006) as it also does in the upper part of the Gilbert-type fan delta bottomset beds (Fig. 12b). Melinte-Dobrinescu *et al.* (2009) concluded that the nannofossil succession in the post-MSC deposits in the Dardanelles Strait area, consistent with that of Fig. 4, suggests marine reflooding older than the base of the Zanclean Stage.

Block Formation in fluvial Messinian canyons around the Mediterranean

Coarse deposits made of large cemented rounded blocks reworked from Mesozoic limestones were described by Clauzon (1978) directly covering the MES in the Var ria (Nice area, southeastern France) and immediately overlain by the foreset beds of the Zanclean Gilbert-type fan delta (Clauzon *et al.*, 1990). This Block Formation is locally known as the Carros Breccia. Clauzon (1980b) described a similar formation at Garrucha near Vera (southeastern Spain) where, in an identical stratigraphic situation, gypsum blocks were deposited, being reworked from the marginal Messinian evaporites (first step of the MSC: Clauzon *et al.*, 1996). Recently, we have identified such coarse deposits (with reworked Messinian gypsum or not) in identical stratigraphic positions around the Mediterranean Basin and adjacent seas, such as the Marmara Sea (more details on outcrop location are given in caption of Fig. 16). We interpret those blocks as river-transported deposits resulting from a debris-flow process in which the fine particles have or have not been cemented (Nemec, 1990). Their stratigraphic position (Fig. 2a) places them after the erosional peak of the MES and prior to the marine sediments of the Gilbert-type fan delta. We are unable, at this stage of the study, to determine if they were deposited in subaerial or submarine conditions, i.e. at the end of the erosional phase or just after the sudden reflooding. According to the literature and mostly to our field observations, about 20 localities displaying such deposits are now recorded; they are shown in the 'Discussion' section. In some localities such as at Carros, the cemented blocks are covered by an iron-rich crust (Fig. 2b), the significance of such a chemical sedimentation being unclear (subaerial water-table iron pan or submarine microbialite?).

DISCUSSION

A two-step reflooding in the Gulf of Lions

The MES, characterized by a badland morphology (Ryan, 1978), has long been interpreted as a subaerial erosional surface (Ryan & Cita, 1978; Gennesseaux & Lefebvre, 1980; Gorini, 1993; Guennoc *et al.*, 2000; Dos Reis, 2001; Lofi *et al.*, 2003, 2005; Dos Reis *et al.*, 2005, 2008). The planation surface 'e' (Figs 5–7) observed seaward the MES, has recently been interpreted as being related to wave erosion at the end of the MSC (Bache, 2008; Bache *et al.*, 2009). This interpretation is supported by the

smooth aspect of surface 'e' over a large horizontal distance, by the erosional truncations of the underlying series, and also by the onlap termination of the overlying series (Figs 5 and 7), which are all characteristic features of transgressive surfaces (Cattaneo & Steel, 2003; Catuneanu, 2006). Past analogues of such transgressive surfaces are known in southeastern France (Champion *et al.*, 2000). These surfaces, related to Miocene transgressions, present an almost horizontal smooth morphology over large distance (Fig 13a and b), which may be compared with the planation surface 'e' highlighted in this study.

Wave erosion is essentially contained between the surf zone and the limit of fair-weather wave base, which is usually located between 10 and 20 m depth (Demarest & Kraft, 1987; Abbott, 1998; Catuneanu, 2006) and can reach up to 40 m depth in the case of extreme wave energy, such as in the Canterbury Plains in New Zealand (Leckie, 1994). Sunamura (1987) also calculated a maximum theoretical depth of 40 m offshore Japan. In the case of extreme storm waves, the wave base can reach 70 m to maximum depth of 200 m in the Irish Sea and Newfoundland (Cattaneo & Steel, 2003; Guillocheau *et al.*, 2009). Consequently, surfaces abraded by wave ravinement during a landward shift of the shoreline can be used to estimate the associated increase in bathymetry. For this purpose, we need to estimate their slope at the time of their formation (see below the 'Quantification of the two steps' section).

Storm events can erode clean sands from the shoreface and deposit them further offshore (between the fair-weather wave base and the storm wave base). These deposits are often enriched in micas and intercalated between offshore silty-clay deposits (Guillocheau *et al.*, 2009). The 50 m of azoic deposits found in the GLP2 well (Fig. 8), corresponding to an alternation of fine to medium micaceous sandstone with subrounded to subangular grains and silty calcareous clays, could be the result of such events. In the Gulf of Lions, wave action has thus reworked the previous deposits and also reshaped the subaerial unconformity into a typical planation surface. This early transgression must have been relatively slow to enable wave erosion, removal of material and smoothing of the surface.

The contact between badland morphology and the planation surface 'e', at constant TWT (two-way time) depth throughout the Gulf of Lions (Fig. 7), has been interpreted as indicating the location of the palaeoshoreline at the end of the wave erosion phase and just before the very rapid reflooding of the Mediterranean (Bache, 2008; Bache *et al.*, 2009). Numerous representative analogues of this situation can be found in areas where wave action affects the present-day shoreline (Fig. 13c and d).

A major transition in the variations of the relative sea level and a two-step reflooding can thus be proposed. First, a slow landward migration of the shoreline smoothed the distal subaerial relief of the deepest part of the MES, and reworked previous regressive deposits (Step I; Fig. 5); and second, very rapid reflooding 'froze' the remaining subaerial surface (MES) without further erosion or deposition because it suddenly became out of the range of wave action (Step II; Fig. 5).

Can the two-step reflooding scenario be extended to the scale of the entire Mediterranean?

The evidence of Gilbert-type fan deltas within several Zanclean rias (Dardanelles area as described above: Melin-

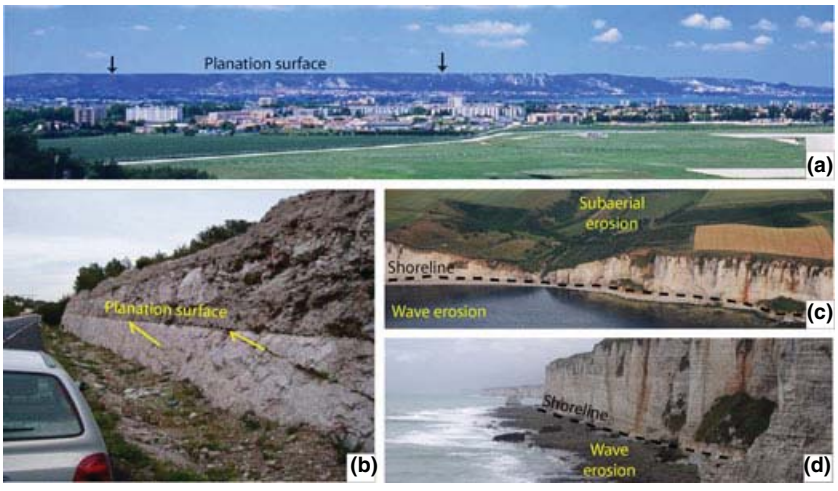

Fig. 13. (a, b) Examples of transgressive surfaces in southeastern France, Nerthe Massif, Provence. These erosional surfaces, related to Miocene transgressions (Champion *et al.*, 2000), present a smooth morphology over large distances, which may be compared with the planation surface 'e' highlighted in this study. (a) Planation surface at the top of the Nerthe Massif, Provence. (b) Cretaceous limestone deposits are truncated and overlain by Miocene transgressive deposits. Photograph: Jean-Loup Rubino. (c, d) Examples of present shore in the North of France where the combined effect of waves and tides leads to erosion of the cliff. These shorelines are representative analogues of our interpretation of the landscape in the Gulf of Lions just before the Step II of reflooding. (c) Vattetot-sur-Mer, Seine Maritime. Photograph: Charlélie Coutinho. (d) Etretat, Seine-Maritime. Photograph: Anne Duperret.

te-Dobrinescu *et al.*, 2009; Antalya Basin in southwestern Turkey: Poisson *et al.*, 2011; many other localities observed by some of us in the northern Aegean, Cyprus and Syria) suggests that both the Western and Eastern Mediterranean basins reflooded in a similar way. One question that arises about the slow reflooding phase (Step I) is whether it is only restricted to the Western Mediterranean (Provence–Algiers Basin) or whether it concerned the whole Mediterranean Basin. In the Western Mediterranean, erosional surfaces (Garcia *et al.*, 2011) or submarine terraces (Estrada *et al.*, 2011) have already been linked with a two-step reflooding scenario. In the Eastern Mediterranean, a comparable wave ravinement surface can be observed off the Nile Delta in the interfluves bordering the Abu Madi canyon, where it contrasts sharply with the lowermost part of the canyon fill (Dalla *et al.*, 1997). A series of flat ravinement surfaces have also been identified in the Levantine Basin and ascribed to wave erosion (Bertoni & Cartwright, 2006;: see their fig. 14 and text p. 112). These surfaces have been interpreted as the effect of repeated phases of base-level change during the MSC. The location of these ravinement surfaces, landward of a subaerial surface linked to the peak of the Mediterranean Sea-level fall during the Messinian desiccation event (Bertoni & Cartwright, 2007), suggests a formation during a reflooding process. The hypothesis of a formation during a regressive trend seems unlikely because in this case, subaerial erosion would have erased the previous topography.

As a consequence, a question arises concerning the Sicily sill, which today separates the two Mediterranean basins (*ca.* 100 m in bathymetry: Fig. 14, profile AB) and controls their water exchanges (Astraldi *et al.*, 1999). Palaeotectonic reconstructions (Jolivet *et al.*, 2006) suggest that a wider space existed between Tunisia and the Italian Peninsula during the Tortonian and early Messinian times, before the opening of the South Tyrrhenian Sea in the Pliocene and subsequent appearance of the Etna volcano in the Mid-Pleistocene. The precise limits and the depth of this probably wider strait are difficult to estimate, although it was likely to be much deeper than what it is today (Jolivet *et al.*, 2006). The map shown in Fig. 15 gives a hypothetical idea about the palaeogeography of the Mediterranean and surrounding regions at the end of Step I of reflooding despite the lack of information on the palaeoshoreline location other than for the Gulf of Lions (Fig. 6).

Tentative age model of the reflooding process and suggested resulting palaeogeographical changes

If the palaeogeography at the end of Step I of reflooding is highly hypothetical (Fig. 15), that after Step II is well-controlled as mapping the early Zanclean marine deposits is achieved inland (see the most recent map published by Jolivet *et al.*, 2006). The map after Step II (Fig. 16) has been significantly completed thanks to some recent publications (Soria *et al.*, 2008; Clauzon *et al.*, 2009; El Euch – El Koundi *et al.*, 2009; Melinte-Dobrinescu *et al.*, 2009; Poisson *et al.*, 2011) and to the intensive field investigations of some of us (G. C., J.-P. S., J.-L. R., L. M.).

The above-mentioned data collected in Sicily (Eraclea Minoa), in the Apennine foredeep (Maccarone) and in the Dardanelles Strait, support that the reflooding of the Mediterranean Basin (i.e. Step II) was completed significantly before 5.332 Ma as suggested by previous studies (Cavazza & Decelles, 1998; Cornée *et al.*, 2006). The classical reflooding at 5.332 Ma (Zanclean GSSP; van Couvering *et al.*, 2000) must be now seriously questioned because of new convergent data obtained from high-resolution studies in deposits just overlying the MES (Cornée *et al.*, 2006; Melinte-Dobrinescu *et al.*, 2009), from the Sicilian Arenazzolo Formation wrongly considered as exclusively composed of reworked microfossils (Londeix *et al.*, 2007), and from an extensive nannofosil research in the Apennine foredeep (Popescu *et al.*, 2007, 2008). Using cyclostratigraphy and astrochronology, it is possible to date this event in Sicily and in the Apennine foredeep. If we apply to the 6.5 dark–lights alternations of the Arenazzolo Unit the same quasi-period as evidenced in the Trubi (i.e. 20 kyr), its duration should be of about 130 kyr. That would date its base, and hence Step II of the Mediterranean reflooding, at 5.46 Ma (Table 1), an age consistent with the basal bottomset beds of the Dardanelles Gilbert-type fan delta preceding the first appearance of *C. acutus* (Fig. 12b) dated at 5.345 Ma (Fig. 4). In the Apennine foredeep, using the established relationship between the pollen ratio SE/AE and eccentricity (Fig. 11b and c), the arrival of marine waters at Maccarone can be dated at 5.36 Ma (Fig. 11; Table 1; Popescu *et al.*, 2007). The slightly delayed entrance of marine waters into the Apennine foredeep is consistent with its potential status as an isolated perched freshwater basin during the peak of the MSC (Fig. 1) (Clauzon *et al.*, 1997, 2005).

The precise age and duration of Step I of reflooding are at the moment impossible to estimate. It is constrained between 5.60 Ma, the consensual age of the sea-level drawdown in the Mediterranean (CIESM, 2008) and the above-proposed age at 5.46 Ma for the sudden Step II of reflooding. Another key-age can be deduced from the dating of the base of the Arenazzolo Unit at 5.46 Ma: the first influx of Paratethyan waters after the MSC at 5.45 Ma (Table 1) indicated by dinoflagellate cysts half a dark–light cycle above the base of Arenazzolo (Fig. 10e).

With respect to the available ages (Table 1), it is possible to propose interpretative palaeogeographical maps at successive times between 5.46 and 5.30 Ma. At 5.46 Ma, fluvial canyons were suddenly filled by marine waters that transformed them into rias, but the connection which existed with the Dacic Basin prior to the MSC through the Balkans (Popescu *et al.*, 2009) has not been re-established (Fig. 16). In many places, a Block Formation (with or without reworked Messinian marginal evaporites) is sandwiched between the MES and Gilbert-type fan delta deposits as shown on Fig. 2a. Such deposits have been interpreted as submarine slumps caused by dissolution

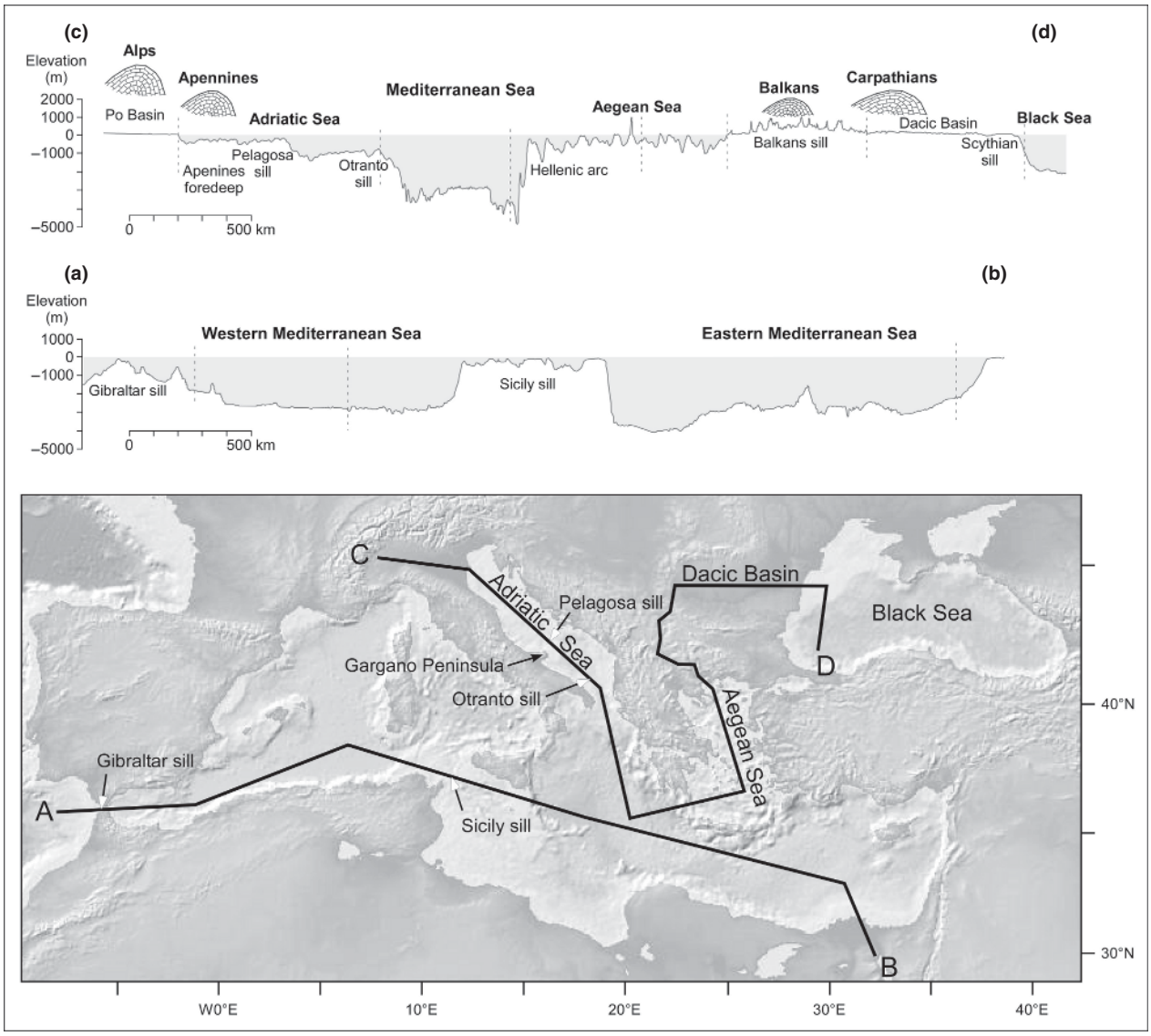

Fig. 14. Two present-day topographic profiles (a–d) illustrating the physiography of the Mediterranean Basin and some peripherial areas just after the Messinian Salinity Crisis. Sills and nearby mountains are indicated. On the profiles, vertical dotted lines indicate direction changes. The map was created using GeoMapApp System developed by Haxby *et al.* (2010).

and collapse (Los Feos, Nijar Basin: Fortuin & Krijgsman, 2003) or as an olitostrome representative of enigmatic tectonics (Garrucha, Vera Basin: Ott D'estevou *et al.*, 1990). We suggest that they are river-transported coarse deposits as shown by Breda *et al.* (2007). The two-step reflooding scenario allows the emplacement of these debris-flow deposits between the end of the drawdown and the beginning of Step II, just after the sudden entrance of marine waters into the proximal part of canyons, completely changing the base-level and stream power of the rivers that become incapable of transporting such blocks. The block deposits are then capped by the arrival of the first prograding sediments of the Gilbert-type fan deltas.

Figure 17 illustrates the re-connection of the Dacic Basin with the Mediterranean at 5.45 Ma (Table 1) attested by dinoflagellate cysts in the Sicilian Arenazzolo Unit (Fig. 10e). This is consistent with the results of Popescu *et al.* (2006b) who obtained an astronomic age of *ca.* 5.40 Ma at the exposed base of bottomset beds of the Zanclean Gilbert-type fan delta at Turnu Severin (SW Romania). As previously suggested by the results obtained by Melinte-Dobrinescu *et al.* (2009) in the Dardanelles area as well as the evidence in the Istanbul region of nearby distinct Messinian fluvial networks (one flowing from the Thrace Basin towards the Black Sea, the other one flowing from the Marmara area towards the Aegean Sea; Suc *et al.*, 2009), the gateway re-connecting the Mediterranean with the Eastern Paratethys was not located in the region of the Marmara Sea. After exploring all the sedimentary basins in the Balkans area, a gateway passing at Serres and Skopje (i.e. in the area drained today by the Strymon–Vardar River), then at Niš before joining the Dacic Basin (i.e. in the area drained today by the Tim-

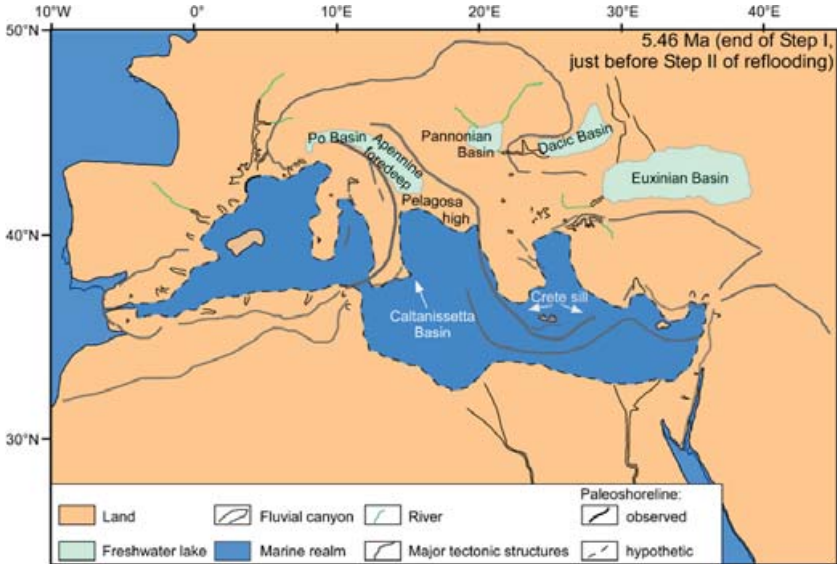

Fig. 15. Palaeogeographical map of the Mediterranean Basin and Eastern Paratethys at the end of Step I of the Mediterranean reflooding, i.e. just before the dramatic rise in sea level at 5.46 Ma. At that time, the water level in the Mediterranean Basin was some 650 m below the Atlantic Ocean, the waters of which flowed into the Mediterranean.

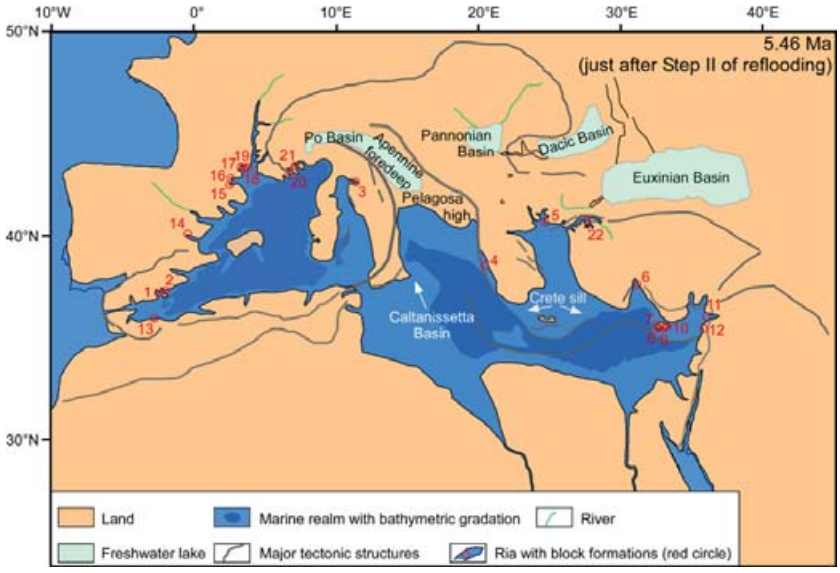

Fig. 16. Palaeogeographical map of the Mediterranean Basin and Eastern Paratethys just after Step II of the Mediterranean reflooding, i.e. just after the dramatic rise in sea level at 5.46 Ma. At that time, the Mediterranean and the Atlantic were connected (i.e. at the same sea level). The Block Formations, now frequently identified (according to literature or our own observations) at the base of the Zanclean marine sediments, are indicated by red circles. Localities with gypsum or anhydrite blocks: Los Feos (1) in the Nijar Basin and Garrucha (2) in the Vera Basin (Clauzon, 1980b) (SE Spain); San Ippolito (3) near Volterra (Central Italy), Kalamaki (4) on the island of Zakynthos; Loutra Eleftheron (5) near Kavala (NE Greece); Gebiz (6) near Antalya (S Turkey) (Glover & Robertson, 1998); Amargeti (7), Pissouri (8) Psematismenos (9) and Boghaz (10) on the island of Cyprus; Mağaracik (11) near Samandağ (SE Turkey); Kferyeho (12) near Lattaquié (Syria). Localities with various rocks: Oued Haddouba and Ikamba (13) in the Melilla area (N Morocco) (Cornée *et al.*, 2006); La Pedrera (14) near San Miguel de Salinas (E Spain) (García-García *et al.*, 2011); Le Boulou (15) and Ille sur Têt (16) near Perpignan (S France); Cessenon (17) and Magalas (18) near Béziers (Ambert *et al.*, 1998) and Tour de Piquet and Bruque-Cabal (19) near Montpellier (Ambert, 2011) (SE France); Carros (20) in the Nice area (SE France) (Clauzon, 1978); Ventimiglia (21) (NW Italy) (Breda *et al.*, 2007); Salzidere (22) in the Bandirma region (S Marmara Sea, N Turkey).

ok River) has been suggested (Clauzon *et al.*, 2005; Popescu *et al.*, 2009; Suc *et al.*, 2009) as shown in Fig. 17. Such a gateway is supported by our recognition of three illustrative Zanclean Gilbert-type fan deltas nested within Miocene deposits, respectively close to

(1)Serres (at Ano Metochi; Fig. 18a), dated by mollusks (abundant *Pecten benedictus* and *Ostrea lamellose*: Karistineos & Georgiades-Dikeoulia, 1985–86) in agreement with the pollen flora (rich in Taxodiaceae, *Liquidambar*, *Zelkova*, *Cathaya*, *Cedrus*, *Picea*, etc.) that we found in the bottomset beds similar to those from the other well-dated pollen localities in the region (Biltekin, 2010);
(2)Skopje (in the Dračevo – Batinci area; Clauzon *et al.*, 2008), dated by the nannofossil *C. acutus* (Fig. 18b and c);

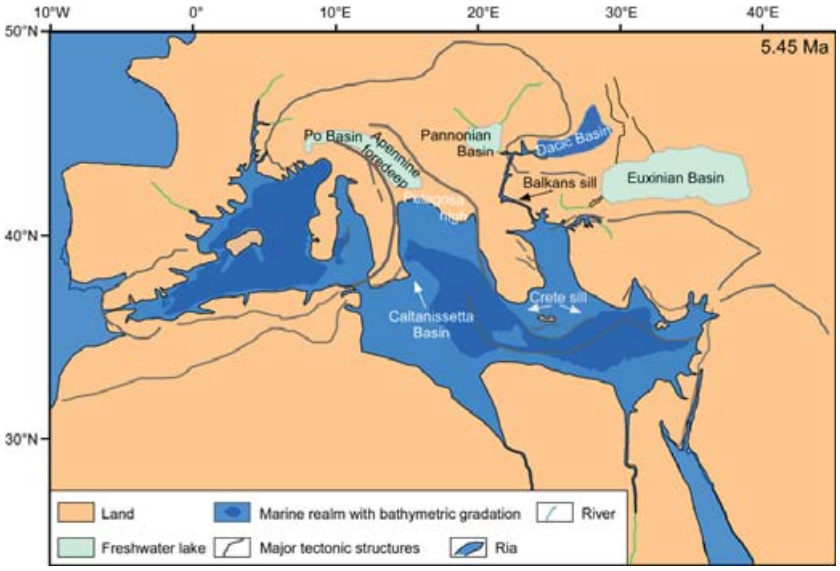

Fig. 17. Palaeogeographical map of the Mediterranean Basin and Eastern Paratethys at 5.45 Ma (after the second step of the Mediterranean reflooding) when the Mediterranean Sea and Dacic Basin reconnected due to continuing rise of global sea level.

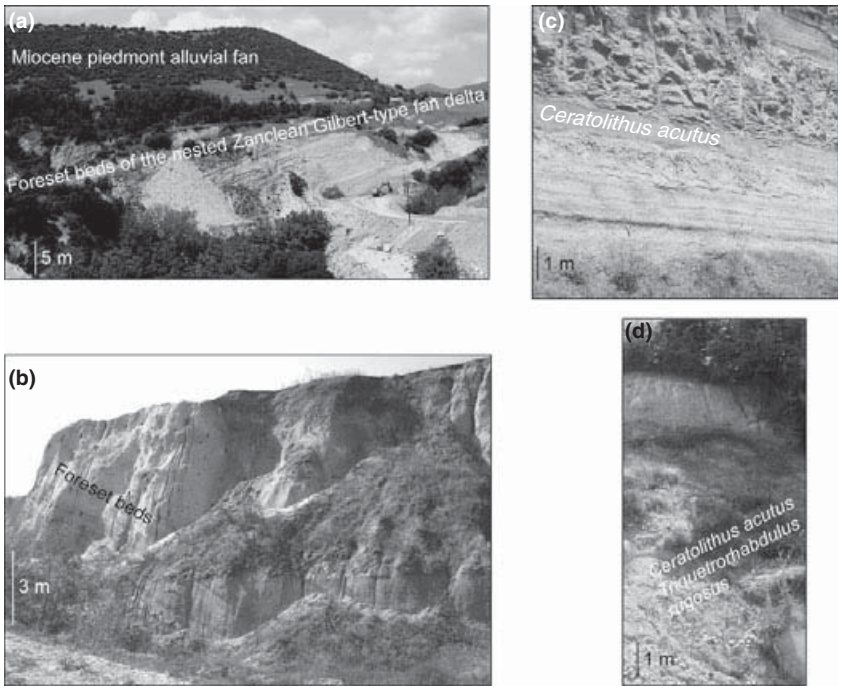

Fig. 18. Zanclean Gilbert-type fan deltas in the Balkans. (a) Serres (Ano Metochi): foreset beds of the Zanclean Gilbert-type fan delta nested within the Miocene piedmont alluvial fan; (b, c) Zanclean Gilbert-type fan delta near Skopje: (b) foreset beds at Dračevo; (c) bottomset beds at Batinci; (d) Niš: bottomset beds of the Zanclean Gilbert-type fan delta at Gabrovačka Reka.

(3)Niš (at Gabrovačka Reka), dated by nannofossils (*C. acutus* and *T. rugosus*) (Fig. 18d).

The delayed invasion of Mediterranean waters into the Dacic Basin was probably caused by the crossing of a sill, here called the Balkans sill, which we tentatively locate east of Skopje (Fig. 17). At Dračevo (Skopje), the marine-continental transition of the Gilbert-type fan delta, i.e. the marker of the early Zanclean coastline, is today at 395 m altitude (Clauzon *et al.*, 2008). This value provides an idea of the post-Pliocene uplift.

On the basis of the eccentricity tuning of the pollen record from the Maccarone section, it is possible to date at 5.36 Ma the arrival of marine waters into the Apennine foredeep (Fig. 11) and hence the re-connection of this lake with the Mediterranean Sea (Fig. 19). The Pelagosa high was probably the obstacle that isolated this lake during the peak of the MSC (instead of the Otranto high proposed by Clauzon *et al.*, 2005). This is supported by the evidence of the Colombacci Formation (affected by influxes of marine waters) only to the north of the Gargano Peninsula (which today is the coastal expression of the Pelagosa sill; Fig. 14, profile CD). This assumption is in agreement with the presence of marine fishes within the Colombacci Formation in the region of Ancona (Carnevale *et al.*, 2006). The Pelagosa sill is today 160 m deep (Fig. 14, profile CD; Gačić *et al.*, 2002). At that time, marine waters had not yet invaded the entire Po Plain (Fig. 19; Mary *et al.*, 1993; Channell *et al.*, 1994; Sprovieri *et al.*, 2007; Violanti *et al.*, 2011).

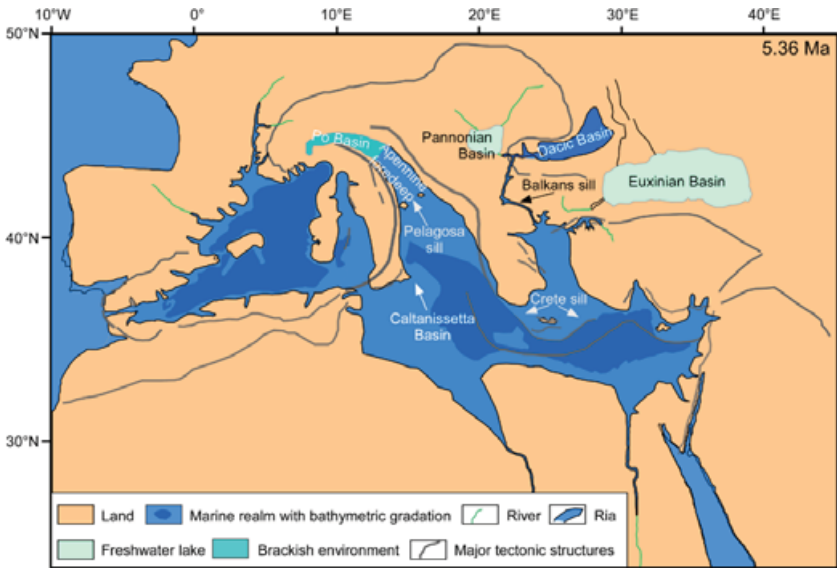

Fig. 19. Palaeogeographical map of the Mediterranean Basin and Eastern Paratethys at 5.36 Ma when the Mediterranean Sea and Apennine foredeep reconnected due to continuing rise of global sea level.

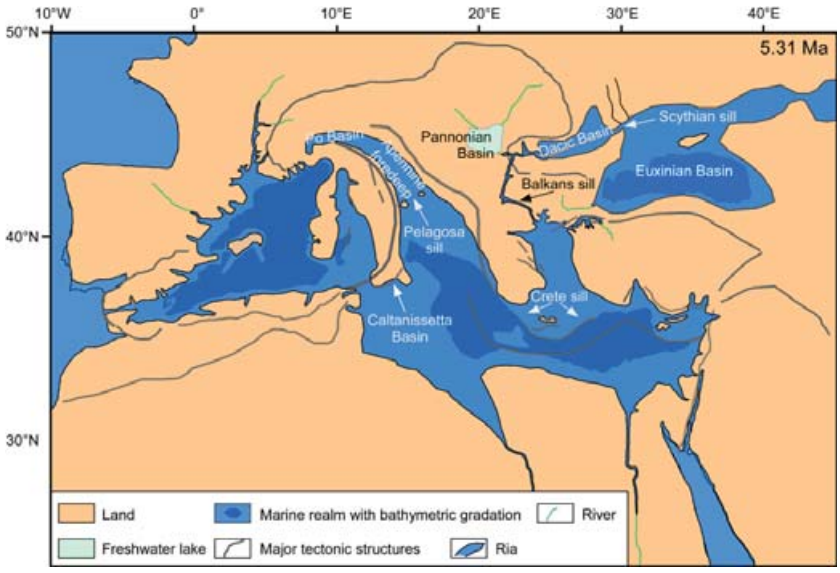

Fig. 20. Palaeogeographical map of the Mediterranean Basin and Eastern Paratethys at 5.31 Ma when the Dacic and Euxinian basins connected (Popescu *et al.*, 2010) due to continuing rise of global sea level.

Finally, the Mediterranean waters crossed the Scythian sill (Fig. 20), i.e. the Reni sill of Semenenko (1995), today exposed in the Dobrogea region (Fig. 14, profile CD). Incursion of Mediterranean species (diatoms: Schrader, 1978; dinoflagellate cysts: Popescu, 2006; calcareous coccoliths including *C. acutus* and *T. rugosus*: Popescu *et al.*, 2010) into the Euxinian Basin is documented by DSDP Site 380 (Fig. 3). It occurred at 5.31 Ma (Table 1; Fig. 20) as established by cyclostratigraphy (Popescu *et al.*, 2010).

Why did these peripheral (Dacic, Apennine and Euxinian) basins not re-connect simultaneously to the Mediterranean at the time of the sudden Step II of the reflooding? Probably because of the presence of sills at different altitude elevations that were successively inundated during the continuing slower global rise of sea level after 5.46 Ma by the end of the late Miocene Antarctic glaciation (Hardenbol *et al.*, 1998; Miller *et al.*, 2005). The minimum 50 m water depth increase between 5.46 and 5.332 Ma could explain the sedimentological differences between the Arenazzolo (prodeltaic muds) and Trubi (white chalky pelagic oozes) units, also reflected by their respective dinoflagellate cysts content (Fig. 10e).

What happened at Gibraltar?

Today, the water circulation within the Mediterranean Sea is controlled by sills and, mostly, by the sill of Gibraltar (Bethoux & Gentili, 1999). Accordingly, what happened at the Strait of Gibraltar is crucial to unravelling the process of the Mediterranean reflooding after the MSC. The erosional activity of the Atlantic flow after initial erosion by a local river (Blanc, 2002), a process that was modelled by Loget *et al.* (2005), has been proposed in contrast to the Gibraltar palaeo-falls (Hsü *et al.*, 1973) or

a major tectonic event (Krijgsman & Garcés, 2004). This is supported by the distance of 30 km separating the strait from the sill that shifted westward as a consequence of this erosion. Recently, Garcia-Castellanos *et al.* (2009) proposed that the Atlantic flow directly cut the Gibraltar channel in a cataclysmic way. Campillo *et al.* (1992) and then Garcia-Castellanos *et al.* (2009) documented the presence in the central Alboran Sea of a major palaeochannel, wich constitutes the relic of a major gateway between the Atlantic Ocean and the Mediterranean Basin.

Step I of reflooding relates to an early stage of (subaerial or marine) erosion at Gibraltar resulting in the entrance of Atlantic waters in moderate quantity whatever its proposed duration (26 years: Blanc, 2002; 100–3000 years: Garcia-Castellanos, 2009), that anyway appears greatly insufficient with regard to the events that occurred during this time-interval:

(1) as a consequence of the erosion at Gibraltar, the volume of entering Atlantic waters should have progressively increased; we estimate that the total volume of water in the Mediterranean Basin at the end of Step I could represent 25% of its capacity;
(2) in the same way, the progressive sea-level rise would form the planation surface.

Step II of reflooding (Fig. 16) is the sudden, fast and massive entrance of Atlantic waters into the Mediterranean Basin as the immediate response to the collapse of the sill suggested by Blanc (2002) and Garcia-Castellanos *et al.* (2009), with similar proposed duration (respectively 10–11 years and a few months to 2 years). The Mediterranean physiography at the time when this rapid influx started is sketched out in Fig. 15. From a rough estimate, including a final catastrophic sea-level rise of 600–900 m, we conclude that *ca.* 50% of the water volume of the Mediterranean Basin entered it just after the collapse as opposed to the 90% proposed by Garcia-Castellanos *et al.* (2009).

The sea-floor topography of the Western Alboran Basin as deduced from seismic lines and structural maps (Alvarez-Marrón, 1999; Comas *et al.*, 1999; Mauffret *et al.*, 2007) seems to have been made of successive small basins at increasing depths from West to East and still infilled by marine waters during the peak of the MSC, into which the Atlantic continuously overflowed, feeding the abyssal plains farther East after their almost complete desiccation. Such a physiography could explain how the Mediterranean biota (molluscs, echinids, bryozoans, etc.) recovered so quickly after the crisis from some Alboran potential refuge basins, providing a possible response to this nagging question pointed out by palaeontologists (Néraudeau *et al.*, 2001; Néraudeau, 2007). This hypothesis is expressed on the map of Fig. 1. Collapse at Gibraltar would have occurred at 5.46 Ma, probably as hypothesized by Blanc (2002) as the result of a significant threshold in the erosion intensity. At that time, the Atlantic water channel through the Gibraltar area would suddenly become a wide strait and the sill would have acquired its approximate present-day morphology. The flow of Atlantic waters across the basins of the sill would have instantaneously supplied the entire Mediterranean Sea with preserved marine endemic benthic organisms.

Quantification of the two steps

The increase in bathymetry during the two steps of reflooding can be estimated. For this purpose, the palaeoshoreline identified between the badland morphology and the planation surface 'e' provides a distinct point of reference. The palaeoshoreline is located at a present-day depth of 1.6 s (TWTT) in the whole Gulf of Lions margin (Fig. 5). We estimate this point at a depth between 1800 and 2100 m taking into account the seismic velocities (Sonic from e-logs) and respective depths found in the nearby Autan1 and Rascasse boreholes. The original depth of the palaeoshoreline can be estimated by subtracting the Pliocene and Quaternary subsidence from its present-day depth (Fig. 21). Rabineau *et al.* (2006), using Pliocene and Quaternary geometries on the shelf, estimated this subsidence at around *ca.* 215 m Ma^{-1} at *ca.* 62 km from the coast in the same area. Considering the age of 5.46 Ma for the end of Step I of reflooding (Table 1 and above), *ca.* 1200 m of subsidence are obtained at this point. We can conclude that the palaeoshoreline was located between 600 m (1800–1200 m) and 900 m (2100–1200 m) below the present sea level at 5.46 Ma. The palaeoshoreline represents the seaward boundary of the MES, which has been preserved during the second step of reflooding. The rapid increase in bathymetry during this second reflooding step thus amounted to between 600 and 900 m.

The increase in bathymetry during the first step of reflooding may also be estimated. We have thus deduced the initial depth of the seaward limit of observation of the planation surface 'e'. This point is located at a maximum distance of 112 km from the coast, at around 3 s (TWTT). We also estimate its depth, taking into account the respective velocities and depths of the GLP2 well and ESP 202 seismic profile, between 3000 and 3400 m. Extrapolating the total subsidence calculated by Rabineau *et al.* (2006) towards the basin with a linear trend (Fig. 21), we obtain a total subsidence of *ca.* 430 m Ma^{-1} at *ca.* 112 km from the coast. Considering the age at 5.46 Ma (Table 1), a subsidence of *ca.* 2300 m is obtained at this point. This limit was thus localized between 700 m (3000–2300 m) and 1100 m (3400–2300 m) below the present sea level at 5.46 Ma. The shoreline displacement, during which the planation surface 'e' formed (Step I), occurred between two points respectively located at 1.6 s TWTT (600–900 m) and 3 s TWTT (700–1100 m) depth before the onset of Pliocene subsidence. The maximum increase in bathymetry during this step was thus around 500 m (1100–600 m) and the corresponding maximum slope value of the planation surface 'e' was 1%. This estimate was made

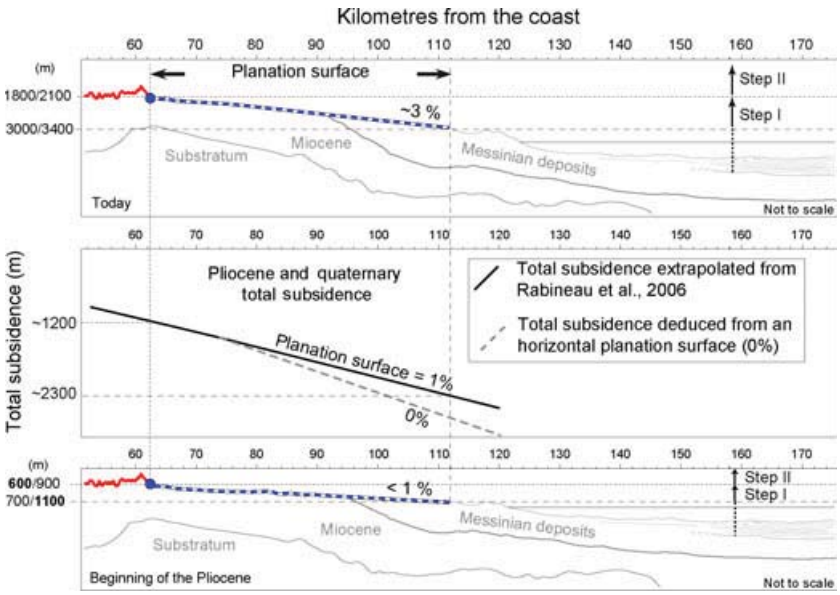

Fig. 21. Estimate of the initial position of the palaeoshoreline and of the planation surface 'e' at the beginning of the Pliocene. The Pliocene and Quaternary total subsidence is deduced from Rabineau *et al.* (2006).

considering an extrapolation of shelf tilting towards the basin as calculated by Rabineau *et al.* (2006), and it is thus a maximum value. Assuming that the minimum value of this slope was 0%, the total increase in bathymetry for the two-step reflooding is estimated between 600 m (600 m for the second step and 0 m for the first step with a slope value of 0%) and 1100 m (600 m for the second step and 500 m for the first step) in the earliest Pliocene. A relative sea-level curve can be proposed for the Gulf of Lions according to this calculation (Fig. 22).

The rate of sea-level rise for the second step of the post-MSC reflooding can be estimated around 60 m kyr^{-1} (at least 600 m in at most 10 000 years). This high rate shows that this transgression was catastrophic and must be related to a special event at Gibraltar (see above). Due to uncertainties on the timing of the first step of reflooding, the corresponding rate cannot be estimated. However, contrasted rates for the two steps of the post-MSC reflooding may explain why the rugged regressive MES has been preserved landward of 1.6 s TWTT and erased by wave erosion seaward of it.

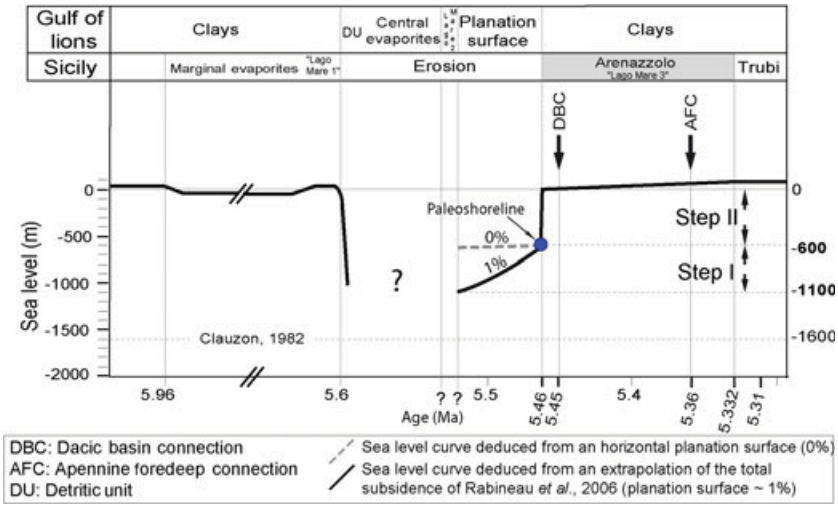

Fig. 22. Variation of the Mediterranean sea level in the Gulf of Lions between 6 and 5.30 Ma encompassing the Messinian Salinity Crisis, with special attention to the reflooding phase. Successive major changes are estimated with respect to present-day sea level (noted '0'). A two-step process is highlighted: the first step (? – 5.46 Ma) is characterized by a relative sea-level rise (500 m at the most). A first transgression flattened previous topography to build a remarkable ravinement surface (slope value between 0% and 1%); the second step (at 5.46 Ma) corresponds to an ultra-rapid Mediterranean sea-level rise contained between 600 and 900 m in amplitude. Just after this outstanding and sudden rise in sea level, Arenazzolo deposition began. After Gilbert-type fan delta sediments began to infill the rias, successive connections of the Mediterranean Basin with adjacent basins formed as global sea level continued to rise: with the Dacic Basin (Eastern Paratethys) at 5.45 Ma, with the Apennine foredeep at 5.36 Ma, at last with the Euxinian Basin (Eastern Paratethys) at 5.31 Ma (see Figs 17–20).

Deposition of the central evaporites (Lower, Mobile and Upper units: Lofi *et al.*, 2011; total thickness: up to 2800 m) requires a continuous input of marine water at the beginning of Step I of reflooding, before the brine concentration reached a critical threshold (Fig. 22). However, it is not excluded that some halite was deposited earlier, i.e. during the sea-level drawdown, and was mixed with detrital deposits. In fact, it can be assumed that two phases are distinguishable and in close succession (Bache *et al.*, 2009): (i) the main erosion phase coeval with the sea-level drop and deposition of detrital material in the almost desiccated basin and (ii) deposition of the major part of evaporites during the beginning of Step I of reflooding, a phase during which fluvial erosion continued on lands and margins. Using modelling, Govers (2009) suggested that most of the evaporites were deposited before sea-level drop. Our data contradict this conclusion because the MES and related detrital products underlie the central basin evaporites (Bache *et al.*, 2009; Montadert *et al.*, 2011), which thus formed after sea-level lowering. Also using modelling, Meijer & Krijgsman (2005) concluded that there were repeated desiccations and re-fillings of the Mediterranean, based on the supposed correspondence of the exposed Sicilian Upper Evaporites and the Upper Unit in the central basins. We oppose this hypothesis too on the basis of the observed relationships between seismic units in the central basins (Bache *et al.*, 2009; Montadert *et al.*, 2011). Duration of evaporite deposition in the central basins, especially the thick halite, was probably brief (<50 000 years in our scenario) in agreement with general assumptions (Lugli *et al.*, 2008), but impossible to define more precisely (Fig. 22).

The transition from massive halite to the Upper evaporitic Unit marks the dilution of Mediterranean waters that increased during the following 'dilution event', generally pointed out as belonging to the 'Lago Mare' episode (Cita *et al.*, 1990; Iaccarino & Bossio, 1999; Rouchy *et al.*, 2001), an assumption clarified by Clauzon *et al.* (2005) who distinguished two kinds of 'Lago Mare' episodes that occurred during three major distinct events (Fig. 22). Two of these so-called 'Lago Mare' events correspond with surface water exchanges between the Mediterranean and Dacic Basin (Eastern Paratethys) through the Balkans gateway, attested by Mediterranean nannoplankton in the Dacic Basin (Drivaliari *et al.*, 1999; Clauzon *et al.*, 2005; Snel *et al.*, 2006) and conversely Paratethyan dinoflagellate cysts in the Mediterranean (Londeix *et al.*, 2007; Popescu *et al.*, 2007, 2009). Such events, called 'Lago Mare' 1 and 3, occurred during high sea levels, respectively just before the desiccation phase and just after Step II of reflooding (Fig. 22). In some exposed sections, they can follow each other in a pseudo-stratigraphic continuity, such as at Eraclea Minoa (Fig. 9e; Londeix *et al.*, 2007; Popescu *et al.*, 2009) and Intepe (Fig. 12b; Melinte-Dobrinescu *et al.*, 2009). 'Lago Mare' 2 is known as a brief dilution event, which seems to characterize the central basins only. Being evidenced by ostracods and geochemical measurements only (see, e.g., Pierre *et al.*, 2006), it could correspond to increased run-off preceding more significant marine water input. Its duration remains unknown and these sediments necessitate new research studies, especially to complete their micropalaeontological content (nannofossils, dinoflagellate cysts), for deciphering their exact origin.

It should be noted that this process of Mediterranean reflooding in two steps after the MSC is unrelated to the debate about scenarios of this dramatic episode, which focuses on the chronological position of evaporitic bodies and fluvial erosion (Rouchy & Caruso, 2006).

CONCLUSION

Considering offshore observations in the Gulf of Lions, a two-step reflooding of the Western Mediterranean Basin is proposed for the end of the MSC (Fig. 22):

(1) Step I (5.56? – 5.46 Ma) is characterized by a relatively moderate and slow sea-level rise (500 m at the most) leading to the landward migration of the shoreline. This first transgression, which was accompanied by the flattening effect of waves and tides, flattened previous highs and formed a remarkable ravinement surface. It resulted from the beginning of a progressively increasing erosion of the Gibraltar barrier.
(2) Step II (instantaneous at 5.46 Ma) was particularly sudden and dramatic, resulting from the collapse of the Gibraltar channel. It caused the so-called 'Pliocene Deluge', being dated prior to the Zanclean GSSP by onshore studies. This violent sea-level rise of 600–900 m flooded the largest part of fluvial canyons, which were suddenly transformed into rias (as attested by numerous Gilbert-type fan deltas), contributing to preserve the MES all around the Mediterranean and the palaeoshoreline evidenced in the Gulf of Lions.

Such a scenario seems to have also been the case in the Eastern Mediterranean Basin, which requires a more detailed research.

We suggest that central basin evaporites were mostly deposited during the beginning of Step I of reflooding. After Step II of rapid Atlantic reflooding of the Mediteranean, sea-level rise slowly but regularly continued as a result of the global rise in sea level and the successive connections between the Mediterranean and the Dacic Basin (at 5.45 Ma), the Adriatic foredeep (at 5.36 Ma), the Euxinian Basin (at 5.31) and finally the Po Plain were established.

In summary, the events that occurred during the MSC appear to have been characterized by high complexity, some being synchronous at the scale of the entire Mediterranean, others diachronous with respect to environmental or regional conditions such as the so-called 'Lago Mare' events, which had a dual nature.

Many new geological aspects may be addressed as a consequence of this work. First of all, the key surfaces observed in the Gulf of Lions provide remarkable points of reference. It will be necessary to correlate them at the scale of the whole Western Mediterranean, as well as within the Eastern Basin. Secondly, as two-step reflooding of the Mediterranean has never been considered before, the quantification of the steps will help constrain future models of reflooding as well as subsidence studies (post-Messinian vertical movements). Finally, kinematic studies can be conducted to confirm the existence of Messinian sills within the Mediterranean Basin (Sicily – Tunisia area for example) and their influence on its reflooding history.

ACKNOWLEDGEMENTS

A. Di Stefano (University of Catania) provided some information on nannoplankton from Eraclea Minoa. Positive comments on the manuscript were made by J. Lofi. Two reviewers, W. Cavazza and an anonymous one, and the Editor of Basin Research, P. van der Beek, are greatly acknowledged for their scrupulous examination of our manuscript and their comments and recommendations, which helped us to significantly improve it. We also thank R. Herzer (GNS Science) for his language corrections and comments on the manuscript. This work is a contribution to ANR 'EGEO' Project, to CNRS/INSU 'Actions Marges' Project (AMEDITER), and to 'Bassins néogènes et manteau en Méditerranée' (TerMEx CNRS/INSU).

SUPPORTING INFORMATION

Additional Supporting Information may be found in the online version of this article:

Figure S1. Uninterpreted seismic profiles of Fig. 5.
Figure S2. Uninterpreted seismic profiles of Fig. 7.
Figure S3. Uninterpreted seismic profiles of Fig. 8.

Please note: Wiley-Blackwell are not responsible for the content or functionality of any supporting materials supplied by the authors. Any queries (other than missing material) should be directed to the corresponding author for the article.

REFERENCES

Abbott, S.T. (1998) Transgressive systems tracts and onlap shellbeds from mid-Pleistocene sequences, Wanganul Basin, New Zealand. *J. Sedim. Res.*, **68**, 253–268.

Alvarez-Marrón, J. (1999) Pliocene to Holocene structure of the Eastern Alboran Sea (Western Mediterranean). In: *Leg 161* (Ed. by R. Zhan, M.C. Comas & A. Klaus) *Proc. Ocean Drill. Progr.*, **161**, 345–355.

Ambert, P. (2011) Messinian and Pliocene continental formations in the Montpellier region and their geological context: geodynamic consequences in the Georges Clauzon model (1996). *Bull. Soc. Géol. France*, **182** (2), 79–85.

Ambert, P., Aguilar, J.-P. & Michaux, J. (1998) Evolution géodynamique messino-pliocène en Languedoc central: le paléo-réseau hydrographique de l'orb et de l'Hérault (Sud de la France). *Geodin. Acta*, **11**(2–3), 139–146.

Astraldi, M., Balopoulos, S., Candela, J., Font, J., Gacic, M., Gasparini, G.P., Manca, B., Theocharis, A. & Tintoré, J. (1999) The role of straits and channels in understanding the characteristics of Mediterranean circulation. *Progr. Oceanogr.*, **44**, 65–108.

Bache, F. (2008) *Evolution Oligo-Miocène des Marges du Micro Océan Liguro-Provençal*. PhD Thesis, Université de Bretagne Occidentale, Brest. Available at: http://tel.archives-ouvertes.fr.

Bache, F., Olivet, J.-L., Gorini, F., Rabineau, M., Baztan, J., Aslanian, D. & Suc, J.-P. (2009) Messinian erosional and salinity crises: view from the Provence Basin (Gulf of Lions, Western Mediterranean). *Earth Planet. Sci. Lett.*, **286**, 139–157.

Bache, F., Olivet, J.-L., Gorini, F., Aslanian, D., Labails, C. & Rabineau, M. (2010) Evolution of rifted continental margins: the case of the Gulf of Lions (Western Mediterranean Basin). *Earth Planet. Sci. Lett.*, **292**, 345–356.

Bentz, F.P. & Hughes, J.B. (1981) New reflection seismic evidence of a Late Miocene Nile Canyon. In: *The Geological Evolution of the River Nile* (Ed. by R. Said), pp. 131–146. Appendix C, Springer-Verlag, New York – Heidelberg – Berlin, 131–146.

Berggren, W.A., Kent, D.V., Swischer, C.C. III & Aubry, M.-P. (1995). A revised Cenozoic geochronology and chronostratigraphy. In: *Geochronology, Time Scales and Global Stratigraphic Correlation: A Unified Temporal Framework for an Historical Geology* (Ed. by W.A. Berggren, D.V. Kent, M.-P. Aubry & J. Hardenbol) *Spec. Publ., Soc. Econ. Paleontol. Mineral.*, **54**, 141–212.

Bertini, A. (1992) *Palinologia ed Aspetti Ambientali del Versante Adriatico Dell'Appennino Centro-Settentrionale Durante il Messiniano e lo Zancleano*. PhD Thesis, University of Florence, Florence.

Bertini, A. (2006) The northern Apennines palynological record as a contribute for the reconstruction of the Messinian palaeoenvironments. *Sedim. Geol.*, **188–189**, 235–258.

Bertoni, C. & Cartwright, J.A. (2006) Controls on the basin-wide architecture of late Miocene (Messinian) evaporites on the Levant margin (Eastern Mediterranean). *Sedim. Geol.*, **188–189**, 93–114.

Bertoni, C. & Cartwright, J.A. (2007) Major erosion at the end of the Messinian Salinity Crisis: evidence from the Levant Basin, Eastern Mediterranean. *Bas. Res.*, **19**, 1–18.

Bessis, F. (1986) Some remarks on the study of subsidence of sedimentary basins: application to the Gulf of Lions margin (Western Mediterranean). *Mar. Pet. Geol.*, **3**, 37–63.

Bethoux, J.P. & Gentili, B. (1999) Functioning of the Mediterranean Sea: past and present changes related to freshwater input and climate changes. *J. Mar. Syst.*, **20**, 33–47.

Biltekin, D. (2010) *Vegetation and Climate of North Anatolian and North Aegean Region Since 7 Ma According to Pollen Anal-*

ysis. PhD Thesis, Université Claude Bernard – Lyon 1 and Istanbul Technical University, Istanbul.

Blanc, P.-L. (2002) The opening of the Plio-Quaternary Gibraltar Strait: assessing the size of a cataclysm. *Geodin. Acta*, **15**, 303–317.

Boccaletti, M., Ciaranfi, N., Cosentino, D., Deiana, G., Gelati, R., Lentini, F., Massari, F., Moratti, G., Pescatore, T., Ricci Lucchi, F. & Tortorici, L. (1990) Palinspastic restoration and paleogeographic reconstruction of the peri-Tyrrhenian area during the Neogene. *Palaeogeogr. Palaeoclimatol. Palaeoecol.*, **77**, 41–50.

Bonaduce, G. & Sgarrella, F. (1999) Paleoecological interpretation of the latest Messinian sediments from southern Sicily (Italy). *Mem. Soc. Geol. It.*, **54**, 83–91.

Breda, A., Mellere, D. & Massari, F. (2007) Facies and processes in a Gilbert-delta-filled incised valley (Pliocene of Ventimiglia, NW Italy). *Sedim. Geol.*, **200**, 31–55.

Brolsma, M.J. (1975) Lithostratigraphy and foraminiferal assemblages of the Miocene-Pliocene transitional strata of Capo Rossello and Eraclea Minoa (Sicily, Italy). *Proc. Kon. Neder. Akad. Van Wetensch. B*, **78**, 341–380.

Brolsma, M.J. (1978) Quantitative foraminiferal analysis and environmental interpretation of the Pliocene and topmost Miocene on the South coast of Sicily. *Utrecht Micropaleontol. Bull.*, **18**, 1–143.

Burrus, J. (1989) Review of geodynamic models for extensional basins; the paradox of stretching in the Gulf of Lions (northwest Mediterranean). *Bull. Soc. Géol. France*, **8**, 377–393.

Butler, R.W.H., Lickorish, W.H., Grasso, M., Pedley, H.M. & Ramberti, L. (1995) Tectonics and sequence stratigraphy in Messinian basins, Sicily: constraints on the initiation and termination of the Mediterranean salinity crisis. *Geol. Soc. Am. Bull.*, **107** (4), 425–439.

Campillo, A.C., Maldonado, A. & Mauffret, A. (1992) Stratigraphic and tectonic evolution of the western Alboran Sea: late Miocene to recent. *Geomar. Lett.*, **12**, 165–172.

Carloni, G.C., Francavilla, F., Borsetti, A.M., Cati, F., D'onofrio, S., Mezzetti, R. & Savelli, C. (1974) Ricerche stratigrafiche sul limite Miocene-pliocene nelle Marche centro-meridionali. *Giornale di Geologia, ser. 2a*, **39**(2), 363–392.

Carnevale, G., Caputo, D. & Landini, W. (2006) Late Miocene fish otoliths from the Colombacci Formation (Northern Apennines, Italy): implications for the Messinian 'Lago-mare' event. *Geol. J.*, **41**, 1–19.

Casero, P. (2004) Structural setting of petroleum exploration plays in Italy. *Ital. Geol. Soc., Spec. Vol.* 189–199.

Cattaneo, A. & Steel, R.J. (2003) Transgressive deposits: a review of their variability. *Earth-Sci. Rev.*, **62** (3–4), 187–228.

Catuneanu, O. (2006) *Principles of Sequence Stratigraphy*. 1st edn, Elsevier, Amsterdam.

Cavazza, W. & Decelles, P.G. (1998) Upper Messinian siliciclastic rocks in southeastern Calabria (southern Italy): palaeotectonic and eustatic implications for the evolution of the central Mediterranean region. *Tectonophysics*, **298**, 223–241.

Champion, C., Choukroune, P. & Clauzon, G. (2000) La déformation post-miocène en Provence Occidentale. *Geodin. Acta*, **13**, 67–85.

Channell, J.E.T., Poli, M.S., Rio, D., Sprovieri, R. & Villa, G. (1994) Magnetic stratigraphy and biostratigraphy of Pliocene "argille azzurre" (Northern Apennines, Italy). *Palaeogeogr. Palaeoclimatol. Palaeoecol.*, **110**, 83–102.

Chumakov, I.S. (1967) Pliocene and Pleistocene deposits of the Nile Valley in Nubia and Upper Egypt (in Russian). *Trans. Geol. Inst. Acad. Sci. USSR*, **170**, 5–111.

Chumakov, I. (1973) Geological history of the Mediterranean at the end of the Miocene-the beginning of the Pliocene according to new data. In: *Leg 13* (Ed. by W.B.F. Ryan & K.J. Hsü, *et al.*) *Init. Rep. Deep Sea Drill. Proj.*, **13**(2), 1241–1242.

CIESM (Antón, J., Çağatay, M.N., de Lange, G., Flecker, R., Gaullier, V., Gunde-Cimerman, N., Hübscher, C., Krijgsman, W., Lambregts, P., Lofi, J., Lugli, S., Manzi, V., McGenity, T.J., Roveri, M., Sierro, F.J. & Suc, J.-P.) (2008) Executive summary. In: *The Messinian Salinity Crisis From Mega-Deposits to Microbiology – A Consensus Report* (Ed. by F. Briand) *CIESM Workshop Monographs*, **33**, 7–28.

Cita, M.B. & Colombo, L. (1979) Sedimentation in the latest Messinian at Capo Rossello (Sicily). *Sedimentology*, **26**, 497–522.

Cita, M.B. & Gartner, S. (1973) Studi sul Pliocene e uli strati di passaggio dal Miocene al Pliocene IV. The stratotype Zanclean foraminiferal and nannofossil biostratigraphy. *Riv. Ital. Paleont.*, **79** (4), 503–558.

Cita, M.B., Racchetti, S., Brambilla, R., Negri, M., Colombaroli, D., Morelli, L., Ritter, M., Rovira, E., Sala, P., Bertarini, L. & Sanvito, S. (1999a) Changes in sedimentation rates in all Mediterranean drillsites document basin evolution and support starved basin conditions after early Zanclean flood. *Mem. Soc. Geol. It.*, **54**, 145–159.

Cita, M.B., Rio, D. & Sprovieri, R. (1999b) The Pliocene Series: chronology of the type Mediterranean record and standard chronostratigraphy. In: *The Pliocene: Time of Change* (Ed. by J.H. Wrenn, J.-P. Suc & S.A.G. Leroy) *Amer. Assoc. Stratigr. Palynol. Found.*, 49–63.

Cita, M.B., Santambrogio, S., Melillo, B. & Rogate, F. (1990) Messinian paleoenvironments: new evidence from the Tyrrhenian Sea (ODP Leg 107). In: *Leg 107* (Ed. by K.A. Kastens & J. Mascle, *et al.*) *Init. Rep. Deep Sea Drill. Proj., Sci. Res.*, **107**, 211–227.

Cita, M.B., Wright, R.C., Ryan, W.B.F. & Longinelli, A. (1978) Messinian paleoenvironments. In: *Leg 42A* (Ed. by K. Hsü & L. Montadert, *et al.*) *Init. Rep. Deep Sea Drill. Proj., Sci. Res.*, **42**(1), 1003–1025.

Civis, J. (1977) Estudios de los Foraminiferos del afloramiento pliocenico de Can Albareda (Barcelona), analisis paleogeologico et biostratigrafico. *Stud. Geol.*, **13**, 105–126.

Clauzon, G. (1973) The eustatic hypothesis and the Pre-Pliocene cutting of the Rhône Valley. In: *Leg 13* (Ed. by W.B.F. Ryan & K.J. Hsü) *Init. Rep. Deep Sea Drill. Proj.*, **13**(2), 1251–1256.

Clauzon, G. (1978) The Messinian Var canyon (Provence, Southern France) – paleogeographic implications. *Mar. Geol.*, **27**, 231–246.

Clauzon, G. (1980a) Le canyon messinien de la Durance (Provence, France): une preuve paléogéographique du basin profond de dessiccation. *Palaeogeogr. Palaeoclimatol. Palaeoecol.*, **29**, 15–40.

Clauzon, G. (1980b) Révision de l'interprétation géodynamique du passage miocène-pliocène dans le bassin de Vera (Espagne méridionale): les coupes d'Antas et de Cuevas del Almanzora. *Riv. Ital. Paleont.*, **86** (1), 203–214.

Clauzon, G. (1982) Le canyon messinien du Rhône: une preuve décisive du "desiccated deep-basin model" (Hsü, Cita et Ryan, 1973). *Bull. Soc. Géol. France, Ser. 7*, **24**(3), 597–610.

Clauzon, G. (1990) Restitution de l'évolution géodynamique néogène du bassin du Roussillon et de l'unité adjacente des Corbières d'après les données écostratigraphiques et paléogéographiques. *Paléobiol. Cont.*, **17**, 125–155.

Clauzon, G. & Cravatte, J. (1985) Révision chronostratigraphique de la série marine pliocène traversée par le sondage Canet (Pyrénées orientales): apports à la connaissance du Néogène du Roussillon. *C. R. Acad. Sci. Paris, Ser. 2*, **301**, 1351–1354.

Clauzon, G., Rubino, J.-L. & Casero, P. (1997) Regional modalities of the Messinian Salinity Crisis in the framework of two phases model. In: *Neogene Basins of the Mediterranean Region: Controls and Correlation in Space and Time* (Ed. by M. Grasso & F. Lentini), pp. 44–46. R.C.M.N.S. Inter.-Coll., Catania, Program and Abstracts.

Clauzon, G., Suc, J.-P., Aguilar, J.-P., Ambert, P., Cappetta, H., Cravatte, J., Drivaliari, A., Doménech, R., Dubar, M., Leroy, S., Martinell, J., Michaux, J., Roiron, P., Rubino, J.-L., Savoye, B. & Vernet, J.-L. (1990) Pliocene geodynamic and climatic evolutions in the French Mediterranean region. *Paleontologia i Evolucio*, **Spec. Vol. 2**, 132–186.

Clauzon, G., Suc, J.-P., Gautier, F., Berger, A. & Loutre, M.-F. (1996) Alternate interpretation of the Messinian salinity crisis: controversy resolved? *Geology*, **24** (4), 363–366.

Clauzon, G., Suc, J.-P., Popescu, S.-M., Marunţeanu, M., Rubino, J.-L., Marinescu, F. & Melinte, M.C. (2005) Influence of the Mediterranean sea-level changes over the Dacic Basin (Eastern Paratethys) in the Late Neogene. The Mediterranean Lago Mare facies deciphered. *Bas. Res.*, **17**, 437–462.

Clauzon, G., Suc, J.-P., Dumurdžanov, N., Melinte-Dobrinescu, M.C. & Zagorchev, I. (2008) The Pliocene Gilbert-type fan delta of Dračevo (Skopje area, Republic of Macedonia): paleogeographic inference. *Geol. Macedonica*, **2**, 21–28.

Clauzon, G., Suc, J.-P., Melinte-Dobrinescu, M.C., Jouannic, G., Jolivet, L., Rubino, J.-L., Popescu, S.-M., Gorini, C., Bache, F. & Estrada, F. (2009) New insights from the Andalusian Sorbas and Vera basins. *Acta Nat. Ateneo Parm.*, **45** (1–4), 334–335.

Comas, M.C., Platt, J.P., Soto, J.I. & Watts, A.B. (1999) The origin and tectonic history of the Alboran Basin: Insights from leg 161 results. In: *Leg 161* (Ed. by R. Zhan, M.C. Comas & A. Klaus) *Proc. Ocean Drill. Progr.*, **161**, 555–580.

Cornée, J.-J., Ferrandini, M., Saint Martin, J.P., Münch, P., Moullade, M., Ribaud-Laurenti, A., Roger, S., Saint Martin, S. & Ferrandini, J. (2006) The late Messinian erosional surface and the subsequent reflooding in the Mediterranean: new insights from the Melilla–Nador basin (Morocco). *Palaeogeogr. Palaeoclimatol. Palaeoecol.*, **230**, 129–154.

Cosentino, D., Cipollari, P., Faranda, C., Florindo, F., Gennari, R., Gliozzi, E., Grossi, F., Laurenzi, M.A., Lo Mastro, S., Sampalmiero, G. & Sprovieri, M. (2009) Integrated analyses of the Maccarone section (northern Apennines, Italy). 13ème Congrès RCMNS Naples. *Acta Nat. Ateneo Parm.*, **45**(1–4), 338–339.

Cravatte, J., Dufaure, P., Prim, M. & Rouaix, S. (1974) Les sondages du Golfe du Lion: stratigraphie, Sédimentologie. *Notes et Mémoires de la Compagnie Française des Pétroles*, **11**, 209–274.

Csato, I., Kendall, C.G.StC. & MOORE, P.D. (2007) The Messinian problem in the Pannonian Basin, Eastern Hungary – Insights from stratigraphic simulations. *Sedim. Geol.*, **201**, 111–140.

Dalla, S., Harby, H. & Serazzi, M. (1997) Hydrocarbon exploration in a complex incised valley fill: an example from the late Messinian Abu Madi Formation (Nile Delta Basin, Egypt). *Lead. Edge*, **16**, 1819–1824.

Decima, A. & Wezel, F. (1971) Osservazioni sulle evaporiti messiniane della Sicilia centro-meridionale. *Riv. Min. Sicil.*, **130–132**, 172–187.

Demarest, J.M. & Kraft, J.C. (1987) Stratigraphic record of Quaternary sea levels: implications for more ancient strata. In: *Sea-Level Fluctuation and Coastal Evolution* (Ed. by D. Nummedal, O.H. Pilkey & J.D. Howard) *SEPM Spec. Publ.*, **41**, 223–240.

Denizot, G. (1952) Le Pliocène dans la vallée du Rhône. *Rev. Géogr. Lyon*, **27**, 327–357.

Dos Reis, A.T. (2001). *La Tectonique Salifère et son Influence sur L'architecture Sédimentaire Quaternaire de la Marge du Golfe du Lion – Méditerranée Occidentale*. PhD Thesis, Université Pierre et Marie Curie, Paris.

Dos Reis, A.T., Gorini, C. & Mauffret, A. (2005) Implications of Salt-sediment interactions for the Architecture of the Gulf of Lions deep-water sedimentary systems – Western Mediterranean Sea. *Mar. Petr. Geol.*, **22** (6–7), 713–746.

Dos Reis, A.T., Gorini, C., Weibull, W., Perovano, R., Mepen, M. & Ferreira, E. (2008) Radial gravitacional gliding indicated by subsalt relief and salt-related structures: the example of the gulf of Lions, western Mediterranean. *Braz. J. Geophy.*, **26** (3), 347–365.

Drake, N.A., EL-Hawat, A.S. & Salem, M.J. (2008) The Development, Decline and Demise of the As Sahabi River System over the Last Seven Million Years. *Garyounis Sci. Bull.* (Spec. Issue), **5**, 95–109.

Drivaliari, A., Ţicleanu, N., Marinescu, F., Marunţeanu, M. & Suc, J.-P. (1999) A Pliocene climatic record at Ţicleni (Southwestern Romania). In: *The Pliocene: Time of Change* (Ed. by J.H. Wrenn, J.-P. Suc & S.A. G Leroy) *Amer. Assoc. Stratigr. Palynol. Found.*, 103–108.

El Euch – El Koundi, N., Ferry, S., Suc, J.-P., Clauzon, G., Melinte-Dobrinescu, M.C., Safra, A. & Zargouni, F. (2009) Messinian deposits and erosion in northern Tunisia. Inferences on the Sicily Strait during the Messinian Salinity Crisis. *Terra Nova*, **21**, 41–48.

Estrada, F., Ercilla, G., Gorini, C., Alonso, B., Vazquez, J. T., Garcia-Castellanos, D., Juan, C., Maldonado, A., Ammar, A. & Elabbassi, M. (2011) Impact of Atlantic water inflow into the Alboran Basin at the time of the Zanclean flooding. *Geo. Mar. Lett.*, in press. DOI 10.1007/s00367-011-0249-8.

Fauquette, S., Suc, J.-P., Bertini, A., Popescu, S.-M., Warny, S., Bachiri Taoufiq, N., Perez Villa, M.-J., Chikhi, H., Subally, D., Feddi, N., Clauzon, G. & Ferrier, J. (2006) How much did climate force the Messinian salinity crisis? Quantified climatic conditions from pollen records in the Mediterranean region. *Palaeogeogr. Palaeoclimatol. Palaeoecol.*, **238**, 281–301.

Fortuin, A.R. & Krijgsman, W. (2003) The Messinian of the Nijar Basin (SE Spain): sedimentation, depositional environments and paleogeographic evolution. *Sedim. Geol.*, **160**, 213–242.

Gačić, M., Poulain, P.-M., Zore-Armanda, M. & Barale, V. (2002) Overview. In: *Physical oceanography of the Adriatic Sea. Past, present, future* (Ed. by B. Cushman-Roisin, M. Gačić, P.-M. Poulain & A. Artegiani), pp. 1–44. Kluwer Academic Publishers, Dordrecht, The Netherlands.

Garcia, M., Maillard, A., Aslanian, D., Rabineau, M., Alonso, B., Gorini, C. & Estrada, F. (2011) The Catalan margin during the Messinian Salinity Crisis: physiography, morphology and sedimentary record. *Mar. Geol.*, **284**, 158–174.

Garcia-Castellanos, D., Estrada, F., Jiménez-Munt, I., Gorini, C., Fernàndez, M., Vergés, J. & De Vicente, R. (2009) Catastrophic flood of the Mediterranean after the Messinian salinity crisis. *Nature*, **462**, 778–781.

García-García, F., Corbí, H., Soria, J.M. & Viseras, C. (2011) Architecture analysis of a river flood-dominated delta during an overall sea-level rise (early Pliocene, SE Spain). *Sedim. Geol.*, **237**, 102–113.

Gaullier, V. (1993) *Diapirisme Salifère et Dynamique Sédimentaire Dans le Bassin Liguro-Provençal*. PhD Thesis, Université de Rennes, Rennes.

Gautier, F., Clauzon, G., Suc, J.-P., Cravatte, J. & Violanti, D. (1994) Age et durée de la crise de salinité messinienne. *C. R. Acad. Sci. Paris, Ser. 2*, **318**, 1103–1109.

Gennari, R., Iaccarino, S.M., di Stefano, A., Sturiale, G., Cipollari, P., Manzi, V., Roveri, M. & Cosentino, D. (2008) The Messinian – Zanclean boundary in the Northern Apennine. *Stratigraphy*, **5** (3–4), 307–322.

Gennesseaux, M. & Lefebvre, D. (1980) Le Golfe du Lion et le Paléo-Rhône messinien. *Géol. Médit.*, **7**, 71–80.

Gilbert, G.K. (1885) The topographic features of lake shores. *U.S. Geol. Survey Rep.*, **5**, 75–123.

Gilbert, G.K. (1890) Lake Bonneville. *Monogr. U.S. Geol. Survey*, **1**, 1–438.

Gillet, H., Lerocilais, G. & Réhault, J.-P. (2007) Messinian event in the black sea: evidence of a Messinian erosional surface. *Mar. Geol.*, **244**, 142–165.

Glover, C. & Robertson, A. (1998) Neotectonic intersection of the Aegean and Cyprus tectonic arcs: extensional and strike-slip faulting in the Isparta Angle, SW Turkey. *Tectonophysics*, **298**, 103–132.

Gorini, C. (1993) *Géodynamique D'une Marge Passive: Le Golfe du Lion (Méditeranée Occidentale)*. PhD Thesis, Université Paul Sabatier, Toulouse.

Gorini, C., Le Marrec, A. & Mauffret, A. (1993) Contribution to the structural and sedimentary history of the Gulf of Lions (Western Mediterranean) from the ECORS profiles, industrial seismic profiles and well data. *Bull. Soc. Géol. France*, **164**, 353–363.

Goudie, A.S. (2005) The drainage of Africa since the Cretaceous. *Geomorphology*, **67**, 437–456.

Govers, R. (2009) Choking the Mediterranean to dehydration: the Messinian salinity crisis. *Geology*, **37** (2), 167–170.

Griffin, D.L. (2002) Aridity and humidity: two aspects of the late Miocene climate of North Africa and the Mediterranean. *Palaeogeogr. Palaeoclimatol. Palaeoecol.*, **182**, 65–91.

Guennoc, P., Gorini, C. & Mauffret, A. (2000) Histoire géologique du Golfe du Lion et cartographie du rift oligo-aquitanien et de la surface messinienne. *Géol. France*, **3**, 67–97.

Guillocheau, F., Dabard, M.P., Robin, C. & Loi, A. (2009) *Les dépôts de tempêtes. Des domaines marins ouverts aux milieux restreints.* Vol. 65 Livre Association des Sédimentologues Français, Rennes. 102 pp.

Haxby, W.F., Melkonian, A.K., Coplan, J., Chan, S.-M. & Ryan, W.B.F. (2010) GeoMapApp freeware software, v.2.3. Lamont-Doherty Earth Observatory, Palisades, http://jgs.geoscienceworld.org/cgi/content/full/168/2/333.

Hardenbol, J., Thierry, J., Farley, M.B., Jacquin, T., de Graciansky, P.-C. & Vail, P.R. (1998) Mesozoic and Cenozoic sequence chronostratigraphic framework of European Basins. In: *Mesozoic and Cenozoic sequence stratigraphy of European Basins* (Ed. by P.-C. De Graciansky, J. Hardenbol, T. Jacquin, & P.R. Vail), *SEPM Spec. Publ.*, **60**, 3–13.

Hilgen, F.J. & Langereis, C.G. (1989) Periodicities of $CaCO_3$ cycles in the Pliocene of Sicily: discrepancies with the quasi-periods of the Earth's orbital cycles? *Terra Nova*, **1**, 409–415.

Hilgen, F.J. & Langereis, C.G. (1993) A critical re-evaluation of the Miocene/Pliocene boundary as defined in the Mediterranean. *Earth Planet. Sci. Lett.*, **118**, 167–179.

Homewood, P., Guillocheau, F., Eschard, R. & Cross, T.A. (1992) Corrélations haute résolution et stratigraphie génétique: une démarche intégrée. *Bull. Centres Rech. Explor.-Prod. Elf-Aquitaine*, **16**, 357–381.

Hsü, K.J., Cita, M.B. & Ryan, W.B.F. (1973) The origin of the Mediterranean evaporites. In: *Leg 13* (Ed. by W.B.F. Ryan & K.J. Hsü *et al.*), *Init. Rep. Deep Sea Drill. Proj.*, **13**, 1203–1231.

Iaccarino, S. & Bossio, A. (1999) Paleoenvironment iof uppermost Messinian sequences in the Western Mediterranean (Sites 974, 975, and 978). In: *Leg 161* (Ed. by R. Zahan, M.C. Comas & A. Klaus), *Proc. Ocean Drill. Progr., Sci. Results*, **161**, 529–541.

Jolivet, L., Augier, R., Robin, C., Suc, J.-P. & Rouchy, J.M. (2006) Lithospheric-scale geodynamic context of the Messinian salinity crisis. *Sedim. Geol.*, **188–189**, 9–33.

Karistineos, N.K. & Georgiades-Dikeoulia, E. (1985-86) The marine transgression in the Serres Basin. *Ann. Géol. Pays Hellén., Ser. 1*, **33**, 1.

Krijgsman, W. & Garcés, M. (2004) Palaeomagnetic constraints on the geodynamic evolution of the Gibraltar Arc. *Terra Nova*, **16**, 281–287.

Krijgsman, W., Hilgen, F.J., Marabini, S. & Vai, G.B. (1999a) New paleomagnetic and cyclostratigraphic age constraints on the Messinian of the Northern Apennines (Vena del Gesso Basin, Italy). *Mem. Soc. Geol. It.*, **54**, 25–33.

Krijgsman, W., Hilgen, F.J., Raffi, J., Sierro, F.J. & Wilson, D.S. (1999b) Chronology, causes and progression of the Messinian salinity crisis. *Nature*, **400**, 652–655.

Krijgsman, W. & Meijer, P.TH. (2008) Depositional environments of the Mediterranean "Lower Evaporites" of the Messinian salinity crisis: constraints from quantitative analyses. *Mar. Geol.*, **253**, 73–81.

Laskar, J., Robutel, P., Joutel, F., Gastineau, M., Correia, A.C.M. & Levrard, B. (2004) A long term numerical solution for the insolation quantities of the Earth. *Astron. Astrophys.*, **428**, 261–285.

Leckie, D.A. (1994) Canterbury Plains, New Zealand – implications for sequence stratigraphic models. *Bull. Am. Assoc. Petrol. Geol.*, **78**, 1240–1256.

Lefèbvre, D. (1980) *Evolution Morphologique et Structurale du Golfe du Lion. Essai de Traitement Statistique des Données*. PhD Thesis, Université Pierre et Marie Curie, Paris.

Li, X.S., Berger, A., Loutre, M.-F., Maslin, M.A., Haug, G. H. & Tiedemann, R. (1998) Simulating late Pliocene Northern Hemisphere climate with the LLN-2D model. *Geophys. Res. Lett.*, **25**, 915–918.

Lofi, J. (2002) *La Crise de Salinité Messinienne: Conséquences Directes et Différées sur L'évolution Sédimentaire de la Marge du Golfe du Lion*. PhD Thesis, Université des Sciences et Techniques, Lille.

Lofi, J., Rabineau, M., Gorini, C., Berné, S., Clauzon, G., de Clarens, P., Dos Reis, T., Mountain, G.S., Ryan, W.B.F., Steckler, M. & Fouchet, C. (2003) Plio-Quaternary prograding clinoform wedges of the Western Gulf of Lions continental margin (NW Mediterranean) after the Messinian Salinity Crisis. *Mar. Geol.*, **198**, 289–317.

Lofi, J., Gorini, C., Berné, S., Clauzon, G., Dos Reis, A.T., Ryan, W.B.F. & Steckler, M.S. (2005) Erosional processes and paleo-environmental changes in the western gulf of Lions (SW France) during the Messinian salinity crisis. *Mar. Geol.*, **217**, 1–30.

Lofi, J. & Berné, S. (2008) Evidences for Pre-Messinian submarine canyons incisions on the Gulf of Lions Miocene slope (Western Mediterranean). *Mar. Petr. Geol.*, **25** (8), 804–817.

Lofi, J., Sage, F., Déverchére, J., Loncke, L., Maillard, A., Gaullier, V., Thinon, I., Gillet, H., Guennoc, P. & Gorini, C. (2011) Refining our knowledge of the Messinian Salinity Crisis records in the offshore domain through Multi-site seismic analysis. *Bull. Soc. Géol. France*, **182** (2), 163–180.

Loget, N., van den Driessche, J. & Davy, P. (2005) How did the Messinian Salinity Crisis end? *Terra Nova*, **17**, 414–419.

Londeix, L., Benzakour, M., de Vernal, A., Turon, J.-L. & Suc, J.-P. (1999) Late Neogene dinoflagellate cyst assemblages from the Strait of Sicily, Central Mediterranean Sea: paleoecological and biostratigraphical implications. In: *The Pliocene: Time of Change* (Ed. by J.H. Wrenn, J.-P. Suc & S. A. G Leroy) *Amer. Assoc. Stratigr. Palynol. Found.*, 65–91, Dallas.

Londeix, L., Benzakour, M., Suc, J.-P. & Turon, J.-L. (2007) Messinian palaeoenvironments and hydrology in Sicily (Italy): the dinoflagellate cyst record. *Geobios*, **40**, 233–250.

Lourens, L.J., Hilgen, F.J., Laskar, J., Shackleton, N.J. & Wilson, D. (2004) The neogene period. In: *A Geological Time Scale* (Ed. by F. Gradstein, J. Ogg & A. Smith), pp. 409–440, Cambridge University Press, Cambridge.

Lugli, S., Manzi, V. & Roveri, M. (2008) New facies interpretation of the Messinian evaporites in the Mediterranean. *CIESM Workshop Monogr*, **33**, 67–72.

Maillard, A., Gorini, C., Mauffret, A., Sage, F., Lofi, J. & Gaullier, V. (2006) Offshore evidence of polyphase erosion in the Valencia basin (Northwestern Mediterranean): scenario for the Messinian Salinity Crisis. *Sedim. Geol.*, **188–189**, 69–91.

Manzi, V., Lugli, S., Roveri, M. & Schreiber, C. (2009) A new facies model for the Upper Gypsum of Sicily (Italy): chronological and palaeoenvironmental constraints for the Messinian salinity crisis in the Mediterranean. *Sedimentology*, **56**, 1937–1960.

Mary, C., Iaccarino, S., Courtillot, V., Besse, J. & Aissaoui, D.M. (1993) Magnetostratigraphy of Pliocene sediments from the Stirone River (Po Valley). *Geophys. J. Int.*, **112**, 359–380.

Matias I Sendra, I. (1990) *Els Nannofossils Calcaris del Plioce de la Mediterrania Nord-Occidental*. PhD Thesis, University of Barcelona, Barcelona.

Mauffret, A., Ammar, A., Gorini, C. & Jabour, H. (2007) The Alboran Sea (Western Mediterranean) revisited with a view from the Moroccan Margin. *Terra Nova*, **19**, 195–203.

Meijer, P.Th. & Krijgsman, W. (2005) A quantitative analysis of the desiccation and re-filling of the Mediterranean during the Messinian Salinity Crisis. *Earth Planet. Sci. Lett.*, **240**, 510–520.

Melinte-Dobrinescu, M.C., Suc, J.-P., Clauzon, G., Popescu, S.-M., Armijo, R., Meyer, B., Biltekin, D., Çağatay, M.N., Ucarkus, G., Jouannic, G., Fauquette, S. & Çakir, Z. (2009) The Messinian Salinity Crisis in the Dardanelles region: chronostratigraphic constraints. *Palaeogeogr. Palaeoclimatol. Palaeoecol.*, **278**, 24–39.

Miller, K.G., Kominz, M.A., Browning, J.V., Wright, J.D., Mountain, G.S., Katz, M.E., Sugarman, P.J., Cramer, B. S., Christie-Blick, N. & Pekar, S.F. (2005) The Phaneorozoic record of global sea-level change. *Science*, **310**, 1293–1298.

Montadert, L., Nicolaides, S., Semb, P.H. & Lie, Ø. (2011) Petroleum systems offshore Cyprus. In: *Petroleum Systems of the Tethyan Region* (Ed. by L. Marlow, C. Kendall & L. Yose) *Amer. Assoc. Petrol. Geol., Spec. Publ.*, in press.

Nemec, W. (1990) Aspects of sediment movement on steep delta slopes. *Spec. Publs int. Ass. Sediment.*, **10**, 29–73.

Néraudeau, D. (2007) Les bioaccumulations néogènes (calcaires à algues, faluns) d'Europe occidentale et leurs relations avec la crise messinienne. *C. R. Palevol.*, **6**, 59–71.

Néraudeau, D., Goubert, E., Lacour, D. & Rouchy, J.M. (2001) Changing biodiversity of Mediterranean irregular echinoids from the Messinian to the Present-Day. *Palaeogeogr. Palaeoclimatol. Palaeoecol.*, **175**, 43–60.

Nesteroff, W. & Glaçon, G. (1977) Le caractère rythmique des evaporites messiniennes en Méditerranée orientale (coupe d'Eraclea Minoa, Sicile). *Bull. Soc. Géol. France, Ser. 7*, **19**, 489–500.

Nicolai, C. (2008) Tracing the As Sahabi Channel System in the Ajdabita Trough, Central Sirt Basin, Lybia. *Garyounis Sci. Bull.* (Spec. issue), **5**, 85–94.

Odin, G.S., Ricci Lucchi, F., Tateo, F., Cosca, M. & Hunziker, J.C. (1997) Integrated stratigraphy of the Maccarone section, Late Messinian (Marche region, Italy). In: *Miocene Stratigraphy – An Integrated Approach* (Ed. by A. Montanari, G.S. Odin & R. Coccioni), pp. 529–544, Elsevier, Amsterdam.

Ott D'estevou, P., Montenat, C. & Alvado, J.-C. (1990) Le basin de Vera – Garrucha. *Doc. Trav. IGAL*, **12–13**, 165–187.

Paillou, P., Schuster, M., Tooth, S., Farr, T., Rosenqvist, A., Lopez, S. & Malezieux, J.-M. (2009) Mapping of a major paleodrainage system in eastern Lybia using orbital imaging radar: the Kufrah River. *Earth Planet. Sci. Lett.*, **277**, 327–333.

Pierre, C., Caruso, A., Blanc-Valleron, M.-M., Rouchy, J. M. & Orszag-Sperber, F. (2006) Reconstruction of the paleoenvironmental changes around the Miocene–Pliocene boundary along a West–East transect across the Mediterranean. *Sedim. Geol.*, **188–189**, 319–340.

Pierre, C. & Fontes, J.-C. (1979) Oxygène 18, carbone 13, deutérium et soufre 34: marqueurs géochimiques de la diagenèse et du paléomilieu évaporitiques du Messinien de la Méditerranée. *Bull. Mus. Nat. Hist. Nat. Paris,* Ser. 4, Sect. C, **1**, 3–18.

Pierre, C., Rouchy, J.-M. & Blanc-Valleron, M.-M. (1998) Sedimentological and stable isotope changes at the Messinian/Pliocene boundary in the Eastern Mediterranean (Holes 968A, 969A, and 969B). In: *Leg 160* (Ed. by A.H.F. Robertson & K.-C. Emeis *et al.*) *Proc. Ocean Drill. Progr., Sci. Results*, **160**, 3–8.

Poisson, A., Orszag-Sperber, F., Kosun, E., Bassetti, M.A., Müller, C., Wernli, R. & Rouchy, J.M. (2011) The Late Cenozoic evolution of the Aksu basin (Isparta angle; SW

Turkey). New insights. *Bull. Soc. Géol. France*, **182** (2), 133–148.

Popescu, S.-M. (2001) Repetitive changes in Early Pliocene vegetation revealed by high-resolution pollen analysis: revised cyclostratigraphy of southwestern Romania. *Rev. Palaeobot. Palynol.*, **120**, 181–202.

Popescu, S.-M. (2006) Late Miocene and early Pliocene environments in the southwestern Black Sea region from high-resolution palynology of DSDP Site 380A (Leg 42B). *Palaeogeogr. Palaeoclimatol. Palaeoecol.*, **238**, 64–77.

Popescu, S.-M., Biltekin, D., Winter, H., Suc, J.-P., Melinte-Dobrinescu, M.C., Klotz, S., Combourieu-Nebout, N., Rabineau, M., Clauzon, G. & Deaconu, F. (2010) Pliocene and Lower Pleistocene vegetation and climate changes at the European scale: long pollen records and climatostratigraphy. *Quat. Intern.*, **219**, 152–167.

Popescu, S.-M., Melinte, M., Suc, J.-P., Clauzon, G., Quillévéré, F. & Sütő-Szentai, M. (2008) Marine reflooding of the Mediterranean after the Messinian Salinity Crisis predates the Zanclean GSSP. Reply to the "Comment to, 'Earliest Zanclean age for the Colombacci and uppermost Di Tetto formations of the "latest Messinian" northern Apennines: new palaeoenvironmental data from the Maccarone section (marche Province, Italy)' by Popescu *et al.* (2007) Geobios 40 (359-373)" authored by Roveri *et al. Geobios*, **41**, 657–660.

Popescu, S.-M., Dalesme, F., Jouannic, G., Escarguel, G., Head, M.J., Melinte-Dobrinescu, M.C., Sütő-Szentai, M., Bakrac, K., Clauzon, G. & Suc, J.-P. (2009) *Galeacysta etrusca* complex, dinoflagellate cyst marker of Paratethyan influxes into the Mediterranean Sea before and after the peak of the Messinian Salinity Crisis. *Palynology*, **33** (2), 105–134.

Popescu, S.-M., Krijgsman, W., Suc, J.-P., Clauzon, G., Marunţeanu, M. & Nica, T. (2006b) Pollen record and integrated high-resolution chronology of the Early Pliocene Dacic Basin (Southwestern Romania). *Palaeogeogr. Palaeoclimatol. Palaeoecol.*, **238** (1–4), 78–90.

Popescu, S.-M., Suc, J.-P. & Loutre, M.-F. (2006a) Early Pliocene vegetation changes forced by eccentricity-precession. Example from Southwestern Romania. *Palaeogeogr. Palaeoclimatol. Palaeoecol.*, **238** (1–4), 340–348.

Popescu, S.-M., Suc, J.-P., Melinte, M., Clauzon, G., Quillévéré, F. & Sütő-Szentai, M. (2007) Earliest Zanclean age for the Colombacci and uppermost Di tetto formations of the "latest Messinian" northern Apennines: new palaeoenvironmental data from the Maccarone section (Marche Province, Italy). *Geobios*, **40** (3), 359–373.

Rabineau, M., Berné, S., Aslanian, D., Olivet, J.-L., Joseph, P., Guillocheau, F., Bourillet, J.-L., Ledrezen, E. & Granjeon, D (2005) Sedimentary sequences in the Gulf of Lions: a record of 1000,000 years climatic cycles. *Mar. Pet. Geol.*, **22**, 775–804.

Rabineau, M., Berné, S., Olivet, J.-L., Aslanian, D., Guillocheau, F. & Joseph, P. (2006) Paleo sea levels reconsidered from direct observation of paleoshoreline position during Glacial Maxima (for the last 500,000 yr). *Earth Planet. Sci. Lett.*, **252**, 119–137.

Raffi, I., Backman, J., Fornaciari, E., Palike, H., Rio, D., Lourens, L. & Hilgen, F. (2006) A review of calcareous nannofossil astrobiochronology encompassing the past 25 million years. *Quat. Sci. Rev.*, **25**, 3113–3137.

Rouchy, J.M. & Caruso, A. (2006) The Messinian salinity crisis in the Mediterranean basin: a reassessment of the data and an integrated scenario. *Sedim. Geol.*, **188–189**, 35–67.

Rouchy, J.-M., Orszag-Sperber, F., Blanc-Valleron, M.-M., Pierre, C., Riviere, M., Combourieu-Nebout, N. & Panayides, I. (2001) Paleoenvironmental changes at the Messinian-Pliocene boundary in the Eastern Mediterranean (southern Cyprus basins): significance of the Messinian Lago-Mare. *Sedim. Geol.*, **145**, 93–117.

Roveri, M., Bassetti, M.A. & Ricci Lucchi, F. (2001) The Mediterranean Messinian salinity crisis: an Apennine foredeep perspective. *Sedim. Geol.*, **140**, 201–214.

Roveri, M. & Manzi, V. (2006) The Messinian salinity crisis: looking for a new paradigm? *Palaeogeogr. Palaeoclimatol. Palaeoecol.*, **238**, 386–398.

Roveri, M., Manzi, V., Gennari, R., Iaccarino, S.M. & Lugli, S. (2008a) Recent advancements in the Messinian stratigraphy of Italy and their Mediterranean-scale implications. *Boll. Soc. Paleontol. Ital.*, **47** (2), 71–85.

Roveri, M., Lugli, S., Manzi, V. & Schreiber, C. (2008b) The Messinian Sicilian stratigraphy revisited: new insights for the Messinian salinity crisis. *Terra Nova*, **20**, 483–488.

Ryan, W.B.F. (1978) Messinian badlands on the southeastern margin of the Mediterranean Sea. *Mar. Geol.*, **27**, 349–363.

Ryan, W.B.F. (2011) Geodynamics responses to a two-step model of the Messinian salinity crisis. *Bull. Soc. Géol. France*, **182** (2), 73–78.

Ryan, W.B.F. & Cita, M.B. (1978) The nature and distribution of Messinian erosional surface – indication of a several kilometer-deep Mediterranean in the Miocene. *Mar. Geol.*, **27**, 193–230.

Said, R. (1982) The geological evolution of the River Nile in Egypt. *Z. Geomorph.*, **26** (3), 305–314.

Savoye, B. & Piper, D.J.W. (1991) The Messinian event on the margin of the Mediterranean Sea in the Nice arc, southern France. *Mar. Geol.*, **97**, 279–304.

Schrader, H.-J. (1978) Quaternary through Neogene history of the Black Sea, deduced from the paleoecology of diatoms, silicoflagellates, ebridians, and chrysomonads. In: *Leg 42B* (Ed. by D.A. Ross & Y.P. Neprochnov *et al.*) *Init. Rep. Deep Sea Drill. Proj.*, **42**(2), 789–901.

Semenenko, V.N. (1995)Geological events at the Miocene/Pliocene boundary in the Eastern Paratethys. *Geol. Soc. Greece*,**4** (Spec. Publ.), 264–268.

Snel, E., Marunţeanu, M., Macaleţ, R., Meulenkamp, J.E. & van Vugt, N. (2006) Late Miocene to Early Pliocene chronostratigraphic framework for the Dacic Basin, Romania. *Palaeogeogr. Palaeoclimatol. Palaeoecol.*, **238** (1–4), 107–124.

Soria, J.M., Caracuel, J.E., Corbí, H., Dinarès-Turell, J., Lancis, C., Tent-Manclús, J.E., Viseras, C. & Yébenes, A. (2008) The Messinian–early Pliocene stratigraphic record in the southern Bajo Segura Basin (Betic Cordillera, Spain): implications for the Mediterranean salinity crisis. *Sedim. Geol.*, **203**, 267–288.

Sprovieri, R., di Stefano, E., Bonomo, S., Tamburini, F. & Mckenzie, J. (2007) The Messinian – Pliocene boundary in the north Italy. *Geophys. Res. Abstracts*, **9**, 06041.

Steckler, M.S. & Watts, A.B. (1980) The Gulf of Lion: subsidence of a young continental margin. *Nature*, **287**, 425–429.

Suc, J.-P. & Bessais, E. (1990) Pérennité d'un climat thermoxérique en Sicile, avant, pendant, après la crise de salinité messinienne. *C. R. Acad. Sci. Paris, Ser. 2*, **310**, 1701–1707.

Suc, J.-P., Clauzon, G., Armijo, R., Meyer, B., Melinte-Dobrinescu, M.C., Popescu, S.-M., Lericolais, G., Gillet, H., ÇağAtay, M.N., Jouannic, G., Brun, J.-P., Sokoutis, D., Ucarkus, G. & Çakir, Z. (2009) The Messinian Salinity Crisis in the Northeastern Aegean – Black Sea region. 13rd RCMNS Congress, Naples. *Acta Nat. Ateneo Parm.*, **45**(1/4), 116–117.

Suc, J.-P., Violanti, D., Londeix, L., Poumot, C., Robert, C., Clauzon, G., Turon, J.-L., Ferrier, J., Chikhi, H., Cambon, G. & Gautier, F. (1995) Evolution of the Messinian Mediterranean environments: the Tripoli Formation at Capodarso (Sicily, Italy). *Rev. Palaeobot. Palynol.*, **87**, 51–79.

Sunamura, T. (1987) Coastal cliff erosion in Nii-Jima Island, Japan: present, past and future. In: *International Geomorphology 1986 Part I. First International Conference on Morphology Proceedings* (Ed. by V. Gardiner), Wiley, Chichester, pp. 1199–1212.

van Couvering, J.A., Castradori, D., Cita, M.B., Hilgen, F. J. & Rio, D. (2000) The base of the Zanclean Stage and of the Pliocene Series. *Episodes*, **23** (3), 179–187.

Violanti, D., Dela Pierre, F., Trenkwalder, S., Lozar, F., Clari, P., Irace, A. & D'atri, A. (2011) Biostratigraphic and palaeoenvironmental analyses of the Messinian/Zanclean boundary and Zanclean succession in the Moncucco quarry (Piedmont, Northwestern Italy). *Bull. Soc. Géol. France*, **182** (2), 149–162.

Warny, S., Bart, P.J. & Suc, J.-P. (2003) Timing and progression of climatic, tectonic and glacioeustatic influences on the Messinian Salinity Crisis. *Palaeogeogr. Palaeoclimatol. Palaeoecol.*, **202**, 59–66.

Zheng, Z. & Cravatte, J. (1986) Etude palynologique du Pliocène de la Côte d'Azur (France) et du littoral ligure (Italie). *Geobios*, **19** (6), 815–823.

Manuscript received 15 July 2010; In revised form 18 June 2011; Manuscript accepted 01 July 2011.

Quantification of Pliocene-Quaternary Subsidence and isostatic readjustment related to the Messinian Crisis (using paleobathymetric markers in the G*ulf of Lion)*

M. Rabineau(1), E. Leroux(1, 3), F. Bache(2), D. Aslanian(3), C. Gorini(4), M. Moulin(5), S. Molliex (1), L. Droz (1), T. Dos Reis(6), JL Rubino (8), JL Olivet(3)

CNRS, UMR6538, Domaines Océaniques, IUEM, 29280 Plouzané, France

IFREMER, DRO/GM,BP 70, 29280 Plouzané, France

(2012)

Abstract

The sedimentary record of the offshore part of continental margins is characterized by an important tectonic and thermic subsidence, which favours a good preservation of sedimentary sequences (as opposed generally to the onshore part of margins). This sedimentation in turn enhances the subsidence because of loading effects. The quantification of this total postrift subsidence and more specifically deciphering the relative effect of the different factors is not easy, especially when no wells are available in the area. We present here a direct estimation based on the geometry and the interpretation of sedimentary markers as seen on seismic data, in the *Gulf of Lion*, to evaluate total subsidence rate from the coast to the outer shelf and in the deep sea from the end of Messinian to present day (the last circa 5.6 Ma) with minimal assumptions.

On the shelf, the Pliocene-Quaternary subsidence shows a seaward tilting reaching a rate of 240-260 m/Ma at the shelf break (70 km from the present day coastline), i.e. a total angle of rotation of 0.88°, with a hinge point (rotation point) located 13 km landward of present day coastline (around Sète city). This rate is the same as the rate calculated for the last 500,000 years at 70 Km (Rabineau *et al.*, 2006, 2007). This suggests that subsidence rate has been constant during the Pliocene-Quaternary, creating, continuously and regularly a large amount of accommodation to be filled by

sediments. A minor reactivation has been detected on the inner shelf that induces a localised deformation of Pliocene-Quaternary sedimentary cover. The amplitude of this deformation is small, but can induce a shift of up to 50 m in the Pliocene series. It is superimposed on deeper faults that seem to have been reactivated at around 1 Ma. The quantification of Pliocene-Quaternary subsidence also enabled to evaluate isostatic rebound on the outer shelf during the messinian crisis (up to 1.3 km uplift at the Herault-Sète canyon heads).

When using older sedimentary marker from the deep-sea (the base of salt deposits, dated at 5.6 Ma) to estimate the subsidence rate on ECORS profile, we also find a seaward tilting subsidence of the slope with a measured angle of 1.44°. The subsidence increases up to 996 m/Ma at 200 Km from the coast. From this point to the deepest part of the basin, the total subsidence is then almost vertical and reaches 1070 m/Ma during the last 5.6 Ma in the deepest part of the basin.

These very high total subsidence rates enable high sedimentation rates along the margin, which in turn enabled the detailed record of climate evolution during Pliocene-Quaternary that make of the *Gulf of Lion* a unique archive.

Abstract: (452 words). Main Text : 4578 words ; 13 Figures.

* Corresponding author and requests for materials should be addressed to Marina Rabineau

(e-mail: marina.rabineau@univ-brest.fr) Tel: (33) (0)2 98 49 87 28 Fax: (33) (0)2 98 49 87 60

Keywords : Subsidence, Passive margins, Sedimentary record, Isostasy, Pliocene-Quaternary, *Gulf of Lion*, Gulf of Lions, Mediterranean Sea, Stratigraphic modelling.

1. Introduction : A rapid overview of Subsidence studies in the *Gulf of Lion*

Subsidence studies in the *Gulf of Lion* margin (**Fig. 1**) have recently been summarized in Bache, 2008 ; Bache et al., 2010. We provide here only a short summary. Subsidence has long been considered as an Atlantic-type passive margin with a general and regular seaward tilt of the shelf (Le Pichon *et al.,* 1971; Watts & Ryan (1976) ; Ryan, 1976; Biju-Duval, Letouzey *et al.*, 1978; Montadert, Letouzey *et al.*, 1978 ; Steckler and Watts, 1980, Burrus, 1989). While uniform extension models (McKenzie, 1978) were largely used to explain the evolution of such margins, many discrepancies with the predictions of these models have been highlighted

in the Gulf of Lions. Steckler and Watts (1980) used biostratigraphic data from commercial wells and described a relatively small volume of syn-rift sediments compared to post-rift sediments. This first type of discrepancy was not corroborated by more recent studies, which described a great thickness of synrift sediments (Bessis, 1986; Guennoc et al., 2000). Bessis (1986) and Burrus (1989) pointed out that the evolution of the subsidence of the Gulf of Lions was qualitatively (rapid initial subsidence during rifting, followed by a slower thermal subsidence after rifting) but not quantitatively in agreement with the uniform stretching model proposed by McKenzie (1978) which led them to introduce the concept of "paradox of stretching" in the Gulf of Lions. Réhault *et al.* (Réhault, Boillot *et al.*,1984), Bessis, Burrus, 1986, Burrus *et al.* (Burrus, Bessis *et al.*, 1987), also tried to compare the vertical evolution of the Liguro-provencal basin to classical models of subsidence in open oceans and concluded that present-day depth of the basin was at least 1000 m deeper than what it should be (if the model is right and applies here).

Other studies in the area have shown that tectonic subsidence associated with rifting was small and local and that most of the subsidence only started in Miocene time as a consequence of postrift thermic cooling enhanced by sediment loading {De Voogd, 1991 #26} {Gorini, 1994 #27}.

Seranne, 1999, observes that the Gulf of Lion margin displays structural and stratigraphic features similar to 'Atlantic-type' margins, however he suggests that the Oligocene rifting of the Gulf of Lion represents the initial stage of a succession of rifting events and back-arc basin formation, due to continuously retreating subduction during convergence of Africa and Europe (Seranne, 1999) (Jolivet et al., 2006). The A colder mantle may account for the abnormal subsidence of the basin (500 m/Ma), and could be a result of the >40 Ma long subduction beneath this area (Serrane et al., 1999 ; Chamot-rooke et al., 1999).

Total subsidence rate of the deep Mediterranean Sea, after deposition of evaporites has first been estimated to be 20 cm/ka (i.e. 200 m/Ma) by Ryan (Ryan, 1976). In the same paper Ryan estimates Pliocene-Quaternary amount of subsidence ranging from >400 m for the inner shelf to >1000m for the outer shelf and >1200 m for the edge of the abyssal plain (Ryan, 1976). For De Voogt et al.1991, the (postrift) total subsidence rates calculated along the margin show an overall regular tilting for the last 20 Ma from the shelf to the slope (apart from the messinian isostatic readjustment). The tectonic subsidence computed was 20 m/Ma on the shelf and 180 m/Ma in the deep basin (at more than 250 km from the coast on ECORS profile). Note that these values correspond to the tectonic subsidence only, a value to which thermal and gravity subsidence (loading) need to be added, to obtain total subsidence. So this estimation gives a

much higher rate of subidence than that calculated by Ryan (1976). Seranne, 1999 estimates the average total subsidence as 500 m/Ma.

Bessis (1986), Burrus (1989), and Burrus & Audebert (1990) note an enhanced total subsidence rate during the Pliocene-Quaternary (5 Ma) in the very deep basin of the Gulf of Lion that remains largely unexplained and that has also been observed in the Ligurian Sea (Réhault et al., 1984). Burrus & Audebert, 1990 interpret this increase as related to Alpine compression.

Bache, 2008 also applied 1D backstripping in the deep Gulf of Lion at the position of ESP 206 (Expanded Spread Profile, see position in fig. 1) (allowing access to thicknesses of the main units), using the empirical age-depth equation of Parsons & Sclater, 1977. Bache, found a general post-messinian subsidence (after the refill of the Mediterranean Sea) of around 1100 m for the last 5.3 Ma ; i.e. 210 m/Ma. The same subsidence including the messinian event, i.e. between 5.96 to present gives a total subsidence of 3,2 km, i.e. : **535 m/Ma** (because of the loading effect of the enormous amount of messinian deposits) (Bache *et al.,* 2009).

For the Pliocene-Quaternary time-period, Lefebre (1980) realised a cartographic synthesis and an isopach map of Pliocene-Quaternary deposits at the scale of the Gulf of Lion based on seismic profiles. He noted the general tectonic stability of the shelf since the messinian.

A conclusion also reached by Lofi *et al.,* 2003 and Mauffret *et al.* 2001*,* when studying the westernmost part of the Gulf of Lion. Most of the faults occur and play in post-aquitanian sediments and are sealed by the messinian unconformity (Gorini *et al.*, 2005). A late Miocene-early Pliocene extensional tectonics has been shown in the westernmost part of the Gulf of Lion, but these faults are active only until the early Pliocene (Mauffret *et al.* 2001). We willl come back to this phase in the discussion.

Lefebre, 1980, Genesseaux & Lefebvre (1980) and Guennoc *et al.* (2000) mapped the messinian erosional surface on the shelf and showed the effect of the deep cutting of the messinian Rhône river on the shelf. Guennoc et al. also produced a reconstructed paleomessinian surface by correcting the present day messinian surface from water and Pliocene-Quaternary sediment loading. The depth of this reconstructed surface on the slope is around 1500 m in the vivinity of the GLP2 drillhole, which is also thought to be the position of the messinian shoreline. Present day depth of the same point (GLP2 is now at 3437 m). On the Aude-Hérault intefluve a point located at present day at 1800 m has been reconstructed at 600 m). On the inner shelf a point at 1500 m is corrected to 500 m. Note that this surface is not exactly the surface at time of deposition because thermal cooling (inducing further

subsidence) was not taken into account (Guennoc *et al.,* 2000). However this correction shows at least 1000 m to 1200 m to 1937 m of subsidence (from the middle to outer shelf to upper slope (GLP2) due solely to water and sediment loading.

Using very high resolution Sparker data from IFREMER, Rabineau (2001), Rabineau *et al.* (2006, 2007) calculated subsidence rate of the western shelf of the Gulf of Lion for the last 540 000 years. In this area, erosional surfaces are related to glacial maxima of 100,000 years cycles and are very well preserved (Aloïsi, 1986, Berné *et al.,* 2004, Rabineau *et al.,* 2005). The effect of subsidence is clearly shown on these seismic profiles where erosion surfaces, which represent the same environment at different times, show angles of inclination that increase with age (with depth below earth surface). The present day depth of paleoshorelines therefore corresponds to the depth below Sea Level (SL) at time of deposition *plus* the movement of the floor after deposition (see Fig. 7 in Rabineau *et al.,* 2006). Rabineau *et al.* 2006 measured the tilt on the seismic profiles by the inclination of successive erosion surfaces; using the ages of erosional surfaces (MIS2, 6, 8, 10 and 12), they obtained the rate of subsidence i.e. 250 m/Ma at 70 km from the coast around the Aude and Hérault canyon heads, the rotation point being 13.5 km offshore of present day coast. This was confirmed using stratigraphic modelling to reconstruct observed geometries (Rabineau *et al.*, 2006, 2007). The recent Promess boreholes PRGL1 and PRGL2 drilled on the shelf and upper slope through the erosional surfaces, lowstand shorefaces and prodeltaic muds further confirmed this interpretation and validated the methodology by giving a ground-truth and detailed age-control of previous interpretation using C14 datings, biostratigraphy and isotope analyses (Bassetti *et al.*, 2008 ; Sierro *et al.*, 2009).

In 2008, Jouet and co-authors modelled late-Quaternary subsidence rates on the shelf using numerical stratigraphic modelling (with Sedflux Model using used the following statement S= GS + WL=(WS + TTS) + WL where GS : geohistory subsidence ; WL : Water loading ; WS : Sediment weight ; TTS : tectonic-thermal Subsidence.) in order to decipher the relative role of parameters (Jouet et al., 2008). These authors showed the importance of water loading variations (between Last Glacial Maximum and high stand of sea-level, like present day situation) reaching 60-65% of total subsidence, whereas tectonic-thermal subsidence contributed only to 35-40 %.

These ealier studies at least, show despite of many discrepencies, that subsidence rate are particularly high in the *Gulf of Lion* whatever the factor responsible for it.

In our paper, we will not deal with mecanisms and origin of subsidence, our purpose is only to measure postrift total rates of subsidence (S) over the entire margin during Mesinian-Pliocene-Quaternary times using sedimentary markers with known paleobathymetry.

3. Data and Methodology:

• 1D and 2D study of Accomodation from Seismic Stratigraphy and Sequence stratigraphy

Many factors of global, regional or local scale have long been recognised to control the overall geometry and deposition of sediments. The method applied in this study is based on the recognition, the interpretation and the dating of paleosurfaces as seen on seismic reflection profiles using concepts of seismic stratigraphy (recognition of stratal termination and configuration). Those surfaces are correlated at a regional scale and are then used as markers to quantify the vertical evolution of the margin and potential tectonic deformation.

Sequence stratigraphy models developed from the pioneer work of Exxon in 1977, and further developed in the 1980-1990s aiming at explaining the formation and the geometries of sequences within a chronostratigraphic framework. Most authors recognize three factors variable in time, that control directly the creation, expression and organisation of sedimentary sequences [Vail, Colin *et al.*, 1987; Jervey, 1988; Posamentier, Jervey *et al.*, 1988a ; Posamentier and Vail, 1988b; Guillocheau, 1991 …] : (1) Eustatism (with absolute sea-level variations), (2) Movements of the substratum (Subsidence s. l. and compaction) (**Figure 2a**) and (3) Sedimentary Fluxes.

Conceptual model are based on the fact that sedimentary series can be described as a logical succession of units, which geometry and localisation on a coast-to-basin depositional profile is a function of varying Relative Sea-Level (also named « Accommodation ») that is variable in space and time. Accommodation represents the total space measured from a fixed point that is open to sedimentation in the basin though time. It is therefore the space comprised between the substratum and the sea-level, that is, the space created either by subsidence and/or by eustatism and is independent of the presence or not of sediments (**Figure 2**). This accommodation in the basin can then be filled, completely or partially, by sediments, which will form depositional sequences. Note that many other parameters have an impact on the detailed nature of the sediments and deposition style, but they have no impact on accommodation, which is therefore a useful concept. Calculation of accommodation at a given point and a given time can be handled in two ways : (1) by additionning the value of subsidence and the value of sea-level that both need to be known (Figure 1a), (2) by

additionning the thickness of sediments and their bathymetry at time of deposition (**Figure 2b).** On passive continental margins, the subsidence often takes the form of a tilt and can therefore be measured with a point of rotation and an angle of rotation (**Figure 2c**).
Variation of Accommodation can then be calculated between two time period, ΔAcco (t2-t1)= Acco (t2) – Acco(t1) = Δsubsi (t2-t1)+ Δ Eustat (t2-t1)= (e2+b2) – (e1+b1)
(Note that Δsubsi is positive for a lowering of the sea-floor between t1 and t2; Eustat is positive if above present day sea-level ; bathymetry (b) is positive below sea-level, Δ Eustat is positive if sea-level rises between t1 and t2)

• In this study we used the database build during the French GDR Marges and Actions Marges Program thanks to the collaboration of TOTAL which gave access to all their conventional standard seismic lines, high resolution multi-channel data (LRM lines in particular) and industrial boreholes (**Figure 1**). Additional high and very high resolution seismic profiles from IFREMER were also used (**Figure 1 and 3**). Seismic Stratigraphy principles were applied to interpret seismic profiles (Payton, 1977 ; Catuneanu et al., 2009 for example) (**Figure 4 and 5**). In order to have as many chronostratigraphic constraints as possible within the sedimentary column, we used seismic profiles of different resolution but at the same position, so that the well-constrained and well-dated Quaternary surfaces can also be placed on lower resolution profiles as shown on **Figure 4**. Key reflectors identified are labelled MES (Margin Erosional Surface in pink), Plio11 (green), q10 (red), D30 (orange).

• Time-depth conversion

The measure of the Pliocene-Quaternary subsidence using observed depositional profiles and key sedimentological reference points (i.e. shoreline, offlap break, toeset break,…), imposes to convert profiles and interpretation from TWTT to depth (in meters), in order to measure directly tilting or movements of the substratum (**Figure 2c**). On the shelf we used velocities measured in two wells: Rascasse and Tramontane (**Figures 1 and 6 A and B)**. Tramontane well is located 30 Km from the coast, 6 km to the SW of LRM18 profile, Rascasse well is located in a more distal part of the profile on the outer shelf at 55 km from the coast (**Figures 1 and 6)**. Measured boreholes velocities were correlated to seismic profiles and showed that we could distinguish specific velocities for different sedimentary packages. We therefore identified the Topset part of big sedimentary prisms, the foreset part, and the toeset part each with specific values of velocities. We therefore defined a 2D velocitiy profile (**Figure 6C**) on the shelf. We then used this 2D profile to convert interpreted reflectors from TWTT to depth

(m) and we therefore obtain a 2D section of interpretated profile LRM18 in depth (**see later in results**).

On the slope and deep sea we used ESP (Expanding Spread Profiles) data that were shot along the ECORS profile (De Voogd, 1991 #26)**,** and that have been interpreted by Pascal *et al.*, 1993, and the velocities obtained by tomographic inversion from new refraction data acquired during the Sardinia Cruise (Gailler et al., 2009) to build the 2D velocity model (**Figure 6D**). We also compared those velocities with measuremets at GLP2 well (1246 m water depth, see position on ECORS line, **Figure 5**) and Figure 6 TFP measurements in GLP2 showed velocities from 1800 m/s at the top of the well to 2500 m/s at 2508 m ; 3000 m/s at 4100 m ; 3180 m/s at 4855 m (at the base on Miocene series), and 3320 m/s at 5345 m (i.e. at 4100 mbsf).

After time-depth conversion, we therefore obtain a 2D section of interpreted reflectors in depth (m) (**Figure 7 and 12**).

• Dating of surfaces

Very high-resolution profiles interpreted in earlier studies (Rabineau, 2001, 2005) showed that the last 5 erosional surfaces correspond to the last five glacial maximum erosions of 100,000 years cycles, with preservation of the shoreline on the outer shelf. The fifth surface D30 was interpreted as MIS12.2 and therefore dated at 434 000 years (according to orbitally tuned isotopic Specmap curve, Imbrie, 1984) (Rabineau *et al.* 2005, 2006). This interpretation and dating has now been confirmed on the shelf thanks to the Promess drillsite (Bassetti *et al.*, 2008, Sierro et al., 2009).

The messinian margin erosional surface (MES) is generally dated at 5.33 Ma according to the GSSP (Global Stratotype Section and Point) of the Lower Pliocene Zanclean Stage dated astronomically by Van Couvering *et al.*, 2000. Most authors also agreed to date the initiation of salt deposition at 5.6 Ma, and the end of the Salinity crisis at 5.33 Ma (CIESM, 2008).

4- Data and Results : measure of subsidence rates

a- On the shelf

The high resolution erosional surface D30 was plotted on LRM18 profile (**Figure 4**). Below this D30 surface, other erosional surfaces could be plotted: surface q10 corresponds to a major erosional surface, that lies around 450 ms (or 400 m) below present day sea-level at

shotpoint 3400 on LRM18 and seals an important incision on the outer shelf. At the base of the profile a proeminent erosional surface appears which corresponds to the well-known messinian margin erosional surface (MES) dated at 5.33 Ma. Above the MES and below the upper two surfaces (D30 and q10) we distinguished a number of large clinoforms (around 500 m high). Clinoforms are named p1 to p14, and all show a gently dipping linear topset part, a highly dipping foreset part curving more or less progressively to a gently dipping bottomset part (**Figure 7**). All clinoforms show these 3 parts organisation, topset parts of clinoforms are all preserved through time, and show an increased topset-slope with increasing age. The overall organisation can be described as a prograding-agrading margin. Clinoform p11 (green) on the shelf shows an important erosion that truncates the topset part of earlier clinoforms p10 and p9. In the upper part of the section some erosional V-shaped filled incisions appear, that are related to paleocanyons heads that have been filled. The organisation and functioning of quaternary canyons have been described in detailed studies in the area (Baztan *et al.*, 2005; Gaudin *et al.*, 2006, Canals, 2008, Lastras et al.…). The oldest observed incision of that type has been observed just above p11 clinoform. Therefore it seems that canyons appear around p11 as also suggested by Lofi et al., 2003.

• Significance of offlap breaks or topset-foreset breaks

The *offlap-break (or clinoform breakpoint)* has often been described in sequence stratigraphy as the inflexion point between topset and foreset (Vail *et al.*, 1991). It has very often been considered as the position of the shoreline, i.e. the «Zero» of sea-level. Topsets sediments were therefore attributed to continental facies. Foresets in that case represent the delta front or shoreface shallow environment. Numerous discussions recently occurred about this notion, and pointed to the abuses of this interpretation (Emery & Myers, 1996, Tropéano, 2001, Cattanéo *et al.*, 2004, 2009, Helland-Hansen, 2009; Henriksen *et al.*, 2009). Those recent publications clearly showed that clinoforms and offlap break occur at very different scales (from current ripples, to shoreline break and shelf-edge break).

Present day situation in the Gulf of Lion also shows two kinds of offlap-breaks of very different scale (**Figure 4**): the offlap break related to the shoreline and the offlap-break related to the shelf break. To avoid confusions we used this specific terminology with a shoreline-offlap break, a shelf-offlap break (**Figures 4 and 7**). At present day those two points lie at a water-depth of 0-10 m and 150-160 m as shown on bathymetric map (Berné *et al.*, 2001; 2002).

Earlier studies also demonstrated that the Last Glacial Maximum (LGM) paleo-shoreline, 20 ka ago, is recorded on the outer shelf, at the top of 30 m-thick sand bodies and at a present day bathymetry of 115 m (Aloïsi, 1986, Berné *et al.* :1998, Rabineau *et al.* 1998, 2005, 2006, Jouet *et al.* 2006, Bassetti *et al.*, 2006, 2008). During the LGM, sea-level is at least 100 m below present day sea-level, so the shelf-offlap break was lying at around 50 m bathymetry.

We therefore think that paleo-shelf-offlap break during Pliocene-Quaternary do not represent the shoreline but the shelf break and that the height of clinoforms represents the slope. Paleobathymetry of this offlap-break can be estimated to be **between 50 and 150 m**. We assumed that this paleobathymetry is the same for all identified shelf-offlap-breaks. Topsets of clinoforms therefore represent several environments from subaerial, fluvial to shoreline and continental shelf all eroded during lowstand. We consider that all Pliocene-Quaternary Topsets are related to the same process and therefore represent the same paleoenvironments and the same paleobathymetry at time of deposition.

Therefore *offlap-breaks* in sedimentary record a paleobathymetry of either 0 (shoreline offlap-break) or 150m (shelf-offlap break). We also identified a toeset-offlap break at the base of foresets that we will use to calculate accommodation (see below).

• Calculation of Pliocene-Quaternary Subsidence rates

We used two distinct methods to calculate total subsidence.

a) Accommodation calculation at two different points (A and B) on profile LRM18 between Zanclean (around 5,3 Ma) and Present Day (**Figure 7**).

   Zanclean accommodation can be estimated using the height of Pliocene prisms between offlap break and toeset break. This height is around 650 m at point A The bottomsets of clinoforms are therefore deposited under a waterdepth of at least 650 m for the most landward clinoforms. To this value we must add the paleowater depth of the offlap break, which can be estimated by analogy to present day situation at 150 m at the most, so that Zanclean accommodation at point A is 800 m. At point B it is more difficult to estimate accommodation with this method because we are lacking appropriate marker to estimate the paleowater depth of initial deposits (just above the messinian). However, we can postulate that it is at least of the same order of magnitude (800m, probably more). Note that this estimate is a regional estimate as locally the messinian erosional surface is very irregular and can induce locally large thickness variations.

-Present Day accommodation is easily estimated as the sum of the thickness of sediments plus present-day bathymetry (i.e. the present day depth of the messinian surface). From the depth profiles at point A this value is 1050 m and at point B it is 2240 m.

So, the amount of accommodation created during Plioquateranry time is: Zanclean Acco –Actual Acco is of 250m at point A on the inner shelf and 1440 (as a maximum) at point B. This creation of accommodation corresponds to the sum of subsidence and eustatism variations (between Zanclean and actual time). If we estimate eustatism at initial time (Zanclean) we can therefore deduce the Pliocene-Quaternary subsidence amount and rate. The early Pliocene is well-known to have been an interval of global warmth. According to global estimates of eustatic variations (Miller *et al.* 2005), sea-level shows a regressive tendancy between Zanclean and present-day time estimated to correspond to a first order sea-level drop of Δeustat = eust final-eust ini= -40m (Shackleton et Opdyke, 1977 ; Blackwelder, 1981). For Miller et al., 2005 the best estimate for sea-level at 5.33 Ma is +48.8 m above present day sea-level. Other estimates of sea-level during very early Pliocene give a sea-level at +25m above sea-level (Kennett & Hoddell, 1993), or +88 m in Haq et al., 1987 compared to presentday sea-level, so we would have a loss of space due to sea-level drop (Δeustat = eust present-eust Zanclean).

We averaged this value to **+50 m in our estimate**.

Finally, the creation of subsidence itself is calculated using the following relation: Δsubsi + Δ eustat = ΔAcco ; Δsubsi= Δacco –Δeustat

And we obtain the following values: ΔSubsi = 300m at point A and <1600 m at point B. If we date initial prism p1 at 5.33 Ma, we obtain subsidence rates of 56m/Ma and <300m/Ma (**Figure 7**).

b) Using the same LRM18 depth-profile we analysed the tilt of erosional surfaces.

In the upper part of the profile quaternary erosional surfaces are well-known and sampled by cores and the new Promess drillsite. Studies at this scale demonstrated that the erosional surface correspond to a polygenic surface related to glacial regression (Rabineau *et al,* 2005*)* slightly reworked during transgression (Bassetti *et al.*, 2006). The erosional surface was mostly subaerial during LGM and now corresponds to the shelf of the Gulf of Lion. This surface can easily be approximated to a line from the middle to the outer shelf, this line has a slope of 1,5 m/km (0,15 %, 0,0859°). This approximation of erosional surfaces in topset areas was done for all plotted clinoforms in the outer part of the profile (from p11 to present)

(**Figure 8**). The lines show an increasing slope with increasing age of clinoforms. Topset of clinoforms (**Figures 2A and 8**) can reach 15m/km (1.5 %, 0,86°) foresets can reach 50-62m/km (5-2.6.2 % or 2.86-3.5 °) and bottomsets 3m/km. All lines showed a common rotation point located at 13 km landward of present day coast. As we assume that topsets represent the same paleoenvironment and the same paleobathymetry at time of deposition which is proven for at least the last 434 000 years (Rabineau et al., 2005, Bassetti et al., 2008), they correspond to a caracteristic slope at time of deposition. We considered this slope to be the same as present day slope of the shelf i. e. 1,5m/km. (≈ 0,086 °). Observed increasing slopes are due to post-depositional tilting of the margin related to subsidence. However detailed analysis of slope adjustment performed on the outer shelf showed that the landward part of clinoforms did not fit well with real observed geometries (figure 8, see zoom 8B). Further investigation on seismic profiles showed that around 32 km from the coast we observed a small but systematic deformation of reflectors (**Figure 7 and 8**). All reflectors from early Pliocene to p14 show the same deformation, whereas reflector q10 is much less deformed and D30 not deformed. We therefore conclude that there is a tectonic deformation with 50 m uplift in the landward part of the section. This deformation can be followed on several lines and mapped in the western area (see discussion and **Figure 9**). The age of reflectors extrapolated between p1 and D30 (see method section) led us conclude that the uplift occurs around q10, i.e. 1 Ma.

If we restore the landward part of the section before this deformation we then find a good adjustment of topsets, that can be propagated down to p1 clinoform with the same previously defined rotation point.

Present-day approximation-line of the sea-floor lies at 150m at Km 70. The tilt between approximation of p1 and the approximation of present day sea-floor brings line-p1 at 1430 m at Km70 Figure 10), i.e. 1280 m of subsidence at 70 km from present-day coast. The angle of tilt (between early Pliocene to present day) is therefore α **=0.88°** (=**1,54%**) (see definition on **Figure 02**). The first visible prism p1 on the shelf (appearing at Km6) lies directly on the messinian surface (dated at 5,33 Ma). If we date this first prism as **5,3 Ma** we found a total subsidence rates of 49 m/Ma at 19 km from the coast to 241 m/Ma at 70 km from the coast. In other words, the tilt of the shelf is of 0,16 °/Ma = 0,28 %/Ma.

The two methods to estimate subsidence rate are in good agreement, this second method is more precise than our calulation of accommodation because it describes the 2D evolution of the subsidence.

This value 241m/Ma is exactly the same order as the subsidence calculated for the last 434,000 years (250 m/Ma) (Rabineau *et al.*, 2006). This common value calculated at two very

different time scale is a strong argument for a **regular and constant subsidence rate during all the Pliocene-Quaternary**. It corresponds to the most **parcimonious** hypothesis (as used in phylogeny reasoning, e.g. Lecointre & Le Guyader, 2001). This "total" subsidence measured from a geometrical point of view is the overall outcome of any processes by which the ground surface has moved at the margin scale.

Of course, an uncertainty is associated with the estimate of subsidence, corresponding to errors in the measurements (+/- 5m), time-depth conversion, paleomorphology variations, paleobathymetries estimates (+/- 20 m), sea-level estimation (+/- 20m), the linear interpolation and the dating of first clinoform p1. So, we estimated this error to ± 45-50 m for the last 5 Ma, i.e. +/- 15m/Ma.

• Defining ages of surfaces

As the rate of subsidence is constant through time, we suggest to extrapolate the datings of reflectors between the Messinian and the upper Quaternary on the shelf. The same amount of tilt between two surfaces implies that the amount of time between the surfaces is the same. We have therefore extrapolated age of surface D30 downwards so that q10 surface is dated around 1 Ma and plio11 around 2.7 Ma.

2- From the upper slope to the deep Basin: the base of the salt used as a marker to measure subsidence

Applying the same methodology as defined on the shelf, we can also analyse the subsidence on the slope and in the deep basin using the ECORS profile transformed in depth (Figure 12). The base of salt surface shows two different segments: a tilted part (between Km 120 and 200 from the Coast) and a nealy flat surface from Km 200 to the very deep basin. We therefore define another hinge point at Km 200 and fit a line through the upper part. The approximated line rotates around a point located at 22 Km onshore of present coastline to Km 200 from coastline (142 km from rotation point) where the surface lies at around 5.6 km. The slope of this surface compared to horizontal is therefore **1.44° (or 2.5 %) (Figure 11)**. Some salt has been deposited on this surface but has then moved creating the well-known salt tectonic in the basin (Dos Reis, 2001, Dos Reis et al., 2004). A few small pillows of salt can still be observed on this surface. The question we do not know is wether this surface had already a slope when the salt has been deposited.

If we consider that this surface was flat at time of deposition, the slope measures directly the amount of subsidence. Recent studies and synthesis on the messinian salinity crisis have been summarized in a consensual paper, CIESM, 2008 where most authors agreed to date the initiation of salt deposition at 5.6 Ma. We can therefore compute a maximum rate of subsidence of 0,26°/Ma for the last 5.6 Ma. At Km 200 from the Coast (222 Km from the rotation point), the maximum total rate of subsidence would be D*tanα = 222000*tan(1.44°)/ 5.6= **996 m/Ma over 5.6 Ma.**

If the basin had a paleomorphology with an already tilted surface, then the subsidence would be of course smaller. On the other hand the subsidence on the slope can not be smaller than the subsidence calculated on the shelf. If we just extrapolate the value measured on the shelf, we found a value of D*tanα = 222000*tan(0.88°)/5.6= **608 m/Ma over 5.6 Ma.**

Between Km 62 and Km 110, another sedimentary paleo-marker has been identified: a planar surface of erosion found in the entire Gulf of Lion (Bache, 2008, Bache *et al.* 2009). This surface occurs from 1.6 twtt around Km 62 (near the Aude-Herault canyon) (Profile LRM16-Ligo20), which corresponds to a depth of 1800-2100 m (using velocities from wells) (Bache et al., 2011). This surface can be followed easily at least down to 2.6 twtt around Km 110. This surface has been interpreted as a transgressive surface that erodes the previous messinian regressive erosional surface and its lowstand deposits (the detritic fans) and occurs at the end of the messinian salinity crisis, before the very rapid transgression which is so rapid that it leaves the shelf unaffected by the transgression (Bache et al., 2011). The landward termination of the surface (the position of the shoreline before the final rapid transgression) lies at 1.6 twtt all along the margin and therefore demonstrates that Pliocene-Quaternary subsidence has been homogeneous in the central part of the margin. On the contrary, the landward terminaison lies at 1.4s only on both edge East and West of the Gulf of Lion.

On profile RM107 (**Figure 12**) a strike line at the base of the slope (see location on **Figure 1**), we observe that messinian reflectors, dip towards the West. The top of the massive salt layer goes from 3.35 to 4.32 twtt and the base of salt from 3.95 twtt to 4.5 twtt. This slope also mimics the general subsidence during Pliocene-Quaternary which increases towards the West and diminishes toward the edge of the Gulf of Lion.

In the deepest part of the basin (from Km 200 around ESP205) the base of salt is clearly imaged on profiles below a transparent layer) (**Figure 11**) and shows a sub-horizontal surface very gently dipping from 5.2 twtt (5.6 km) at Km200 to a maximum of 5.4 s twtt around

41°30’ (profiles PROGRES e.g.pgstk06, pgstk09 and Sardinia) which corresponds to a depth around 6 km at 270 km from the coast. The average dip of this surface is therefore around 0,005 % or 0,003°. We have an additional subsidence of the deepest central part of the basin of 70 m/Ma compared to the Km200 point. In the deepest part of the basin, all potential postdepositional movements of the margin have been nearly **vertical** as the base of salt remains nearly horizontal in this domain.

6- DISCUSSION

Tectonic and Geodynamic implications: deformation and isostatic rebound

• Deformation and rotation point

The detailed interpretation of erosional surfaces enabled us to demonstrate a small but visible deformation in the inner part of the shelf. The position of the break in slope induced by the deformation coincides with the position of major pre-messinian faults as mapped by Bache, 2008 (**Figure 9B**). Dating of the surfaces (see previous section) further enabled us to date this deformation slightly before 1 Ma. All the reflectors below the q10 marker are highly deformed (see plio11 for example on **Figure 9A**), whereas q10 itself (dated at 1 Ma) is less affected so part of the deformation occurred before and finally q5 (0,5 Ma) is not affected at all.

In this study we found a rotation point 22 km landward of the coast on ECORS NW-SE, at 13 km landward of the coast on LRM18 and a small deformation of the inner part of the shelf occurring around 1 Ma. This rotation point is somewhat different to that calculated for the last 500,000 years that was found at 13 Km seaward of the coast (Rabineau *et al.*, 2006). This difference can be explained by the deformation occurring at 1 Ma which uplifts the inner part of the shelf, this would have prevented deposition of younger strata on the inner shelf and shifted depocenter 30 km seaward resulting in a pinchout of Quaternary sequences and erosional surfaces at 13 Km offshore from the coast from this period (1 Ma) to present day. Position of this rotation point must be further investigated in 3D and compared to onshore studies.

• Isostasy

Caluclation of Pliocene-Quaternary on the margin showed that subsidence rate reached 250 m/Ma at shelf break. Observation of Miocene strata underneath the messinian erosional

surface however appear to be about planar and parallel to each other in this area. Wells on the shelf showed that those Upper Miocene deposits are very shallow (Cravatte *et al.*, 1974 describes a brackish to inner shelf environment at both Mistral and Tramontane ; In Autan1 well (which is located much further on the upper slope) paleoenvironments are described as inner to middle shelf. We therefore think that hose Miocene deposits have been deposited as horizontal strata. The amount of Pioquaternary subsidence should therefore have tilted them, which is not what we observe. We therefore think that Miocene strat have been deformed before the Pliocene-Quaternary which is probably related to an isostatic re-adjustement related to the Messinian erosional and salinity crisis. This suggestion has been proposed by many authors (Ryan, 1976 ; Norman & Chase, 1986; Mauffret *et al.*, 2001, Gorini *et al.*, 2005 ; Ryan, 2011). The drop of sea-level, the intense erosion on the shelf (over 1.5 twtt amount of sediments that have been eroded in our area Bache, 2008, Bache *et al.* 2009) must have generated an isostatic rebound. Our results on Pliocene-Quaternary subsidence therefore also give, a direct estimate of this isostatic rebound. Miocene strata have been uplifted during the MSC and then subsided again during the Pliocene-Quaternary. As they are back to horizontal at present day, the amount of Plioquateranry subsidence equals the amount of uplift during the crisis (i.e. 1280 m at Km 70). **We can therefore approximate the rebound during the crisis to be about 1.3 Km in this area**. This value is of the same order than that evaluated by Mauffret *et al.*, 2001 who found 1.7 km of uplift in the offshore part of the Albères Massif (i.e. about 20 km south of our estimate near the Pyrenees) which is not fully compensated by Pliocene-Quaternary subsidence as the landward dipping geometry of the strata on the outer shelf demonstrate. Considering the duration of the crisis to be 700 000 ka at the most (CIESM, 2008) we found **a rate of more than 1830 m/Ma which shows how rapid vertical movement can be**.

The value we found here is far greater than the values obtained with isostatic modelling by Govers *et al.*, (2009) in the Gulf of Lion. Govers described both the effect of the dessication creating an uplift of the margin and the effect of evaporites deposition (creating a load) (see his figure 9). But this uplift is limited to 300 to 600 m (from 100 Km offshore to present-day shoreline), furthermore the uplift is partly compensated by subsidence effect of evaporites deposition. However the model does not take into account the huge amount of erosion on the shelf (more than 1 km thick, Bache *et al.*, 2009) nor the huge amount of terrigeneous and evaporitic deposits (over 3 km thick Bache *et al.*, 2009).

• Meaning of the hinge point between subsidence values at 200 Km relation to deep structure of the margin.

This study also demonstrated an abrupt change of the subsidence around Km 200 (on ECORS profile). From 30 Km onshore to this point, the subsidence corresponds to a strong tilt of the margin (1.44° of tilt since the beginning of salt deposition at 5.6 Ma). This area of strong tilt on the slope is located in the domain II of highly thinned continental crust just above the T-reflector described by De Vogt et al., 1991. From Km200 seaward, the subsidence of the margin is nearly vertical allowing the preservation of the tabular salt. The value of total subsidence may have reach up to 1070 m/Ma in the center of the Basin. The point at Km 200 falls in the Domain III above the "undetermined crust" between the strongly thinned continental crust domain II and the oceanic crust domain IV (Bache *et al.*, 2010). Further studies and modelling will need to investigate the detailed relation between these observations.

Such high and vertical subsidence rates in the center of the basin allows the deposition of thick amount of sediments that do not fit classical conservational extensional models as has been also observed in much older open ocean, like the South Atlantic (Moulin *et al.,* 2005; Aslanian *et al.,* 2009) leading to new models for the evolution of margins (Aslanian et al., 2009 ; Bache et al., 2010).

8. Conclusions

The seismic shows that our studied area subsided regularly without substantial local deformation nor variations in rates; this enables us to propose a model for the subsidence with a linear and constant tilt during Plioquateranry. The rate increases with the distance from the Coast, the rotation point is located 13 Km landward of the coast, it reaches a rate of 250 m/Ma at 70 km from the coast, for the last 5,3 Ma, i.e. with an angle of rotation of 0.88° for the last 5 Ma. The same measurement on a larger scale (Ecors profile) also show an inclined base of salt surface up to Km 200 with an angle of 1.41° for the last 5,6 Ma. From 200 Km seaward there is a break in slope, subsidence is nearly constant and vertical from this point to the central part of the Provence basin where it may reach 1070 m/Ma for the last 5.6 Ma. The total subsidence rates are very high in the Gulf of Lion and allow an extremely detailed record of climate history and consequences on the sedimentary system (erosion/deposition). This work needs to be further extended in space and time to provide full 3D description of subsidence history of the margin. Ideally, IODP drillings on the shelf and in the deep Gulf of Lion would enable to better constrain this scenario of subsidence quantification.

Acknowledgements:

The original idea to undertake this work was initiated by J-L Olivet (Ifremer) who greatly contributed to the initial interpretations and results.

The velocity model and time-depth conversion of the profiles were made with the help of H. Nouzé (previously at Ifremer) and M. Moulin (Lattex). Interpretation of Pliocene-Quaternary strata on profiles were performed by M. Rabineau, J-L Olivet, E. Leroux on the shelf and by L. Droz, T. Dos Reis, E. Leroux in the deep-sea. Interpretation of Messinian and Miocene strata on profiles (both on the shelf and the deep-sea) were performed by F. Bache, J-L Olivet & C. Gorini. Interpretation of subsidence rates and consequences were made by M. Rabineau, D. Aslanian and JL Olivet with inputs from the team.

The final manuscript greatly benefited from the comments and advices of XXX. We thank YYY for fruitful discussions and a critical review of the manuscript and Alison Chalm and Barbara Harris-Rabineau for their final review as English native speakers. This research was mainly funded by CNRS and IFREMER, with additional support from the French GDR Marges-Actions-Marges program. TOTAL (Jean-Loup Rubino) and Melrose Ressources (Richard Bunt) are also acknowledge for providing seismic data.

Figure Captions

Figure 01 Location of Study Area, Dataset and bathymetry of the *Gulf of Lion (*modified from Berné *et al.,* 2002*)*. Red triangles correspond to industrial wells. Blue triangles correspond to the two PROMESS European boreholes. Big green dots represent the ESP data, small green dots repsent OBS data on Sardinia profiles. Thick lines (black, green or red) correspond to seismic lines shown in this paper. The blue thick line represents the end of the smooth surface (at 1.6 twtt) and the pink thick line represents the limit of salt (from Bache, 2008, Bache *et al.*, 2009)

Figure 02- Definition of Accommodation or relative sea-level

A) Accommodation is a function of Subsidence and Eustatism, it does not depend on sedimentary fluxes, nor hydrodynamics or autocyclic factors.

Accommodation = Subsidence + Eustatism

Accommodation = Thickness (e) + Bathymetry (b)

B) Example of accommodation variation between t1 and t2,

Accommodation in each time step is calculated as the sum of the thickness of sediment + bathymetry above sediments at ti.

Acco2-Acco1=(e2+b2) -(e1=b1) = (Δ Subsi) + (Δ Eustat)

Variation in Accommodation is positive when new space is created (either by subsidence or by eustatism (sea-level rise) or both)

In this example subsidence is not varying so variation of accommodation are solely due to increase in sea-level. On the other hand, resulting geometry does not depend only on accommodation variations but also on sediment fluxes and hydrodynamic in the basin. In case B) shown observed geometry implies a high sediment flux between t1 and t2.

C) Calulation of the angle of subsidence

Figure 03-resolution.ai

Seismic Profiles with three different resolution but located at the same place. A) Sparker profile 1049 from BASAR1 cruise ; B) Multichannel high resolution profile SMAVH07 and C) conventionnal industrial LRM18 (TOTAL) together with their frequency spectrum. The distance between P1049 and SMAVH07 is less than 100 m; distance between SMAVH 07 and LRM18 is less than 1 kilometer. Note that the combination of profiles from different resolution enables to follow and recognise sedimentarystructures on the different scales. For

example here the LGM sandy prism (red dot) clearly imaged on Sparker data (with highly dipping reflectors) can just be guessed on the LRM line.

Figure 4 Seismic Profile LRM18 in TWTT (s) and interpretation of prograding clinoforms. Black pins on top show cross-lines, Wells Tramontane (TR) and Rascass (RA) are projected on the profile. Shelf-Offlap breaks and Slope-toeset breaks and shoreline breaks have been identified on profile. Key reflectors are labelled and highlighted in colors MES (pink), p11 (green) , q10 (red), q5(orange) and sea-floor. Location of Figure 3 (Zoom) on this profile is also shown.

Figure 05 –ECORS

Line drawing of Profile ECORS NW-SE (in seconds TWTT)

(modified from Olivet, 1996 ; Bache, 2008; Bache et al., 2009 ; Bache et al., 2010 ; name of messinian surfaces adapted from Lofi et al. 2011).

Thick lines represent respectively from deepest to shallowest : base of continental crust (CC), top of substratum (S), basal messinian erosional surface Dm (in red), base of presumed evaporites in blue LU1 ; base of probable turbidites (LU0), margin messinian erosional surface (MES in pink), base and top of salt (MU), and sea-floor.

Figure 06- velocity models.ai

A) and B) Interval velocities measured in TRAMONTANE and RASCASSEwells positionned on dip-profile LRM10 and LRM16 (see location on Figure 1).

Main reflectors have been identified : q5 (435,000 ka) ; q10 (around 1 Ma) ; plio11 (around 2,7 Ma) and the messinien margin erosional surface MES (5,3 Ma) (in pink) and light green reflector (Miocene) below the messinian on LRM16 (see age estimates in discussion). Note in orange on LRM10, a paleo-canyon cut along its course and sealed by the q10 erosional surface.

Note on LRM16, the presence of a Fault that offsets the light green Miocene reflector (from Bache, 2008).

In green nice clinoforms are developped with topsets, forestes and bottomsets, the last clinoform of this package is the PlioXX surface. Below the blue surface, reflexions are sub-plane and correspond to bottomsets of previously deposited clinoforms.

C) 2D evolution of velocites based on wells Tramontane and Rascasse projected on Profile LRM18 (see Figure 1 for location). Enveloppes for velocity intervals are based on geometries

of deposits as observed on seismic profiles (velocities appeared to change from topsets to foresets and bottosets). Note also that those limits are not time-lines but related to major lithology changes. Within enveloppes interval velocities show linear variations and jumps at interfaces. Note also that extrapolation towards upper-slope is subject to caution as the evolution of velocities might be very different (in part due to the presence of canyons).
D) Velocity model used for time-depth conversion using Velocities as measured on ESP data (Pascal et al., 1993) and Sardinia data (Gailler et al., 2009) and interpretation of seismic profile

Figure 7-LRM18Acco.ai
Seismic Profile LRM18 **in depth** (m) used for calculation of 1D accommodation and subsidence at points A et B. Black pins on top show cross-lines, Wells Tramontane and Rascass are projected on the profile.
Initial accommodation corresponds to early Pliocene stage. Final accommodation corrresponds to present-day stage. Here we considered that offlap breaks represent the shelf breaks with a constant paleowater depth approximated to 150 m. Eustatism at initial stage (early Pliocene) is considered to be between 40 and 70 m (Haq *et al.*, 1987), we took 50m in this estimate, eustatism at final stage (present -day) is equal to 0 m. Accomodation has been estimated by measuring the height of clinoforms (between offlap breaks and toeset breaks) which corresponds to the minimal space that enables clinoform deposition ; we added to this value the paleo-water depth of the offlap break (150 m). Accomodation = Eustatism + Subsidence. The rate of subsidence is calculated using a duration for Plioquateranry of 5.33 Ma (occurring after the Messinian Salinity Crisis).

Figure 8-ApproxTopsets.ai

A) Seismic Profile LRM18 in depth (m) used for calculation of 2D subsidence along the profile. Black pins on top show cross-lines. Topsets of reflectors p11 to present day sea-floor are well approximated to straight lines on the outer part of the shelf (from Km36 to Km70. Lines are inclined seaward, inclination increases with the age of reflectors. All lines have a common rotation point which is located 13 km landward of present-day coast.
B) Inset B) shows the misfit of those lines in the inner part of the shelf. Note around the blue arrow (at Km 32) how reflectors plio11 to plio14 are deformed.

Figure 9-LRM16.ai

A) Zoom on Seismic Profile LRM16 in TWTT (s) and interpretation of Miocene and Pliocene-Quaternary strata. Wells Tramontane is on the profile. Note the deformation of plio11 refelctor and q10 reflector just above a major deeper Fault F1. Interpretation of Miocene strata slightly modified from Bache, 2008. Another deformation can be suspected in the landward most part of the profile See position of profile and Faults on Figure B.

B) Mapping of Major Faults and thickness of Miocene deposits (without messinian deposits) (in seconds twtt) from Bache, 2008. The thick line represent the position of Seismic Profile LRM16 shown in A). Major Fault F1 is localised near the Tramontane well (green dot) on the profile.

Figure 10-Rectot.ai

Seismic Profile LRM18 in depth (m) used for calculation of 2D subsidence along the profile. Black pins on top show cross-lines. The inner part of the shelf (Km 0 to Km 36) has been reconstructed to correct the effect of post-depositional deformation (large scale deformation). In this configuration topsets of reflectors p1 to present day sea-floor are well approximated to straight lines both on the inner and outer part of the shelf. All lines are inclined seaward, their inclinations increase with the age of reflectors. All lines have also a common rotation point which is located 13 km landward of present-day coast. The tilting of the margin from p1 to present day can be measured directly on the profile, it reaches 1280 m at Km 70 from the coast. Considering that the first clinoform p1 can be dated as early Pliocene (just after the Zanclean reflooding) we estimated its age between 5.3 and 5 Ma. This allows us to calculate a subsidence rate going from 0 m/Ma at -13 Km landward of the coast to 240-255 m/Ma at Km 70 seaward from the coast (near the upper slope).

Figure 11 – A) ECORS profile converted in depth (using previous velocity law-figure 06). Dm : discontinuity at the base of Messinian deposits; LU0, LU1 : lower unit of messinian age ; MU : mobile unit (salt) ; according to Bache et al., 2009. For a more detailed interpretation of Miocene and messinian deposits see recently published paper from Bache *et al.*, 2009 ; Bache et al., 2010. The vertical dashed red line indicates a change in the direction of the seismic profile. B) Approximation of the messinian surface to the base of salt with a straight line inclined seaward. The line has a rotation point which is located 22 km landward of present-day coast.

Figure 12 – RM107

Seismic Profile RM01-107 (Courtesy Melrose Ressources) in TWTT (s) (see location on figures 1) and interpretation of Pliocene-Quaternary deep-sea fan deposits. Black pins on top show cross-lines, Well GLP 2 is projected on the profile.

I, II, III: Lower, Intermediate and Upper Series, respectively. I-3: channel/levee system 3 of Series I (1 to n from the oldest to the youngest). Q10 (in red) and Plio11 (in green) represent majour erosional boundaries respectiveley between Series I-II and Series II-III. Stratigraphic interpretation from the shelf correlated to the deep sea suggest ages of 2.7 Ma for Plio11 and 1 Ma for q10 (see discussion). Thin red lines are local erosional unconformities; pink bodies are local or regional MTDs.

Differencial subsidence is imaged by the inclinaison of the base of salt deposit (in pink). Local defomation, pull-downs can be observed below canyons, they are artefact due low water velocities in canyons compared to adjacent sediments. Note that the general westernward inclination is also observed in underlying deposits (yellow reflectors).

The rate of subsidence is calculated using a duration for Salt and Plioquateranry of 5.6 Ma (an age agreed by most authors, see CIESM, 2008).

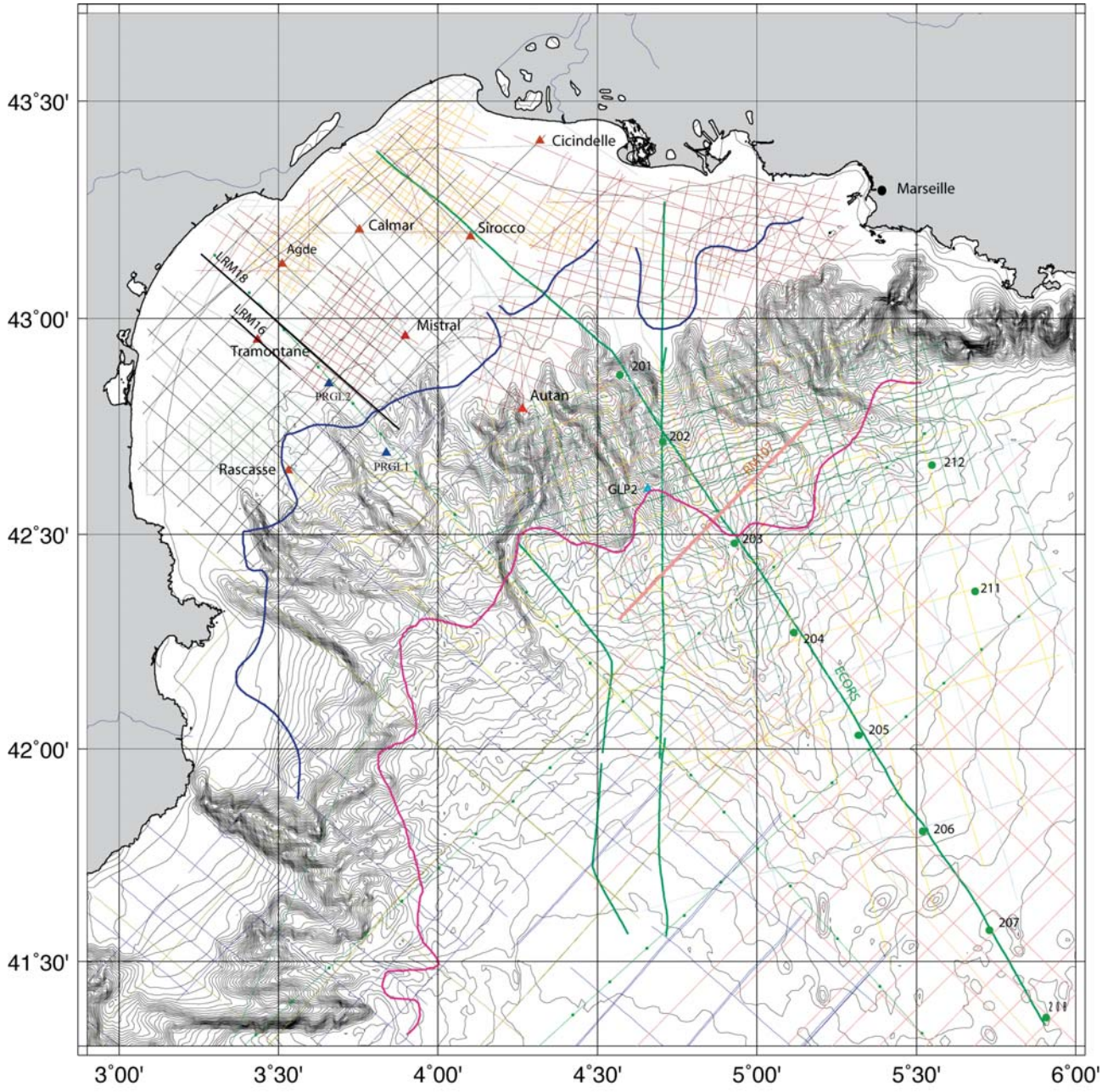

Figure 1 Dataset location in th eGulf of Lion . Red triangles correspond to industrial wells. Blue triangles correspond to the two PROMESS European boreholes. Big green dots represent ESP data (Expanding Spread Profiles), small green dots repsent OBS data on Sardinia profiles. Thick lines (black, green or red) correspond to seismic lines shown in this paper. The blue thick line represents the end of the smooth surface (at 1.6 twtt) and the pink thick line represents the limit of salt (from Bache, 2008, Bache et al., 2009). Bathymetry of the Gulf of Lion (from Berné et al., 2002)

FIGURE 1 –

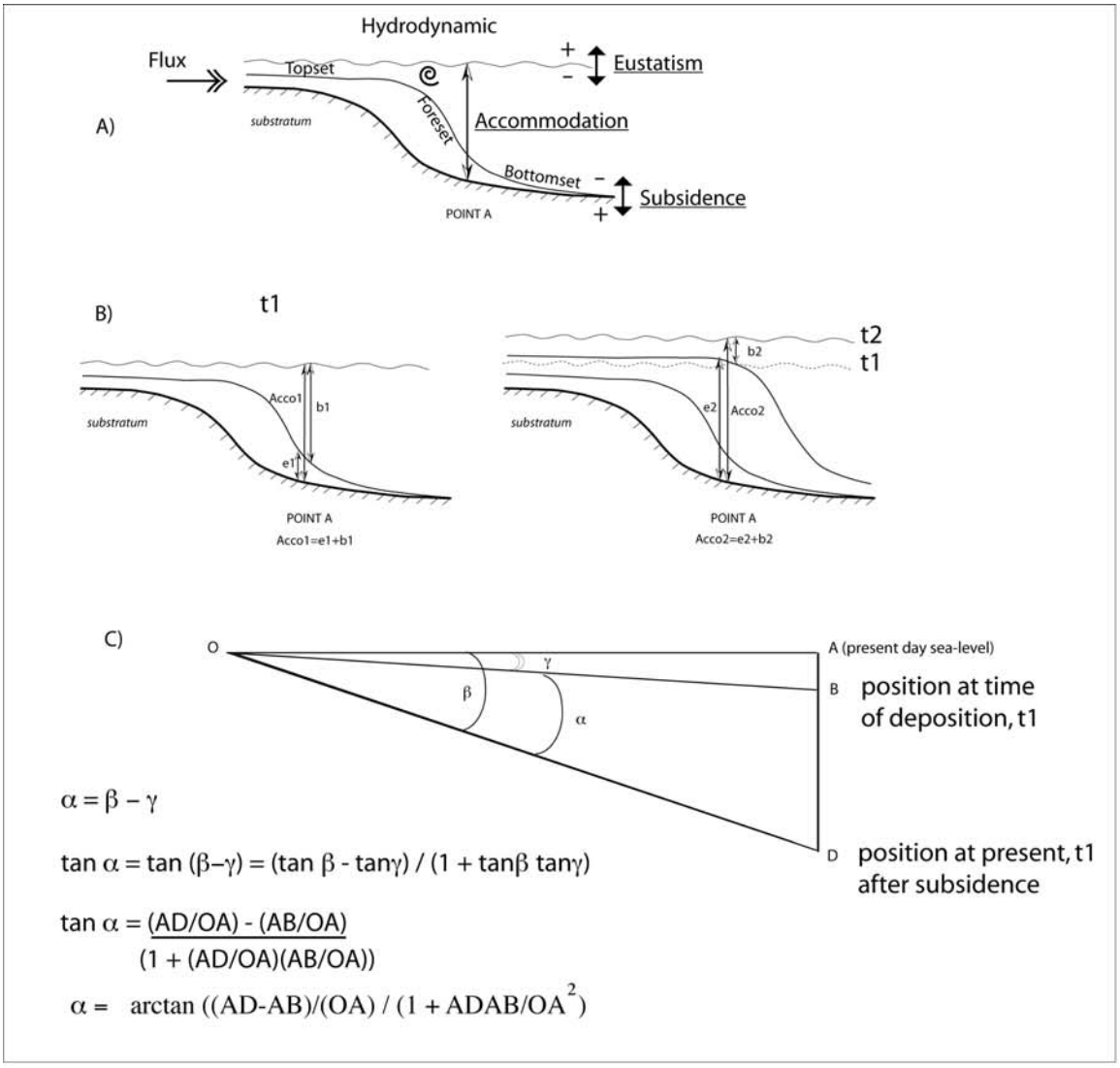

Figure 2- Definition of Accommodation or relative sea-level
A) Accommodation is a function of Subsidence and Eustatism, it does not depend on sedimentary fluxes, nor hydrodynamics or autocyclic factors.
Accommodation = Subsidence + Eustatism
Accommodation = Thickness (e) + Bathymetry (b)
B) Example of accommodation variation between t1 and t2,
Accommodation in each time step is calculated as the sum of the thickness of sediment + bathymetry above sediments at ti.
Acco2-Acco1=(e2+b2) -(e1=b1) = (Delta Subsi) + (Delta Eustat)
Variation in Accommodation is positive when new space is created (either by subsidence or by eustatism or both)
In this example subsidence is not varying so variation of accommodation are solely due to increase in sea-level.
On the other hand, resulting geometry does not depend only on accommodation variations but also on sediment fluxes and hydrodynamic in the basin. In case B) the observed geometry implies a high sediment flux between t1 and t2.
C) Defining α, the angle of subsidence, between t1 and t2 and the rate of subsidence $\alpha/(\tau 2 - \tau 1)$ (°/Ma).

FIGURE 2 –

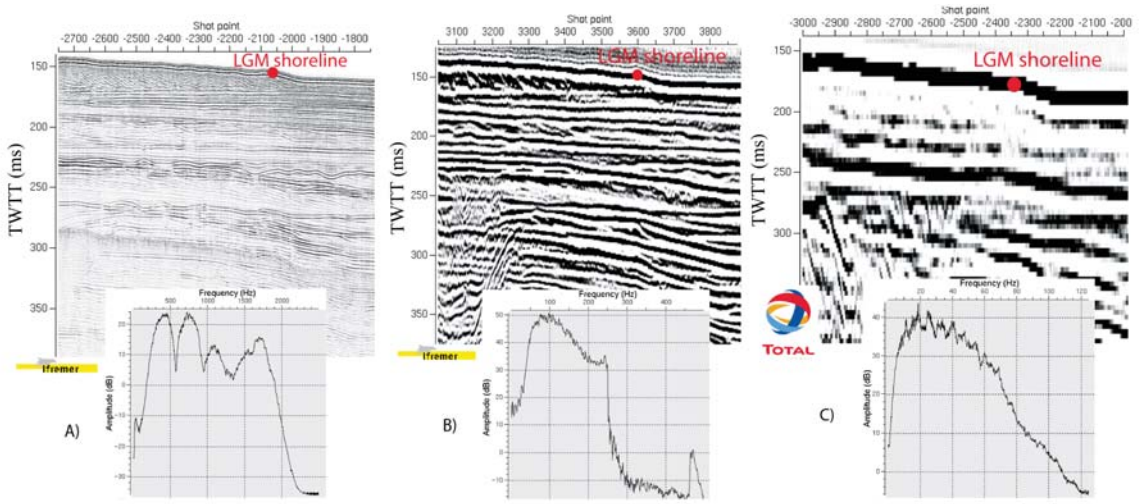

Figure 3- Seismic Profiles with three differente resolution but located at the same place. A) Sparker profile 1049 from BASAR1 cruise ; B) Multichannel high resolution profile SMAVH07 and C) conventionnal industrial LRM18 (TOTAL) *together with their frequencie spectrum. Note that the combination of profiles from different resolution enables to follow and recognise sedimentarystructures on the different scales. For example here the LGM sandy prism (red dot) clearly imaged on Sparker data (with highly dipping reflectors) can just be guessed on the LRM line.*

FIGURE 3 –

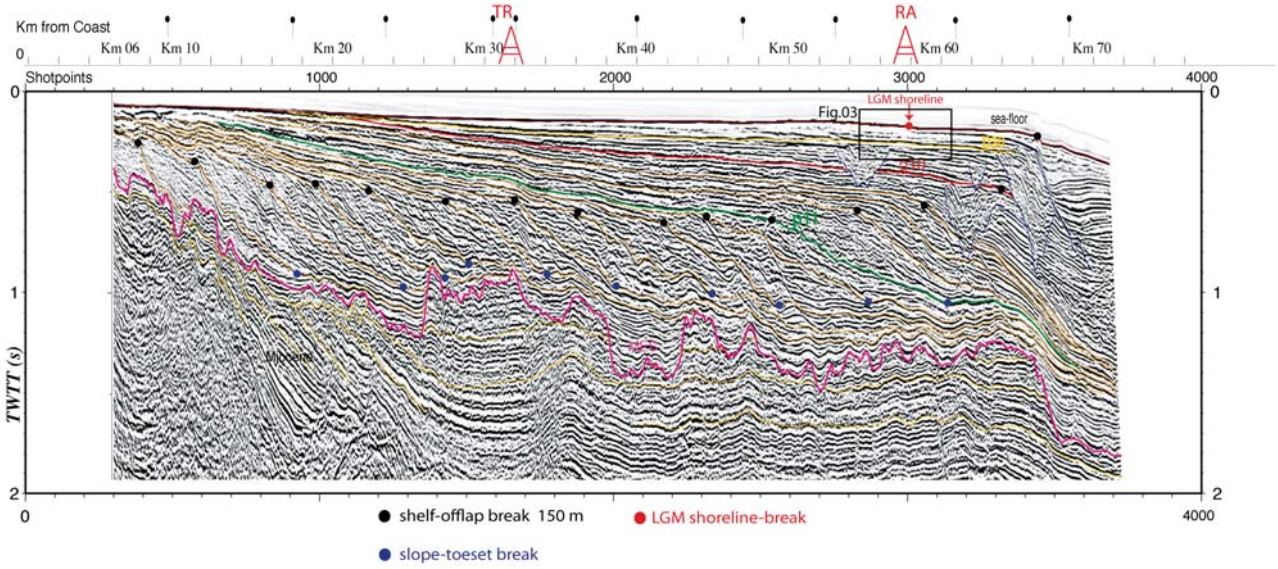

Figure 4 Seismic Profile LRM18 in TWTT (s) and interpretation of prograding clinoforms*. Black pins on top show cross-lines, Wells Tramontane (TR) and Rascass (RA) are projected on the profile. Shelf-Offlap breaks and Slope-toeset breaks and shoreline breaks have been identified on profile. Key reflectors are labelled and highlighted in colors MES (pink), p11 (green) , q10 (red), q5(orange) and sea-floor. Location of Figure 3 (Zoom) on this profile is also shown.*

FIGURE 4 –

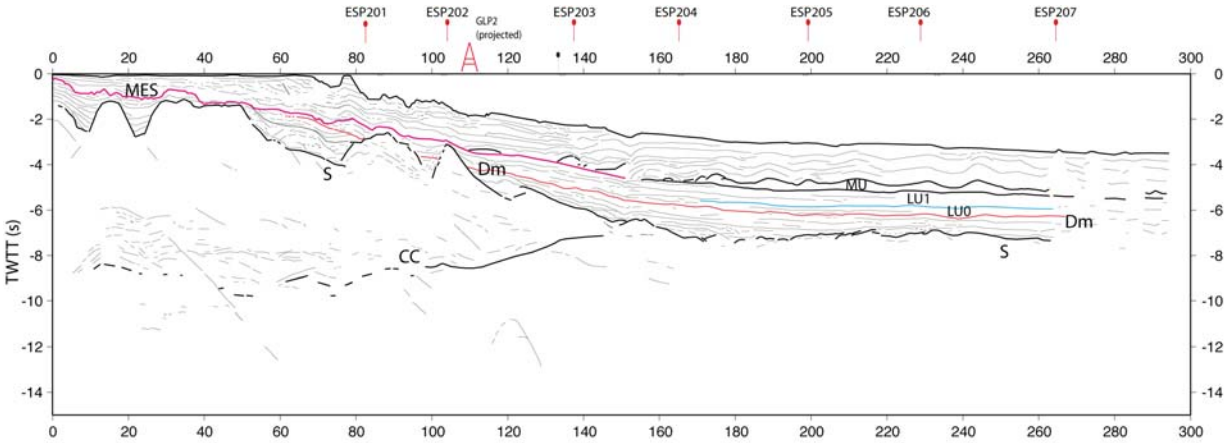

Figure 05 - line drawing of Profile ECORS NW-SE (in seconds TWTT)
(modified from Olivet, 1996 ; Bache, 2008; Bache et al., 2009 ; Bache et al., 2010 name of messinian surfaces adapted from Lofi et al. 2011).
Thick lines represent respectively from deepest to shallowest : base of continental crust (CC), top of substratum (S),
basal messinian erosional surface Dm (in red), base of presumed evaporites in blue LU1 ; base of probable turbidites (LU0),
margin messinian erosional surface (MES in pink), base and top of salt (MU), and sea-floor.

FIGURE 5 –

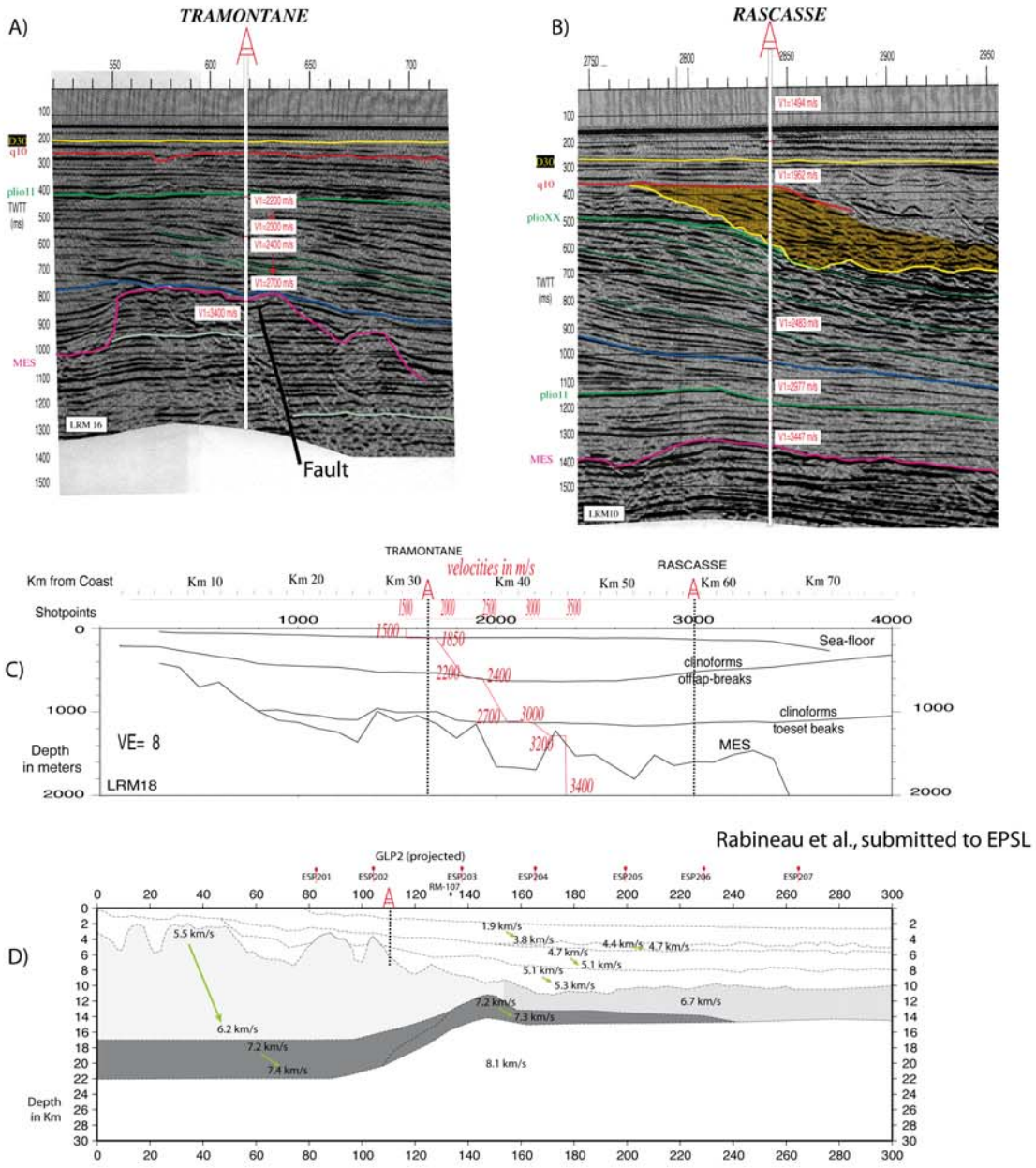

Figure 6-Velocity models

A) and B) Interval velocities measured in TRAMONTANE and RASCASSE; wells positionned on dip-profile LRM10 and LRM16 (see location on Figure 1).
Main reflectors have been identified : D30 (434,000 ka) ; q10 (around 1 Ma) ; plio11 (around 2,7 Ma) and the messinien margin erosional surface MES (5,3 Ma) (in pink) and light green reflector (Miocene) below the messinian on LRM16 (see age estimates in discussion). Note in orange on LRM10, a paleo-canyon cut along its course and sealed by the q10 erosional surface.
Note on LRM16, the presence of a Fault that offsets the light green Miocene reflector (from Bache, 2008).
In green nice clinoforms are developped with topsets, forestes and bottomsets, the last clinoform of this package is the PlioXX surface. Below the blue surface, reflexions are sub-plane and correspond to bottomsets of previously deposited clinoforms.
C) 2D evolution of velocites based on wells Tramontane and Rascasse projected on Profile LRM18 (see Figure 1 for location). Enveloppes for velocity intervals are based on geometries of deposits as observed on seismic profiles (velocities appeared to change from topsets to foresets and bottosets). Note also that those limits are not time-lines but related to major lithology changes. Within enveloppes interval velocities show linear variations and jumps at interfaces. Note also that extrapolation towards upper-slope is subject to caution as the evolution of velocities might be very different (in part due to the presence of canyons).
D) Velocity model used for time-depth conversion using Velocities as measured on ESP data (Pascal et al., 1993) and Sardinia data (Gailler et al., 2009)
and interpretation of seismic profile

FIGURE 6 –

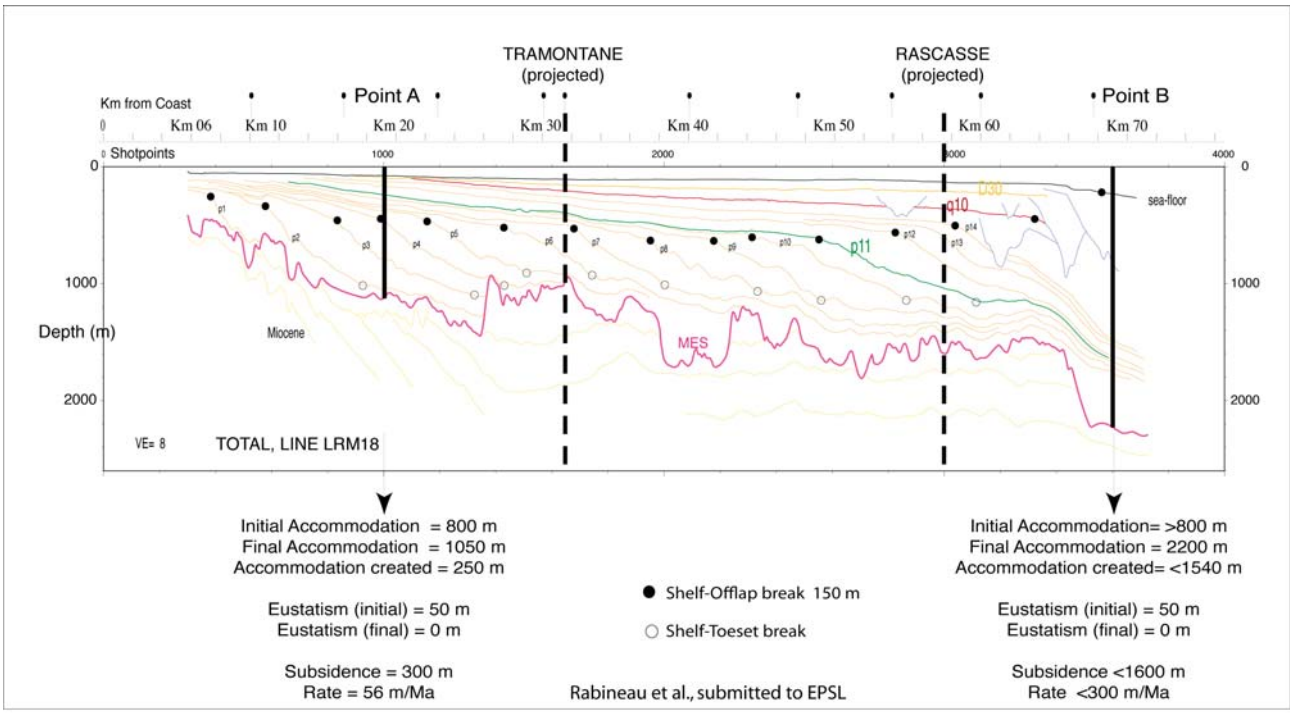

Figure 7- Seismic Profile LRM18 in depth (m) used for *calculation of 1D accommodation and subsidence at points A et B. Black pins on top show cross-lines, Wells Tramontane and Rascass are projected on the profile.*
Initial accommodation corresponds to early Pliocene stage. Final accommodation corrresponds to present-day stage. Here we considered that offlap breaks represent the shelf breaks with a constant paleowater depth approximated to 150 m. Eustatism at initial stage (early Pliocene) is considered to be betwween 40 and 70 m (Shackleton et Opdyke, 1977 ; Haq et al., 1987), here we used 50 m; eustatism at final stage (present -day) is equal to 0 m. Accomodation has been estimated by measuring the height of clinoforms (between offlap breaks and toeset breaks) which corresponds to the minimal space that enables clinoform deposition ; we added to this value the paleo-water depth of the offlap break (150 m). Accomodation = Eustatism + Subsidence. The rate of subsidence is calculated using a duration for Plioquateranry of 5.33 Ma (occurring after the Messinian Salinity Crisis).

FIGURE 7 –

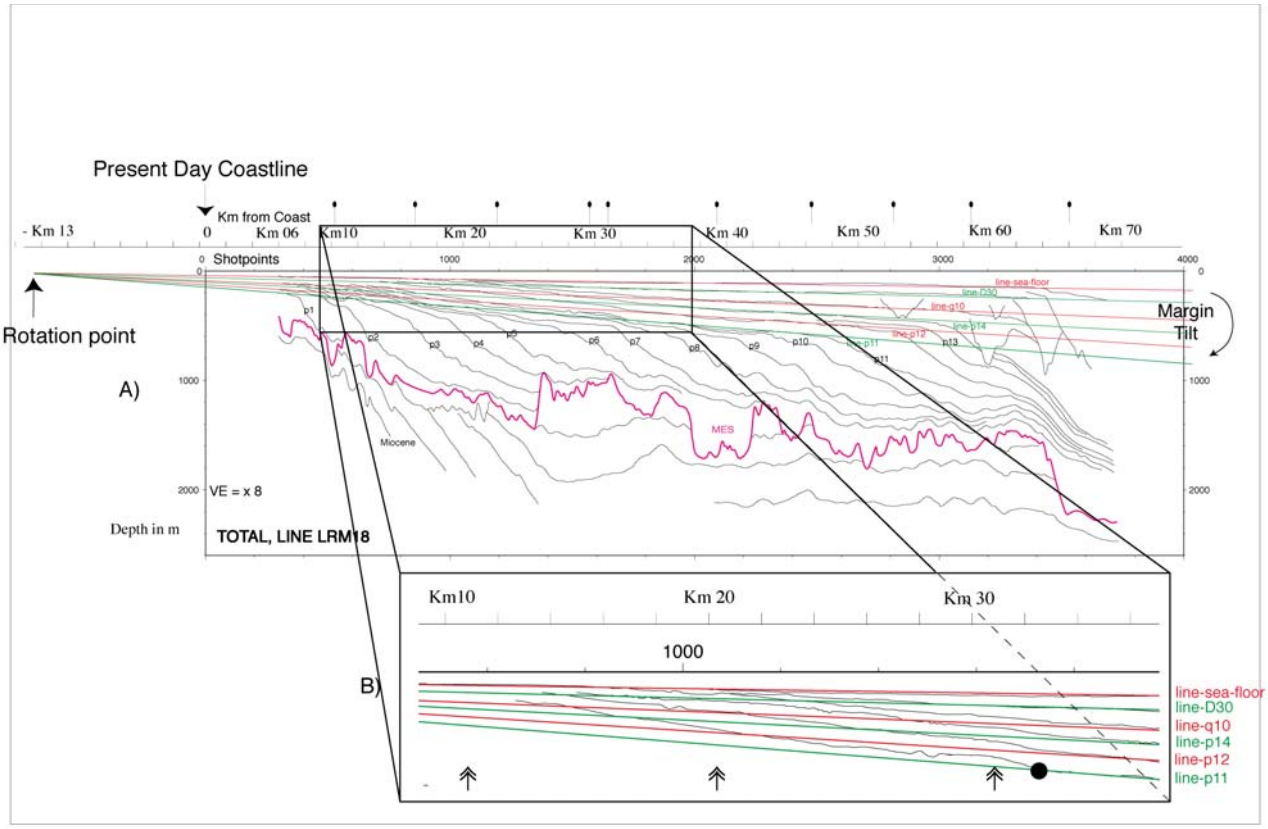

Figure 8 A) Seismic Profile LRM18 in depth (m) used for *calculation of 2D subsidence along the profile. Black pins on top show cross-lines. Topsets of reflectors p11 to present day sea-floor are well approximated to straight lines on the outer part of the shelf (from Km36 to Km70. Lines are inclined seaward, inclination increases with the age of reflectors. All lines have a common rotation point which is located 13 km landward of present-day coast. Inset B) shows the misfit of those lines in the inner part of the shelf. Note the black point (at Km 32) from which reflectors plio11 to plio14 are deformed (uplift of the inner part of the shelf) as well as q10 but to a lesser extent.*

FIGURE 8 –

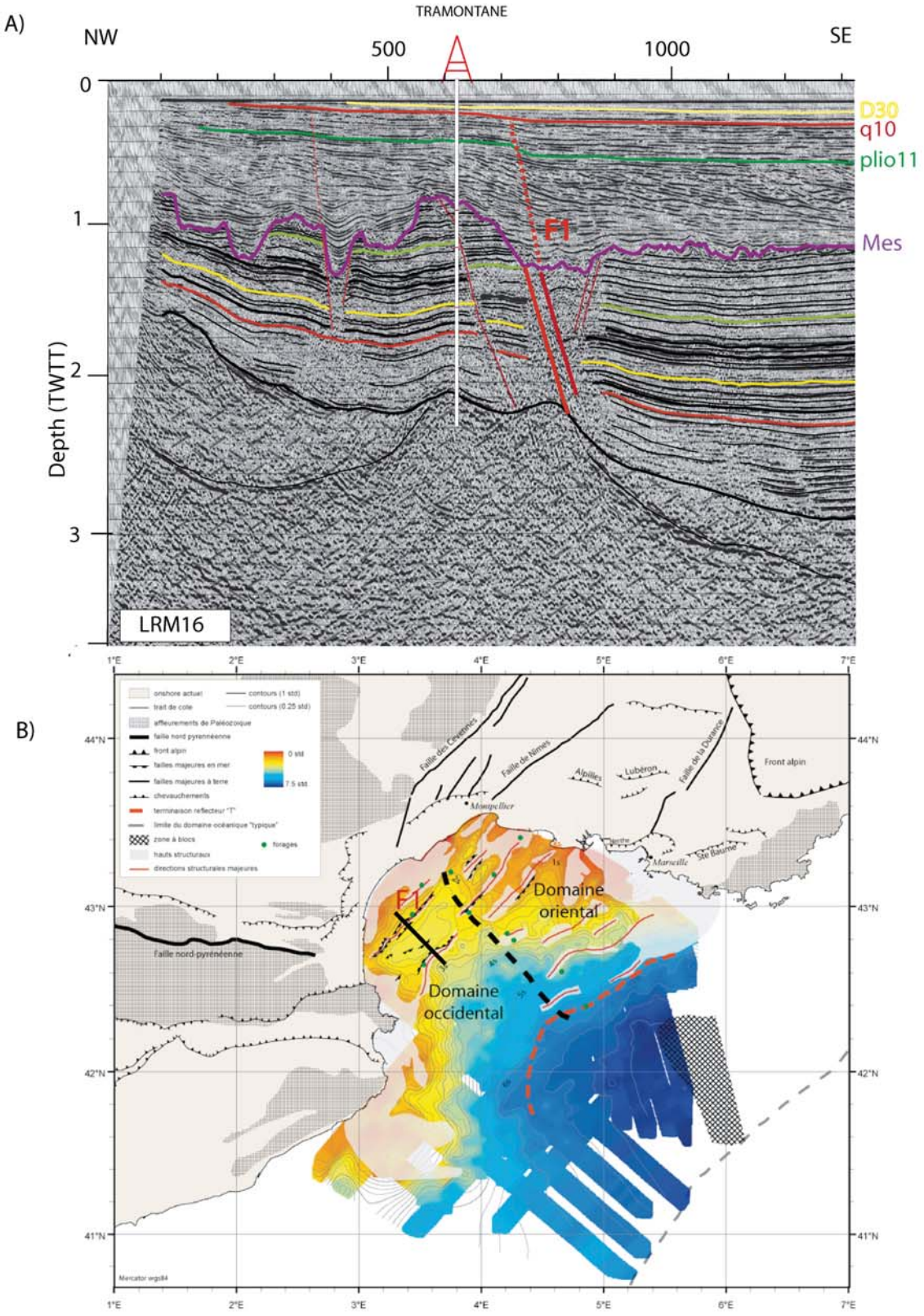

Figure 9 A) Zoom on Seismic Profile LRM16 in TWTT (s) and interpretation of Miocene and Plioquaternary strata. *Wells Tramontane is on the profile. Note the deformation of plio11 refelctor and q10 reflector just above a major deeper Fault F1. Interpretation of Miocene strata slightly modified from Bache, 2008. Another deformation can be suspected in the landward most part of the profile See position of profile and Faults on Figure B. B)* ***Mapping of Major Faults and depth of Substratum (in seconds twtt) from Bache, 2008. The thick line represent the position of Seismic Profile LRM16 shown in A). Major Fault F1 is localised near the Tramontane well*** *(green dot) on the profile.*

FIGURE 9 –

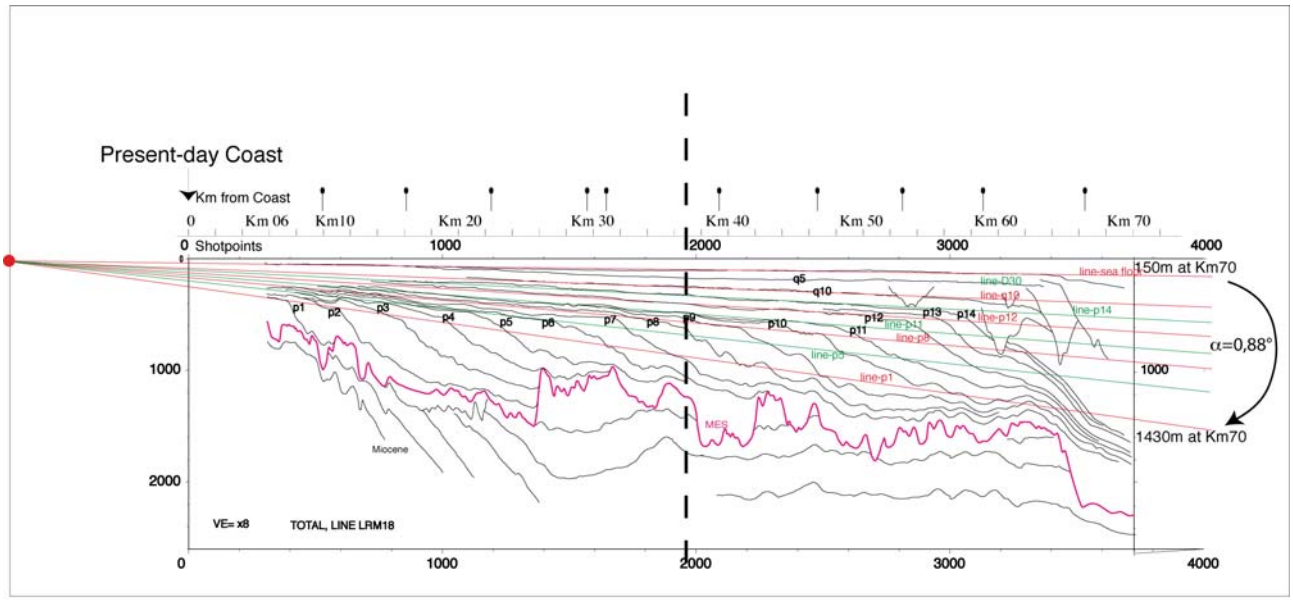

Figure 10 Seismic Profile LRM18 in depth (m) used for *calculation of 2D subsidence along the profile. Black pins on top show cross-lines. The inner part of the shelf (Km 0 to Km 36) has been reconstructed to correct the effect of post-depositional deformation (large scale deformation). In this configuration topsets of reflectors p1 to present day sea-floor are well approximated to straight lines both on the inner and outer part of the shelf. All lines are inclined seaward, their inclinations increase with the age of reflectors. All lines have also a common rotation point which is located 13 km landward of present-day coast. The tilting of the margin from p1 to present day can be measured directly on the profile, it reaches 1430 - 150 =1280 m at Km 70 from the coast. Considering that the first clinoform p1 can be dated as early Pliocene (just after the Zanclean reflooding) we estimated its age between 5.3 and 5 Ma. This allows us to calculate a subsidence rate going from 0 m/Ma at -13 Km landward of the coast to 240-255 m/Ma at Km 70 seaward from the coast (near the upper slope) or an angleof 0,88° (see figure 2).*

FIGURE 10 –

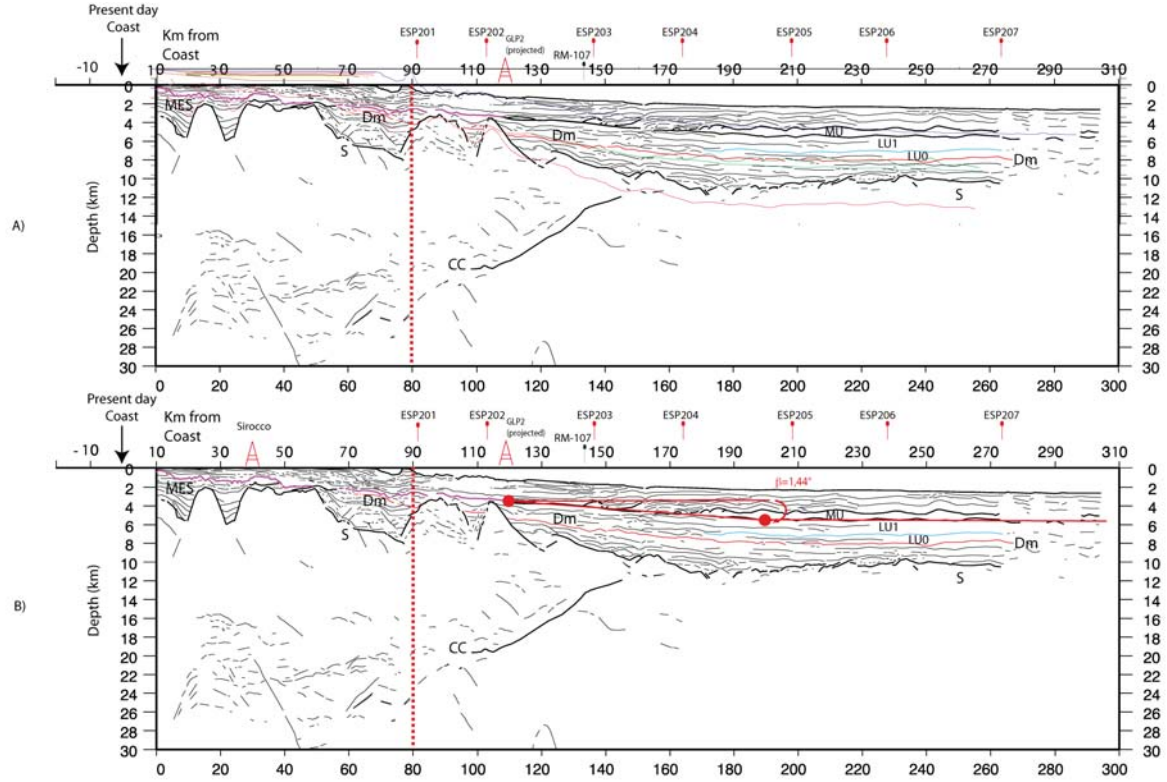

Figure 11– A) ECORS profile converted in depth (using previous velocity law-figure 06). Dm : discontinuity at the base of Messinian deposits; LU0, LU1 : lower unit of messinian age ; MU : mobile unit (salt) ; according to Bache et al., 2009, CC : Continental Crust. For a more detailed interpretation of Miocene and messinian deposits see recently published paper from Bache et al., 2009 ; Bache et al., 2010. The vertical dashed red line indicates a change in the direction of the seismic profile.

B) Approximation of the messinian surface to the base of salt with a straight line inclined seaward. The line has a rotation point which is located 22 km landward of present-day coast.

FIGURE 11 –

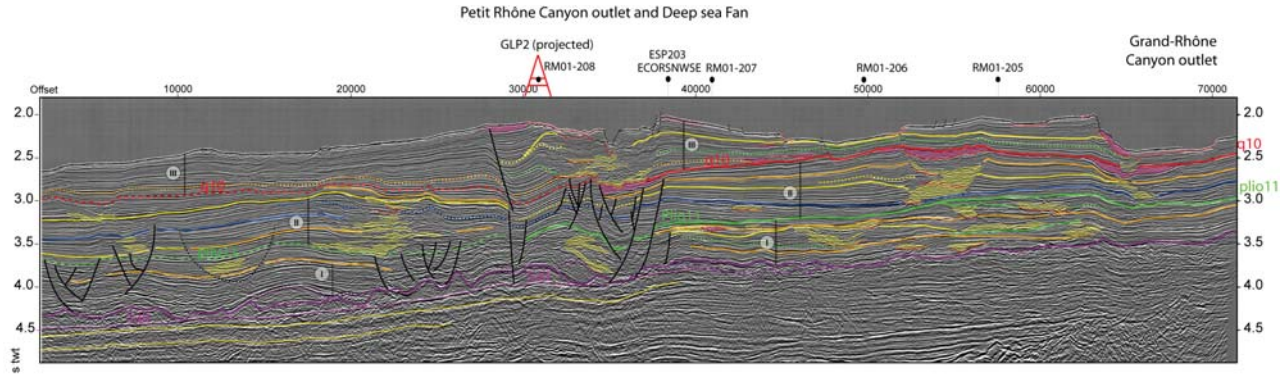

Figure 12
Seismic Profile RM01-107 (Courtesy Melrose) in TWTT (s) *(see location on figures 1)* ***and interpretation of Plioquaternary deep-sea fan deposits.***
Black pins on top show cross-lines, Well GLP 2 is projected on the profile.
I, II, III: Lower, Intermediate and Upper Series, respectively. I-3: channel/levee system 3 of Series I (1 to n from the oldest to the youngest). q10 (in red) and plio11 (in green) represent majour erosional boundaries respectiveley between Series I-II and Series II-III. Stratigraphic interpretation from the shelf correlated to the deep sea suggest ages of 2.7 Ma for Plio11 and 1 Ma for q10 (see discussion). Thin red lines are local erosional unconformities; pink bodies are local or regional MTDs.
Differencial subsidence is imaged by the inclinaison of the base of salt deposit (in pink). Local defomation, pull-downs can be observed below canyons, they are artefact due low water velocities in canyons compared to adjacent sediments . Note that the general westernward inclination is also observed in underlying deposits (yellow reflectors).

The rate of subsidence is calculated using a duration for Salt and Plioquateranry of 5.6 Ma (an age agreed by most authors, see CIESM, 2008).

FIGURE 12 –

Detailed process of the peak of the Messinian Salinity Crisis: Evidences from the Gulf of Lions (NW Mediterranean)

François Bache[1*]; Julien Gargani[2]; Jean-Pierre Suc[3,4]; Christian Gorini[3,4]; Marina Rabineau[5]; Jean-Louis Olivet[6]; Speranta-Maria Popescu[7]; Estelle Leroux[5,6]; Gwenaël Jouannic[2]; Damien Do Couto[3,4,8]; Jean-Loup Rubino[9]; Georges Clauzon[10]; Antonio Tadeu Dos Reis[11] & Daniel Aslanian[6]

[1] GNS Science, P.O. BOX 30368, Lower Hutt 5040, New Zealand.

[2] Université Paris-Sud, Laboratoire IDES, UMR 8148, Orsay, F-91405, France.

[3] UPMC Univ. Paris 6, UMR 7193, ISTEP, F-75005, Paris, France.

[4] CNRS, UMR 7193, ISTEP, F-75005, Paris, France.

[5] IUEM, Domaines océaniques (UMR 6538), 1 place Nicolas Copernic, 29280 Plouzané, France.

[6] IFREMER, Géosciences marines, LGG, BP 70, 29280 Plouzané Cedex, France.

[7] Geo-Biostrat-Data Consulting, 385 route du Mas Rillier, 69140 Rillieux la Pape, France

[8] TOTAL, 2 place Jean Millier, 92400 La Défense, Paris, France

[9] TOTAL, TG/ISS, CSTJF, Avenue Laribeau, 64018 Pau Cedex, France.

[10] C.E.R.E.G.E. (UMR 6635), Université Paul Cézanne, Europôle de l'Arbois, BP 80, 13545 Aix-en-Provence Cedex 04, France.

[11] Departamento de Oceanografia Geologica/UERJ-Brazil, Rua São Francisco Xavier, 524, 4º Andar, Maracaña, Rio de Janeiro RJ CEP: 20.550-900, Brazil.

*GNS Science P.O.BOX 30368, Lower Hutt 5040, New Zealand. f.bache@gns.cri.nz. Tel.: +64 4 5704686; fax: +64 4 570 4600.

1. Abstract

The Messinian Salinity Crisis is well-known to have resulted from a significant drop of the Mediterranean Sea level after its isolation from the world ocean at the end of the Miocene. This outstanding event has been intensely studied within the Mediterranean basins however new offshore observations from central basins have been collected to better constrain conceptual scenarios and numerical models. In this study, we review geological markers of the Messinian Salinity Crisis in the Gulf of Lions and show that detrital prisms deposited prior to the central evaporites, the precipitation of which occurred in a context of sea-level rise. These results highlight three steps for the evolution of the central Mediterranean basins during the peak of the Messinian Salinity Crisis. The first step immediately follows the major and fast sea-level drawdown and corresponds to a transfer of clastics from eroded margins to central basins. The second step corresponds to the deposition of thick central evaporites and *pro parte* contemporaneous wave abrasion during a slow landward migration of the shoreline. The third step is the catastrophic instantaneous reflooding of the Mediterranean. A numerical simulation of the Messinian evaporite precipitation shows that this scenario can be modelled assuming a value of evaporation minus precipitation when the basin was dried up higher than today.

Keywords: Messinian, Mediterranean, Erosion, Evaporites.

2. Introduction

The largest known sea-level fall on the Earth occurred as a result of the isolation of the Mediterranean Sea from the world ocean at the end of the Miocene. This isolation, associated with a significant evaporation rate led to the deposition of a thick series of evaporites in the central Mediterranean basins (Hsü et al., 1973) and intense subaerial erosion at its periphery

(Barber, 1981; Barr and Walker, 1973; Chumakov, 1973; Clauzon, 1973, 1978, 1982; Denizot, 1952; Ryan and Cita, 1978; Savoye and Piper, 1991). This event was the paroxysm of the Messinian Salinity Crisis (MSC). The well-accepted "desiccated, deep basin" model (Cita, 1973; Hsü, 1972; Hsü et al., 1973; Ryan, 1973) is based on a demonstrated deep Mediterranean Sea (over 1500 m) at the onset of its desiccation phase. In the 1990s, the peripheral Mediterranean basins, easily accessible to field studies, were used to constrain the timing of the MSC (Gautier et al., 1994; Hilgen and Langereis, 1993; Krijgsman et al., 1999; Lourens et al., 2004; Van Couvering et al., 2000). These advances have resulted in several new conceptual scenarios, mostly derived from the initial "desiccated, deep basin" model. Two groups of conceptual scenarios are usually referred to (Fig. 1): one that favours a synchronous deposition (at 5.96 Ma) of the first evaporites in all the Mediterranean basins before the huge sea-level fall (Krijgsman et al., 1999; Rouchy and Caruso, 2006), and the second that favours a diachronous deposition of the evaporites through two phases of desiccation (Butler et al., 1995; Butler et al., 1999; Clauzon et al., 1996; Riding et al., 1998). According to the second scenario, peripheral basins experienced deposition of evaporites (at 5.96 Ma) before the onset of a major sea-level fall and erosion and central basins experienced deposition of evaporites only after the onset of the sea-level fall. The peak of the MSC is the phase that begins with the huge sea-level fall and that ends with the catastrophic marine reflooding (phase 2 on figures). There is a large agreement on the age of the beginning of this paroxysm phase (5.60 Ma; CIESM, 2008), but its duration is still debated (70 kyrs: Krijgsman et al., 1999; *ca.* 140 kyrs: Bache et al., 2012; Butler et al., 1995; *ca.* 270 kyrs: CIESM, 2008) as also the age of its end (5.46: Bache et al., 2012; 5.332: CIESM, 2008; Krijgsman et al., 1999). Anyway, its brevity, together with the magnitude of the associated sea-level variation (Clauzon, 1982; Savoye and Piper, 1991), make this event quite unique in terms of depositional processes.

Despite the fact that the history of the peripheral basins is reconstructed in a satisfactory way, the relationship with that of the central basins is still unclear because the geophysical investigation of the central basins is often incompletely worked. Several aspects of the peak of the MSC have been undertaken using numerical models, in particular the huge sea-level fall and the following reflooding (Blanc, 2000; Blanc, 2006; Garcia-Castellanos et al., 2009; Govers, 2009; Govers et al., 2009; Krijgsman and Meijer, 2008; Meijer and Krijgsman, 2005; Ryan, 2008). Here, in order to clarify the succession of events which have affected the Mediterranean central basins, we re-visit the geological markers of the MSC in the Gulf of Lions showing the marginal transition to the Provence central Basin (Fig. 2) and we particularly study in detail the relationships between the subaerial erosional surface and the central evaporites. New constraints for conceptual scenarios of the MSC are provided and submitted to a first test with a numerical model.

3. Data and method

The Gulf of Lions (Fig. 2) is weakly deformed by Pliocene and Quaternary tectonics and characterised by a relatively high subsidence rate which has continuously created accommodation space (Bache et al., 2010; Bessis, 1986; Burrus, 1989; Rabineau et al., 2005; Steckler and Watts, 1980). This configuration, together with the availability of a large set of seismic reflection data (Fig. 2), has permitted accurate descriptions of the relationships between the Messinian halite and the sedimentary units of the Gulf of Lions margin (Bache, 2008; Bache et al., 2009; Gorini, 1993; Lofi et al., 2005). In this study, conventional and high-resolution seismic reflection data are interpreted using the principles of seismic stratigraphy (Vail et al., 1977). We identify seismic units using configurations of seismic reflectors including reflector continuity and termination. The extensive coverage of seismic data enabled an integrated seismic stratigraphy to be developed. Interpretation and correlation

of seismic reflectors have been assisted by biostratigraphic and lithostratigraphic data from eleven wells that sampled Miocene and younger sedimentary cover. Seismic two-way travel-time (TWT) has generally been tied to formation tops in wells using sonic logs.

4. Observations in the Gulf of Lions

4.1. Key surfaces and seismic units previously defined

Several sedimentary and erosional features related to the MSC have been previously observed in the Gulf of Lions. From the shelf to the deep basin, four key elements provide crucial information for constraining the interpretation of the MSC (Figs. 2 and 3).

(1) The Messinian Erosional Surface (MES) corresponds to the subaerial morphology preserved at the end of the MSC, just before the catastrophic reflooding of the Mediterranean (Bache et al., 2012). This surface has been used to estimate the maximum (>1500 m) sea-level fall (Clauzon, 1982). However, the seaward extension of this subaerial morphology has been smoothed by a transgressive ravinement surface (Bache et al., 2009) that does not allow to precisely locate the shore corresponding to the lowest sea level. The MES deeply eroded older deposits (Miocene shelf). Previous estimates indicate that more than 10,000 km^3 have been eroded from both the Rhône Valley and shelf of the Gulf of Lions (Bache et al., 2009). This represents twice the Storegga slide volume or three times the Mount Everest volume that has fed the central basin by the momentary subaerial exposure of only a small part of the Mediterranean periphery. The total amount of eroded volumes around the Mediterranean has yet to be evaluated in order to constrain mass variations and resulting regional isostatic response of the crust (Norman and Chase, 1986).

(2) Detrital prisms (Dm) have been identified at the outlet of the Messinian drainage systems in the distal part of the Gulf of Lions (Bache et al., 2009; Lofi et al., 2005). These units are sandwiched between the prograding pre-Messinian Crisis shelf and overlying Pliocene

126 sediments. The lower part of these prisms extends toward the basin beneath the earliest
127 central evaporites, and the upper part is contemporaneous with deposition of the central
128 evaporites (Bache et al., 2009). Two conflicting interpretations of the lower part have been
129 proposed. The first interpretation attributes these detrital prisms to submarine erosion forced
130 by pre-Messinian sea-level falls (Lofi and Berné, 2008). The second interpretation attributes
131 the same deposits to the subaerial erosion of the Gulf of Lions shelf during the Messinian sea-
132 level drawdown (Bache et al., 2009).
133 (3) The evaporite series of the Western Mediterranean central basin is usually divided into
134 “lower evaporites”, “halite” and “upper evaporites”. In the Provence Basin, the first evaporitic
135 unit (LU1), previously considered about 500-600 m thick (Lofi et al., 2005; Montadert et al.,
136 1978), has been recently revaluated at about 1500 m thick using more recent and dense
137 seismic reflection and refraction data (Bache et al., 2009). The total thickness of evaporites
138 (lower unit LU1, halite MU, upper unit UU) in the Western Mediterranean Basin is therefore
139 estimated to be on the order of 3 km. This reappraisal has significant consequences for
140 numerical models which typically use a total evaporite thickness of around 1500 m (Blanc,
141 2006; Govers, 2009; Govers et al., 2009; Meijer and Krijgsman, 2005) in the Western
142 Mediterranean.
143 (4) A transgressive ravinement surface (TRS) truncates detrital prisms in the region extending
144 from the evaporite domain to the shelf where the MES is observed (Bache et al., 2009; Bache
145 et al., 2012). The boundary between this surface and the MES has been interpreted as a
146 paleoshoreline and clearly highlights a two-step reflooding process (Bache et al., 2009; Bache
147 et al., 2012). We consider that the first step of reflooding (step I in Bache et al., 2012) was
148 sufficiently slow to allow wave abrasion and reshaping of previous topography (by the TRS).
149 The second step (step II in Bache et al., 2012) was so rapid that the MES has been preserved
150 from wave erosion in the landward part of the shelf. The preserved shoreline at the above

mentioned point just before the catastrophic reflooding represents a new reference for all studies of the MSC. The initial position of this paleoshoreline has been estimated between 600 m and 900 m below the present sea level (Bache et al., 2012) by subtracting the Pliocene and Quaternary subsidence from its present-day position. The rapid increase in water depth during the catastrophic reflooding was thus between 600 and 900 m. This reappraisal provides new information for numerical models that until now have commonly used a minimum value of 1000 m for the catastrophic reflooding (Blanc, 2006; Garcia-Castellanos et al., 2009; Loget and Van Den Driessche, 2006; Loget et al., 2005).

4.2. New observations

The transition between Pre-Messinian Crisis deposits and Messinian evaporites and the transition between evaporites and the TRS have been accurately examined in order to better constrain the beginning and the end of the peak of the MSC.

4.2.1. Pre-salt seismic units

Clinoforms dipping steeply basinward (Dm) fill two major incisions located at the outlet of the Messinian fluvial network (Figs. 2 and 3). These prisms have been sampled by GLP2 and Autan 1 wells where an undifferentiated Burdigalian to Tortonian age has been proposed (Brun et al., 1984; Cravatte et al., 1974; Guennoc et al., 2000). However foraminifer assemblages poor in stratigraphic markers from these wells do not allow to reject a Messinian age for Dm unit. The seismic unit located beneath Dm prisms is characterised by parallel reflectors in the Gulf of Lions shelf area and by sigmoidal progradations toward the basin (Fig. 4). Five reflectors (Mi1 to Mi5) are observed within this unit and analysed by wells, giving age constraints for Dm prisms. The youngest reflector preserved from Messinian erosion (Mi5) intersects three wells at the exact position of an obvious sedimentary boundary (in Mistral 1) or above it (in Tramontane 1 and Calmar 1) (Fig. 5). In Tramontane 1 and

Mistral 1 this boundary, respectively located at 1540 and 1675 m depth, corresponds to a transition from marine to littoral conditions (Fig. 5; Cravatte et al., 1974). The sediments overlying this boundary and located below the base of Dm are dated in these wells from Middle to Upper Miocene (Cravatte et al., 1974). In Calmar 1, the boundary is located at 1400 m and has been ascribed to the Serravallian/Tortonian transition (Fig. 5; Guennoc et al., 2000), leading to a younger age for the deposition of Dm prisms.

4.2.2. Transgressive evaporites

The TRS identified in the Gulf of Lions highlights the existence of a slow landward migration of the shoreline before the catastrophic reflooding of the Mediterranean (Bache et al., 2009; Bache et al., 2012). Seismic units onlapping this surface were not clearly identified due to the unclear seaward extent of this surface and the lack of seismic data to accurately observe this transition. First interpretations assumed that only the Upper Evaporites (UU) and 52 m of sandstones drilled in GLP2 well between 3437 and 3385 m (Brun et al., 1984) were deposited during this transgressive step (Bache et al., 2009; Bache et al., 2012). The sandstone unit contains a clayey level at 3426.70 m depth which provided a calcareous nannoflora with *Amaurolithus primus* and *A. tricorniculatus* (Fig. 7; Brun et al., 1984), that can be precisely dated between 5.54 and 5.35 Ma (Di Stefano and Sturiale, 2010; Raffi et al., 2006), *i.e.* in agreement with chronology of the reflooding proposed by Bache et al. (2012) (Fig. 8).

The TGS-NOPEC seismic line (Fig. 6) acquired in the Gulf of Lions in 2001 allows us to refine our interpretation of the transition from the TRS to the evaporite units. The TRS is characterised by its smooth aspect, the erosional truncation of the underlying series and by the onlap termination of the overlying series (Fig. 7). Thickness map of the seismic unit immediately above the TRS (Fig. 9) confirms its onlap configuration seaward of the paleoshoreline preserved just before the catastrophic reflooding. Toward the basin the base of

this seismic unit can be followed within the upper part of LU1 and its top corresponds to the top of UU. This configuration means that the upper part of LU1 and the overlying MU and UU units were deposited in a transgressive context, during the landward migration of the shoreline that led to the formation of the TRS. An heterogenous evaporitic body (thick of 266 m) has been drilled in GLP2 well between 3703 and 3437 m depth (Fig. 7; Brun et al., 1984). It is made of an alternation of halite, clays and anhydrite. The Messinian age of these evaporites is supported by the occurrence of *Amaurolithus tricorniculatus* in the overlying unit and attested by that of *Globigerina nepenthes* at 3508.70 m depth (Brun et al., 1984). This interval probably corresponds to the seismic facies mapped above the TRS (Figs. 7 and 9). In addition the clays sandwiched between the evaporitic bodies are characterized by 80% of planktonic foraminifers (at 3508.70 m from a side well core; Fig. 7), that is consistent with their deposition in a context of sea-level rise (Brun et al., 1984).

5. Scenario of the peak of the Messinian Salinity Crisis

These new observations lead to subdivide the peak of the MSC (phase 2) into three distinct steps including instantaneous events at the geological scale (Figs. 8, 10 and 11): (i) the sea level drop at 5.60 Ma which followed the high sea-level episode of Lago Mare 1, (ii) a slow rise in sea level at the origin of the TRS, and (iii) the very fast catastrophic marine reflooding at 5.46 Ma which caused the high sea-level episode of Lago Mare 3 (Clauzon et al., 2005; Bache et al., 2012). Lago Mare 2 is still an imperfectly explained episode of unknown duration, which only concerned the central basins (Clauzon et al., 2005; Fig. 6).

5.1. Step I, sea level drop: subaerial erosion and detrital deposition

The lower part of Dm prisms and its distal counterpart have been interpreted as deposited before the initiation of the Messinian drawdown dated at 5.60 Ma, *i.e.* during the Middle-Upper Miocene (Lofi and Berné, 2008), maybe at the Serravallian/Tortonian transition

226 characterised by the most pronounced global drawdown prior to the Messinian (Haq et al.,
227 1987). Arguments for this interpretation are the identification of five successive generations
228 of submarine canyons at the base and within the seismic unit that contains the prisms and
229 aggradational geometry of the topsets beds observed within one of the interpreted canyons,
230 which appeared to Lofi *et al*. (2008) as hardly compatible with the major Messinian lowering
231 phase.
232 An alternative interpretation links Dm prisms with the MES (*i.e.* the major Messinian
233 drawdown) (Bache et al., 2009). This interpretation is supported by the position of the prisms
234 at the outlet of the Messinian subaerial erosional network, the consistency between the
235 volume of sediments eroded by the MES and the volume of Dm prisms and the magnitude of
236 sea-level fall necessary to produce the erosional surface identified at the base of the prisms
237 (Bache et al., 2009). Our observations provide further arguments to support this interpretation.
238 The younger reflector identified on the Gulf of Lions shelf (Mi5) beneath the base of Dm unit
239 has been dated at around the Serravallian/Tortonian transition (Fig. 5). Description of the
240 interval that includes this reflector in boreholes and of a Serravallian/Tortonian fluvial
241 incision in the Rhône Valley (Besson et al., 2005) are consistent with a global sea-level fall at
242 the Serravallian/Tortonian transition (Haq et al., 1987). It means that Dm prisms have been
243 deposited after and independently of the Serravallian/Tortonian sea-level fall. The lower part
244 of Dm prisms extends within the basin deep beneath the halite (MU) and just beneath LU1,
245 which has been interpreted as the first evaporite unit (Lower Evaporites) deposited in the
246 Provence Basin (Bache et al., 2009). It suggests that the main Messinian sea-level drawdown
247 responsible of the formation of the MES (step I) occurred before the main phase of evaporite
248 precipitation (step II). The existence of submarine canyons within Dm units is not in
249 contradiction with a Messinian regressive environment. These canyons could have been

250 formed in a very short time at the beginning of the Messinian drawdown, when the shelf was
251 already exposed to subaerial erosion but before the almost complete desiccation of the basin.
252 Further observations support a deposition of Messinian evaporites in the Provence Basin after
253 the main Messinian sea-level drawdown. The MES is commonly described as extending
254 below the salt (MU) in the Gulf of Lions (Clauzon et al., 1996; Lofi et al., 2005). Lofi *et al.*
255 (2005) suggested that the MES could also be traced at the base of the Lower Evaporites (LU1)
256 based on the onlap termination of their seismic reflectors. Our observations highlight that the
257 most significant erosion in the basin is located at the base of Dm prisms (Fig. 3). Erosional
258 surfaces have been observed within the evaporitic units (LU1-MU-UU) but of lesser
259 significance, suggesting that a huge sea-level drawdown after a first stage of evaporite
260 deposition under a significant water column is unlikely.
261 An Upper Miocene tectonic phase has also been highlighted in the western part of the Gulf of
262 Lions (Mauffret et al., 2001). Lofi *et al.* (2008) suggested that this episode, probably
263 accompanied by an increase of clastic sediment supply, is a possible origin for the formation
264 and subsequent filling of the submarine canyons observed within Dm prisms. In order to
265 decipher the tectonic and eustatic origin of theses canyons, the same authors suggested
266 looking for the existence of submarine canyons on the eastern Gulf of Lions which was not
267 affected by Upper Miocene tectonics. The identification of Dm prisms and of their basal
268 incision in the eastern part of the Gulf of Lions (Fig. 3; see also Bache et al, 2009) allows to
269 discard such a tectonic hypothesis.
270 Observation of clastic deposits beneath the central evaporites in the Gulf of Lions provides
271 new perspectives for the interpretation of pre-evaporites deposits elsewhere in the
272 Mediterranean. Dives have been performed offshore the region of Nice where a Messinian
273 low sea-level detritic cone has been described by Savoye and Piper (1991) who did not
274 provide clear relationships between detritals and the central evaporites. The clastics are

constituted by rounded pebbles with buff-coloured sandstones suggesting a subaerial deposition (Savoye and Piper, 1991). Clastic deposits related to the MES and contemporaneous with central evaporites have been identified on the Sardinian (Sage et al., 2005), Valencia (Maillard et al., 2006) and Ligurian (Obone-Zue-Obame et al., 2011) margins. Unlike the Gulf of Lions, seismic data used for these studies did not allow to interpret seismic units beneath the evaporites. Even if terrigenous input was probably higher in the Gulf of Lions due to the strong fluvial network dominated by the powerful Rhône River, detrital deposits linked with the MES beneath the central evaporites near these margins cannot be excluded.

Thick clastic deposits within a channelled system are overlain by the Messinian evaporites offshore Cyprus according to Montadert et al. (in press) who refer them to the Nile input during the Mediterranean desiccation. In the Levantine Basin, identical relationships between clastic deposits and Messinian evaporites were identified offshore Israel by Bertoni and Cartwright (2007). The similarity of the events which affected the Western and Eastern Mediterranean basins is thus suggested, starting by the desiccation phase at the origin of the MES and thick clastic deposits (step I) followed by evaporite deposition (step II).

The sea level drop is generally accepted to have been very fast, *ca.* 1500 yrs (Benson et al., 1991) but the duration of the clastic deposition episode cannot be estimated. Accordingly, the age of the upper limit of the detrital deposition episode on Figure 7 is fully speculative.

5.2. Step II, onset of the reflooding: evaporite deposition and marine abrasion

The large amount of salt precipitated during the MSC requires the evaporation of about 8 times the volume of the Mediterranean and thus continuous water inputs from oceans to the Mediterranean during the precipitation stage (Benson et al., 1991; Blanc, 2006; Hsü et al.,

1977; Ryan, 2009). To explain this crucial point, precipitation in all the basins (peripheral and central) before the huge Messinian sea-level fall and before the total isolation of the Mediterranean (Krijgsman et al., 1999) is often referred to and quite easy to reproduce with numerical modelling (Blanc, 2006; Garcia-Castellanos and Villasenor, 2011; Meijer and Krijgsman, 2005; Ryan, 2008). However sedimentary geometries in the central Mediterranean basins do not support this hypothesis, which would imply erosion and detritic deposits after the deposition of thick evaporites.

Our observations show a significant detrital phase (step I) followed by evaporite precipitation (step II). The age of the detrital episode deduced from the relationship between the MES and central basin evaporites and the relationship between evaporitic sequences and the TRS identified in the Gulf of Lions suggests that a significant part of the evaporites (upper part of LU1, MU and UU) has been deposited after the main Messinian drawdown and during a transgressive episode (step II), which occurred before the catastrophic reflooding of the Mediterranean (step III). Therefore, precipitation of the lower part of LU1 during the massive drawdown cannot be excluded. Similar conclusions can be assumed for the Eastern Mediterranean because of the location of the Messinian evaporites above the clastic deposits (Bertoni and Cartwright, 2007; Montadert et al., in press).

Duration of deposition of central evaporites is currently impossible to predict. The authors agree for a very fast process for halite and potash salt deposition (for example, 50 kyrs, even less, are suggested for the Sicilian halite, thick of about 700-800 m if undeformed; Bertini et al., 1998; CIESM, 2008).

A landward migration of the shoreline (step II) implies an increase of accommodation space for sedimentation. This process can be explained by (i) subsidence, (ii) by a rise of the Mediterranean sea-level or (iii) by a combination of both. Transfer of sediment from the eroded margins to the basin accompanied by a high precipitation rate of evaporites can

generate subsidence in the central basins. However the observation of transgressive ravinement surfaces in the Valencia Trough (García et al., 2011) and possibly in the Alboran margin (Estrada et al., 2011) as well as the necessity of water inputs from oceans to precipitate evaporites suggest a combination of subsidence and increase of the Mediterranean sea-level (Bache et al., 2012). This context coupled with a high evaporation rate was favorable to precipitate thick evaporites at the centre of the Mediterranean after the major Messinian drawdown dated at 5.60 Ma (Butler et al., 1995; Butler et al., 1999; CIESM, 2008; Clauzon et al., 1996; Riding et al., 1998) and before the catastrophic reflooding of the Mediterranean at 5.46 Ma (Bache et al., 2012), followed by a continuing sea-level rise well-documented at 5.332 Ma (Hilgen and Langereis, 1993; Lourens et al., 2004; Van Couvering et al., 2000).

Here, we assume sufficient water inputs from ocean after the Messinian drawdown and before the catastrophic reflooding. Recent numerical models suggest that such water input is insufficient or unlikely to occur after the closure of the Rifian Corridor (Blanc, 2002; Garcia-Castellanos et al., 2009; Govers, 2009; Govers et al., 2009). The numerous uncertainties on models constraints (erodibility, uplift rate, climate data…) and the lack of alternative conceptual scenarios consistent with our observations do not allow to discard our assumptions. Loget et al. (2005) have shown that intense regressive erosion developed inevitably in the Gibraltar area after the Messinian drawdown. It should be a likely process to explain a continuous input of marine waters necessary to precipitate enough evaporites in the desiccated Mediterranean Basin.

In the Eastern Mediterranean, wave ravinement surfaces comparable to the TRS observed in the Gulf of Lions have been observed off the Nile Delta in the interfluves bordering the Abu Madi canyon, where it contrasts sharply with the lowermost part of the canyon fill (Dalla et al., 1997). A series of flat ravinement surfaces have also been identified in the Levantine

Basin and ascribed to wave erosion (Bertoni and Cartwright, 2006). Our interpretation of the TRS in the Gulf of Lions (and Western Mediterranean) provides good perspectives to discuss the occurrence of step II in Eastern Mediterranean and to compare the evolution of these two parts of the Mediterranean during the peak of the MSC.

5.3. Step III, instantaneous catastrophic reflooding: prograding Gilbert-type fan deltas and completed inundation

In several places in the Mediterranean Basin, it has been observed that the post-Crisis marine reflooding preceded the Zanclean GSSP (Calabria: (Cavazza and DeCelles, 1998); Dardanelles Strait: (Melinte-Dobrinescu et al., 2009); Sicily: (Londeix et al., 2007); Apennine Foredeep: (Popescu et al., 2007)). Indeed, this extremely fast reflooding has been dated at 5.46 Ma (Bache et al., 2012), *i.e.* about 128 kyrs before the Zanclean GSSP corresponding to the base of the Trubi Formation in Sicily dated at 5.332 Ma (Lourens et al., 2004; Van Couvering et al., 2000). The excessively brief duration of this episode [comprised between <2 yrs (Garcia-Castellanos et al., 2009) and *ca.* 36 yrs (Blanc, 2002)] is attested by prograding sediments within the fluvial valleys (suddenly transformed into marine rias): debris flows with large blocks stopped just at the front of subaerial - submarine deposits, overlain by conglomeratic to sandy foreset beds of Gilbert-type fan deltas (Bache et al., 2012). Then, the continuing sea-level rise in the Mediterranean is illustrated at 5.332 Ma by the Trubi deposits onlapping the fanglomerate deposits in Calabria (Cavazza and DeCelles, 1998) and the Arenazzolo Unit in Sicily (Bache et al., 2012; Popescu et al., 2009), and the Argille Azzurre Formation onlapping the Colombacci Formation in the Apennine Foredeep (Bache et al., 2012; Popescu et al., 2007). Later, continuing sea-level rise is indicated by some marine incursion(s) into the sedimentary filled and emerged rias (*e.g.*: Roussillon Basin at Trouillas: (Suc, 1976); Var area at Saint-Isidore: (Clauzon et al., 1990); Níjar Basin at Gafares: (Bassetti

et al., 2006)). Cavazza and DeCelles (1998) proposed to refer this "additional sea-level rise" to the isostatic readjustment resulting from the Mediterranean Basin reflooding. The time-interval which separates the catastrophic reflooding in Sicily evidenced at the base of the Arenazzolo Unit (estimated at 5.460 Ma; Bache *et al*., 2012) from the base of the Trubi Formation (dated at 5.332 Ma; Van Couvering *et al*., 2000; Lourens *et al*., 2004), 128 kyrs, is too long to be ascribed to the isostatic downlift which should be of the order of about ten thousand years only if we refer to the relatively low amplitude sea-level rise of the Holocene (Lambeck and Bard, 2000). Bache *et al*. (2012) preferred to consider the continuing global sea level rise after the catastrophic reflooding to explain the wider inundation observed after 5.332 Ma around the Mediterranean.

6. Test by numerical modelling

In order to discuss the relevancy of the proposed scenario, several numerical experiments have been performed. The aim of these numerical experiments is to test if the scenario is reliable taking into account realistic hydro-climatic conditions. The results are not used to support the scenario, but to illustrate the consistency of our interpretation of the geological observations.

The tested numerical model allows to estimate a water and a salinity budget of the Western Mediterranean Basin. As a complementary interest, it allows to predict the level of the Mediterranean Sea and the evaporite thickness in the Western central Basin, an output that can be compared with data. The method to perform such a numerical experiment is already indicated in several studies (Blanc, 2000; Blanc, 2006; Gargani et al., 2008; Gargani and Rigollet, 2007; Meijer, 2006; Meijer and Krijgsman, 2005) and details are also reported in the supplementary material. Basically, the quantitative influence of the Atlantic sea-water inflow, river discharge and rainfall is taken into account and counterbalanced by the rate of water

evaporation. The relevant factors controlling the water budget are the climatic conditions (precipitation, evaporation, and the resulting river discharge) and the context of the Atlantic/Mediterranean connection (sea-water inflow). In this simple model, the mechanism that reduces/increases the input of Atlantic waters (tectonic uplift or relaxation, erosion of the paleo-sill, isostatic rebound, global sea-level variations) and the modified regional and global climatic contexts are not considered.

On the other hand, several constraints have been considered in the numerical experiments such as our age model, the proposed steps of the peak of the MSC and the corresponding estimates of the Mediterranean sea level (see previous section; Bache et al., 2012). Indeed, the input data (precipitation, evaporation, river discharge, Atlantic sea-water inflow) of the numerical model have been chosen in order to fit the geological observations presented above and their interpretation (a 1500 m sea-level drawdown at 5.60 Ma; deposition of the thick evaporite body starting after the sea-level fall and during a slow sea-level rise from -1500 m to -900/-600 m depth until 5.46 Ma; a catastrophic instantaneous reflooding at 5.46 Ma). The numerical experiment (Fig. 12) shows that it is possible to obtain a significant quantity of evaporites (>2000 m in thickness) in accordance with the seismic data when considering a value of E-P at the time of the drop of sea level of 1.75 $m^3/m^2/yr$ and a river discharge of 7500 m^3/s.

7. Discussion

The data from the Gulf of Lions presented in this paper and their interpretation, consistent with the interpretation of similar data from the Eastern Mediterranean (Bertoni and Cartwright, 2007; Montadert et al., in press), lead to revise the debated conceptual scenarios and to conceive new constraints for numerical models.

7.1. Revision of conceptual scenarios

Mediterranean evaporites have been deposited in peripheral and central basins. No physical link has been established between these two domains, and evaporites from the central basins have not been fully sampled or accurately dated. Therefore the timing of evaporites deposition in the central basins may be quite different from that of the peripheral basins (5.96-5.60 Ma; Clauzon et al., 1996; CIESM, 2008).

The synchronous scenarios imply that evaporites from the central basins have been formed under a high water column. The diachronous scenarios involve the isolation of peripheral sub-basins and evaporite deposition in relation with an initial sea-level fall (~150 m) followed by deposition of central evaporites after the major drop in sea level (~1500 m) (Fig. 1). Only a diachronous scenario is consistent with step I of the peak of the MSC in the Gulf of Lions (Figs. 8, 10 and 11), that we interpret as corresponding to the subaerial exposure of the shelf and deposition of huge detrital prisms before the precipitation of evaporites.

Hardie and Lowenstein (2004) re-interpreted the cores from DSDP Legs 13 and 42A and suggest that evaporites of the central Mediterranean were deposited under relatively deep-water (below wave base) conditions. Considering that only a small part of the upper stratigraphic units of the evaporitic body have been sampled (tens of metres), these authors specified: "*Until we have deep cores that penetrate the entire evaporite section we cannot hope to unravel more from existing DSDP cores than the depositional history of the very last phase of the Messinian evaporite body that lies beneath the floor of the Mediterranean Sea*". Deep-water (below wave base) conditions for this last episode is in agreement with the end of our proposed step II of the peak of the MSC in the Gulf of Lions (Figs. 8, 10 and 11), which would correspond to the deposition of central evaporites in a context of sea-level rise.

An extensive discussion resulted in a consensus now largely accepted (CIESM, 2008), following the proposal of Clauzon et al. (1996) in separating the desiccation cycles of the

449 peripheral basins during which the Mediterranean was full of water (5.96 – 5.60 Ma) from the
450 almost complete drying up of the central basins (5.60 – 5.46 Ma), which constitutes the peak
451 of the MSC. Our study supports this scenario. However, controversy continues about the
452 status of two Mediterranean regions:

453 - Sicily: a peripheral basin (relatively deeper than the others) for many authors (Bache
454 et al., 2012; Bertini et al., 1998; Butler et al., 1995; Clauzon et al., 1996; Clauzon et
455 al., 2005; El Euch-El Koundi et al., 2009; Pedley and Grasso, 1993; Pedley et al.,
456 2007; Popescu et al., 2009; Suc et al., 1995) or a central deep basin uplifted during the
457 Pliocene and Quaternary (Krijgsman et al., 1999; Krijgsman and Meijer, 2008; Manzi
458 et al., 2009; Manzi et al., 2011; Rouchy and Caruso, 2006; Rouchy and Saint Martin,
459 1992; Roveri et al., 2008a; Roveri et al., 2008b);
460 - Apennine Foredeep: an appendix of the central deep Ionian Basin (Roveri and Manzi,
461 2006; Roveri et al., 2008b) or a perched relatively deep basin isolated during the peak
462 of the MSC (Bache et al., 2012; Clauzon et al., 1997; Clauzon et al., 2005; Corselli
463 and Grecchi, 1984; Popescu et al., 2007).

464 Even if similar data characterize the West and East Mediterranean basins as mentioned
465 above, continuing investigations are necessary not only in these debated areas but also in
466 coring the central evaporites to reach a consensus at the size of the entire Mediterranean
467 and, as a consequence, to perform a new generation of numerical modellings at this scale.
468

469 ### *7.2. Constraints for numerical models*

470 During the last decade, several numerical models have been performed to complete the
471 history of the MSC insufficiently elucidated from field and analytic data:

- geomorphological models (Messinian erosion) (Babault et al., 2006; Garcia-Castellanos et al., 2009; Gargani, 2004a, b; Loget and Van Den Driessche, 2006; Loget et al., 2005)
- sedimentological models (Messinian evaporites) (Blanc, 2002; Blanc, 2000; Garcia-Castellanos and Villasenor, 2011; Gargani et al., 2008; Krijgsman and Meijer, 2008; Meijer, 2006; Meijer and Krijgsman, 2005)
- geodynamical models and vertical movement (isostasy) modelling (Duggen et al., 2003; Gargani, 2004a, b; Gargani et al., 2010; Govers, 2009; Govers et al., 2009; Norman and Chase, 1986)
- oceanographic and atmospheric modelling (Alhammoud et al., 2010; Gladstone et al., 2007; Meijer and Tuenter, 2007; Murphy et al., 2009; Schneck et al., 2010)
- complex interaction modelling (between climate, global sea-level, tectonic, sea-water inflow and river discharge) (Garcia-Castellanos and Villasenor, 2011; Gargani et al., 2008; Gargani and Rigollet, 2007)

These models have probably contributed to improve the understanding of the MSC and highlighted the complexity of this event. Indeed, various complex feedback processes were involved in this crisis and justify the use of a modelling approach. Furthermore, modelling approach allows to test quantified data. As a consequence, modelling results have led to generate new ideas.

Such results are used to argue for and against synchronous or diachronous scenarios. It is often concluded from modelling that the evaporitic sedimentation in the central Mediterranean basins began before any drawdown of sea-level at 5.60 Ma (Blanc, 2006; Govers, 2009; Govers et al., 2009; Krijgsman and Meijer, 2008; Meijer and Krijgsman, 2005). To support this hypothesis, the authors invoke a rise in salinity sufficient to precipitate evaporites before the sea-level drop (Blanc, 2006), either argue that a complete blocking of

497 Atlantic seawater exchange (caused by flexural uplift) after the major drawdown would
498 prevent the deposition of thick evaporites at that time (Govers, 2009), or consider that
499 evaporite thickness (ca. 3 km where undeformed) calculated for shallow-water deposition of
500 the so-called "Lower Evaporites" in the central basins is unrealistic (Krijgsman and Meijer,
501 2008).
502 Modelling outputs depend on the data available as well as assumptions that could not be
503 completely constrained nor tested. We believe that models do not demonstrate that a specific
504 interpretation is the "truth", but could allow verifying a minimum of coherency and
505 plausibility in the interpretation.
506 Our numerical simulation (see supplementary material and Figure 12) shows that (1) the sea
507 level in the central basins and the thickness of the evaporites are strongly dependent of
508 evaporation/precipitation rates and Atlantic water flux; (2) a value of E-P>1.75 $m^3/m^2/yr$ is
509 required to reproduce a precipitation of thick evaporites (>2000 m) in the central basins after
510 the major sea-level drawdown, assuming a river discharge comparable to the present-day of
511 about 7500 m^3/s (Gargani and Rigollet, 2007; Meijer and Krijgsman, 2005; Struglia et al.,
512 2004).
513 In the absence of any alternative, previous studies of water and salt budget have used present-
514 day hydrological fluxes with E-P ranging between 0.5 and 1 $m^3/m^2/yr$ (Meijer and Krijgsman,
515 2005). E-P value of 0.9-1 $m^3/m^2/yr$ during the peak of the MES is also suggested from recent
516 climate modelling (Murphy et al., 2009). The higher value of E-P (1.75 $m^3/m^2/yr$) required in
517 our model to reproduce a mass of evaporites in agreement with our observations is however
518 consistent with the reconstructed climatic parameters at the time of the MSC indicating lower
519 annual precipitations and higher mean annual temperature than today in the southwest
520 Mediterranean lands (Fauquette et al., 2006; Van Dam, 2006).

521 In the Dead Sea, which can be compared to the Mediterranean Basin at the time of the MSC,
522 the rate of evaporation has been measured between 1.7 $m^3/m^2/yr$ and 1.25 $m^3/m^2/yr$ between
523 1944 and today (Yechieli et al., 1998). With regard to the low precipitation rate (about 0.1
524 $m^3/m^2/yr$) at the shore of the Dead Sea (Neumann et al., 2010), an average E-P value of 1.5
525 $m^3/m^2/yr$ can be considered. The E-P value of 1.75 $m^3/m^2/yr$ required to reproduce a
526 precipitation of thick evaporites (>2000 m) in the Mediterranean central basins after the major
527 sea-level drawdown is thus acceptable. Moreover, evaporation rates >2 $m^3/m^2/yr$ have been
528 recorded in various lakes in arid regions (Abd Ellah, 2009; Kotwicki and Isdale, 1991).
529 A higher E-P value than today is all the more suitable so as it probably increased during the
530 desiccation phase (2-II), an evolution which is suggested by the momentary migration of the
531 subdesertic plants 3° northward their habitat at the onset of the MSC (Fauquette et al., 2006;
532 Popescu et al., 2007).
533 New observations in the Gulf of Lions provide good perspectives to constrain the other types
534 of modelling the MSC process. In particular, sedimentary transfers implied by step I (erosion
535 at the Mediterranean periphery and huge detrital deposits in the central basins) should be
536 taken into account when modelling the isostatic response to the outstanding changes in sea
537 level.
538

539 ## 8. Conclusion

540 Using seismic lines and data from wells in the Gulf of Lions, we show that detrital prisms
541 have been deposited before and during the deposition of evaporites in the Mediterranean
542 Provence-Algiers central Basin. The upper part of these evaporites has been deposited
543 contemporaneously with the formation of a transgressive ravinement surface, during the
544 landward migration of the shoreline. Three successive steps subdividing the peak of the MSC
545 (5.6-5.46 Ma) are defined to characterise this sedimentary pattern: step I (5.6-? Ma)

546 corresponds to the deposition of detritals in relation with intensive subaerial erosion
547 immediately after the fast Messinian major sea-level drawdown; step II (?-5.46 Ma) is
548 characterised by deposition of evaporites (more than 2 kilometers in thickness) since the sea-
549 level drawdown and during a slow sea-level rise resulting in landward migration of the
550 shoreline; step III is the instantaneous catastrophic reflooding of the Mediterranean at 5.46
551 Ma.
552 This scenario, the first to be expressed for the peak of the MSC, has been numerically
553 modelled for the Western Mediterranean and the expected thickness of evaporites implies that
554 precipitation minus evaporation (E-P) was higher than today when the basin was dried up.
555 Because of similar observations, this scenario should be expandable to the whole
556 Mediterranean. The missing pieces for continuing to improve the understanding of the peak of
557 the MSC at the scale of the whole Mediterranean are ground-truth observations of the pre-
558 evaporite geometries as well as an accurate datation of the corresponding sediments.
559 Recognition at larger scale of the critical stratigraphic markers identified in the Gulf of Lions
560 in other Mediterranean basins should allow:
561 1/ a finer chronostratigraphic constraint of the MSC leading to comparisons between different
562 basins. In particular, the understanding of the connections between Western and Eastern
563 Mediterranean and the role of sill that probably separated these basins is necessary to model
564 the MSC for the whole Mediterranean (Bache et al., 2012; Gargani et al., 2008; Gargani and
565 Rigollet, 2007; Leever et al., 2011; Leever et al., 2010);
566 2/ the quantification of vertical movements across the whole Mediterranean that will lead to
567 better understanding of the behaviour of the lithosphere (its rigidity) in response to rapid
568 variations of load during the MSC (sedimentary transfers, sea-level variations).
569 New data acquisition (geophysical and sampling) is needed in the central basins to provide
570 accurate dating of the Messinian events, for example in drilling the pre-salt sedimentary

deposits. In addition, another important perspective relates the Messinian climate. A precise estimate of evaporation and precipitation rates as well as Atlantic water flux is needed to constrain numerical modelling of the MSC. Anyway, this refined scenario of the MSC, with particularly a first complete reconstruction of the peak of the crisis, opens new and promising perspectives for a significant progress in deciphering this outstanding episode.

9. Supplementary material

To obtain the requested sea-level variation and to predict the observed evaporite thickness in the Western Mediterranean Basin, it is necessary to calculate the water budget and to take into account the geometry of the basin. The water budget of the Western Mediterranean Basin is estimated by summing the discharge from rivers Q_{river}, the precipitation P and the Atlantic Ocean flux Q_{ocean}. The fresh water loss by evaporation E is also taken into account. Starting from an initial volume of sea water V_0 of the Western Mediterranean Basin a new volume $V(t)$ is calculated at the time t. The water budget is given by:

$$\Delta V = V_0 - V(t) = V_0 + Q_{river} + P + Q_{ocean} - E$$

During the Messinian Salinity Crisis in the Mediterranean area, the evaporation E was higher than the sum of the water influx triggering a drawdown of the Mediterranean sea-level. The sea level $Z(t)$ is calculated from the surface area $S(t)$ using the equation $Z(t)=a.S(t)+Z_0$, where a and Z_0 are parameters that depend on the geometry of the Western Mediterranean Basin at the Messinian time. For the Western Mediterranean Basin a and Z_0 are assumed to be equal to 4461.5×10^{-12} m^{-1} and to -3123 m respectively. The surface area $S(t)$ is obtained using the relation

$$\Delta V = a.[S^2(t+\Delta t) - S^2(t)]/2$$

where Δt is the time step.

595 To calculate the evaporite thickness, it is necessary to know the water volume and the salt
596 concentration. The salinity of the Mediterranean at the beginning of the crisis C_0 is considered
597 to be 35 g/l, equal to the salinity of the Atlantic Ocean C_{ocean}. The salinity of rivers C_{river} is
598 assumed to be of 1 g/l. The salt concentration of the Western Mediterranean Basin at time t is
599 therefore given by:
600 $C(t) = [M_0 + M_{river}(t) + M_{ocean}(t)] / V(t)$
601 where $V(t)$ is the volume of the sea water at the time t and $M_0 = C_0.V_0$ is the mass of
602 evaporites when all the water in the Western Mediterranean is evaporated. $M_{river}(t) =$
603 $Q_{river}(t).C_{river}.t$ is the mass of evaporites which come from river discharge Q_{river},
604 $M_{ocean}(t)=Q_{ocean} .C_{ocean} . t$ is the mass of evaporites which come from the Atlantic Ocean
605 through an oceanic inflow Q_{ocean} when Atlantic waters overflooded the Gibraltar sill. The salt
606 precipitates when $C(t)$ >130 g/l. This precipitation allows the formation of evaporite minerals.
607 The salt density used to calculate the volume of evaporites is 2170 kg/m^3.
608

609 ## 10.Acknowledgments

610 We thank Bertrand Meyer, Vaughan Stagpoole and Bilal Haq for critical discussions and
611 reading of a preliminary version of the manuscript. We thank TGS-Nopec and Total for
612 making their data available and in particular Jacqueline Camy-Peyret (Total) for her help in
613 working with the database.
614

615 ## 11.References cited

616 Abd Ellah, R.G., 2009. Evaporation rate at Wadi El-Rayan Lake, Egypt. World Applied
617 Sciences Journal 6, 524-528.
618 Alhammoud, B., Meijer, P., Dijkstra, H.A., 2010. Sensitivity of Mediterranean thermohaline
619 circulation to gateway depth: A model investigation. Paleoceanography 25, PA2220.

620 Babault, J., Loget, N., Van Den Driessche, J., Castelltort, S., Bonnet, S., Davy, P., 2006. Did
621 the Ebro basin connect to the Mediterranean before the Messinian salinity crisis?
622 Geomorphology 81, 155-165.
623 Bache, F., 2008. Evolution Oligo-Miocène des marges du micro océan Liguro Provençal.
624 Editions Universitaires Européennes, Saarbrücken.
625 Bache, F., Olivet, J.-L., Gorini, C., Aslanian, D., Labails, C., Rabineau, M., 2010. Evolution
626 of rifted continental margins: the case of the Gulf of Lions (Western Mediterranean
627 Basin). Earth and Planetary Science Letters 292, 345-356.
628 Bache, F., Olivet, J.-L., Gorini, C., Rabineau, M., Baztan, J., Aslanian, D., Suc, J.-P., 2009.
629 The Messinian Erosional and Salinity Crises: View from the Provence Basin (Gulf of
630 Lions, Western Mediterranean). Earth and Planetary Science Letters 286, 139-157.
631 Bache, F., Popescu, S.-M., Rabineau, M., Gorini, C., Suc, J.-P., Clauzon, G., Olivet, J.-L.,
632 Rubino, J.-L., Melinte-Dobrinescu, M.C., Estrada, F., Londeix, L., Armijo, R., Meyer,
633 B., Jolivet, L., Jouannic, G., Leroux, E., Aslanian, D., Reis, A.T.D., Mocochain, L.,
634 Dumurdžanov, N., Zagorchev, I., Lesić, V., Tomić, D., Namik Çağatay, N., Brun, J.-P.,
635 Sokoutis, D., Csato, I., Ucarkus, G., Çakir, Z., 2012. A two-step process for the
636 reflooding of the Mediterranean Basin after the Messinian Salinity Crisis. Basin
637 Research 24, 125-153.
638 Barber, P.M., 1981. Messinian subaerial erosion of the Proto-Nile delta. Marine Geology 44,
639 253-272.
640 Barr, F.T., Walker, B.R., 1973. Late Tertiary channel system in Northern Lybia and its
641 implications on Mediterranean sea level changes, in: Ryan, W.B.F., Hsü, K.J., al. (Eds.),
642 Initial Reports of Deep Sea Drilling Project. (U.S. Government Printing Office),
643 Washington, pp. 1244-1255.

644 Bassetti, M.A., Miculan, P., Sierro, F.J., 2006. Evolution of depositional environments after
645 the end of Messinian Salinity Crisis in Nijar basin (SE Betic Cordillera). Sedimentary
646 Geology 188-189, 279-295.
647 Benson, R.H., Rakic-El Bied, K., Bonaduce, G., 1991. An important current reversal (influx)
648 in the Rifian Corridor (Morocco) at the Tortonian-Messinian boundary: The end of the
649 Tethys Ocean. Paleoceanography 6, 164-192.
650 Bertini, A., Londeix, L., Maniscalco, R., Di Stefano, A., Suc, J.-P., Clauzon, G., Gautier, F.,
651 Grasso, M., 1998. Paleobiological evidence of depositional conditions in the Salt
652 Member, Gessoso-Solfifera formation (Messinian, Upper Miocene) of Sicily.
653 Micropaleontology 44, 413-133.
654 Bertoni, C., Cartwright, J.A., 2006. Controls on basin-wide architecture of Messinian salt
655 deposits, eastern Mediterranean. Sedimentary Geology 188-189, 93-114.
656 Bertoni, C., Cartwright, J.A., 2007. Clastic depositional systems at the base of the late
657 Miocene evaporites of the Levant region, eastern Mediterranean., in: Schreiber, B.C.,
658 Lugli, S., Babel, M. (Eds.), Evaporites through space and time. Geological Society,
659 London, Special Publications, pp. 37-52.
660 Bessis, F., 1986. Some remarks on the study of subsidence of sedimentary basins. Application
661 to the Gulf of Lions margin (Western Mediterranean). Marine and Petroleum Geology
662 3, 37-63.
663 Besson, D., Parize, O., Rubino, J.-L., Aguilar, J.-P., Aubry, M.-P., Beaudoin, B., Berggren,
664 W.A., Clauzon, G., Crumeyrolle, P., Dexcote, Y., Fiet, N., Michaux, J., von Salis, K.,
665 Suc, J.-P., Reynaud, J.Y., Wernli, R., 2005. Latest Burdigalian network of fluvial
666 valleys in southeast France (western Alps): characteristics, geographic extent, age,
667 implications. Comptes Rendus Geoscience 337, 1045-1054.

668 Blanc, P.-L., 2002. The opening of the Plio-Quaternary Gilbraltar Strait : assessing the size of
669 a cataclysm. Geodinamica Acta 15, 303-317.
670 Blanc, P.-L., 2000. Of sills and straits: a quantitaive assessment of the Messinian Salinity
671 Crisis. Deep-Sea Research 47, 1429-1460.
672 Blanc, P.-L., 2006. Improved modelling of the Messinian Salinity Crisis and conceptual
673 implications. Palaeogeography, Palaeoclimatology, Palaeoecology 238, 349-372.
674 Brun, L., Castet, A., Grosdidier, P., Moreau, P., Prestat, B., Seyve, C., Cussey, R., Fajerwerg,
675 R., Brevart, O., Chennaux, G., Severac, J.P., Barlier, J., Palacios, C., Poumot, C., 1984.
676 Sondage Golfe du Lion profond n°2 GLP2, France, études de laboratoire. SNEA(P)
677 Direction Exploration, Division recherches et applications en géologie, Boussens.
678 Burrus, J., 1989. Review of geodynamic models for extensional basins; the paradox of
679 stretching in the Gulf of Lions (northwest Mediterranean). Bulletin de la Societe
680 Geologique de France 8, 377-393.
681 Butler, R.W.H., Lickorish, W.H., Grasso, M., Pedley, H.M., Ramberti, L., 1995. Tectonics
682 and sequence stratigraphy in Messinian basins, Sicily: constraints on the initiation and
683 termination of the Mediterranean salinity crisis. Geological Society of America Bulletin
684 107, 425-439.
685 Butler, R.W.H., McClelland, E., Jones, R.E., 1999. Calibrating the duration and timing of the
686 Messinian salinity crisis in the Mediterranean: linked tectonoclimatic signals in thrust-
687 top basins of Sicily. Journal of the Geological Society, London 156, 827-835.
688 Cavazza, W., DeCelles, P.G., 1998. Upper Messinian siliciclastic rocks in southeastern
689 Calabria (southern Italy): palaeotectonic and eustatic implications for the evolution of
690 the central Mediterranean region. Tectonophysics 298, 223-241.

691 Chumakov, I.S., 1973. Pliocene and Pleistocene deposits of the Nile Valley in Nubia and
692 Upper Egypt., in: Ryan, W.B.F., Hsü, K.J., al. (Eds.), Initial Reports of Deep Sea
693 Drilling Project. (U.S. Government Printing Office), Washington, pp. 1242-1243.
694 CIESM (Antón, J., Çağatay, M.N., De Lange, G., Flecker, R., Gaullier, V., Gunde-Cimerman,
695 N., Hübscher, C., Krijgsman, W., Lambregts, P., Lofi, J., Lugli, S., Manzi, V.,
696 McGenity, T.J., Roveru, M., Sierro, F.J., & Suc, J.-P.), 2008. Executive Summary, in:
697 Briand, F. (Ed.), The Messinian Salinity crisis from mega-deposits to microbiology - A
698 consensus report. CIESM Workshop Monographs, Monaco, pp. 7-28.
699 Cita, M.B., 1973. Mediterranean evaporite: paleontological arguments for a deep-basin
700 desiccation model, in: Drooger, C.W. (Ed.), Messinian events in the Mediterranean.
701 North-Holland Publ. Co, Amsterdam, pp. 206-228.
702 Clauzon, G., 1973. The eustatic hypothesis and the pre-Pliocene cutting of the Rhône valley.,
703 in: Ryan, W.B.F., Hsü, K.J., al. (Eds.), Initial Reports of Deep Sea Drilling Project.
704 (U.S. Government Printing Office), Washington, pp. 1251-1256.
705 Clauzon, G., 1978. The Messinian Var canyon (Provence, Southern France) -
706 Paleogeographic implications. Marine Geology 27, 231-246.
707 Clauzon, G., 1982. Le canyon messinien du Rhône : une preuve décisive du "dessicated deep-
708 basin model" (Hsü, Cita et Ryan, 1973). Bulletin de la Societe Geologique de France
709 24, 597-610.
710 Clauzon, G., Rubino, J.-L., Casero, P., 1997. Regional modalities of the Messinian Salinity
711 Crisis in the framework of a two phases model. In: Neogene basins of the
712 Mediterranean region: controls and correlation in space and time, R.C.M.N.S. Interim-
713 Colloquium, Catania, Program and Abstracts, 44-46.
714 Clauzon, G., Suc, J.-P., Aguilard, J.-P., Ambert, P., Cappeta, H., Cravatte, J., Drivaliari, A.,
715 Doménech, R., Dubar, M., Leroy, S., Martinell, J., Michaux, J., Roiron, P., Rubino, J.-

716 L., Savoye, B., Vernet, J.-L., 1990. Pliocene geodynamic and climatic evolutions in the
717 French Mediterranean region. Paleontologia i Evolucio Memoria Especial 2, 132-186.
718 Clauzon, G., Suc, J.-P., Gautier, F., Berger, A., Loutre, M.-F., 1996. Alternate interpretation
719 of the Messinian salinity crisis: controversy resolved ? Geology 24, 363-366.
720 Clauzon, G., Suc, J.-P., Popescu, S.-M., Mărunțeanu, M., Rubino, J.-L., Marinescu, F.,
721 Melinte, M.C., 2005. Influence of Mediterranean sea-level changes on the Dacic Basin
722 (Eastern Paratethys) during the late Neogene: the Mediterranean Lago Mare facies
723 deciphered. Basin Research 17, 437-462.
724 Corselli, C., Grecchi, G., 1984. The passage from hypersaline to hyposaline conditions in the
725 Mediterranean Messinian: Discussion of the possible mechanisms triggering the “Lago
726 Mare” facies. Paleobiologie Continentale 14, 225-239.
727 Cravatte, J., Dufaure, P., Prim, M., Rouaix, S., 1974. Les sondages du Golfe du Lion:
728 Stratigraphie, Sédimentologie, Notes et Mémoires n°11. Compagnie Française des
729 Pétroles, Paris, pp. 209-274.
730 Dalla, S., Harby, H., Serazzi, M., 1997. Hydrocarbon exploration in a complex incised valley
731 fill: An example from the late Messinian Abu Madi Formation (Nile Delta Basin,
732 Egypt). The Leading Edge 16, 1819-1824.
733 Denizot, G., 1952. Le Pliocène dans la vallée du Rhône. Revue de Géographie de Lyon 27,
734 327-357.
735 Di Stefano, A., Sturiale, G., 2010. Refinements of calcareous nannofossil biostratigraphy at
736 the Miocene/Pliocene Boundary in the Mediterranean region. Geobios 43, 5-20.
737 Duggen, S., Hoernle, K., Boggard, P.V.D., Rüpke, L., Morgan, J.P., 2003. Deep roots of
738 Messinian salinity crisis. Letters to nature 422, 602-606.
739 El Euch-El Koundi, N., Ferry, S., Suc, J.-P., Clauzon, G., Melinte-Dobrinescu, M.C., Gorini,
740 C., Safra, A., Zargouni, F., 2009. Messinian deposits and erosion in northern Tunisia:

741 inferences on Strait of Sicily during the Messinian Salinity Crisis. Terra Nova 21, 41-
742 48.
743 Estrada, F., Ercilla, G., Gorini, C., Alonso, B., Vazquez, J., Garcia-Castellanos, D., Juan, C.,
744 Maldonado, A., Ammar, A., Elabbassi, M., 2011. Impact of pulsed Atlantic water
745 inflow into the Alboran Basin at the time of the Zanclean flooding. Geo-Marine Letters,
746 1-16.
747 Fauquette, S., Suc, J.-P., Bertini, A., Popescu, S.-M., Warny, S., Bachiri Taoufiq, N., Perez
748 Villa, M.-J., Chikhi, H., Subally, D., Feddi, N., Clauzon, G., Ferrier, J., 2006. How
749 much did climate force the Messinian salinity crisis? Quantified climatic conditions
750 from pollen records in the Mediterranean region. Palaeogeography, Palaeoclimatology,
751 Palaeoecology 238, 281-301.
752 Garcia-Castellanos, D., Estrada, F., Jiménez-Munt, I., Gorini, C., Fernandez, M., Vergés, J.,
753 De Vicente, R., 2009. Catastrophic flood of the Mediterranean after the Messinian
754 salinity crisis. Nature 462, 778-781.
755 Garcia-Castellanos, D., Villasenor, A., 2011. Messinian Salinity Crisis regulated by
756 competing tectonics and erosion at the Gibraltar arc. Nature 480, 359-363.
757 García, M., Maillard, A., Aslanian, D., Rabineau, M., Alonso, B., Gorini, C., Estrada, F.,
758 2011. The Catalan margin during the Messinian Salinity Crisis: Physiography,
759 morphology and sedimentary record. Marine Geology 284, 158-174.
760 Gargani, J., 2004a. Eustatism, erosion and flexural isostasy: numerical modelling applied to
761 the Messinian Rhône. Comptes Rendus Geoscience 336, 901-907.
762 Gargani, J., 2004b. Modelling of the erosion in the Rhone valley during the Messinian crisis
763 (France). Quaternary International 121, 13-22.
764 Gargani, J., Moretti, I., Letouzet, J., 2008. Evaporite accumulation during the Messinian
765 Salinity Crisis: the Suez Rift case. Geophysical Research Letter 35, L02401.

766 Gargani, J., Rigollet, C., 2007. Mediterranean Sea level variations during the Messinian
767 salinity crisis. Geophysical Research Letter 34, L10405.
768 Gargani, J., Rigollet, C., Scarselli, S., 2010. Isostatic response and geomorphological
769 evolution of the Nile valley during the Messinian Salinity Crisis. Bulletin de la Societe
770 Geologique de France 181, 19-26.
771 Gautier, F., Clauzon, G., Suc, J.-P., Cravatte, J., Violanti, D., 1994. Age and duration of the
772 messinian salinity crisis. Comptes Rendus de l'Académie des Sciences - Series IIA -
773 Earth and Planetary Science 318, 1103-1109.
774 Gladstone, R., Flecker, R., Valdes, P., Lunt, D., Marwick, P., 2007. The Mediterranean
775 hydrologic budget from a Late Miocene global climate simulation. Palaeogeography,
776 Palaeoclimatology, Palaeoecology 251, 254-267.
777 Gorini, C., 1993. Géodynamique d'une marge passive: le Golfe du Lion (Méditerranée
778 Occidentale). Université Paul Sabatier, Toulouse, p. 256.
779 Govers, R., 2009. Choking the Mediterranean to dehydration: The Messinian salinity crisis.
780 Geology 37, 167-170.
781 Govers, R., Meijer, P., Krijgsman, W., 2009. Regional isostatic response to Messinian
782 Salinity Crisis events. Tectonophysics 463, 109-129.
783 Guennoc, P., Gorini, C., Mauffret, A., 2000. Histoire géologique du Golfe du Lion et
784 cartographie du rift oligo-aquitanien et de la surface messinienne. Géologie de la France
785 3, 67-97.
786 Haq, B.U., Hardenbol, J., Vail, P., 1987. Chronology of fluctuating sea levels since the
787 Triassic (250 million years ago to present). Science 235, 1156-1167.
788 Hardie, L.A., Lowenstein, T.K., 2004. Did the Mediterranean sea dry out during the Miocene?
789 A reassessment of the evaporite evidence from DSDP legs 13 and 42A cores. Journal of
790 Sedimentary Research 74, 453-461.

791 Hilgen, F.J., Langereis, C.G., 1993. A critical re-evaluation of the Miocene-Pliocene
792 boundary as defined in Mediterranean. Earth and Planetary Science Letters 118, 167-
793 179.
794 Hsü, K.J., 1972. When the Mediterranean dried up. Sci. Am. 227, 44-51.
795 Hsü, K.J., Cita, M.B., Ryan, W.B.F., 1973. The origin of the Mediterranean evaporites, in:
796 Ryan, W.B.F., Hsü, K.J., al. (Eds.), Initial Reports of Deep Sea Drilling Project. U.S.
797 Government Printing Office, Washington, pp. 1203-1231.
798 Hsü, K.J., Montadert, L., Bernoulli, D., Cita, M.B., Erickson, A.J., Garrison, R.E., Kidd, R.B.,
799 Mélières, F., Müller, C., Wright, R., 1977. History of the Mediterranean salinity crisis.
800 Nature 267, 399-403.
801 Kotwicki, V., Isdale, P., 1991. Hydrology of Lake Eyre, Australia: El Nino link.
802 Palaeogeography, Palaeoclimatology, Palaeoecology 84, 87-98.
803 Krijgsman, W., Hilgen, F.J., Raffi, I., Sierro, F.J., Wilson, D.S., 1999. Chronology, causes
804 and progression of the Messinian salinity crisis. Nature 400, 652-655.
805 Krijgsman, W., Meijer, P.T., 2008. Depositional environments of the Mediterranean “Lower
806 Evaporites” of the Messinian salinity crisis: Constraints from quantitative analyses.
807 Marine Geology 253, 73-81.
808 Lambeck, K., Bard, E., 2000. Sea-level change along the French Mediterranean coast from
809 the past 30 000 years. Earth and Planetary Science Letters 175, 203-222.
810 Leever, K.A., Matenco, L., Garcia-Castellanos, D., Cloetingh, S., 2011. The evolution of the
811 Danube gateway between Central and Eastern Paratethys (SE Europe): insight from
812 numerical modelling of the causes and effects of connectivity between basins and its
813 expression in the sedimentary record. . Tectonophysics 502, 175-195.

814 Leever, K.A., Matenco, L., Rabagia, T., Cloetingh, S., Krijgsman, W., Stoica, M., 2010.
815 Messinian sea level fall in the Dacic Basin (Eastern Paratethys): palaeogeographical
816 implications from seismic sequence stratigraphy. Terra Nova 22, 12-17.
817 Lofi, J., Berné, S., 2008. Evidence for pre-messinian submarine canyons on the Gulf of Lions
818 slope (Western Mediterranean). Marine and Petroleum Geology 25, 804-817.
819 Lofi, J., Gorini, C., Berné, S., Clauzon, G., Dos Reis, A.T., Ryan, W.B.F., Steckler, M.S.,
820 2005. Erosional processes and paleo-environmental changes in the Western Gulf of
821 Lions (SW France) during the Messinian Salinity Crisis. Marine Geology 217, 1-30.
822 Loget, N., Van Den Driessche, J., 2006. On the origin of the strait of Gibraltar. Sedimentary
823 Geology 188-189, 341-356.
824 Loget, N., Van den Driessche, J., Davy, P., 2005. How did the Messinian Salinity Crisis end?
825 Terra Nova 17.
826 Londeix, L., Benzakour, M., Suc, J.-P., Turon, J.-L., 2007. Messinian paleoenvironments and
827 hydrology in Sicily (Italy): The dinoflagellate cyst record. Geobios 40, 233-250.
828 Lourens, L.J., Hilgen, F.J., Laskar, J., Shackleton, N.J., Wilson, D., 2004. The Neogene
829 Period, in: Gradstein, F.M., Ogg, J., Smith, A. (Eds.), A Geological Time Scale.
830 Cambridge University Press, Cambridge, pp. 409-440.
831 Maillard, A., Gorini, C., Mauffret, A., Sage, F., Lofi, J., Gaullier, V., 2006. Offshore evidence
832 of polyphase erosion in the Valencia Basin (Northwestern Mediterranean): Scenario for
833 the Messinian Salinity Crisis. Sedimentary Geology 188-189, 69-91.
834 Manzi, V., Lugli, S., Roveri, M., Schreiber, C., 2009. A new facies model for the Upper
835 Gypsum of Sicily (Italy): chronological and palaeoenvironmental constraints for the
836 Messinian salinity crisis in the Mediterranean. Sedimentology 56, 1937-1960.
837 Manzi, V., Lugli, S., Roveri, M., Schreiber, C., Gennari, R., 2011. The Messinian "Calcare di
838 Base" revisited. Geological Society of America Bulletin 123, 347-370.

839 Mauffret, A., Durand de Grossouvre, B., Dos Reis, A.T., Gorini, C., Nercessian, A., 2001.
840 Structural geometry in the eastern Pyrenees and western Gulf of Lion (Western
841 Mediterranean). Journal of Structural Geology 23, 1701-1726.
842 Meijer, P., 2006. A box model of the blocked-outflow scenario for the Messinian Salinity
843 Crisis. Earth and Planetary Science Letters 248, 471-479.
844 Meijer, P., Krijgsman, W., 2005. A quantitative analysis of the desiccation and re-filling of
845 the Mediterranean during the Messinian Salinity Crisis. Earth and Planetary Science
846 Letters 240, 510-520.
847 Meijer, P., Tuenter, E., 2007. The effect of precession-induced changes in the Mediterranean
848 freshwater budget on circulation at shallow and intermediate depth. Journal of Marine
849 System 68, 349-365.
850 Melinte-Dobrinescu, M.C., Suc, J.-P., Clauzon, G., Popescu, S.-M., Armijo, R., Meyer, B.,
851 Biltekin, D., Çağatay, M.N., Ucarkus, G., Jouannic, G., Fauquette, S., Çakir, Z., 2009.
852 The Messinian Salinity Crisis in the Dardanelles region: Chronostratigraphic
853 constraints. Palaeogeography, Palaeoclimatology, Palaeoecology 278, 24-39.
854 Montadert, L., Letouzey, J., Mauffret, A., 1978. Messinian event : seismic evidence, in: Hsü,
855 K.J., Montadert, L., al (Eds.), Initial Reports of the Deep Sea Drilling Project, Volume
856 42, Part 1. (U.S. Government Printing Office), Washington, pp. 1037-1050.
857 Montadert, L., Nicolaides, S., Semb, P.H., Lie, Ø., in press. Petroleum systems offshore
858 Cyprus, in: Marlow, L., Kedall, C., Yose, L. (Eds.), Petroleum Systems of the Tethyan
859 Region. American Association of Petroleum Geologists.
860 Murphy, L., Kirk-Davidoff, D.B., Mahowald, N., Otto-Bliesner, B.L., 2009. A numerical
861 study of the climate response to lowered Mediterranean Sea level during the Messinian
862 Salinity Crisis. Palaeogeography, Palaeoclimatology, Palaeoecology 279, 41-59.

Neumann, F.H., Kagan, E.J., Leroy, S.A.G., Baruch, U., 2010. Vegetation history and climate fluctuations on a transect along the Dead Sea west shore and their impact on past societies over the last 3500 years. Journal of Arid Environments 74, 756-764.

Norman, S.E., Chase, C.G., 1986. Uplift of the shores of the western Mediterranean due to Messinian desiccation and flexural isostasy. Nature 322, 450-451.

Obone-Zue-Obame, E.M., Gaullier, V., Sage, F., Maillard, A., Lofi, J., Vendeville, B., Thinon, I., Rehault, J.P., and-the-Mauresc-Shipboard-scientific-party., 2011. The sedimentary markers of the Messinian salinity crisis and their relation with salt tectonics on the Provençal margin (western Mediterranean): results from the "MAURESC" cruise. Bulletin de la Societe Geologique de France 182, 181-196.

Pedley, H.M., Grasso, M., 1993. Controls on faunal and sediment cyclicity within the Tripoli and Calcare di Base basins (late Miocene) of central Sicily. Palaeogeography, Palaeoclimatology, Palaeoecology 105, 337-360.

Pedley, H.M., Grasso, M., Maniscalco, R., Esu, D., 2007. The Monte Carrubba Formation (Messinian, Sicily) and its correlatives: New light on basin-wide processes controlling sediment and biota distributions during Palaeomediterranean-Mediterranean transition. Palaeogeography, Palaeoclimatology, Palaeoecology 253, 363-384.

Popescu, S.-M., Dalesme, F., Jouannic, G., Escarguel, G., Head, M.J., Melinte-Dobrinescu, M.C., Sütő-Szentai, M., Bakrac, K., Clauzon, G., Suc, J.-P., 2009. *Galeacysta etrusca* complex, dinoflagellate cyst marker of Paratethyan influxes into the Mediterranean Sea before and after the peak of the Messinian Salinity Crisis. Palynology 33, 105-134.

Popescu, S.-M., Suc, J.-P., Melinte, M., Clauzon, G., Quillévéré, F., Sütő-Szentai, M., 2007. Earliest Zanclean age for the Colombacci and uppermost Di tetto formations of the "latest Messinian" northern Apennines: New palaeoenvironmental data from the Maccarone section (Marche Province, Italy). Geobios 40, 359-373.

888 Rabineau, M., Berné, S., Aslanian, D., Olivet, J.-L., Joseph, P., Guillocheau, F., Bourillet, J.-
889 F., Ledrezen, E., Granjeon, D., 2005. Sedimentary sequences in the Gulf of Lion: a
890 record of 100,000 years climatic cycles. Marine and Petroleum Geology 22, 775-804.
891 Rabineau, M., Berné, S., J.L., O., Aslanian, D., Guillocheau, F., Joseph, P., 2006. Paleo sea
892 levels reconsidered from direct observation of paleoshoreline position during Glacial
893 Maxima (for the last 500,000 yr). Earth and Planetary Science Letters 252, 119-137.
894 Raffi, I., Backman, J., Fornaciari, E., Pälike, H., Rio, D., Lourens, L., Hilgen, F., 2006. A
895 review of calcareous nannofossil astrobiochronology encompassing the past 25 million
896 years. Quaternary Science Reviews 25, 3113-3137.
897 Riding, R., Braga, J.C., Martin, J.M., Sanchez-Almazo, I.M., 1998. Mediterranean Messinian
898 salinity crisis: constraints from a coeval marginal basin, Sorbas, southeastern Spain.
899 Marine Geology 146, 1-20.
900 Rouchy, J.M., Caruso, A., 2006. The Messinian salinity crisis in the Mediterranean basin: A
901 reassessment of the data and an integrated scenario. Sedimentary Geology 188, 35-67.
902 Rouchy, J.-M., Saint Martin, J.-P., 1992. Late Miocene events in the Mediterranean as
903 recorded by carbonate-evaporite relations. Geology 20, 629-632.
904 Roveri, M., Lugli, S., Manzi, V., Schreiber, B.C., 2008a. The Messinian Sicilian stratigraphy
905 revisited: toward a new scenario for the Messinian Salinity Crisis. Terra Nova 20, 483-
906 488.
907 Roveri, M., Manzi, V., 2006. The Messinian salinity crisis: Looking for a new paradigm?
908 Palaeogeography, Palaeoclimatology, Palaeoecology 238, 386-398.
909 Roveri, M., Manzi, V., Gennari, R., Iaccarino, S.M., Lugli, S., 2008b. Recent advancements
910 in the Messinian stratigraphy of Italy and their Mediterranean-scale implications.
911 Bollettino della Società Paleontologica Italiana 47, 71-85.

912 Ryan, W.B.F., 1973. Geodynamic implications of the Messinian crisis of salinity, in: Drooger,
913 D.W. (Ed.), Messinian events in the Mediterranean. Elsevier, Amsterdam, pp. 26-38.
914 Ryan, W.B.F., 2008. Modelling the magnitude and timing of evaporative drawdown during
915 the Messinian salinity Crisis. Stratigraphy 5, 227-243.
916 Ryan, W.B.F., 2009. Decoding the Mediterranean salinity crisis. Sedimentology 56, 95-136.
917 Ryan, W.B.F., Cita, M.B., 1978. The nature and distribution of Messinian erosional surface-
918 indication of a several kilometer-deep Mediterranean in the Miocene. Marine Geology
919 27, 193-230.
920 Sage, F., Gronefeld, G.V., Déverchère, J., Gaullier, V., Maillard, A., Gorini, C., 2005.
921 Seismic evidence for Messinian detrital deposits at the western Sardinia margin,
922 northwestern Mediterranean. Marine and Petroleum Geology 22, 757-773.
923 Savoye, B., Piper, D.J.W., 1991. The Messinian event on the margin of the Mediterranean Sea
924 in the Nice area, southern France. Marine Geology 97, 279-304.
925 Schneck, R., Micheels, A., Mosbrugger, V., 2010. Climate modelling sensitivity experiments
926 for the Messinian Salinity Crisis. Palaeogeography, Palaeoclimatology, Palaeoecology
927 286, 149-163.
928 Steckler, M.S., Watts, A.B., 1980. The Gulf of Lion: subsidence of a young continental
929 margin. Nature 287, 425-429.
930 Struglia, M.V., Mariotti, A., Filograsso, A., 2004. River discharge into the Mediterranean
931 Sea: climatology and aspects of observed variability. Journal of Climate 17, 4740-4751.
932 Suc, J.P., 1976. Apports de la palynologie à la connaissance du Pliocène du Roussillon (sud
933 de la France). Geobios 9, 741-771.
934 Suc, J.-P., Violanti, D., Londeix, L., Poumot, C., Robert, C., Clauzon, G., Turon, J.L., Ferrier,
935 J., Chikhi, H., Cambon, G., Gautier, F., 1995. Evolution of the Messinian

Mediterranean environments: the Tripoli Formation at Capodarso (Sicily, Italy). Review of Palaeobotany and Palynology 87, 51-79.

Vail, P.R., Mitchum, R.M., Todd, R.G., Widmier, J.M., Thompson, S., Sangree, J.B., Bubb, J.N., Hatlelid, W.G., 1977. Seismic stratigraphy and global changes of sea-level. Seismic stratigraphy-applications to hydrocarbon exploration. Memoir 26. American Association of Petroleum Geologists, Tulsa.

Van Couvering, J.A., Castradori, D., Cita, M.B., Hilgen, F.J., Rio, D., 2000. The base of the Zanclean Stage and of the Pliocene Series. Episodes 23, 179-187.

Van Dam, J.A., 2006. Geographic and temporal patterns in the late Neogene (12-3 Ma) aridification of Europe: The use of small mammal as paleoprecipitation proxies. 238, 190-218.

Yechieli, Y., Gavrieli, I., Berkowitz, B., Ronen, D., 1998. Will the Dead Sea die? Geology 26, 755-758.

12. Figure captions

Figure 1. The synchronous and diachronous scenarios for the deposition of the Messinian evaporites.

According to the synchronous scenario, phase 1 corresponds to a limited sea-level fall and rise leading to evaporite deposition in the peripheral basins. Phase 2 (*i.e*. the peak of the MSC) is characterised by a huge sea level drop, evaporite deposition in the central basins, and subaerial erosion of the margins.

According to the diachronous scenarios, evaporites in the central basins were deposited during minimum sea level (phase 2) and after the deposition of evaporites in the peripheral basins (phase 1).

961 The synchronous scenario considers that evaporites have been deposited at variable sea levels.
962 Duration of phase 2 is indicated according to (1) Krijgsman et al. (1999) for the "synchronous
963 scenario" (70 kyrs), and (2) Butler et al. (1995) and Bache *et al*. (2012) on the one hand and
964 CIESM (2008) on the other hand for the "diachronous scenarios" (140 and 270 kyrs
965 respectively).
966
967 **Figure 2.** Map showing the data used for this study and location of Messinian seismic
968 markers in the Gulf of Lions. The Transgressive Ravinement Surface (TRS) related to the end
969 of the Messinian Salinity Crisis and its limit with the subaerial Messinian Erosional Surface
970 (MES), which is interpreted as a paleoshoreline preserved just before the catastrophic
971 reflooding, are highlighted. Dm detrital prisms, located at the outlet of the Messinian drainage
972 networks, are truncated by the TRS. Upstream limit of the halite is deduced from the
973 upstream limit of the listric faults. Boreholes: *Ca1*, Calmar1; *Ci1*, Cicindelle1; *Am1*, Agde
974 Maritime1; *Si1*, Sirocco1; *Mi1*, Mistral1; *Tra1*, Tramontane1; *Ra1*, Rascasse1; *Au1*, Autan1;
975 *Au2*, Autan2; *GLP1*, Golfe du Lion Profond 1; *GLP2*, Golfe du Lion Profond 2.
976
977 **Figure 3.** Sedimentary and morphological evolution of the Gulf of Lions from the margin to
978 basin at the time of the MSC.
979 (a) Seismic cross-section showing the markers of the MSC. Location of the cross-section in
980 Fig. 2.
981 (b) Chronostratigraphic chart based on seismic interpretation that suggests the precipitation of
982 central evaporites only after the major sea-level fall (this study). Note that the vertical scale of
983 the chart is time in Ma. This chart highlights a depositional hiatus on the shelf and erosion and
984 reworking of sediments deposited before the major drawdown.

985 Subdivisions of the MSC: 1, First phase leading to evaporite deposition in the peripheral
986 basins; 2, Second phase (*i.e.* the peak of the MSC) characterised by a huge sea level drop,
987 evaporite deposition in the central basins, and subaerial erosion of the margins.
988 Subdivisions of the peak of the MSC: step I, detrital deposition in the central basins after the
989 huge sea-level drop; step II, step during which central evaporites were deposited and the TRS
990 developed; step III, instantaneous catastrophic reflooding.
991
992 **Figure 4.** Uninterpreted and interpreted seismic profile across the Gulf of Lions shelf (LRM
993 28) showing the position of reflectors Mi1 to Mi5 beneath Dm unit. A Serravallian/Tortonian
994 age for Mi5 leads to a younger age for the deposition of Dm prisms. Location of seismic
995 profiles in Fig. 2.
996
997 **Figure 5.** Stratigraphic correlation between Tramontane 1, Calmar 1 and Mistral 1 wells in
998 the Gulf of Lions shelf. Stratigraphic boundaries and interpretation of depositional
999 environments come from Cravatte et al., (1974) for Tramontane 1 and Mistral 1 and from
1000 Guennoc et al., (2000) for Calmar 1. Mi5 intersects the three wells at the exact position (in
1001 Mistral 1) or above (in Tramontane 1 and Calmar 1) an obvious sedimentary boundary (bold
1002 black line). In Tramontane 1 and Mistral 1 this boundary, respectively located at 1540 and
1003 1675 m depth, corresponds to a transition from marine to littoral conditions. In Calmar 1, the
1004 boundary is located at 1400 m and corresponds to the Serravallian/Tortonian transition,
1005 leading to a younger age for the deposition of Dm prisms, which are younger than Mi5.
1006
1007 **Figure 6.** Uninterpreted and interpreted seismic profile (TGS-NOPEC) across the Gulf of
1008 Lions showing the transition from the shelf to the evaporite units. Dm prisms and their distal
1009 counterpart are respectively represented in yellow and blue. The Transgressive Ravinement

1010 Surface (TRS), characterised by its smooth aspect, the erosional truncations at the underlying
1011 series and by the onlap termination of the overlying series, can be confidently interpreted
1012 from the shelf domain to the GLP2 well. Seaward of GLP2 the surface can be followed in the
1013 upper part of LU1 and clearly below MU. Location of seismic profiles in Figure 2.
1014
1015 **Figure 7.** Zoom of the TGS-NOPEC seismic profile (Fig. 6) showing onlap configuration of
1016 the seismic unit (in green) that overlies the TRS in correspondence with the evaporitic unit
1017 drilled by well GLP2 (3703 – 3437 m depth). The (52 m thick) overlying sandstones and
1018 clays (3437 – 3385 m depth) are indistinct on the seismic profile.
1019
1020 **Figure 8.** Chronology of events which affected the Mediterranean peripheral (including the
1021 Sicilian Caltanissetta Basin and the Apennine Foredeep) and central basins with respect to sea
1022 level changes (modified from Bache et al., 2012).
1023 Subdivisions of the MSC: 1, First phase leading to evaporite deposition in the peripheral
1024 basins; 2, Second phase (*i.e.* the peak of the MSC) characterised by a huge sea level drop,
1025 evaporite deposition in the central basins, and subaerial erosion of the margins.
1026 Subdivisions of the peak of the MSC: step I, detrital deposition in the central basins after the
1027 huge sea-level drop; step II, step during which central evaporites were deposited and the TRS
1028 developed (the formation of TRS corresponds to the step I of Bache et al., 2012); step III,
1029 instantaneous catastrophic reflooding (step II of Bache et al., 2012).
1030
1031 **Figure 9.** Thickness map (in ms TWT) of the seismic unit that overlies the TRS (in green on
1032 Figure 7) showing the pinch-out of the unit seaward of the paleoshoreline preserved just
1033 before the catastrophic reflooding. This configuration suggests that this unit (and its lateral

1034 equivalent represented by UU-MU-upper part of LU1) has been deposited during the
1035 landward migration of the shoreline that led to the formation of the TRS.
1036
1037 **Figure 10.** Scenario of the MSC deduced from the data available onland for the peripheral
1038 basins (see Bache et al., 2012) and for the central basins from the seismic interpretation which
1039 supports a precipitation of central evaporites only after the major sea-level fall (this study).
1040 The stages of this scenario are detailed in the text.
1041 Subdivisions of the MSC: see Figure 7.
1042
1043 **Figure 11.** Variation of the Mediterranean sea level in the Gulf of Lions between 6 and 5.30
1044 Ma encompassing the MSC (modified from Bache et al. (2012)). Successive major changes
1045 are estimated with respect to present-day sea level (noted "0"). The initial position of the
1046 paleoshoreline just before the catastrophic reflooding (step 2-III) has been estimated between
1047 600 m and 900 m below the present sea level by (Bache et al., 2012) by subtracting the
1048 Pliocene and Quaternary subsidence deduced by (Rabineau et al., 2006) from its present-day
1049 position. The rapid increase in water depth during step 2-III was thus between 600 and 900 m.
1050 Solid and dashed black lines are constrained by an increase of 600 m and 900 m respectively.
1051 Subdivisions of the MSC: see Figure 7.
1052
1053 **Figure 12.** Numerical simulations constrained by the interpretation of seismic data supporting
1054 a precipitation of central evaporites after the major sea-level fall. The water budget has been
1055 comprehended to introduce 1/ the existence of a detrital episode in relation with the maximum
1056 desiccation phase (step 2-I) prior to the precipitation of evaporites and 2/ a two-step
1057 reflooding (step 2-II during which evaporites deposited, and step 2-III, which ended the
1058 MSC). The value of E-P has been chosen at 1.75 $m^3/m^2/yr$. River discharge = 7500 m^3/s.

1059 Variation of sea level is in blue and that of water budget in black. The resulting simulation of
1060 evaporite thickness is in purple. Solid and dashed lines are constrained by the initial position
1061 of the paleoshoreline just before step 2-III, respectively at 600 m and 900 m below the present
1062 sea level (Bache et al., 2012)**.** The geometry of the basins is identical to that previously used
1063 by (Meijer and Krijgsman, 2005). Evaporites begin to precipitate when water salinity reaches
1064 130g/l (Gargani et al., 2008; Meijer and Krijgsman, 2005). The water budget is calculated
1065 using river and Atlantic Ocean flow as well as precipitation and evaporation (Gargani and
1066 Rigollet, 2007). See the supplementary materials for further details.

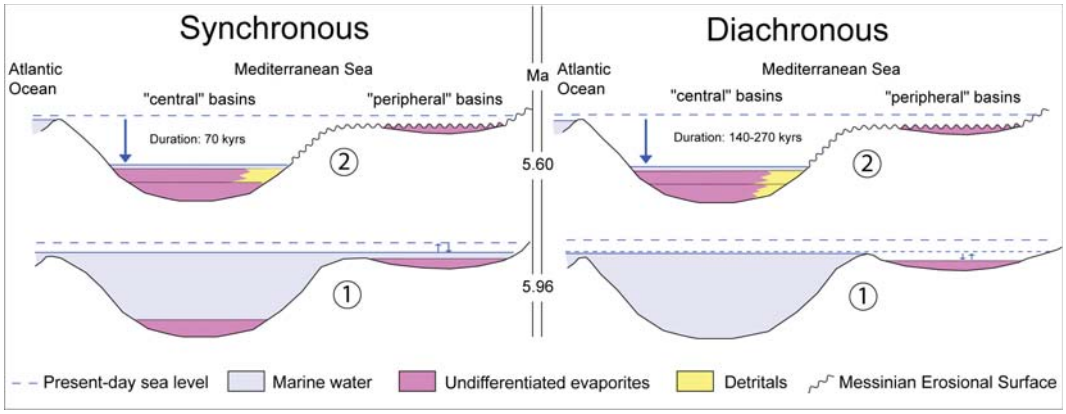

FIGURE 1 –

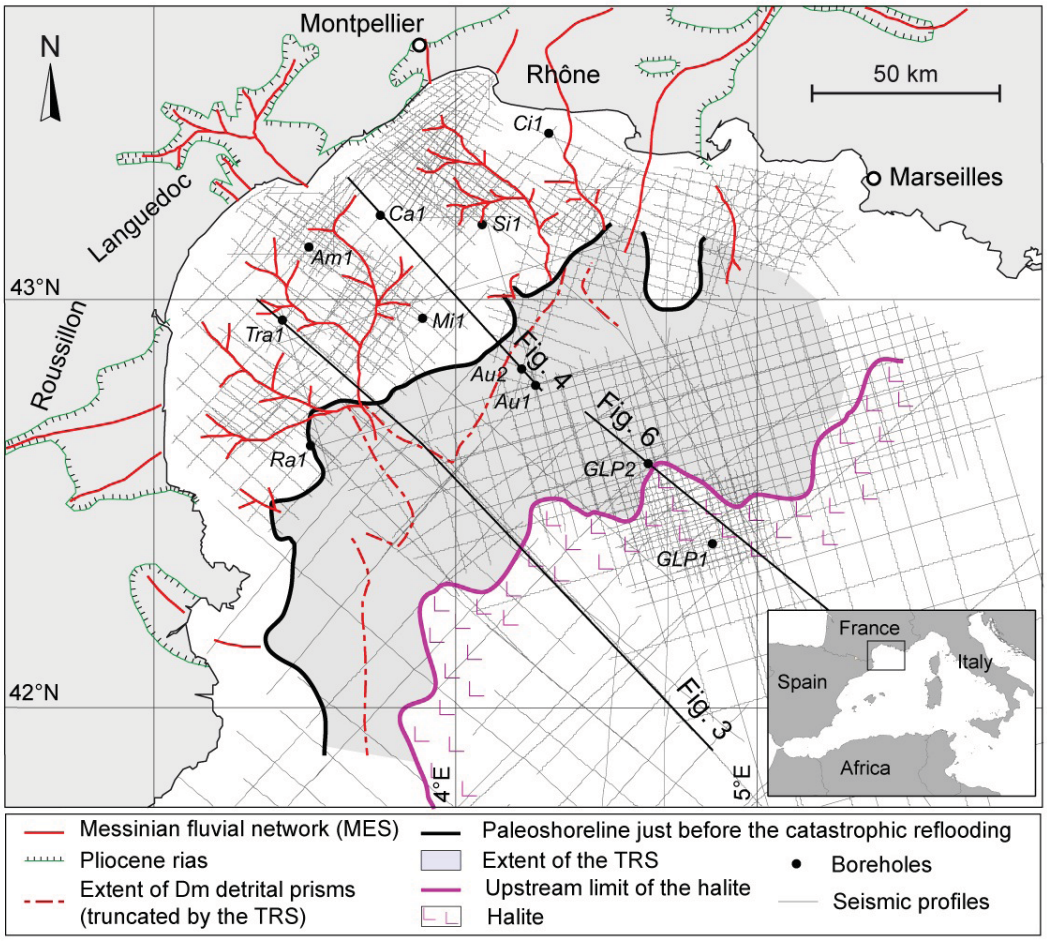

FIGURE 2 –

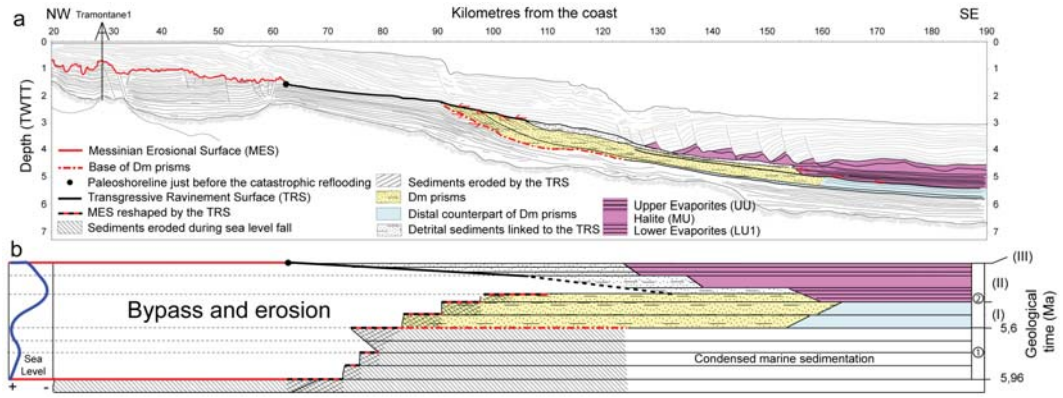

FIGURE 3 –

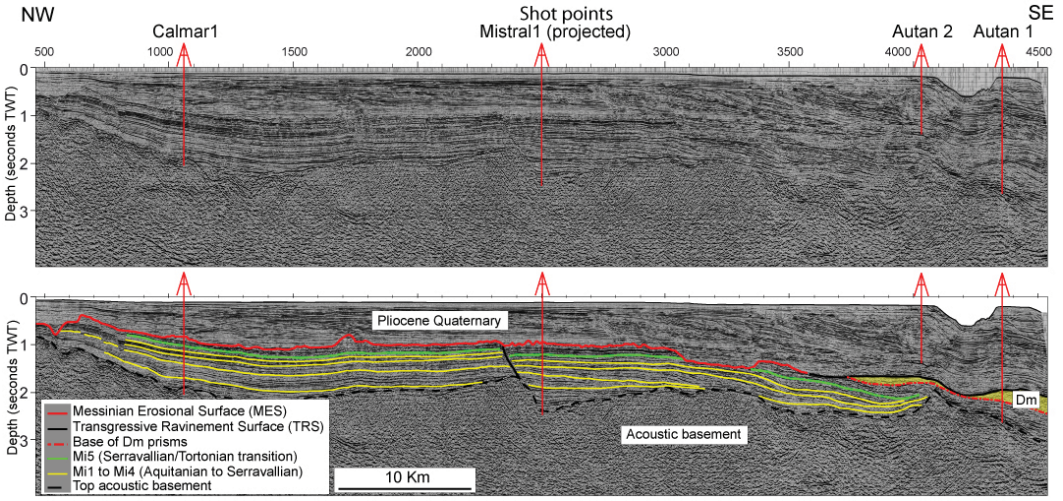

FIGURE 4 –

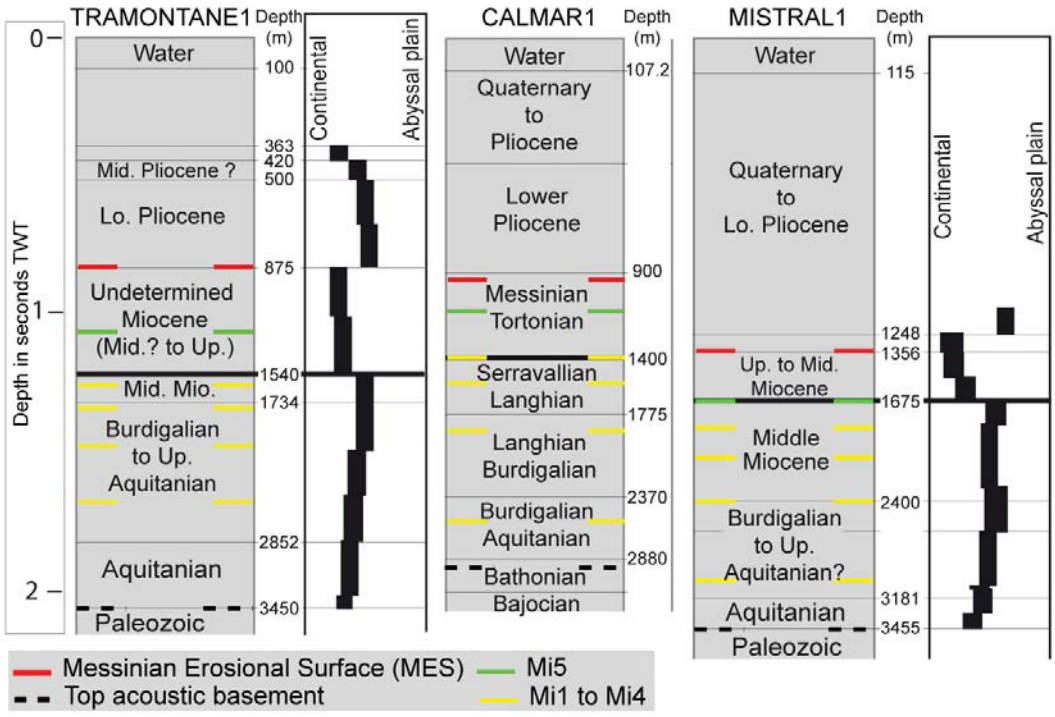

FIGURE 5 –

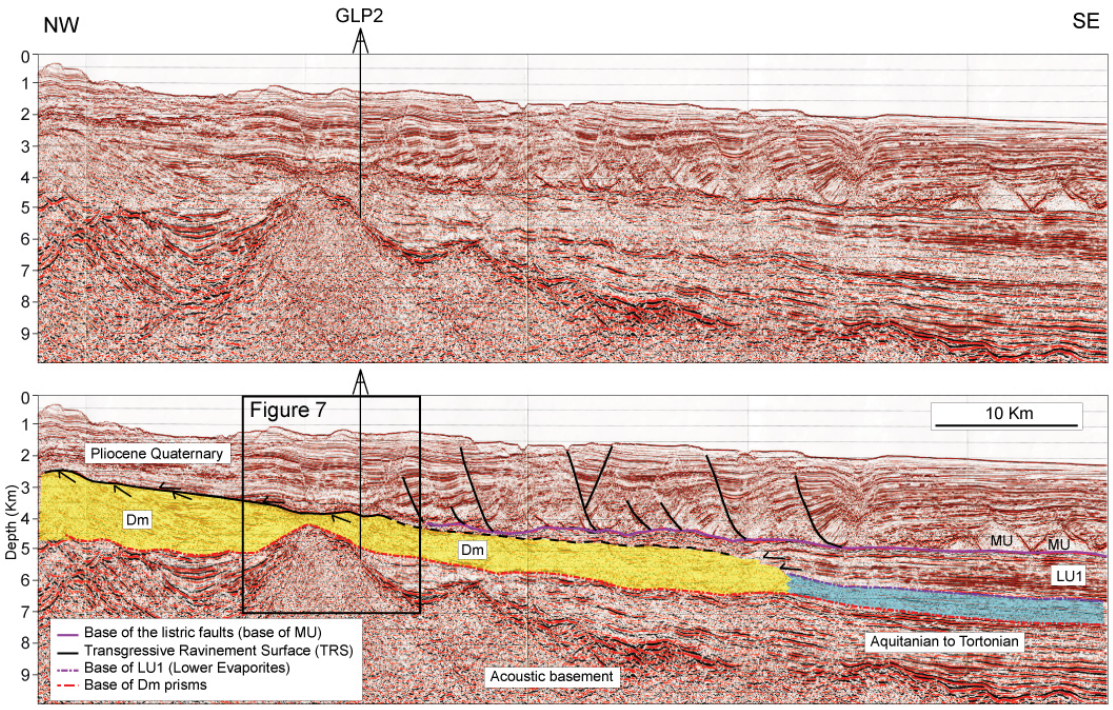

FIGURE 6 –

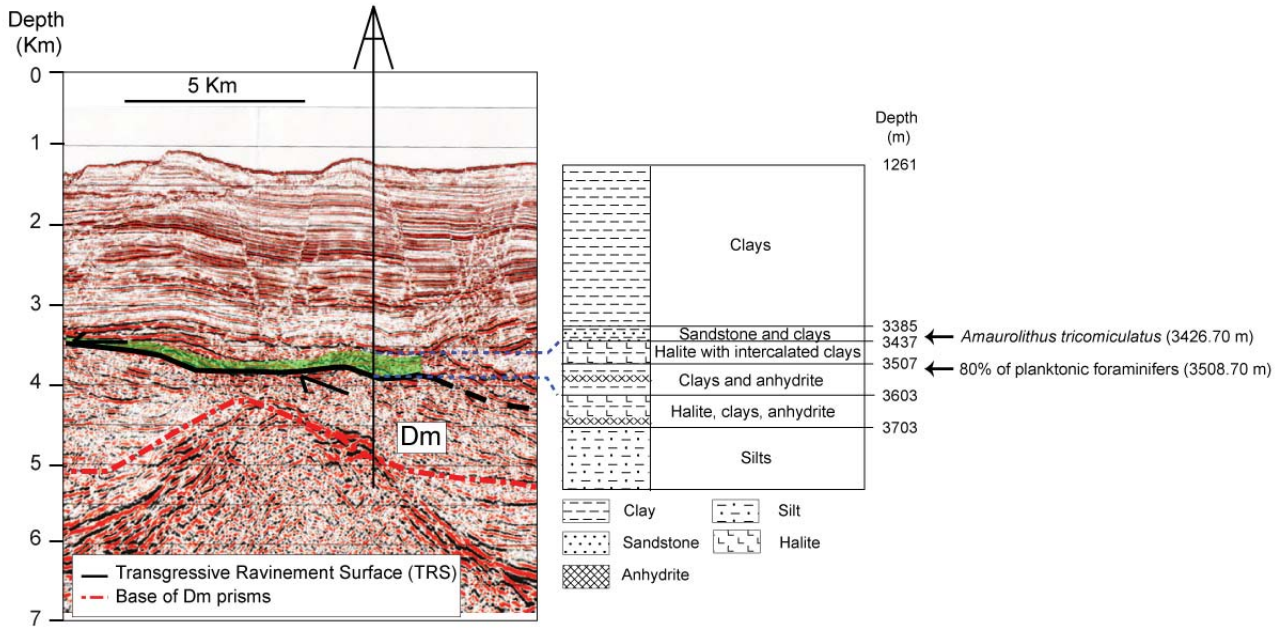

FIGURE 7 –

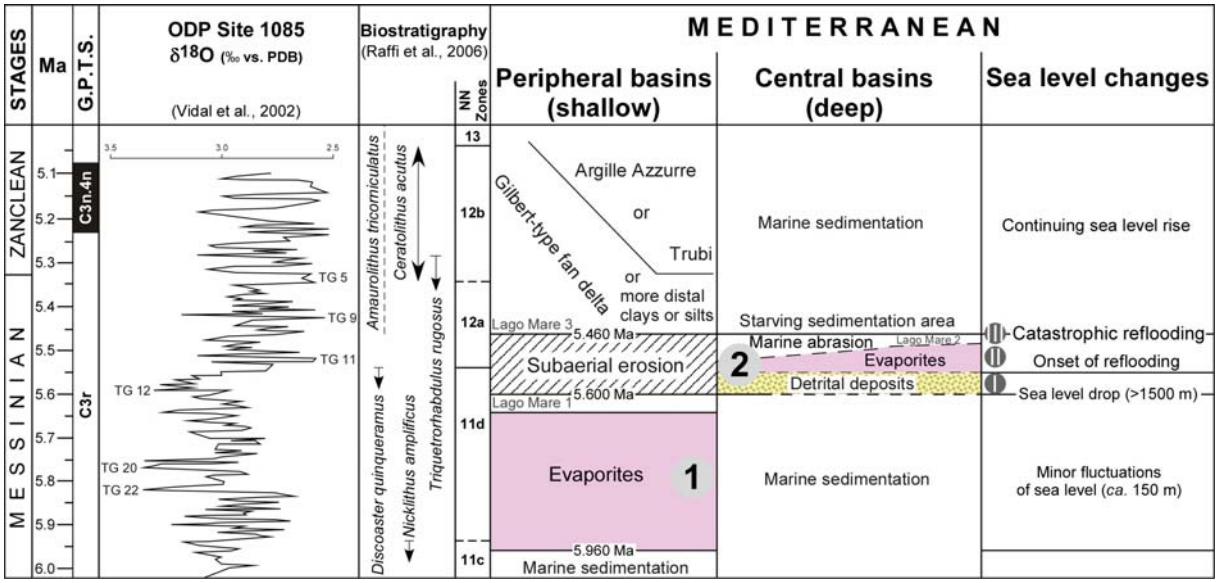

FIGURE 8 –

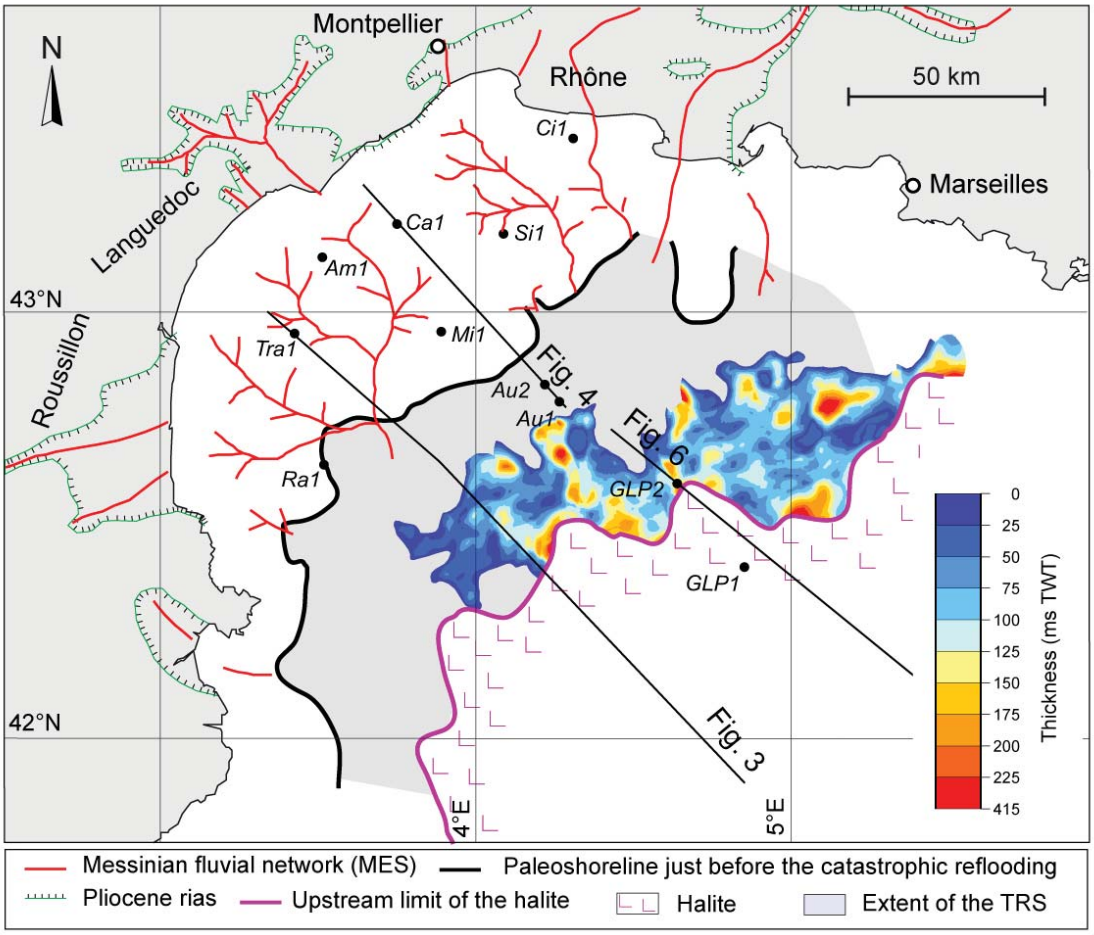

FIGURE 9 –

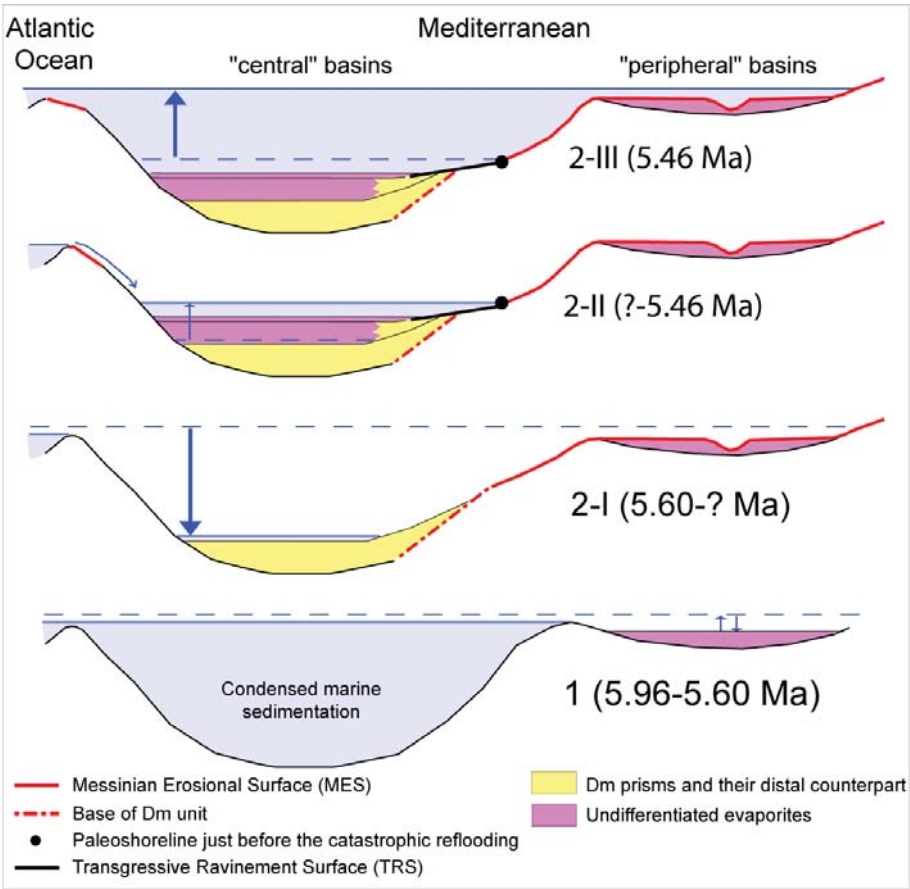
Atlantic Ocean
Mediterranean
"central" basins
"peripheral" basins
2-III (5.46 Ma)
2-II (?-5.46 Ma)
2-I (5.60-? Ma)
Condensed marine sedimentation
1 (5.96-5.60 Ma)
Messinian Erosional Surface (MES)
Base of Dm unit
Paleoshoreline just before the catastrophic reflooding
Transgressive Ravinement Surface (TRS)
Dm prisms and their distal counterpart
Undifferentiated evaporites

FIGURE 10 –

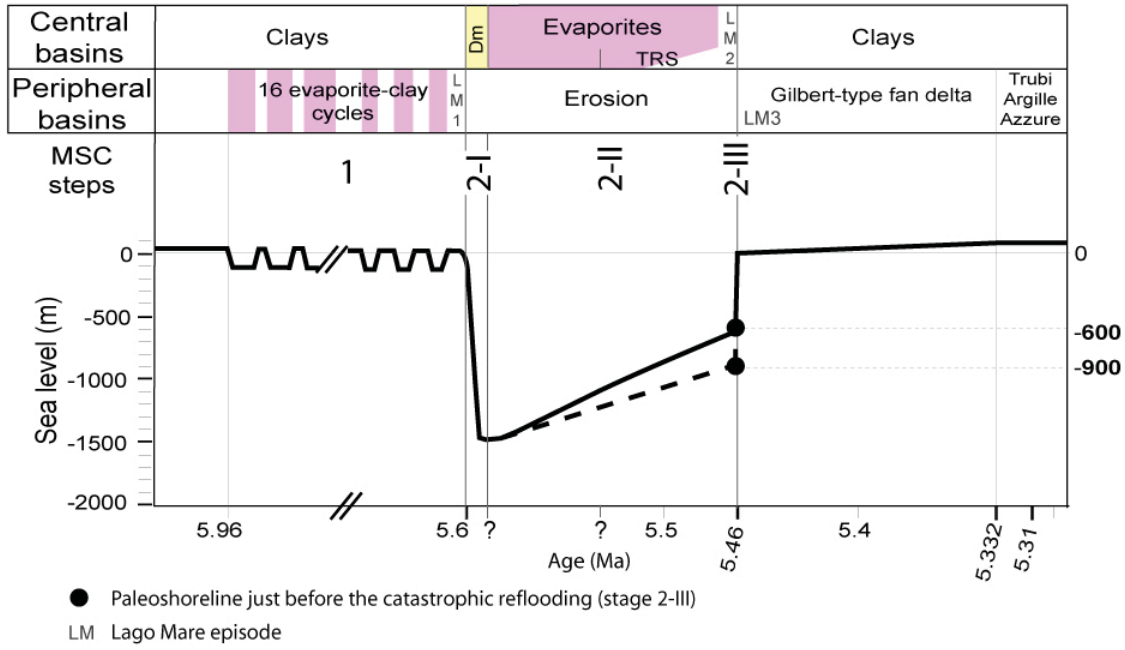

FIGURE 11 –

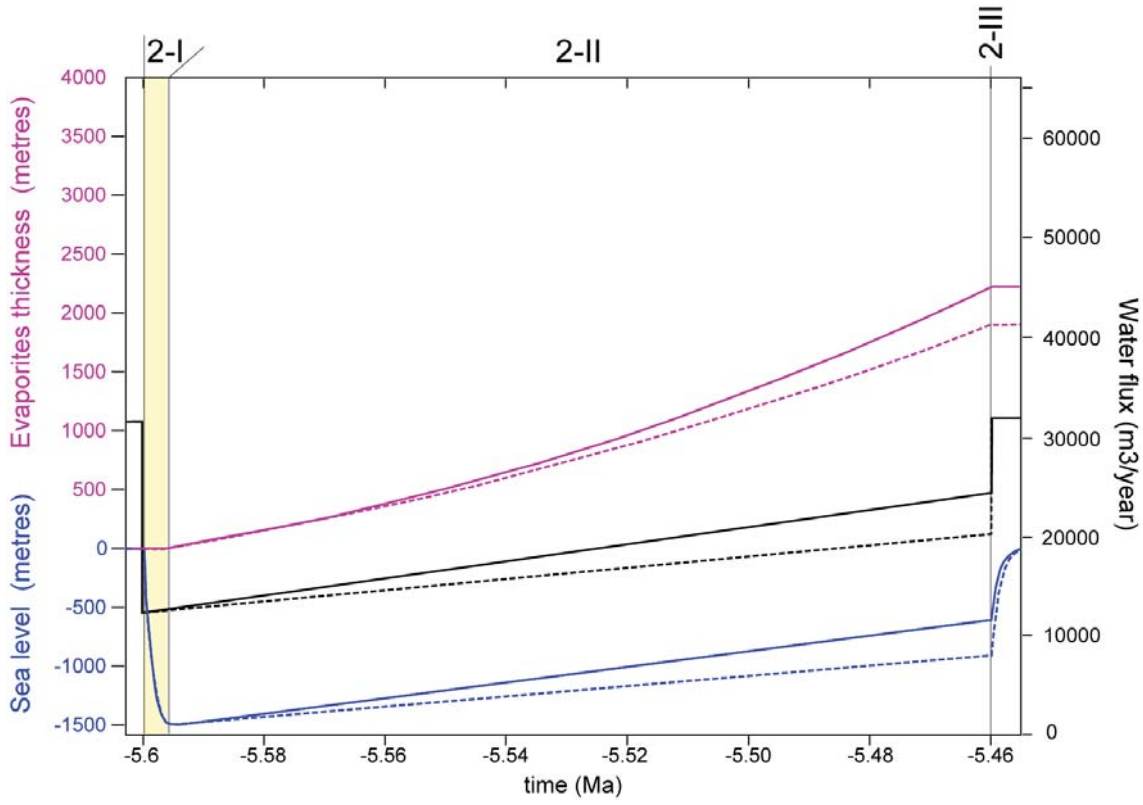

FIGURE 12 –

Structure and evolution of the Gulf of Lions : the Sardinia seismic experiment and the GOLD (Gulf of Lions Drilling) project

D. Aslanian, M. Rabineau, F. Klingelhoefer, M. Moulin, P. Schnurle, A. Gailler, F. Bache, E. Leroux, C. Gorini, A. Droxler, N. Eguchi, J. Kuroda, K. Alain, F. Roure, B. Haq.

Since the well-known models of McKenzie (1978) and Wernicke (1985), understanding the formation of passive continental margins, that is to say the way continental lithosphere is thinned and leads to subsidence, is one of the main challenges in Earth Sciences. These conservational models, i.e. simple shear, pure shear or polyphase models, which exclude exchanges between lower continental crust and upper mantle, are usually proposed to explain lithospheric stretching and consequent crustal thinning of passive continental margins. These models imply huge amount of horizontal movement, however, these movement are not observed in the field and authors suggested that lower continental crust may have been removed from its original place and have flowed towards the middle part of the system (allochthonous domain, part 2 in Figure 1) or/and it may also have flowed towards both extremities of the system.

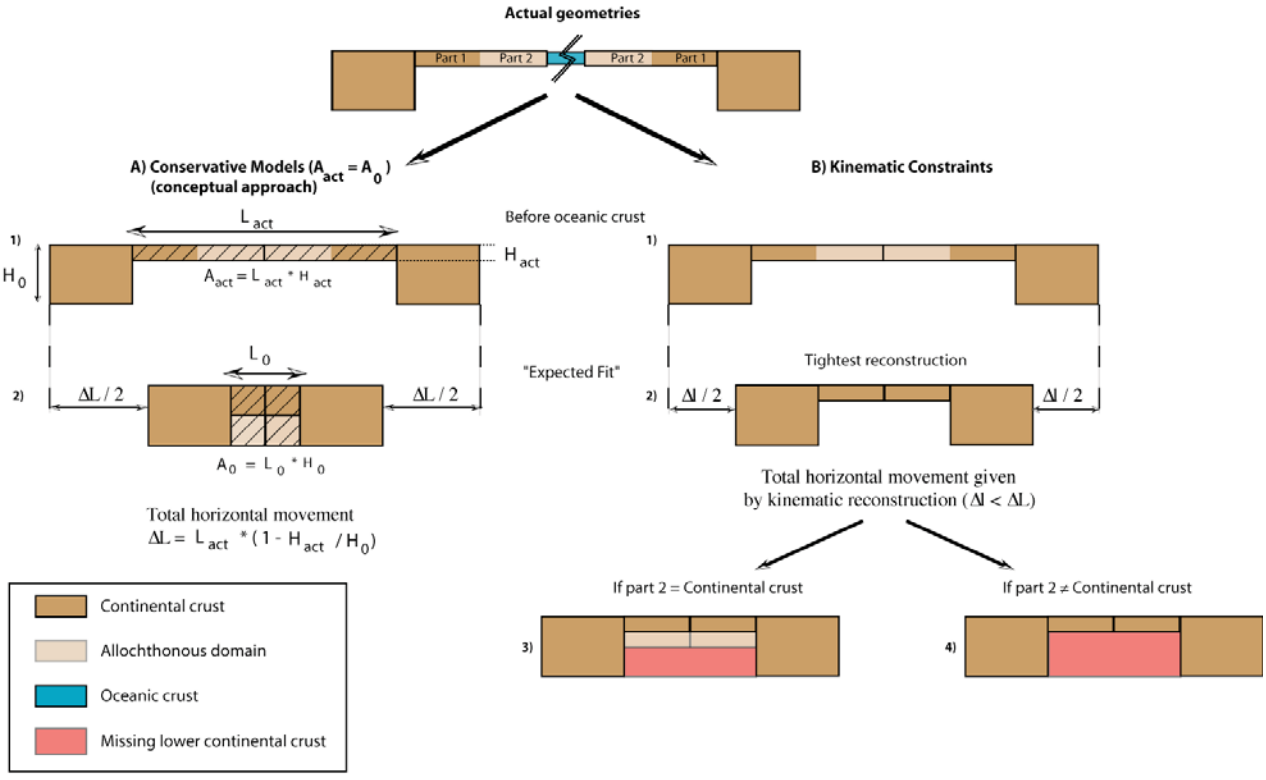

Figure 1: Continental crust thinning process: conceptual versus kinematic approaches. Top: Simplified geometries of a system of conjugate margins. Drawn after the conjugate Angola and Espirito Santo continental passive margins. A) Conceptual approach (conservational model): The actual area of continental crust is intrinsically strictly equal to the initial area, the continental crust thinning process can be converted in the horizontal movement. B) Kinematic Constraints: the horizontal movement is given by precise kinematic reconstruction. A wide thinned basin remains in that case. The allochthonous domains (part 2) of each margin overlap each other and are not shown on figure B-2. The quantity of « missing » lower continental crust depends on the nature (lower continental or not) of the allochthonous domain. After Aslanian & Moulin, GSL, 2012.

Therefore, one of the main impediment to our understanding of margin formation is the unknown nature of the intermediate domain between the unthinned continental crust and the true oceanic crust. Another unknown is how do margin evolve from a margin in a high position during all its

formation, with the presence of subaerial deposition of basalts, shallow water evaporites, subaerial erosion, or carbonates platform construction, towards a basin affected by strong subsidence during the plate divergent phases. Passive margins seem to be close to sea level position during a long time, even after the break-up as carbonates are post-dating the oceanic crust (e.g. on central and south Atlantic margins).

The Gulf of Lion: an unique natural laboratory. The Gulf of Lion (Figure 2) has appeared in the last years as an unique natural laboratory to study both evolution and interaction of deep processes (geodynamics, tectonics, subsidence, isostasy) and more surperficial processes (rivers behaviour, sedimentary fluxes, sea-level changes, climate impact and evolution...) due to a number a peculiar characteristics:

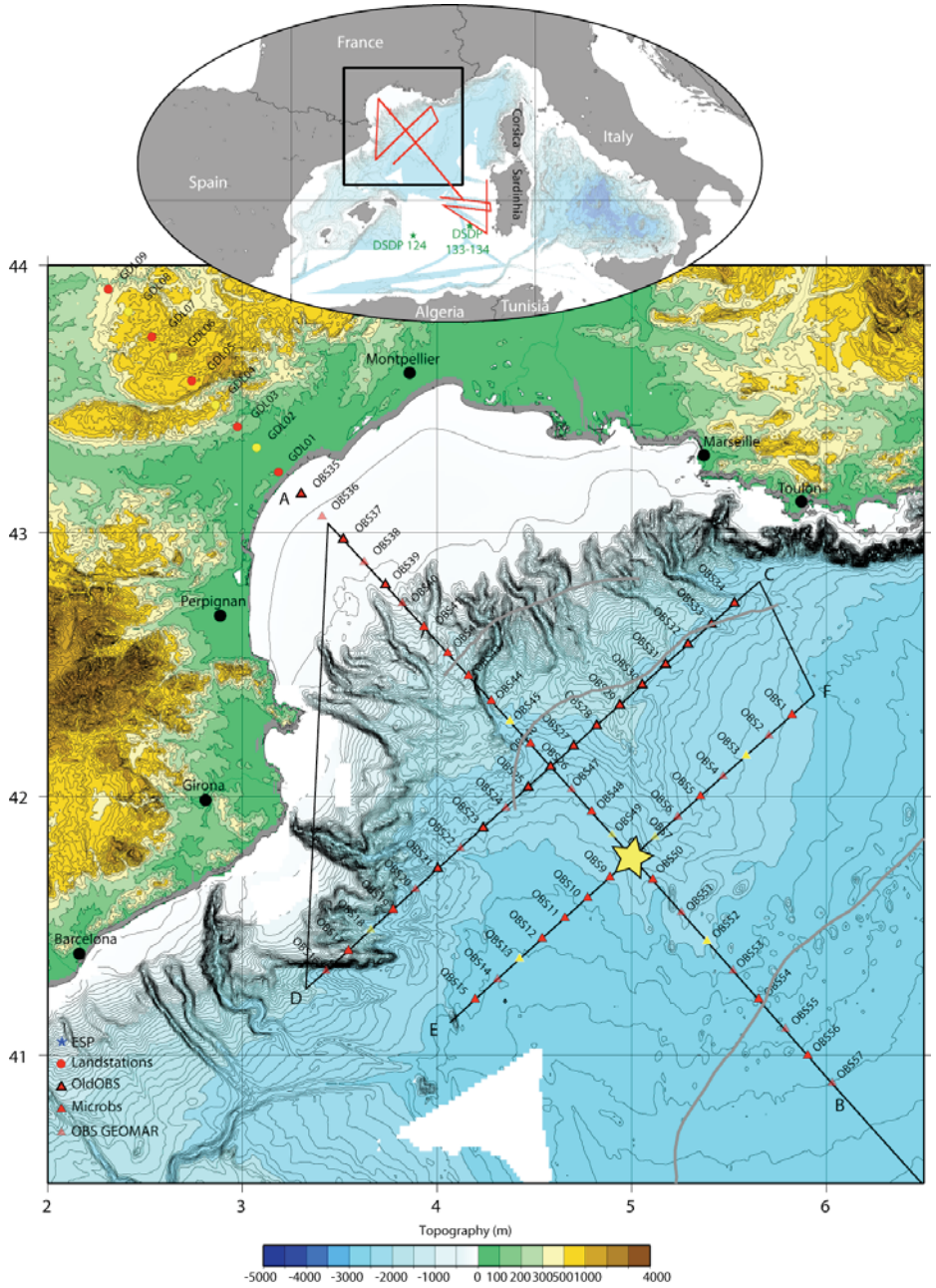

Figure 2 : Localisation of Sardinia profiles (red lines in the top-figure) and the GOLD project in the Gulf of Lion. The NW-SE profile was prolongated onland (dots). The brown lines represent the limits of the different crustal domains (see more details in the text). After Moulin et al.,JGI submitted

• It represents a segment of a continental margin which is both young (less than 35 Ma) and with a low slope gradient (less than 1°). This allows the precise observation of its structure and the detailed analysis of its huge (up to 7.7 km) of sedimentary cover (because of a small amount of instabilities); its homologous margin, the Sardinia margin, is equally accessible. Such an entire system in a small area, is a very rare object that needs to be used to validate models of continental break-up and subsidence evolution

• The sedimentary series are continuous and complete, neither affected by substratum tectonics nor by recent tectonics or gravity processes (Figure 3). Interpretation of sediment strata provides therefore three kinds of information: information on paleoclimatic history, information on tectonical history of the margin (vertical movements), and finally, as correlations are possible all along the margin, it allows for a precise evaluation of sedimentary fluxes and erosion/sedimentation balance.

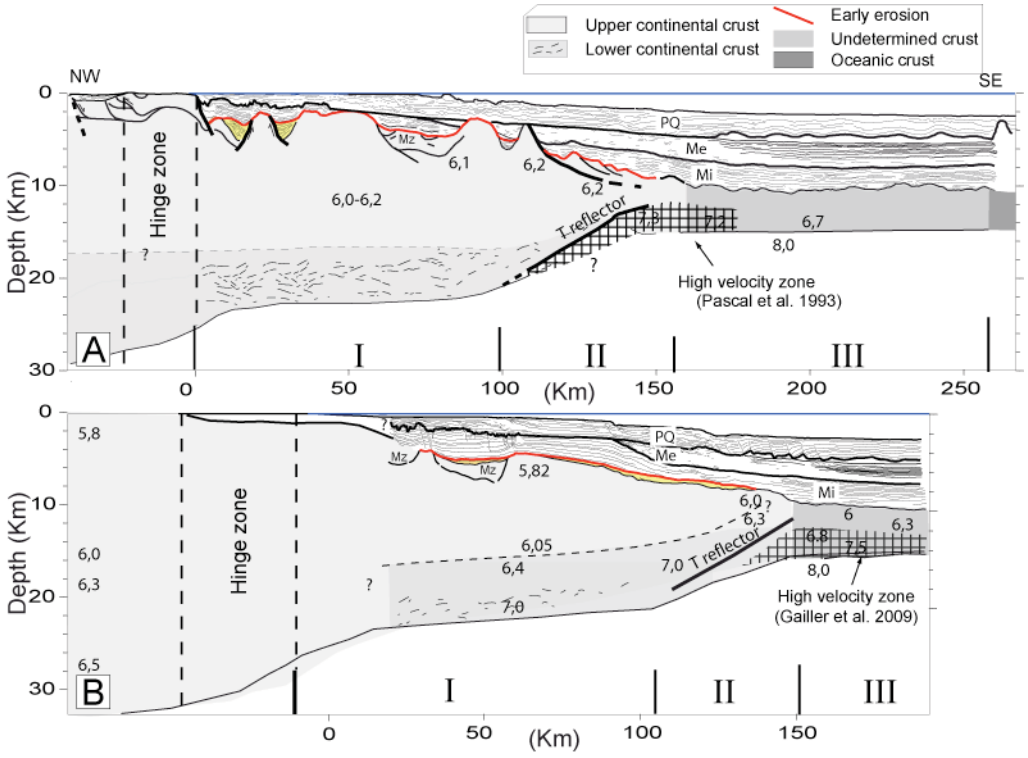

Figure 3- ECORS NWSE and Sardinia 1 profile showing the thickness of Miocene and plio-quaternary sequences, separated by the messinia. Note the presence of a strong reflector T, the High velocity zone and the sub-aerial erosion (red ligne) recorded before the first miocene sediment. Latin numbers represent the different domains (see text for details). After Bache et al., EPSL 2010, modified with results form Gailler et al, ESPL 2009 and Moulin et al., JGI submitted

• The time span of the basin (30 Ma) records some key events in climate évolution. Cenozoic records indeed show a global drop in temperatures and overall cooling of climate and the onset of glacial-intergalcial climatic cycles. The cooling did not occur gradually, but in "steps", with intervals of sudden change, alternating with stable intervals. The Mediterranean is particularly sensitive to the record of astronomically induced oscillations in climate. This has already been extensively studied in the Mediterranean. However, the Gulf of Lions enables to link these oscillations to their effect on sea-level and the erosion/sedimentation behaviour of sedimentary systems.

• Except during the Messinian Event, the Mediterranean Sea has been connected to the global ocean so that sea level variations are directly linked to Antarctic then both Arctic and Antarctic ice caps fluctuations. Shelf and slope of the Gulf of Lion have recorded with a great detail the successive glacio-eustatic fluctuations with a reconstruction of paleoshoreline positions. This has been intensively studied for the last 500,000 years on the shelf and related to sea-level amplitude and finally confirmed by the PROMESS European drilling project. This approach needs to be extended back in time. Such detailed paleobathymetric markers, such as those of the Messinian surface or Pliocene-Quaternary shorelines, will give markers with a precision never reached before to reconstruct paleogeographies (and also sea-level changes) and to better constraint the evolution of the subsidence of margin.

• The margin is the final sink for sediments coming from the second largest rivers in Mediterranean: the Rhône. Its drainage basin responds to climate change, with for example the influence of mountain glaciers over the Alps during the Pliocene and Quaternarywhich has to be compared to periods without glaciers (Miocene and Messinian periods). This influence has never been quantified on large time scale. Erosion/sedimentation balance in this closed basin should answer the question of sedimentary fluxes variability.

• The large shelf and the low continental gradient (less than 1°) in the Gulf of Lion enables the best possible observations for understanding the Messinian Mediterranean Event as a whole. Here, we can measure subaerial erosion on the shelf, observe markers of marine transgression on the slope and at the toe of the slope and map the succession of detritic units and their lateral seaward evolution and correlation to the evaporites. The deep basin is the only area with a full record of evaporite deposits. It is also in the Western Mediterranean Sea that the history of Mediterranean-Atlantic connections is the most direct and complete.

• The Gulf of Lion is the only place in the world where we will be able to evaluate the effect of the magnitude of sea-level variations on the sedimentary system and on sediments budgets with amplitudes varying from 1500 m drop and rise, 100 m drop and rise and 50 m drop and rise. Because the Western Mediterranean is a closed system, no sediment is lost and we can have access to a real Source to Sink system with quantified sediment fluxes.

•Finally, thanks to an exceptionally huge quantity of data (seismic profiles of different resolution, cores, drillings) coming from both industry and academia, the Gulf of Lion appears to be the very place to discuss precisely fundamental questions about passive margins, paleo-climate, sea-level and Messinian Crisis and deep Biosphere and fully integrate results of the ultra-deep drill. Intensive work (seismic interpretation, 3D mapping) has already been done by french academic teams (Universities, CNRS, IFREMER, BRGM, IFP) with a support from the Industry (TOTAL) in the Framework of the French GDR Marges and « Actions-Marges » Programs, (http://gdrmarges.lgs.jussieu.fr ; http://www.actionsmarges.univ-rennes1.fr/).

Geodynamical setting

The Liguro–Provencal basin reveals a structure and evolution corresponding to a pair of rifted margins formed by the rupture and counterclockwise rotation of the Corso–Sardinian micro-continent with respect to the Ibero–European plate from the end of Eocene (Priabonian, 33.7 Ma), in a general context of collision between Africa and Europe. The opening took place at the southern end of the intra-European rift system, in back-arc situation, in response to a SE rollback of

the slab of the African plate subducting beneath the European plate during an extensional phase. This Corso–Sardinian micro-continent rotation resulted in the emplacement of an oceanic crust, starting in the Late Aquitanian (23 Ma to 19 Ma) and ended at the Langhian (about 15 Ma). Although rifting in back-arc basins might differ in some points from cratonic rifting, the mechanics of thinning the continental crust should remain similar. Therefore the conjugate margins of the Gulf of Lions and West Sardinia represent a unique natural laboratory to address fundamental questions on rifting (e.g., on crustal thinning, on the nature of the continent–ocean transition zone and on the style of rifting), because of their young age, complete sedimentary layers and accessibility.

Seven domains can be indentified in the Liguro-Provençal basin on the base of gravity, magnetic, reflection and wide-angle seismic data. The figure 2 shows the Gulf of Lion side, with the four western domains. Domain I represents a 20km thick continental crust, domain II, the necking zone, domain III the intermediate crust and Domain IV the oceanic domain. Both ECORS-CROP and Sardinia 1 reflection seismic profile show the existence of a prominent landward dipping reflector located in the crust at the SE limit of the continental slope and called the T-reflector (Figure 3). Both images show a wide zone of high velocities southeastward of this reflector. These high velocities could be the expression of flowing lower continental crust underplated and intruded by partial melt, or represent serpentinized peridotite material exhumed during the initial opening of the basin. Based on these findings an opening along a lithospheric detachment fault (possibly represented by the T-reflector) has been proposed for the basin with the Sardinia margin representing the upper crustal plate, with exhumation of the mantle or lower crustal material occurring on the Gulf of Lions side. But the lack of deep crustal seismic data from the Sardinia margin has until now prevented to test this hypothesis and assess the asymmetry in depth.

Sardinia Experiment

Wide-angle seismic data can be used to quantify the continental crustal thickness, determine the degree of symmetry of rift structures and hence address fundamental questions concerning the mechanisms of rifting. During the SARDINIA experiment of the Ifremer French R/V L'Atalante, six coincident wide-angle and reflection multi-channel seismic (MCS) profiles, as well as CHIRP and bathymetry profiles, were acquired: three located in the Gulf of Lion area and three located on the conjugate margin offshore Sardinia. The main aims of the Sardinia wide-angle seismic cruise were to image continuously the deep crustal structure of the paired conjugate margins, to verify the existence of a high-velocity zone on the Sardinia margin and to constrain the nature of the ocean–continent transition zone.
First results based on tomographic modelling of the two main conjugate profiles of this experiment showed a symmetrical distribution of seismic velocities on both sides (Figure 4 and ???) (no figure for the other side).

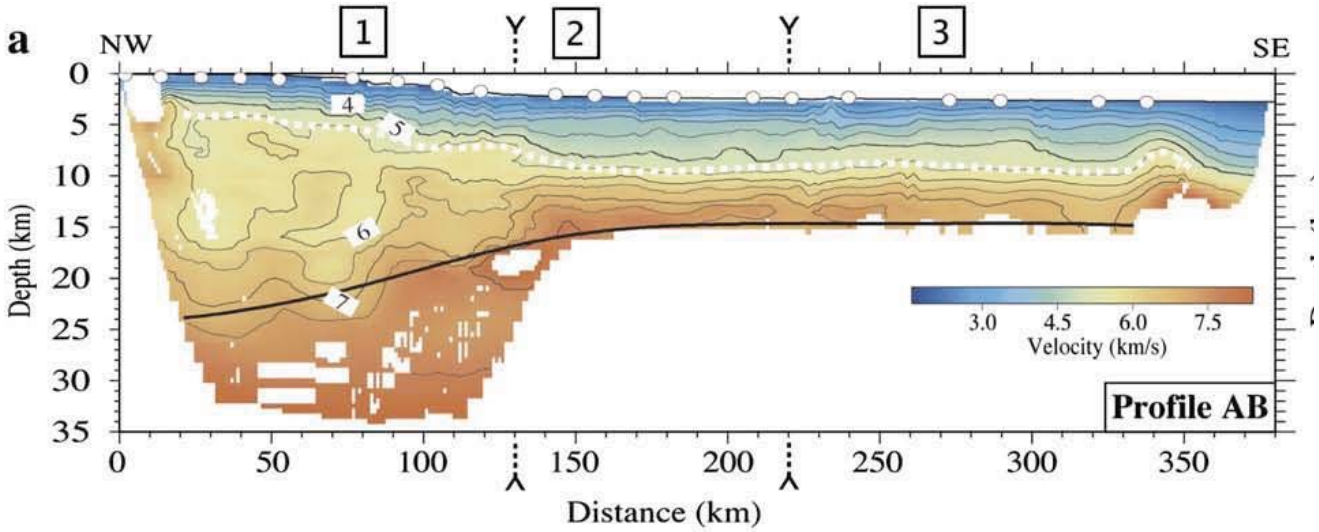

Fig. 4. Final velocity models resulting from the tomographic inversion of Pg, Pn and PmP arrivals. White circles: OBS/OBH locations; solid black lines: location of the Moho interface inverted from PmP arrivals; white dashed line: approximate location of the top of the crust, based on previous work from ESP and wide-angle modelling; black dashed ticks: limits of the 3 different Regions determined from variations of the crustal velocity structures modelled here. From Gailler et al, ESPL 2009.

Along both profiles, the resulting 2D velocity models show a similar evolution of the long-wavelength crustal velocity structures from the continental platform to the deep basin. Three different regions can be distinguished on this tomographic inversion image (Fig. 4).
In Region 1, which corresponds to domain I and II, Moho depth reaches 24 km in its inner part and decreases progressively to 18 km in its distal part (~130 km distance). This implies a thinning of the crust from 22 to 12 km. This crust is characterised by low velocities and a very low vertical velocity gradient. The upper mantle velocity is also low, confirming the previous observation on the ECORS profile. This high-velocity zone which is imaged on both margins of the basin might corresponds to lower crustal material or a mixture of serpentinized upper mantle material with lower crustal material. The existence of this zone on both sides of the margin does not support a hypothesis of a simple shear style opening along a lithospheric detachment fault.
Region 2 is interpreted as the continental-oceanic transition zone, as the crustal velocity structure is not typical of either continental nor oceanic crust. The thickness is about 6 km. Region 3, with a thickness of only 5km, has seismic velocities and vertical velocity gradients which are typical of oceanic crust, with the upper layer showing a high-velocity gradient (Layer 2) and a second layer with a lower velocity gradient (Layer 3). The transition to Region 3 might occur over a distance of 20–30 km probably corresponding to the onset of seafloor spreading.

High velocities found in lower crust have been interpreted in different ways, such as:

a) Exhumed mantle material
b) Highly thinned continental or oceanic crust overlying serpentinized mantle
c) Exhumed lower crust or mixture of lower crustal and upper mantle material

The high velocities found in the lower crust along the margin of the NW-Mediterranean basin (Figure 3 & 4) have been associated to mantle material exhumed during the initial opening of the basin and serpentinized by fluid flow through faults in the crust. In this case the late reflections found in OBS records should correspond to the base of the serpentinization front, as has been

observed on the Iberian and Canadian margins, where they have weak amplitude compared to the phases corresponding to reflection between lower crust and upper mantle material on the same profile. In our OBS record, PmP arrivals show the same amplitude in Regions 2 and 3, which does not clearly support an origin from serpentinized mantle material only.
Highly thinned continental crust or thin oceanic crust overlying serpentinized mantle material is proposed on magma-poor margins. This crustal geometry would produce a PmP reflection above the serpentinized mantle layer and possibly a second reflection from the serpentinization front, which is not supported by our data, where the single PmP reflection can clearly be associated to the base of the high-velocity zone (Figure 5).

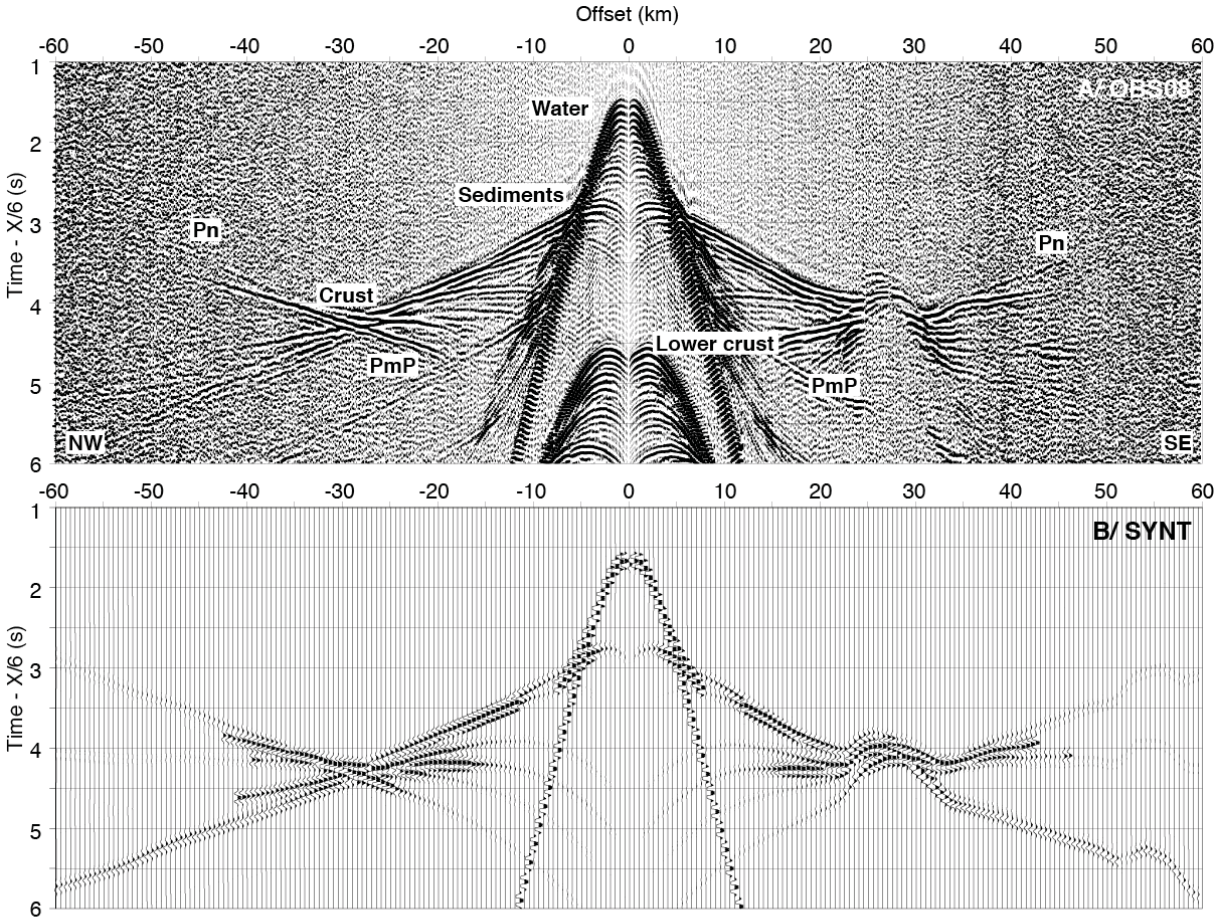

Figure 4 Bandpass filtrered (5–20 Hz) data from OBS 8 on profile AB, on the location of the GOLD project. The data are gain-adjusted according to the offset and reduced to velocity of 6 km/s. B/ Synthetic seismograms calculated from the model for the same station using the asymptotic approach of ray theory from the Zelt code (Zelt & Smith, 1992). The synthetic seismograms are calculated every 500 m, with a sampling rate of 120 Hz, obtained by convolution of the impuls response with a 29-point low passed Ricker wavelet. From Moulin et al., JGI submitted.

The last possibility, namely exhumed lower crustal material or a mixture of lower crustal and upper mantle material would produce one reflection with amplitude similar to that of a "normal" PmP reflection. This last interpretation is in good agreement with our data.

Ground Truth experiment: the GOLD project

The aim of the GOLD project (Gulf Of Lion Drillings) is to realise the first ever deep drilling in the Gulf of Lion, offshore the french coast. The drill site, situated by 2400 m water depth at the toe of

the slope, would go through 6,2 km of sediments deposited during the last 23 Millions years, down to the substratum. This drilling imposes the use of a drill ship equipped with a BOP (*Blow Out Preventer*) in order to go through the 1 km thick Messinian salt layer that has never been reached.

The project gathers a large range of Marine Science disciplines (geology, microbiology, geochemistry, geophysics, biology) as well as Engineering Sciences (instrumentation, signal processing)

- **Major challenges and innovative aspects**

The major challenges of this drilling project are focused around 6 major scientific, social and economic themes

1) *Greenhouse gases storage*: the drilling would enable to estimate potential greenhouse gases Storage in sandy reservoirs located below the Messinian salt layer, in the deep offshore of the Gulf of Lion in an area near major north Mediterranean industrial centres (Marseille-Fos, Barcelone).

2) Energy Ressources: the drilling below the salt would enable to evaluate potential hydrocarbon resources in the Mediterranean Sea. The only well know source rock is Messinian in age and are generally immature in most of the Algero-Provencal basin. We need to explore deeper and older series (Aquitanien, Burdigalien, Langhien et Tortonien). On another hand, the drill site also offers strong potential for geothermal energy. The concentration of Lithium in the thick evaporites layer (3000 m) should also be evaluated.

3) Climate and Sea-level changes: the Gulf of Lion is a unique place to study exceptionnally well-preserved sedimentary archives. The quantity of sediments deposited is directly dependant on the existence of the northern hemisphere Ice sheet, and its variations in size and thickness. These variations are related to climate changes, so that we can read glacioeustatic cyclicities in teh sediments. This has been demonstrated using a dense grid of seismic lines for the last 500 000 years and validated by the shallow Promess drill site on the shelf. The new very deep drilling would extend this type of results to the last 23 Ma.

4) Geodynamic, thermicity and margin formation: The formation of the sedimentary basins and continental passive margins have long been explained by numerous physical models, usually built on only one passive margin considered as the reference. However, The recent ante-salt discoveries,the presence of carbonate at the end of the passive margin building... demonstrate that these models fail usually to fit the observations. Passive continental margins are so diverse that the existence of a unique thinning process must be re-considered and discussed. However, the recurrence of some general features (abrupt thinning, large transitional domain, whatever the nature of the crust oceanic, continental or mixed) pleads in favour of general rules. No margin presents all the features needed to support a general model, but each margin supplies pieces of the jigsaw. Drilling the substratum of a deep margin, studying the paleo-envirronement of the first deposits in order to reconstruct the geodynamic history of this margin, is not common. Few places have already been drilled in that purpose. None of them occurs in a young Basin, built in a back-arc context. We need this information to understand the thinning of the continental crust, the building of the passive margins and the continental basins. What is the nature of the crust in the intermediate domain? In what kind of environment are the first sediments deposited? The drilling will offer the ground-truth necessary to constrain models of margin formation and subsidence and their consequences on potential hydrocarbon resources.

5) Deep Biosphere and the limits of Life: What is the maximum depth where life exists? What form does it take ? Today's maximum depth where signals of life have been proven is 1626 m below sea-floor, but this is only the maximum depth where life has been searched for. The deep drilling (7.7 km) is a unique opportunity to constrain the physicochemical limits of life in extreme conditions in terms of

either salinity (in the salt layer), pressure and temperature (as we go deeper) and the composition, function and adaptation of microbial community (bacteries, archea, virus, microeucaryotes) in the deep Mediterranean Sea. The drilling gives us a unique opportunity to better understand the beginning of Life and its potential adaptationto extrem envirronments.

6) Extreme events : the nearly complete dry out of the Mediterranean Sea during the Messinian event represents a unique hydrological, sedimentological and biological event in Earth history. This catastrophic crisis affects all the Mediterranean Sea with a sea-level fall of more than 1500 m inducing a gigantic erosion on the continent and the shelf. Nearly 3000m of evaporites and salt are also deposited in less than 500 000 years. DSDP, IODP drillings only sampled the first meters of this serie. The deep drilling will enable to sample the entire section and definitely test the contradictory models that exist for the process and consequences of this crisis. Quantification of mass movement involved will give essential data set to study and understand the dynamic of underlying mantle (inducing isostatic adjustment).

Finally, the drill site could also be instrumented as a permanent and unique observatory.

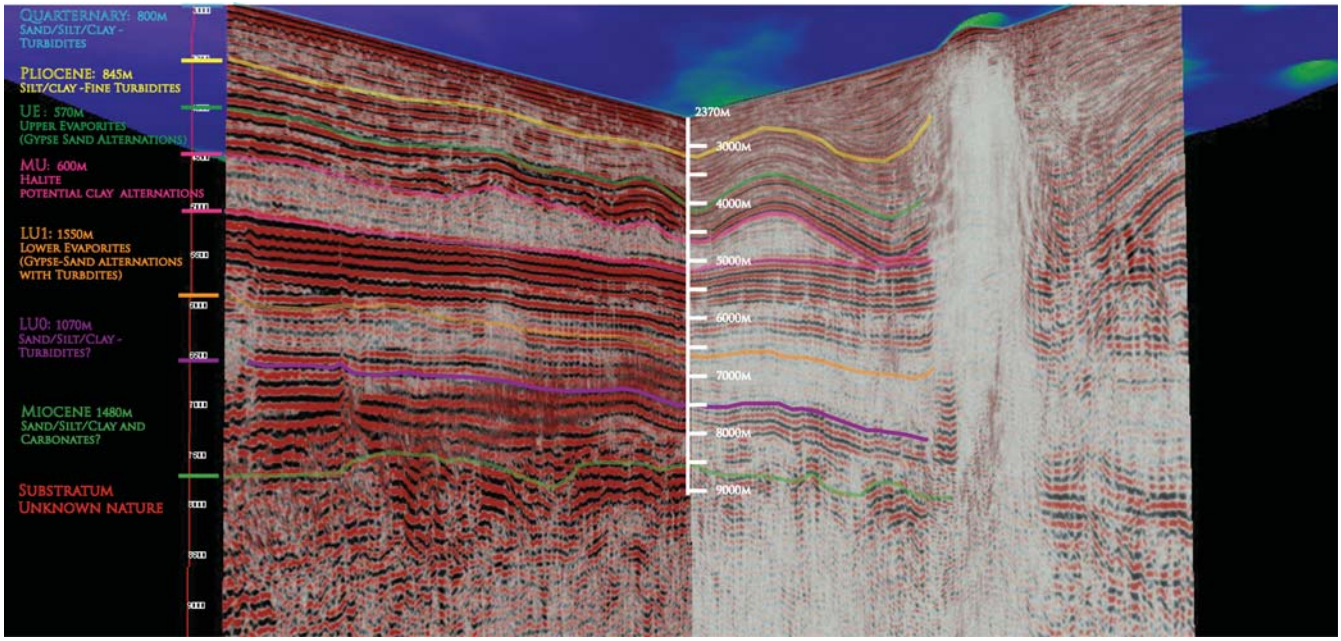

Figure 6 : Gold position on the two Sardinia crossing seismic profiles. The multi-channel seismic reflection data was acquired using a 4.5 km long, 360 trace digital streamer and a tuned airgun array of 8260 in3. The shot-interval was 60 s at an average speed of 5 knots, which translates to a shot-spacing of about 140-150 m. The airgun array consisted of 16 airguns with volumes ranging from 100 in3 G-guns to 16 L Bolt airguns, tuned to the first bubble and towed at depths of 18-28 m, in order to enhance low frequencies and ensure a good seismic penetration. The processing sequence consists of: data geometry and binning, noise editing, time-variant band-pass filtering (6-20-48-62 Hz at sea-floor to 2-12-24-32 Hz 4 s bellow), RMS velocity analysis at 2.5 km spacing, and pre-stack Kirchhoff depth migration.

The GOLD project will be submitted to the IODP Panel in april 2012. It final overall goal is to sample most strata from Upper Evaporites to Miocene strata down to the basement and focuse on Extreme paleoenvironements, their geodynamic and deep biosphere consequences and to reach the intermediate domain, which nature is crucial to identify to understand passive margin genesis and evolution.

The GOLD project will gather a unique group of expertises. A Public-Private Consortium is envisioned with representatives from Universities, public insitutions (Ifremer, IFP-energies nouuvelles, BRGM…) and private companies from petroleum world and other industrial technical or environmental world. Please contact aslanian@ifremer.fr and marina.rabineau@univ-brest.fr.

Suggested reading:

The results and observations presented here are discussed in full in: Crustal structure of a young margin pair: New results across the Liguro–Provencal Basin from wide-angle seismic tomography, by Gailler *et al.* (EPSL, 2009); Evolution of rifted continental margins: The case of the Gulf of Lions (Western Mediterranean Basin), by Bache *et al* (EPSL, 2010); Kinematic consequences of conservative models in the South Atlantic Ocean, by Aslanian & Moulin, 2012.

Recently this GOLD project has been identified as a key initiative of the "Chantier Méditerranée" within **MISTRALS** national initiative **(Mediterranean Integrated Studies at Regional And Local Scales)** an initiative of CNRS-INSU, CIO-E and ANCRE (Comité Inter-Organismes-Environnement and Alliance Nationale de Coordination de la Recherche pour l'Energie, involving CNRS, IFP, BRGM, IFREMER, IRD and CEA) and more specifically as a key initiative and priority within its **TERMEX** (Mediterranean Earth sciences experiment) component (Rabineau et al., 2012, special volume on TERMEX). See also: http/ :www.esf.org/magellan (click on *Science Meetings)* and http://www.congres.upmc.fr/gold/.